UNIVERSITÀ DEGLI STUDI DI TRIESTE

UNIVERSITÀ CÀ FOSCARI VENEZIA

XXXII CICLO DEL DOTTORATO DI RICERCA IN CHIMICA

HETEROCHIRAL SHORT PEPTIDES FOR SELF-ASSEMBLY INTO ANTIMICROBIAL HYDROGELS

Settore scientifico-disciplinare: CHIM/06

DOTTORANDA

MARINA KURBASIC

COORDINATORE

PROF. BARBARA MILANI

SUPERVISORE DI TESI

PROF. SILVIA MARCHESAN

ANNO ACCADEMICO 2018/2019

TABLE OF CONTENTS

Abstract

Antimicrobial peptides (AMPs) have potential properties as next-generation therapeutics to combat the spread of drug-resistant classical antibiotics. Most AMPs consist of long molecules (>>10-15 amino acids), for which the preparation on a large scale can be expensive and not straightforward. By contrast, self-assembling ultrashort antimicrobial peptides are attractive candidates considering their ease of preparation and benign fate in biological settings and in the environment. Moreover, the vast majority of these systems require synthetic N-capping groups (*e.g.*, Fmoc, Nap, etc.) for self-assembly. For biological applications, however, it is preferable to avoid such moieties. The use of both D- and L-amino acids is an alternative strategy to drive self-assembly and attain defined conformation and resistance to proteases. Hydrogels formed by tripeptide ^{D}Leu-^{L}Phe-^{L}Phe display mild antimicrobial activity against *Gram negative* bacteria, including a clinical isolate, whilst not eliciting cytotoxicity nor haemolysis. Inspired by these results, a series of 22 tripeptide analogues was prepared, where the effects of halogenation, and changes in amino acid stereoconfiguration and sequence were evaluated on gelation and antimicrobial activity. Structural analysis has been performed by several techniques, including single-crystal XRD, NMR, LC-MS, circular dichroism, TEM. All compounds designed to self-assemble formed nanostructured hydrogels at physiological pH and displayed mild antimicrobial activity only in the assembled state, giving scope to use assembly/disassembly as a means to switch on/off activity. Although general rules for a structure-activity relationship were not found, two compounds demonstrated improved activity against *E. coli*, resistance to protease-mediated degradation, and negligible haemolytic side effects. In light of the growing issue of drug pollution into the environment, we believe these biodegradable systems stand as an interesting starting point towards the development of antimicrobial materials composed of conveniently simple building blocks, which can be switched on/off on as required, simply assembling or disassembling superstructures *on demand*, as demonstrated for instance by heating/cooling, besides changing of pH values. Tripeptide antimicrobial materials could find application in surgery procedures, as coating of medical devices, or for topical use against infections.

Riassunto

I peptidi antimicrobici (AMPs) sono molto promettenti per combattere le resistenze dei batteri agli antibiotici. La maggior parte degli AMPs consistono in lunghe sequenze (>>10-15 amino acidi), per cui la loro preparazione su scala industriale può risultare molto costosa e difficoltosa. Al contrario, brevi sequenze peptidiche capaci di organizzarsi in strutture supramolecolari e aventi proprietà antimicrobiche sono preferibili, in quanto sono sia facili da preparare che biocompatibili e biodegradabili. La vasta maggioranza di questi composti però richiede la presenza di gruppi protettivi (*e.g.*, Fmoc, Nap, etc.) per riuscire ad auto organizzarsi in strutture supramolecolari. Tuttavia, per le applicazioni biologiche è preferibile evitare l'uso di questi gruppi per via della loro citotossicità. Per superare questo problema, secondo gli ultimi studi, l'uso di aminoacidi D- e L- nella stessa sequenza peptidica è un'utile strategia per formare delle strutture supramolecolari, organizzate in maniera ordinata e aventi una maggior resistenza alla degradazione enzimatica rispetto ai classici peptidi antimicrobici. Basato su questa strategia di self-assembly, recentemente è stato riportato che il tripeptide ^{D}Leu-^{L}Phe-^{L}Phe presenta una lieve attività antimicrobica nei confronti dei batteri *Gram negativi* ed è in grado di formare in condizioni fisiologiche un idrogel supramolecolare privo di citotossicità ed attività emolitica *in vitro*, entrambi effetti indesiderati che spesso si accompagnano all'uso degli AMPs. Sulla base di questo risultato una serie di 22 tripeptidi è stata preparata, valutando l'effetto dell'alogenazione, la stereoconfigurazione, e la sequenza amminoacidica sulle loro proprietà di auto-organizzarsi in strutture più grandi e sull'attività antimicrobica. Le analisi strutturali dei composti sono state testate tramite diverse tecniche, come ad esempio la cristallografia a raggi X, NMR, LC-MS, dicroismo circolare e TEM. Tutti i composti designati per il self-assembly hanno formato idrogel nanostrutturati che presentano lieve attività antimicrobica, ma solo nello stato assemblato, dando la possibilità in questo modo di attivare/disattivare l'attività di questi composti *on demand (Figure 1).* Nonostante non sia stata trovata una relazione generale tra struttura e attività, due composti sono stati identificati con promettente attività antimicrobica, resistenza alla degradazione enzimatica e assenza di effetto emolitico. La possibilità di spegnere l'attività antimicrobica semplicemente rompendo i legami deboli presenti nelle strutture supramolecolari (per esempio con cambio di temperatura o pH) è un passo avanti nell'ottenimento dei farmaci ecologici. Questi materiali supramolecolari basati su tripeptidi possono trovare diverse applicazioni, come ad esempio negli interventi chirurgici come rivestimenti dei dispositivi sanitari o per applicazioni topiche che contrastino le infezioni.

1. INTRODUCTION

1.1. Present and Future for Antimicrobial Peptides

1.1.1 Towards a post-antibiotic era

In recent years, most pharmaceutical companies had severely reduced their R&D investments in new antimicrobial agents, because of the poor returns for antibiotics that were approved to market in the last decades. [1] By contrast, today, research towards new antimicrobial agents is reviving, in light of the worldwide emergency we are facing in terms of antimicrobial resistance (AMR). The term antimicrobial includes antibiotics, anti-viral and anti-malarial agents. The causes of AMR spreading are varied (*Figure 1.1*), and they include misuse of such agents to treat humans and animals, especially in countries where antimicrobials use is not regulated, and they are readily available without medical prescription. There is also the need for clear guidelines concerning the safe disposal of unused and expired antibiotics. This is important to reduce the amount of antibiotics that persist in the environment and could cause further spreading of AMR. The serious risk is that, if the current trend does not stop, we will soon be entering the "post-antibiotic" era, where simple infections could be again the leading cause of death for many humans worldwide. [2]

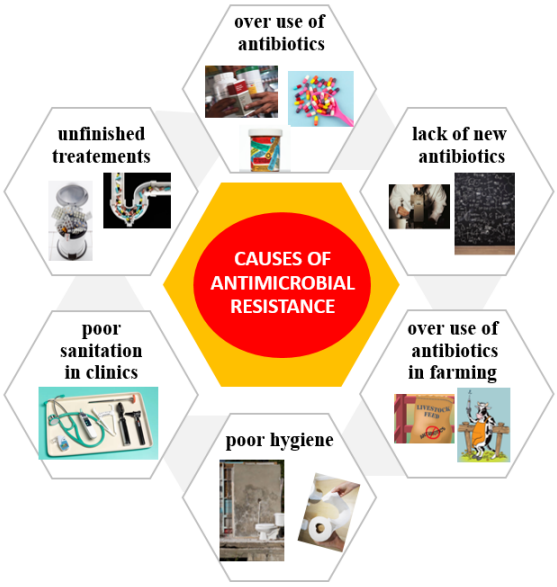

Figure 1.1 Common causes of antimicrobial resistance (AMR).

To circumvent the issue of AMR, research for new antimicrobials has been extended well beyond conventional drug molecules, to include also nanomaterials, such as nanoparticles [3] and peptide-derivative nanostructures. [4] In particular, the latter are attracting wide interest due to their inherent biocompatibility and the fact that endogenous antimicrobial peptides are widely known, and nature has shown they can be very effective against infections. [5] Peptides can easily be modified at the level of their primary sequence, for instance to introduce non-natural moieties that may extend their half-time *in vivo* and may also improve their activity.[6–10] Unfortunately, prediction of the effects of such modifications on their secondary and tertiary structure, and especially on their supramolecular organization, hence bioactivity, is very difficult to anticipate. This introduction will thus focus on recent developments in the research areas of antimicrobial peptides in common with amyloid peptides and self-assembling peptides that can help in the development of the next generation supramolecular, smart, antimicrobial systems.

1.1.2. Antimicrobial peptides

Antimicrobial peptides (AMPs) are considered promising treatment alternatives owing to their broad variety of structural and amino acid composition motifs, as well their broad range of activity and their mode(s) of action being different from those of conventional antibiotics. AMPs include hydrophobic residues and positive charge residues provided by arginine, lysine or, in acid environment, by histidine. The cationic and amphipathic nature of many AMPs contributes to their binding to the anionic bacterial cell surface and insertion into the cytoplasmic membrane, resulting in membrane perturbation and killing of the target microorganism. Thus, unlike antibiotics, AMPs typically do not act on a specific target but preferably attack the cell membrane and are thought to be less likely to induce resistance.[11,12] Moreover, studies with synthetic all-D antimicrobial peptides are a proof that many peptides act directly on the membrane lipid bilayer, rather than on a receptor protein.[13] Subsequent studies with some peptides, however, have shown that all-L and all-D enantiomer peptides do not present equal activity, with results that appear to be species-dependent.[14] Furthermore, higher activity was demonstrated for different peptides explained with their increased affinity to peptidoglycan. Peptide chiral components of peptidoglycan are involved in this preferential interaction. This study is confirmed also by other studies in which the activity of peptides containing D-amino acids is higher if compared to peptide containing L- amino acids, as well their stability towards enzymatic degradation.[15]

The secondary structure of many antimicrobial peptides include a) α-helical structures, b) β- stranded structures due to presence of two or more disulfide bonds, c) β-hairpin or loop due to presence of one disulfide bond and/or cyclisation of the peptide and d) extended structure (*Figure 1.2*).[16–18] Many

peptides have α-helical structures and the majority of them as mentioned above are cationic and amphipathic, but also hydrophobic α-helical antimicrobial peptides exist. In addition, some β-sheet peptides have antimicrobial activity, and also antimicrobial α-helical peptides, which have been modified to possess a β-structure, retain part of their antimicrobial activity.[19] There are even antimicrobial peptides which are rich in a specific amino acid, such as His or Trp or thio-ether rings, some are lipopeptides or present macrocyclic Cys-based motifs.[20–24]

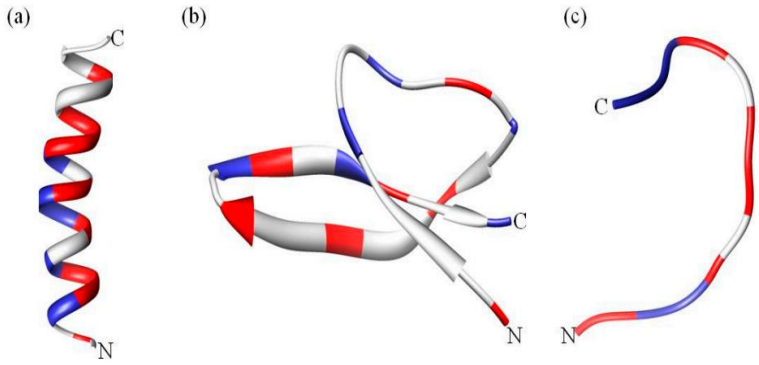

Figure **1.2** Conformation diversity of antimicrobial peptides.
Adapted with permission from ref.[18] © 2018 MDPI.

In humans, the two main classes of antimicrobial peptides are defensins and cathelicidins. Defensins have a β-sheet rich fold and aframework of six disulphide-linked cysteines, with the two main defensin families being α- and β-defensins. Cathelicidin essentially conforms to four structural types, although some of them can contain more than one structural AMP type. A common feature of most of these peptides is a marked cationic nature that favours interaction with bacterial membranes, although this feature can also lead to cytotoxicity due to interaction with mammalian cell membranes.[25]

1.1.3. Mode of action of different AMPs

Different membrane disruption mechanisms are strongly dependent on peptide and lipid interactions. Not all peptides insert into and disrupt the membrane or form pores. Many studies have shown that the same peptides apply their lytic activities *via* different mechanisms, depending on peptide concentration and on peptide-lipid ratio.

The most common mechanism of action can be described by non-poration models, especially the carpet model. In this case, AMPs attach with a parallel orientation to the membrane (*Figure 1.3c*).

Alternatively, AMPs at a high concentration breach the membrane in a detergent-like way (*Figure 1.3d*). In both these models, peptides accumulate at the membrane surface and create permeation and leakage pathways for ions and small molecules across lipid bilayers. Another mechanism proposed is the "charge lipid cluster model" when the presence of cationic AMPs causes the aggregation of anionic lipids and leads to phase separation in membranes (*Figure 1.3e*). The "all-or-none kinetic mechanism" is the case of formation of stable or transient pores in the membrane (*Figure 3 a,b,f*) that facilitates AMPs insertion into and across membranes.[26] All of these models show strong dependence on peptide concentrations.

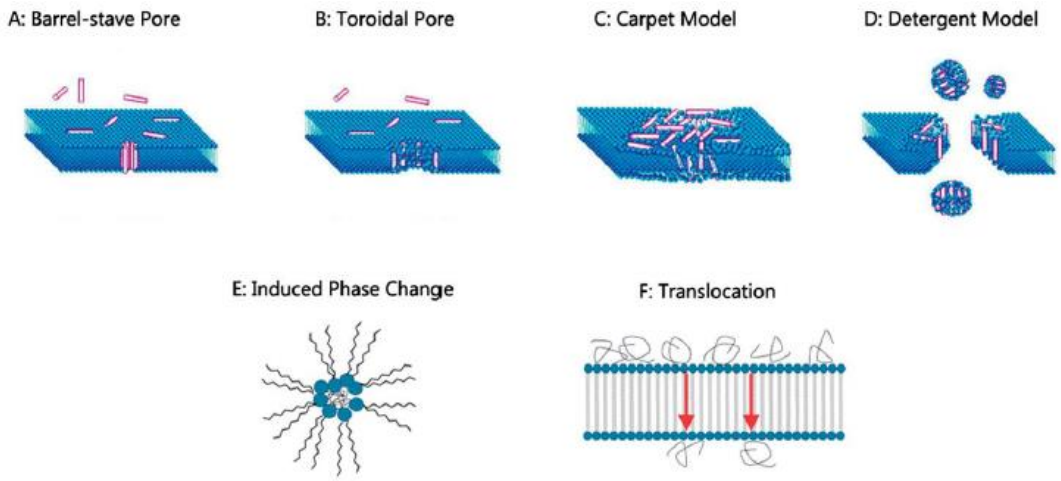

Figure 1.3. Modes of action of antimicrobial peptides.
Adapted with permission from.26[26] © 2013 Biophysical Society by Elsevier Inc.

Some peptides have disordered structures in physiological bulk solution and approach bacterial membranes as such and being cationic are electrostatically attracted to the anionic bacterial surface. Helical peptides undergo a transition from an unstructured globule to an extended, amphipathic, helical conformation that inserts into the membrane and when a critical concentration is reached, the AMPs interact with the membrane bilayer in a detergent-like manner.[27–29] Some helical peptides however, adopt a helical structure already in bulk solution, and this drives aggregation. These peptides approach the membrane as oligomeric bundles and this favours the formation of toroidal pores (*Figure 1.3b*), also peptides with β-sheet structure usually interact with this mechanism. Pro/Arg-rich peptides bind to the bacterial surface and are then internalized by specific bacterial transport proteins.[30] Trp/Arg-rich peptides bind at the membrane surface interface and then translocate into the bacterial cytoplasm.[31] Gly/Ser-rich peptides have intrinsically disordered structures and remain on the bacterial surface. Their precise mechanism of action is unknown, but the antimicrobial activity is quite salt-sensitive and not principally membranolytic.[32]

1.1.4 Ideal properties for AMPs

The starting point to efficiently design AMPs is to identify a natural one and operate some modifications to optimise it. The most important peptide requirements are the following: selective broad spectrum of activity, toxicity for the bacterial target and few side-effects, minimal risk of bacterial resistance, favorable costs.[33,34]

- Broad spectrum of activity. Although AMPs present significant and broad *in vitro* activity, this often decreases under physiological conditions *in vivo*. Besides, it has been described that AMPs show the same activity towards wild-type and resistant strains of bacteria. Natural sources produce AMPs in low quantities with a limited activity compared to enhanced synthetic AMPs.
- Toxicity. If not highly selective for bacterial membranes, AMPs can be toxic to eukaryotic cells, as their mechanism of action principally relies on interaction with membranes. This potential toxicity also represents a crucial obstacle for clinical application. An interesting option is the combination of AMPs with antibiotics in a synergistic manner to allow for reduced doses of each, thus reduced side-effects.
- Minimal risk of bacterial resistance. AMPs have potential properties as next-generation therapeutics to combat the spread of drug-resistant classical antibiotics, thanks to their unique mode of action that targets membranes.
- Cost. This is the principal difficulty to overcome. Commercial-scale production platforms to synthesize AMPs are essential. Shorter AMP sequences that exploit self-assembly mechanisms to mimic longer peptides may offer interesting opportunities.

In terms of antimicrobial hydrogel design, the supramolecular nanofibers and the rheological properties of the hydrogels can be highly effective for improving the antimicrobial activity. [35] Amyloids have also been demonstrated to be able to form transmembrane pores in both anionic and zwitterionic lipid membranes, in a mechanism similar that utilised by antimicrobial peptides for membrane permeabilisation, suggesting common folding and functions of both class of compounds.[36–40]

1.2 Peptide-based hydrogels

Hydrogels are soft materials that incorporate and retain a vast amount of water and are ideal candidates to mimic natural tissues, and especially the extracellular matrix. Therefore, they are highly attractive in the medicinal field for applications that span from tissue engineering, to wound healing, to advanced media for drug release.[6] They can be composed of chemical or physical networks made of a variety of molecules, such as synthetic polymers, polysaccharides, or protein/peptides. They can also be designed to include nanomaterials and further improve their physico-chemical properties. [7–10,41] Indeed, nanomaterials can introduce additional features not only for a quantitative, but rather a qualitative leap in nanomedicine.[42]

Amongst the various types of hydrogels, those composed of ultrashort peptides (*i.e.*, 2-3 amino acids) are particularly attractive, for a number of reasons. Firstly, peptides can easily be produced with a variety of methods, of which the most popular are chemical synthetic approaches for short sequences. It should be noted, though, that solid-phase approaches require a large excess of reagents and solvents, and generate a vast amount of waste. Secondly, costs increase exponentially with the length of the sequence, making amino acid derivatives, di- and tri-peptides amongst the more economically viable options. Thirdly, only such simple compounds can easily be produced in liquid-phase, at significantly lower cost.[43] Furthermore, short peptides are far more chemically robust than large proteins that require correct folding for bioactivity relying on non-covalent, weak interactions that can easily get disrupted.[9] In addition, as small molecules of synthetic origin, they allow for a higher and simpler level of control over chemical exact composition, with very high batch-to-batch reproducibility, in contrast with proteins of natural origin or other macromolecules. Finally, as small molecules, they pose significant lower risks of immune response relative to polypeptides and proteins.

Perhaps one of the most important reasons that gives a net advantage to supramolecular hydrogels over conventional macromolecular systems is the ability to use a simple molecule of exact chemical composition that can self-assemble into a macroscopic, dynamic material. Indeed, macromolecular hydrogels are often composed by several compounds of similar chemical nature; poor control over the molecular weight results in more heterogeneous systems that do not allow for precise control over their physico-chemical behavior. Additionally, hydrogels composed of covalent linkages require far more energy for their disruption and reformation. By contrast, self-assembling small molecules offer a simple means to achieve a macroscopic system of defined chemical composition that can be disrupted and reformed with a small energy requirement, since it is based on weak interactions. A system of this kind allows finer control over its formation and disassembly. As a result, supramolecular hydrogels can be envisaged as dynamic systems that can easily be switched between two states; *i.e.*, assembled (gel) and

disassembled (sol). A plethora of different stimuli have been developed in recent years to trigger transformations of this kind in smart systems, and their description can be found elsewhere.[44]

Stimuli-responsive systems are indeed attractive in light of the fact they can adapt to the environment and evolve over time, an ability typically found in living organisms. Importantly, in the context of AMR, the dynamic behavior can be envisaged as a means to control bioactivity. For instance, if a supramolecular system has antimicrobial activity only in its assembled state, then it could be "switched on" when needed to treat infections, then "switched off" to avoid release of antimicrobial agents in the environment (*Figure 1.4*). In this manner, the antimicrobial activity would be exerted with spatiotemporal control exquisitely to address therapeutic needs.

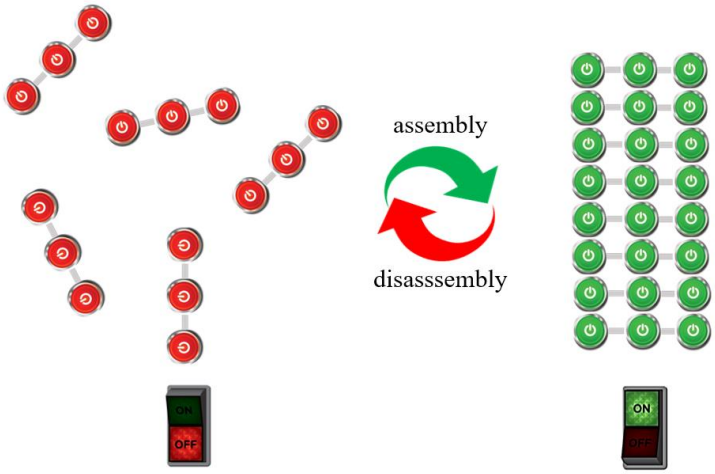

Figure 1.4 Assembly/disassembly of a small molecule can be used as a means to switch on/off a system if a certain function (e.g., antimicrobial activity) lies only within the assembled state. As an example, tripeptide molecules (represented by three red beads for molecules in solution and three green beads for molecules in hydrogel state)

This avenue might be highly promising for the treatment of infections, and could be envisaged not only for topical treatments, such as wound dressings and hydrogel applications on mucosae, but also for advanced formulations containing nanogels for oral administration. However, the way ahead is still long and full of challenges, therefore it requires collaborative efforts from different scientific areas and disciplines that could help in the design of new therapeutic solutions, as described further below.

1.3 Peptide self-assembly

1.3.1 Ultrashort peptide self-assembly

Self-assembly of ultrashort peptides into supramolecular structures for hydrogelation has been the subject of intense studies, yet it is not completely understood. A direct correlation between peptide structure and self-assembly for the design of new gelators is currently lacking, although structural variation is known to have an important impact on self-assembly, and hydrophobicity stands out as a key requirement for molecular aggregation in water.[45] In a minimalistic search, Gazit and collaborators discovered that one or two units of phenylalanine are powerful self-assembling motifs towards supramolecular fibers.[46,47] However, stable hydrogels are not obtained from the latter, unless the dipeptide is cyclized to the corresponding 2,5-piperazinedione.[48,49]

Another very useful approach to promote hydrogelation of the Phe-Phe motif consists of adding rigid, protective groups at the peptide N-terminus that can template self-assembly and engage in aromatic interactions driving supramolecular organization (*Figure 1.5*).[50] Many examples of this approach can be found in the literature; the most popular moieties employed to this end are the fluorenylmethyloxycarbonyl (Fmoc) moiety or naphthalene (Nap) derivatives.[51,52] Recently, also heterocycles, such as indole or carbazole, proved effective as alternatives for this purpose.[53] However, the use of polyaromatic synthetic units raised concerns in terms of their fate *in vivo* and potential toxicity arising from biological applications of such materials.[54,55] For this reason, there is a very active search towards self-assembling ultrashort peptides that do not contain such capping groups. However, this task is very challenging due to the high inherent flexibility of peptide molecules, as exemplified by the finding of only four new hydrogelators from the *in silico* screening of all 8,000 combinations of L-amino acids in tripeptides.[45]

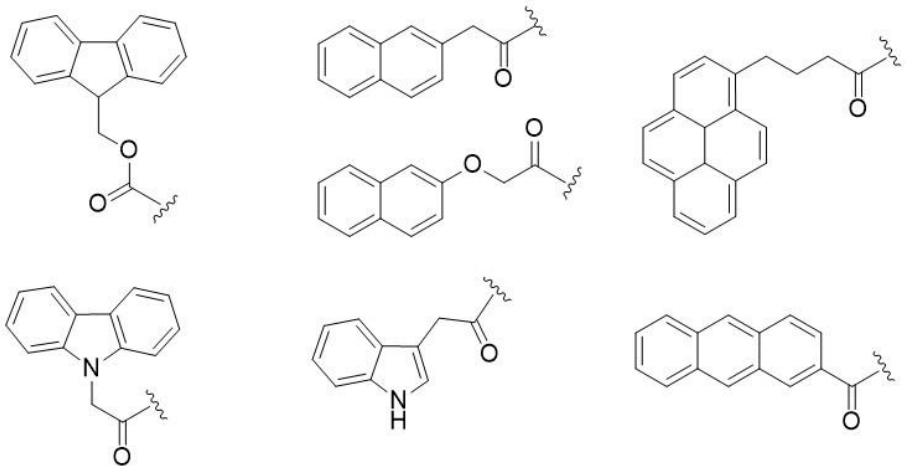

Figure 1.5. N-capping groups successfully used in the design of ultrashort peptide hydrogelators.

Alternatively, the combination of D- and L-amino acids proved to be a successful strategy for the design of hydrophobic, self-assembling, unprotected tripeptides.[56–58] Net segregation of hydrophilic and hydrophobic components is key to achieve an amphiphilic supramolecular organization that renders the hydrogels stable.[58] Only recently, the divergent path of L-homochiral and D,L-heterochiral tripeptides towards self-assembly was monitored *as a continuum* from single molecules to macroscopic hydrogels, highlighting key differences between stereoisomers.[56] Heterochiral hydrogelators offer a number of advantages over their homochiral counterparts.[59] In particular, an attractive feature of these systems is the possibility to fine-tune their protease-mediated degradation rate; this does not only depend on the number and position of D-amino acids along the sequence, but also on the level of supramolecular packing that can effectively mask sensitive peptide bonds from hydrolytic enzymes.[60] These hydrogels are also reversible, so that simple triggers such as variations of temperature or pH could be used to switch back and forth between assembled and disassembled states, as shown for instance in *Figure 1.4*.[56,57]

1.3.2 Amyloid peptides for self-assembly

As described above, diphenylalanine is one of the most popular self-assembling motifs and it was identified by Reches and Gazit through a reductionist approach from the Aβ sequence. The study searched for the minimalist sequence of the peptide involved in Alzheimer's disease that displayed a strong tendency towards self-assembly into amyloid fibrils.[47] Indeed, the vast majority of self-assembling ultrashort peptides have a certain amyloid character, defined in terms of supramolecular organization in the so-called cross-beta pattern, and with characteristic fibril nanomorphology and ability to bind amyloid markers, such as Congo Red (leading to birefringence) or Thioflavin T (leading to fluorescence).[61,62] However, there is no straightforward correlation between amino acid sequence and amyloid character. In any case, the strong link between naturally-occuring amyloids and designed self-assembling materials has been long recognized.[63] Attractive amyloid features lie on the ability to recruit many units of the same protein so that even a weak biological activity can transform in a potent one through repetition and avidity.[64] Additionally, amyloids can self-replicate and evolve over time. On one hand, this property is interesting for the development of smart and dynamic materials; on the other, it relates to pathological aspects of infectivity and toxicity.[64]

According to the official definition of amyloid, 36 amyloid proteins have been found in humans, of which 14 are strictly associated with systemic amyloidoses, 19 occur only locally, and 3 are found in both.[65] Traditionally, amyloids have been associated to pathological states and this fact calls for caution when the intent is to use amyloid peptides for biological applications. However, in recent times, scientists have challenged this paradigm, since an increasing number of functional, non-pathological amyloids

have been found also in humans.[66,67] Understanding how functional amyloids avoid toxicity (*Figure 1.6*) can provide useful elements for the design of amyloid-inspired bioactive materials.[68]

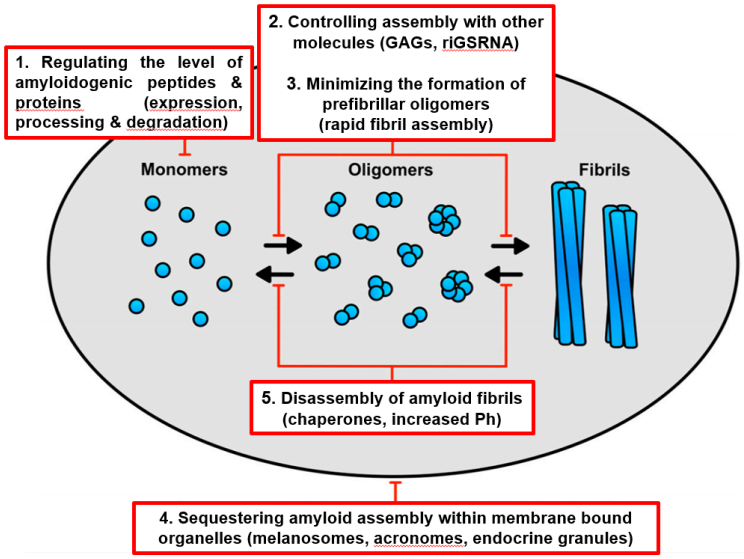

Figure 1.6 Mechanisms employed in nature to avoid functional amyloid toxicity. Reproduced with permission from ref. 68 © 2017 MDPI.

1.4. Amyloids and antimicrobial agents

1.4.1 Functional amyloids in microbes

As described above, the amyloid state was traditionally viewed as a consequence of protein misfolding and aggregation and it is most notorious for its association with human diseases. However, a growing list of examples of "functional amyloids" challenges this bad reputation. In fact, many organisms can employ the biophysical properties of amyloid for their benefit.[69] Interestingly, microbes are amongst such organisms (*Figure 1.7*). For instance, amyloids fulfill important microbial functions, including structure in biofilms and in the cell wall of bacterial spores, or host binding for subsequent internalization, such as the case of adhesins.[70] In addition, a recent study carried out by Seviour and co-workers established the specific binding affinity of quorum-sensing molecules to functional amyloids, which are important for cell signaling within biofilms.[67] Biofilms are communities of bacteria encased in an extracellular matrix of proteins and polysaccharides, and in many of them, amyloids are the major proteinaceous component. Within biofilms, amyloid fibers are well suited for the role of protein scaffolds, they are effective on promoting adherence, and even resistance to a variety of environmental insults.[71] It is thus not surprising that inhibitors of amyloid aggregation, such as natural polyphenols, are being studied also to target biofilm formation.[72]

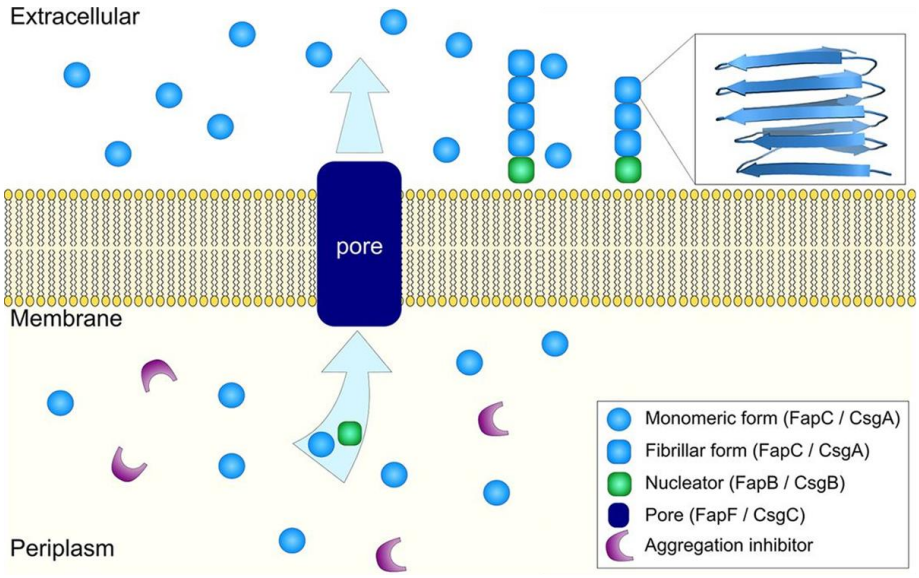

Figure 1.7 Schematic mechanism of the formation of fibrils for functional bacterial amyloids in vivo with common components for *P. fluorescens* and *E. coli*.
Adapted with permission from ref.73[73] © 2019 American Society for Microbiology

1.4.2 Amyloid Aβ as antimicrobial peptide

A recent investigation has provided data supporting an *in vivo* function for Aβ as an antimicrobial peptide. The experiments carried out reveal that Aβ exerts antimicrobial activity against eight clinically relevant microorganisms with a potency analogous to, or in some cases even higher than, LL-37, an archetypal human antimicrobial peptide.[74] Besides bacteria and fungi, also viruses can be effectively targeted by Aβ peptides.[75,36,74] These findings, together with the observation that Aβ is highly conserved across vertebrates suggest that it may act as important and natural defense against microbial infections.[76,77] Evidence in this direction has been recently reviewed.[78]. As a result of these investigations, the traditional "amyloid cascade hypothesis", which sees exclusively a pathological role for Aβ, has been challenged with new theories that call for a role for infections in Alzheimer's disease, and possibly a dysregulation of the innate immune response.[79]

1.5. Ultrashort peptides as antimicrobial agents

Self-assembling ultrashort peptides designed to form nanoarchitectures and even (nanostructured) macroscopic hydrogels hold great potential as novel antimicrobial materials.[4] They can also be envisaged as vehicles to work in synergy with antibiotics or antibacterial agents, including nanoparticles.[80,81] The latter can also be formed *in situ* by including a metal-coordinating motif in the peptide sequence, thus yielding an antibacterial metallogel.[81] As mentioned above potential triggers for enhance inherently self-assembling gel formation for antimicrobial activity might include pH, ionic strength, temperature, light and microbial enzymes.

1.5.1. Self-assembly activation *via* pH and ionic strength

Charge interactions are essential factors in self-assembly, and they are related to the pKa of the peptide ionisable groups. Moreover, salts may play an important role by screening charges or mediating ionic interactions. Recent research of Liu's group introduced the rational design of pH-dependent antimicrobial peptide self-assembly of two peripheral $(KIGAKI)_3$-NH_2 parts conjugated to both ends of a tetrapeptide linker.[82] RADA16 is a well-studied self-assembled peptide with antimicrobial activity at physiological conditions that also supports cell growth and enhances wound healing.[83] Another example of self-assembling peptide is MAX1 peptide (VKVKVKVKV^{D}PPTKVKVKVKV-NH_2) developed by Schneider group that forms supramolecular structures at alkaline pH. MAX1 adopts a β-sheet secondary structure and the central part V^{D}PPT forms a β-turn, resulting in an overall hairpin conformation that displays a hydrophobic core and a hydrophilic cationic lysine-rich portion. The polycationic surface of this peptide is selective for negatively charged bacterial membranes causing in this way leakage of the bacterial cell, and consequent bacterial death (*Figure 1.8*). The use of pH triggered self-assembly has good potential applicability in antimicrobial therapies. For example, in urinary catheter associated infections, the pH increases due to presence of the urease enzyme synthetised by Gram negative *Protens mirabilis*; if the peptide self-assembled at this alkaline conditions, it could work as a protective barrier and also avoid the need for catheter removal.[84]

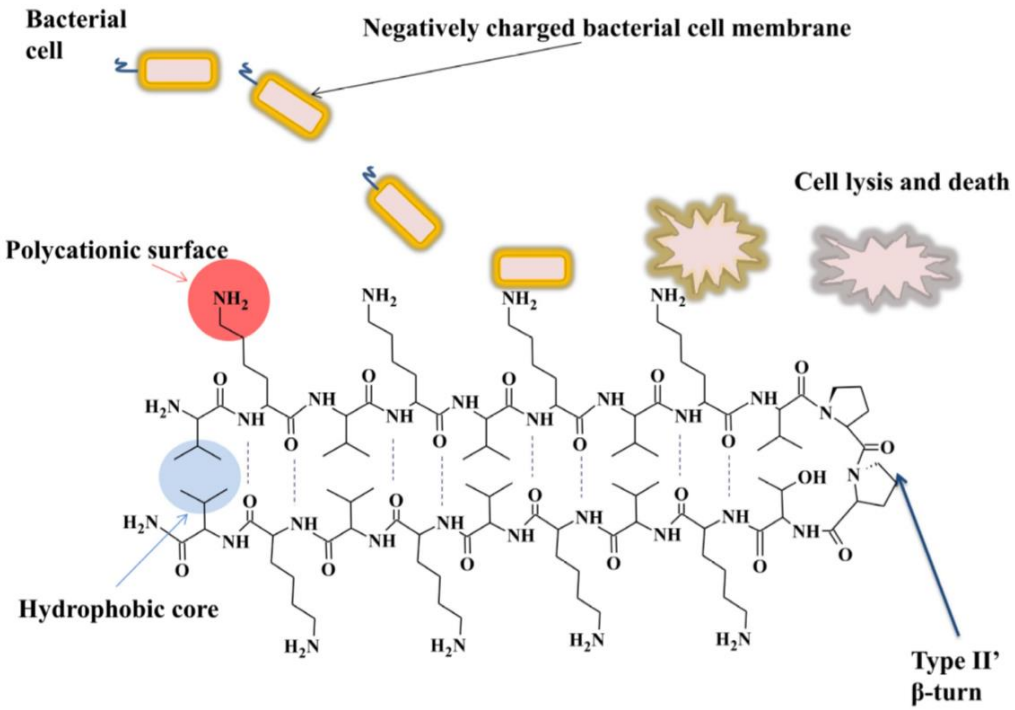

Figure 1.8 The antimicrobial mechanism of action of self-assembling β-sheet forming MAX1 peptide. Reproduced with permission from ref.84 © 2014 MDPI

1.5.2. Photo-activation of self-assembly

In this type of activation, self-assembly starts when a cytocompatibile photo-initiator and a peptide are exposed to a specific wavelength. McCoy developed an antimicrobial material based on tetracationic porphyrin that, thanks to visible-light activation, generates short-lived singlet oxygen at the device surface, thus resulting in antimicrobial activity.[83] Kim and co-workers developed the photosensitizer-peptide conjugate that is composed of eosin and the amphiphilic sequence $(KLAKLAK)_2$; upon irradiation with visible light, this conjugate kills a broad spectrum of bacteria, with no observable cytotoxicity to human cells.[85] Another example is reported by Haines *et al.* that describe MAX-series peptides that are able to self-assemble into a hydrogel after UV irradiation, although they did not investigate if the peptide retains antimicrobial activity after exposure to light.

1.5.3 Thermo-responsive self-assembling peptides

The use of temperature to trigger peptide self-assembly usually is simply based on the hydrophobicity of the molecule.[86] Self-assembling and thermo-responsive peptide systems are reported in different studies.[57,82,84,87,88] Interestingly, it was reported that, depending on the stereoconfiguration, hence the

position of D-amino acids along the sequence, uncapped tripeptide isomers could self-assemble with a higher or lower level of supramolecular order, thus resulting in peptides with different thermoresistance.[60,89] In particular, while ^{D}VFF hydrogels disassemble at temperatures higher than ca. 60 °C, V^{D}FF hydrogels disassemble at temperatures close to the physiological range (ca. 35-40 °C), thus opening opportunities for the thermoregulation of assembly/disassembly for biomedical applications.[60]

1.5.4 Bacterial Enzymatic Self-Assembling process

Enzyme-mediated self-assembly affects the peptide primary sequence and has the advantage to occur at physiological conditions.[90] For instance, Ulijn's group demonstrated enzymatic self-assembly of ultrashort peptides by alkaline phosphatase.[91] In this system, alkaline phospathase facilitates the removal of the phosphate group from a Tyr side-chain, so that the resulting product is more hydrophobic and can effectively self-assemble.[91] Other enzyme triggers can be, for instance, esterases such as subtilisin, which acts on a Fmoc-dipeptide methyl ester to allow self-assembly.[92]

1.6 Future perspectives of ultrashort peptides as supramolecular antimicrobials

As mentioned above, the rapid development of peptide based nanoassemblies offers new approaches for biomedical materials advancement. We can distinguish different chemical classes of peptide gelators, of which numerous examples have been described in the literature and principal problems with peptide designed are high cost and susceptibility to protease degradation.[58] However, if we restrict the focus to small molecules featuring up to three amino acids, with assembling ability and antimicrobial properties, then the list of examples reduces drastically. In particular, we can distinguish lipopeptides, Fmoc-amino acids and Fmoc-peptides, and unprotected peptides, as described below.

1.6.1. Lipopeptides

Das and collaborators reported a series of gelling cationic dipeptide amphiphiles (*Figure 1.9*) that showed remarkably low minimum inhibitory concentrations (MICs) in solution against the growth of both *Gram positive* and *Gram-negative* bacteria. Despite the cationic character, no cytotoxicity was observed against mammalian cells *in vitro*.[80]

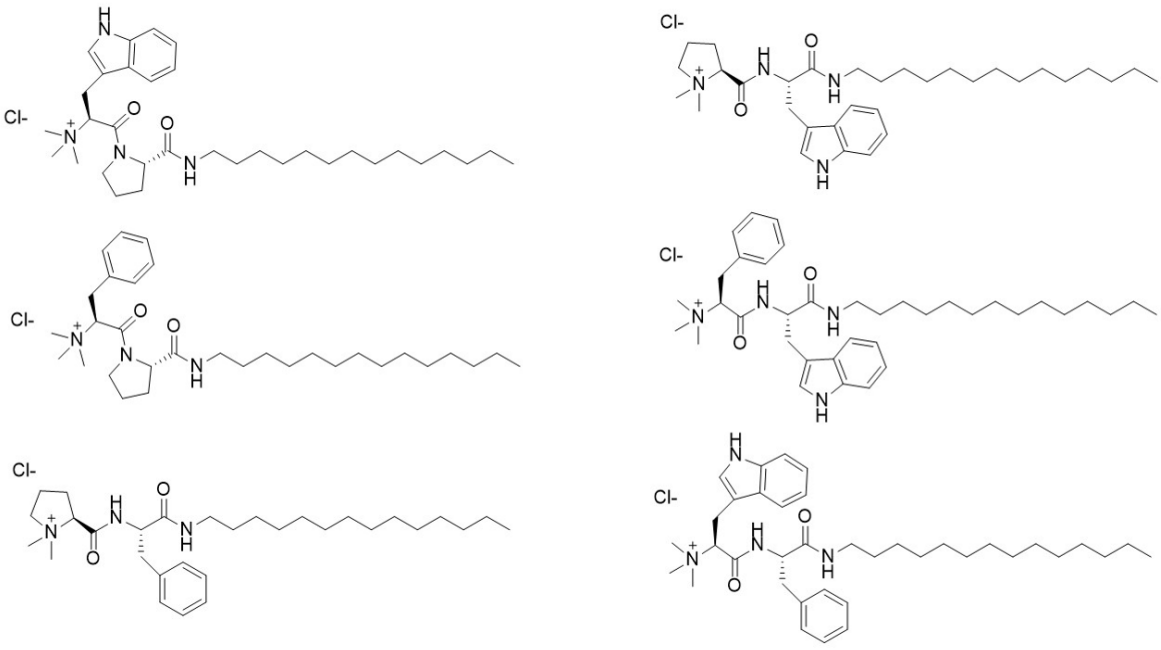

Figure 1.9 Gelling cationic dipeptide amphiphils with antibacterial activity
Reported with permission from Ref.90 © (2004) Elsevier Ltd.

More recently, diphenylalanine conjugated at the N-terminus with a long aliphatic chain was reported to effectively self-assemble into a hydrogel at physiological conditions and display antimicrobial activity against *Gram negative* strains, namely *E. coli* and *P.aeruginosa*.[93] Interestingly, substitution of one phenylalanine with phenylglycine hindered gelation and had a negative impact on the antimicrobial activity observed.[93]

1.6.2 Fmoc-peptides

Fmoc-Phe displayed antibacterial activity against *Gram positive* bacteria including methicillin-resistant *Staphylococcus aureus* (MRSA), both in solution and hydrogel phase.[94] The bactericidal activity was noted also at concentrations equal to, or above, the critical micelle concentration, while bacterial growth was inhibited also at lower amounts.[94] It was inferred that the hydrogel exerted activity mainly through the release of Fmoc-Phe in solution, which acted as a surfactant.[94]

Das and co-workers have also demonstrated that cationic derivatives of Fmoc-Phe, Fmoc-Phe-Phe, and similar analogues, modified at the C-terminus with a pyridinium moiety, displayed antibacterial activity in solution against *Gram positive* and *Gram negative* strains.[95] At higher concentrations, these compounds were also capable of self-organization into supramolecular hydrogels, giving scope for their use as bioactive soft materials.[95]

Fmoc-Phe could also co-assemble with Fmoc-Leu to form a *Gram-positive* selective bactericidal hydrogel that did not elicit mammalian cell cytotoxicity, giving scope for its use as active coating for sanitation in clinical settings.[96] Fluorination of the benzene unit of Fmoc-Phe to the pentafluoro-derivative also proved to be an effective strategy to obtain antibacterial composites when combined with a resin material.[97]

1.6.3 Unprotected peptides

Despite the fact that the discovery of diphenylalanine self-assembly dates back to 2003, only in 2017 it was shown to be able to disrupt bacteria cell membranes in its self-assembled form.[98] Unfortunately, the fibrils did not yield stable hydrogels on their own, but can be incorporated into hydrogels to confer them with antibacterial properties.[48,49,9797,98]

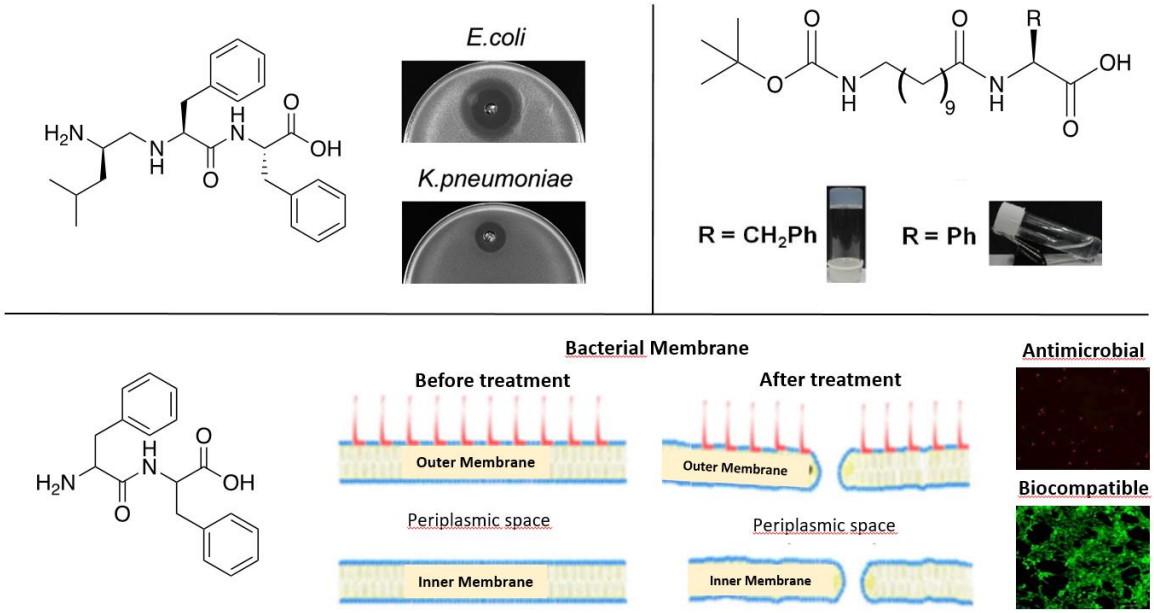

Figure 1.10 Ultrashort unprotected self-assembling antimicrobial peptides.
Adapted with permission from Ref.91, 93, 98

Simple addition of a third amino acid to yield a D,L-heterochiral sequence is sufficient to obtain a supramolecular hydrogel at physiological conditions.[99] This hydrogel demonstrated mild antibacterial activity against *Gram negative* strains, including a clinical isolate.[100] Importantly, this activity could synergize with that of antibiotics, if they participate in the supramolecular organization of the hydrogel for sustained release.[100] This approach could be highly attractive for the prolonged delivery of poorly

soluble drugs, and could be extended to anti-inflammatory molecules for a combined therapy, or even to fluorescent dyes for theranostics.[101,102] Unfortunately, achieving co-assembly between this hydrogelator and drug molecules is far from trivial, and rather difficult to predict based solely on chemical structures.[103] Indeed, the ability of multiple small molecules to participate together in the formation of co-assembled or self-sorted supramolecular hydrogels is a research area that has attracted wide interest amongst chemists.[104,105]

2. AIM OF THE PROJECT

The research areas of antimicrobial peptides and supramolecular hydrogels are fast-moving fields that recently have shown common traits. Knowledge transfer between them has the potential to accelerate progress towards the development of smart supramolecular systems for innovative therapeutic solutions. Considering the worldwide emergency we face in terms of spreading of antimicrobial resistance to antibiotics, we cannot afford to miss the research advancement opportunities that lie at the interface between these areas. The Holy Grail is now the development of smart systems that acquire potent antibacterial activity through self-assembly only when and where needed, to then disassemble into inactive and biodegradable components that are innocuous for the environment and the ecosystems.

To this end, the aim of this project is to get the first insights towards the structure-activity relationship that can provide important guidelines for the design of biocompatible peptide hydrogels with antimicrobial activity. The work will focus on the synthesis and characterisation of different heterochiral short-peptide sequences to be tested as antimicrobial agents, based on the previous identification of the tripeptide ^{D}Leu-^{L}Phe-^{L}Phe as mild antimicrobic compound against Gram negative bacteria. This tripeptide will be considered the *"hit compound"* onto which a series of modifications will be carried out to build a small library of approximately 20 peptides. In particular, such modifications will have the aim to study the consequences of 1) different peptide stereoconfiguration, 2) scrambled sequences, 3) aliphatic side chain elongation or branching, and 4) halogenation. Peptides will be synthesised by solid-phase, purified by reverse-phase HPLC, and characterised by a number of spectroscopic methods as well as single crystal XRD. Their self-assembly into hydrogels at physiological conditions will be assessed, and the supramolecular systems will be characterised by a number of spectroscopic and microscopic technique. Next, the antimicrobial activity *in vitro* against *E.coli* cultures will be tested. Moreover, additional biological tests will include cytotoxicity on human red cells as well stability towards enzymatic degradation.

Important questions to answer are 1) whether any antimicrobial activity is obtained, and ideally improved relative to the hit compound, 2) whether the activity is present at the non-assembled state to use self-assembly as a trigger to switch-on bioactivity, 3) whether enantiomers show analogous effects, confirming the hypothesis that no receptor is involved in the activity and 4) whether it is possible to gain insights into the structure-activity relationship of these novel systems.

3. RESULTS AND DISCUSSION

3.1. Peptide rational design

This project started with the synthesis and characterisation of ^{D}Leu-^{L}Phe-^{L}Phe (**1)** to confirm its antimicrobial activity as previously reported.[100] Next, a library of peptides were designed for self-assembly to allow the assessment of various structural modifications (*Table 3.1*) to get the first insights into the structure-activity relationship:

1. Different peptide stereoconfigurations (*i.e.*, DLL, LDD, LLL, LDL, DLD)
2. Presence of different aliphatic side chains (*i.e.,* Xaa-Phe-Phe, Xaa=Leu, Ile, Nle, Val)
3. Scrambled sequences (*i.e.*, Phe-Xaa-Phe, Xaa= Leu, Ile, Nle)
4. Effect of halogenation on peptide sequences *(i.e.,* R_1, R_2 = H, F, I)

In particular, the specific choice of stereoconfiguration and amino acid sequence was based on recent findings from previous studies, from which simple rules towards self-assembling sequences started to emerge, exploiting the diphenylalanine motif for self-assembly.[50,106,107] Halogenation was introduced because it was reported to favour self-assembly, also by means of halogen bonding.[108,109]

In particular, the library of peptides was selected to evaluate a number of factors on self-assembly and antimicrobial activity. First of all, the enantiomer of **1,** *i.e.,* **2**, was prepared to assess whether the antimicrobial effect is receptor mediated (in which case **2** should be inactive) or simply physical, suchas in the case of membrane disruption as typically occurs for antimicrobial peptides and self-assembled Phe-Phe, in which case **2** should be as active as **1**.[98] Next the homochiral analogue **3** was chosen as control, due its inability to form a nanostructured hydrogel, thus to confirm whether the antimicrobial effect was due to the supramolecular organisation. Moreover, different structural modifications were evaluated (*Table 3.2*, *3.3* and *3.4*), such as different peptide stereoconfiguration, presence of different aliphatic side chains, scrambled sequences and finally effect of halogenation.

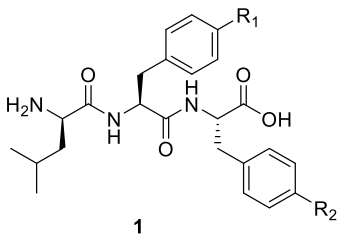

1

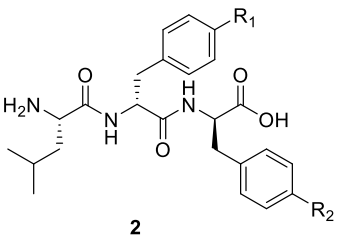

2

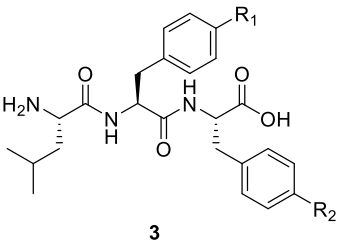

3

Xaa-Phe-Phe

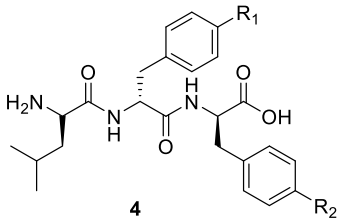

4

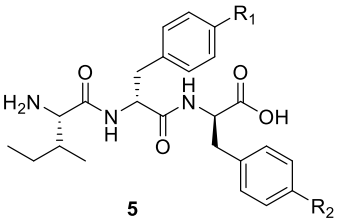

5

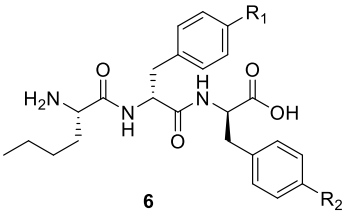

6

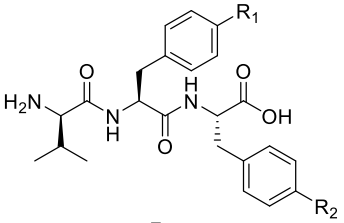

7

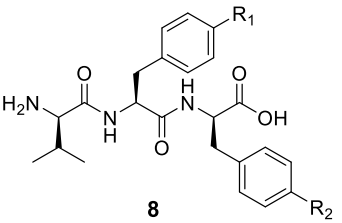

8

Phe-Xaa-Phe

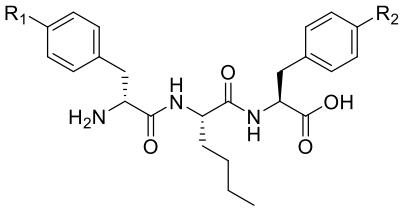

9

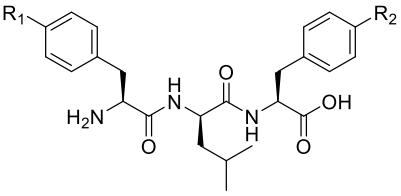

10

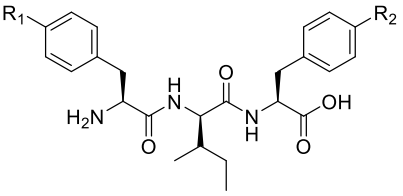

11

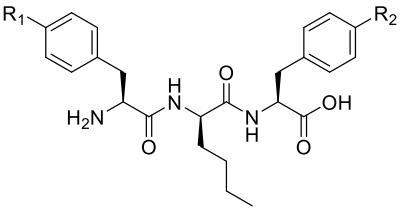

12

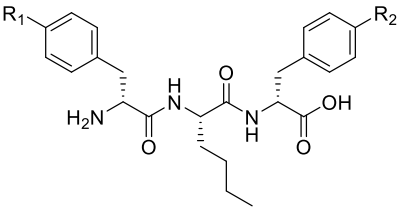

13

Table 3.1 Peptide library synthesised in this project. Compounds with R_1=R_2 =H are denominated ***a***; R_1 = I, R_2 = H ***b***; R_1=H, R_2=I ***c***, R_1=F, R_2=H ***d***; R_1=H, R_2=F ***e*** and R_1=I, R_2=F ***f*** (see Table 3.2, 3.3. and 3.4).

Effect of Chirality

Sequence	Compound name	Chirality	R1	R2
Leu-Phe-Phe	**1a**	**D**LL	H	H
	2a	L**DD**		
	3a	LLL		
	4c	**DDD**	H	I
Val-Phe-Phe	**7a**	**D**LL	H	H
	8a	**D**L**D**		
Phe-Nle-Phe	**9c**	**D**LL	H	I
	13c	**D**L**D**		

Table 3.2 Effect of chirality on self-assembly and antimicrobial activity.

Effect of Amino Acid Side Chain

Sequence	Compound name	Chirality	R1	R2
Leu-**Phe-Phe**	**2a**	L**DD**	H	H
Ile-**Phe-Phe**	**5a**			
Nle-**Phe-Phe**	**6a**			
Val-Phe-Phe	**7a**	**D**LL		
Phe-**Leu**-Phe	**10a**	L**D**L		
Phe-**Ile**-Phe	**11a**			
Phe-**Nle**-Phe	**12a**			

Table 3.3 Effect of aa side chain on self-assembly and antimicrobial activity.

Effect of Halogenation

Sequence	Compound name	Chirality	R1	R2
Leu-**Phe**-**Phe**	**2b**	L**DD**	**I**	H
	2d		**F**	H
	2e		H	**F**
	2f		**I**	**F**
Phe-Nle-**Phe**	**13b**	**D**L**D**	**I**	H
	13c		H	**I**
	13d		**F**	H
	13e		**H**	**F**
	13f		**I**	**F**

Table 3.4 Effect of halogenation on self-assembly and antimicrobial activity.

3.1.1. Peptide synthesis

All peptides (*Table 3.1*) were synthesised according to standard Fmoc-based solid phase peptide synthesis (SPPS) *via* *O*-(benzotriazol-1-yl)-*N,N,N′,N′*-tetramethyluronium hexafluorophosphate (HBTU) and with 1-hydroxy-7-azabenzotriazole (HOAt) activation, using 2- 2-chlorotrityl chloride resin as solid support. Reactions were performed in a sintered funnel with continuous stirring since the forming-peptide is anchored to the resin. After the loading of the first amino acid and the following deprotection of the Fmoc-group at the N-terminus, coupling reactions of two more amino acids were performed, each of them followed by protecting group removal. The completion of each synthetic step was monitored by two colorimetric tests: acetaldehyde/chloranil and bromophenol blue tests. The tripeptide was next cleaved from the resin by using a mixture of trifluoroacetic acid and dichloromethane *Figure 3.1*). Crude peptides were too hydrophobic to be precipitated in cold ether, thus the majority of TFA was evaporated under air flow, and the remaining oil was dissolved in a mixture of acetonitrile/water and purified by reverse-phase HPLC. Compounds were then freeze-dried to yield the corresponding peptide as a white solid, in a yield of 80-100%.

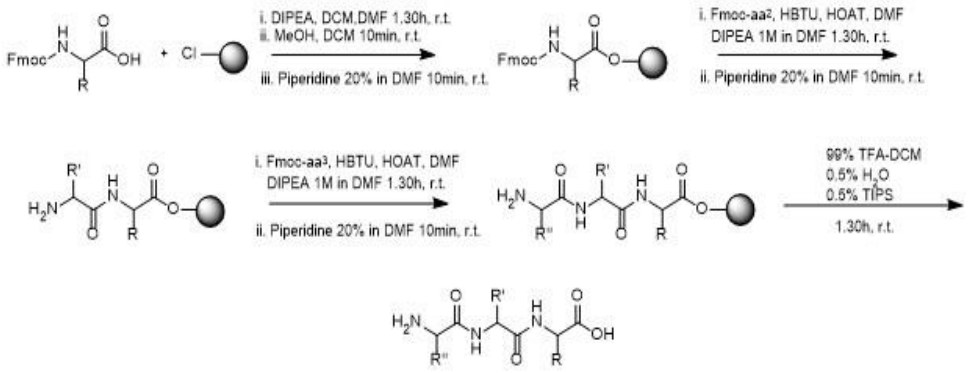

Figure 3.2 General scheme of solid-phase peptide-synthesis.

3.1.3. Peptide characterisation

All peptides were characterised using ^{1}H-NMR, and LC-MS analyses. A typical ^{1}H-NMR peptide spectrum presented specific regions of interest at different ppm values. At low fields, it was possible to identify the signals of amine protons of the N-terminus and protons of amide bonds (~8-9 ppm) and aromatic protons (~7-7.5 ppm), followed by the signals of the hydrogen atoms bound to α-carbon atoms (3-5 ppm), while at higher fields, the signals of hydrogen atoms bound to β, γ, and δ carbon

atoms were detected. LC-MS spectra confirmed compounds purity and their molecular ion peak (all spectra and details are provided in Chapter 6 – Appendix).

3.2. Peptide self-assembly

Peptide self-assembly into hydrogels requires a correct interaction between peptide molecules and between peptides and water, which occurs through a fine balance between hydrophilic and hydrophobic components.[56] It is worth noting that hydrogelation of unprotected tripeptides is really difficult to predict.[45] Indeed, as mentioned in the introduction, usually a popular alternative involves the use of protecting aromatic moieties that easily stack, although they may lead to cytotoxicity and require the use of organic solvents for their dissolution.[54] Therefore, for biological applications it is preferable to avoid such moieties, and self-assembly in this case can be achieved based on appropriate use of both chirality amino acids in a tripeptide sequence.[106,107] Moreover the use of fluorine or iodine can help self-assembly.[108,109] The presence of D- and L-amino acids in the same peptide structure can avoid above mentioned problems and can give us also other advantages, such as higher proteases resistance of compounds containing non-natural amino acids and the possibility to obtain different biological activity if compared to homochiral peptides.[59]

3.2.1. Hydrogel preparation and minimum gelling concentration (mgc)

The protocol for hydrogelation used in this work was already reported and it is based on peptide dissolution in phosphate buffer at alkaline pH thanks to repulsion between negatively charged peptide molecules, followed by a pH trigger to neutral, at which the zwitterionic form of peptides start to self-assemble.[99] Typically, gelation starts with nucleation of zwitterionic molecules that, after sometime, depending on peptide structure and experimental conditions proceeds towards formation of fibrils/fibres that ultimately entangle in a network that composes a macroscopic hydrogel (*Figure 3.2*) The lowest concentration of peptide at which we can observe a stable hydrogel (MGC) generally depends on peptide structure and experimental conditions. In this work, most peptides rapidly form supramolecular hydrogels and their mgc is reported in *Table 3.5*.

Mgc is determined by a combination of factors, including peptide hydrophobicity (as measured by logP and/or HPLC retention times reported in *Table 3.5*), stereoconfiguration, etc. In this case, despite the general similarity across the peptides composing the library, a general trend between

hydrophobicity and mgc was not found. Halogenation appeared to increase peptide hydrophobicity at the expense of solubility, since peptides **2d**, **2e** and **2f** particularly difficult to dissolve, as they required use of ultrasonication for up to 1 hour and/or prolonged heating up to 80°C.

Importantly, it was possible to confirm how heterochirality of the selected peptide sequences was a key factor for supramolecular hydrogelation of ultrashort peptides, as demonstrated previously.[107] The peptides containing only L-amino acids **3a** and iodinated **4c** did not lead to stable gels. While **3a** precipitated, **4c** formed a transient hydrogel which after 20 h converted into crystals, suggesting the former was a kinetic product, and the latter the thermodynamic product.[110] Furthermore, the presence of fluorine in **2d** hindered hydrogelation, and increasing the peptide concentration led to precipitation. By contrast, the presence of iodine at the same position in **2c** led to immediate hydrogelation, thus indicating a complex combination of factors influencing peptide self-assembly. This is not too surprising since self-assembly is a cooperative process through which subtle variations are amplified in an often-unpredictable manner.

A

Compound name	Log P	HPLC R_T (min)	MGC (mM)
1a	2.37	7.9	5.0
2a	2.37	7.9	5.0
3a	2.37	7.5	✕
4c	3.73	9.0	5.0 t.g.*
7a	2.03	8.2	20.0
8a	2.62	7.9	24.0
9c	2.62	9.6	5.0
13c	2.62	9.1	7.5

B

Compound name	Log P	HPLC R_T (min)	MGC (mM)
2a	2.37	7.9	5.0
5a	2.44	8.2	10.5
6a	2.46	8.9	8.0
7a	2.03	8.2	20.0
10a	2.37	8.4	5.0
11a	2.44	8.3	8.0
12a	2.46	8.4	5.0

C

Compound name	LogP	HPLC R_T (min)	MGC (mM)
2b	3.73	8.5	5.0
2d	2.53	8.7	✕
2e	2.53	8.9	15.0
2f	3.89	9.6	15.0
13b	3.82	8.8	7.5
13c	3.82	8.8	7.5
13d	2.62	8.5	7.5
13e	2.62	8.3	7.5
13f	3.98	9.9	2.5

Tables 3.5 A,B,C LogP, HPLC R_T and Minimum gelling concentration (MGC) of peptides
t.g.* = transition of gel in crystals (in 20-24 hours), ✕ not gelling peptide

3.2.2. Tube inversion test, gel reversibility and melting temperature determination

The tube inversion test was used as a quick method to assess peptide gelation, which is approximately related to the fact that a solid that withstands gravity can be seen (*Figure 3.3)*. Photographs of non-gelling peptides **3a** and **1d** are reported in the Appendix.

Effect of chirality

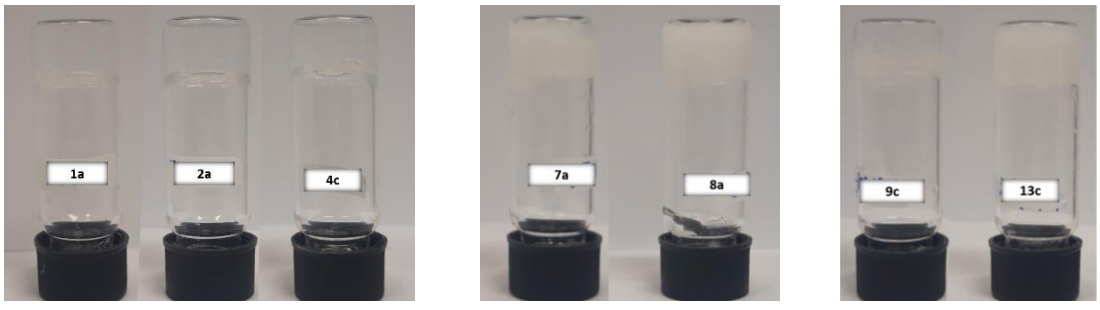

Effect of aa sequence

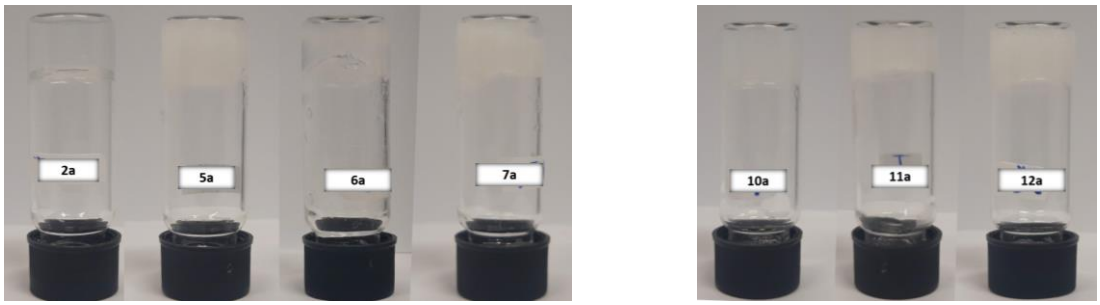

Effect of halogenation

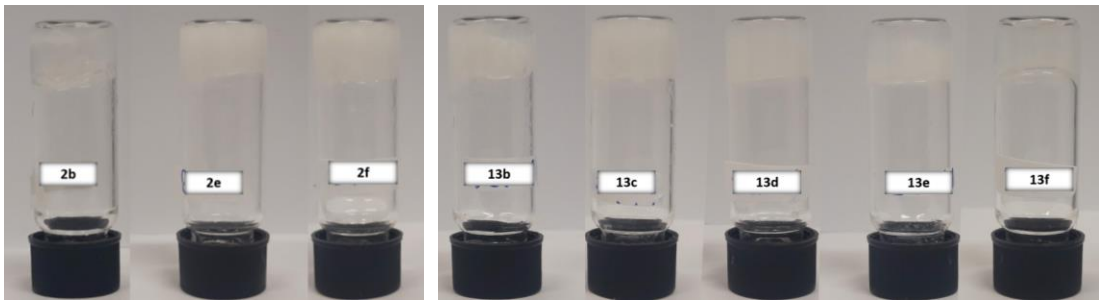

Figure 3.3 Tube inversion test for gelling peptides.

One of the advantages of supramolecular hydrogels is the possibility to form smart systems that can be assembled/disassembled *on demand*. To this end, we evaluated the reversibility of gel disassembly by heating up to the melting temperature (Tm), followed by cooling to room temperature (T*able 3.6 A-C).* The gel-to-sol transition implies the loss of the 3D network that forms the gel matrix, and not necessarily the complete loss of the fibril nanostructure. However, the observed transition is compatible with amyloid fibril melting and the loss of the amyloid nanostructure, as reported by several others and recently reviewed.[60,111] Interestingly, disassembly was reversible for all peptides, except for those with amino acid sequence corresponding to Leu-Phe-Phe, regardless of stereoconfiguration and halogenation, which thus do not give the scope to assemble/disassemble the gel to switch on/off antimicrobial activity *on demand.* Moreover, the thermal behaviour of enantiomers was similar, as expected in achiral environments, and for DLL and DLD stereoisomers, the former displayed higher thermoresistance, in agreement with previous studies on similar sequences.[60] At the tested conditions, the lowest Tms were found for **4c** (38-46 °C) and **8a** (42-55 °C). In all the other cases, a higher Tm in the range of 65-80 °C was found, as typically observed for amyloids.[111] Halogenation did not appear to influence gel thermostability.

A

Compound name	Tm (°C)		Reversibility
	S	D	
1a	55	80	✗
2a	60	80	✗
4c	42	55	✗
7a	54	70	✓
8a	38	46	✓
9c	60	70	✓
13c	56	68	✓

B

Compound name	Tm (°C)		Reversibility
	S	D	
2a	60	80	✗
5a	50	74	✓
6a	72	81	✓
7a	54	70	✓
10a	53	65	✓
11a	58	70	✓
12a	51	65	✓

C

Compound name	Tm (°C)		Reversibility
	S	D	
2b	60	70	✗
2e	70	75	✗
2f	70	80	✗
13b	55	77	✓
13c	50	60	✓
13d	50	75	✓
13e	45	65	✓
13f	50	65	✓

Tables 3.6 A,B,C Peptide hydrogels melting point Tm and reversibility
S temperature at which gel starts to lose water, **D** temperature of complete gel disruption.

3.2.3. Peptide hydrogel characterisation

3.2.3.1. Rheological properties

Oscillatory rheology is the technique of choice to assess the viscoelastic properties of a material and to confirm the hydrogel nature. At the gel point, the material changes from a viscoelastic liquid to a viscoelastic solid. In linear oscillatory rheometry, a sample material is subjected to a small oscillatory strain (or stress) (*1*) and the resulting response of the material is measured.

$$\gamma = A\sin(\omega t) \qquad (1)$$

From the material response, the complex shear modulus G* can be obtained and it can be separated into the fraction that is in-phase with the deformation and the part that is out-of-phase with the

deformation. These are generally represented in terms of the elastic G' and viscous G" shear moduli (*2*).

$$G' \propto \sin(\omega t), \quad G'' \propto \cos(\omega t), \quad G^* = \left(G'^2 + G''^2\right)^{1/2}, \quad \tan(\delta) = \frac{G''}{G'} \qquad (2)$$

As it is possible to observe from equation (2) the phase angle δ shows the relative importance of the liquid-like viscous modulus G" and the solid-like elastic modulus G'. For an elastic (solid) material, stress and strain are in phase, while for a viscous (fluid) material, stress and strain are out of phase, and when $0° < \delta < 90°$, the response is viscoelastic.

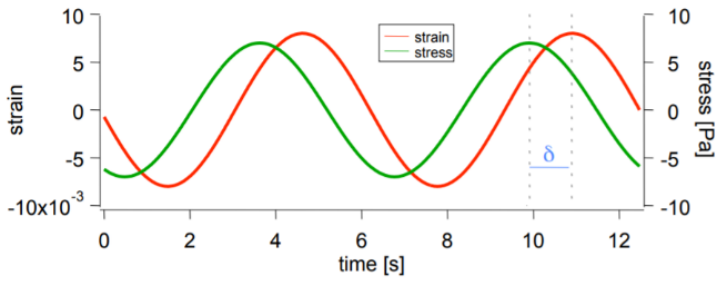

Figure 3.4 Oscillatory strain (or stress) and the resulting response of the material

Moreover, hydrogels typically present an elastic modulus G' higher in value (Pa) than the viscous modulus G". G' measures the sample elasticity and its ability to store energy, while G" measures the sample viscosity, hence its ability to dissipate energy as heat.[112] All studies performed in this work consist in measuring gelation kinetics over time, and gel stability across a range of applied frequencies and of increasing stress until a gel-to-sol transition occurs.

The measurements were performed at mgc and also at 5 mM (*i.e.*, the concentration at which most of the compounds were able to form a hydrogel) to allow a meaningful comparison across samples. Peptides **10a**, **11a**, **12a** were already reported to form supramolecular hydrogels at 5 mM, 8 mM and 5 mM respectively, and their rheological properties have been previously determined both at mgc and 5 mM.[56]

Leu-Phe-Phe enantiomers **1a** and **2a** display, as expected, analogous G' (1.3-1.6 kPa) that increases to 5-6 kPa with increasing the concentration to 15 mM. The homochiral analogue **3a** was confirmed not to gel, yet halogenation to **4c** resulted in the highest G' of the set (*Figure 3.6*).[99]

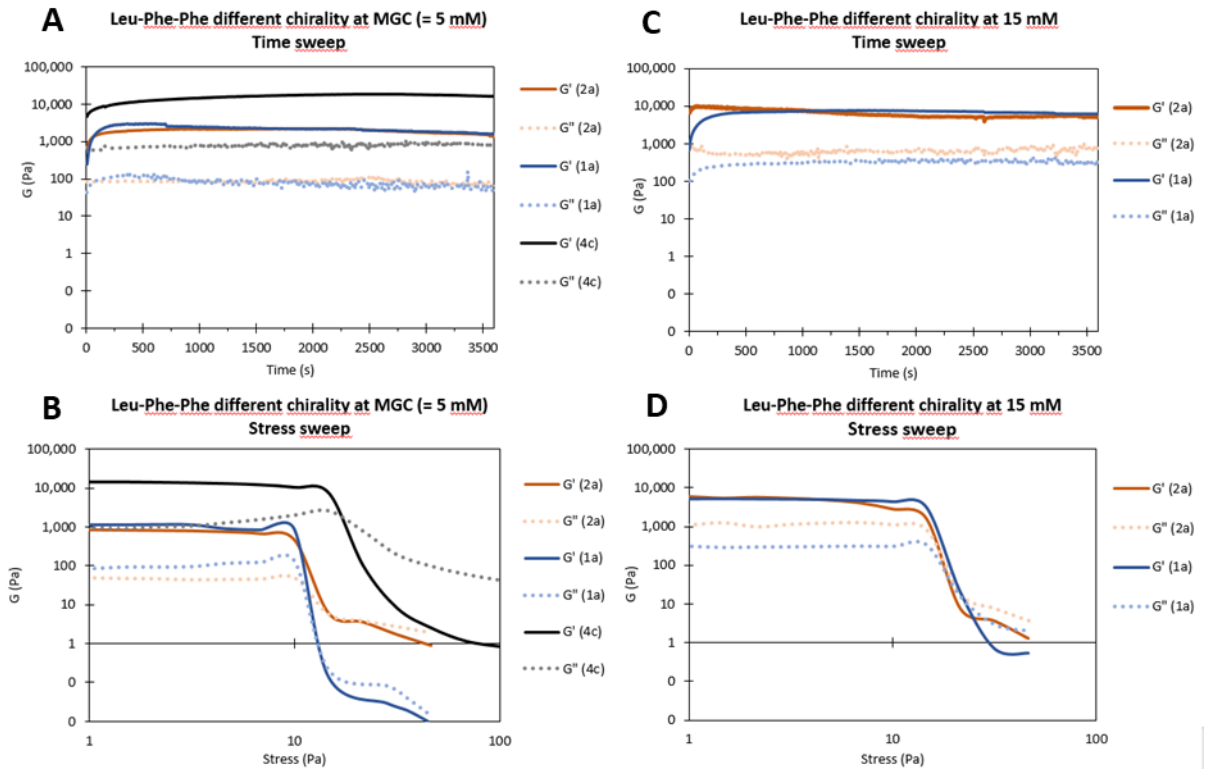

Figures 3.6 A-D Strain and stress sweep of Leu-Phe-Phe different chirality at MGC (= 5 mM) and at 15 mM.

Val-Phe-Phe peptide stereoisomers **7a** and **8a** were already reported to gel, but not analysed at 5mM, thus their gels were tested on the rheometer.[106] They are more hydrophilic than the other compounds containing Leu, Ile or Nle, and not surprisingly they display a higher mgc, since they do not gel at 5 mM. Both form stable hydrogels, with a high G' as well as high resistance to stress, especially for the DLL streoconfiguration relative to LDL (*Figure 3.7*). A similar trend was observed for compounds 9c and 13c, whereby the DLL streoconfiguration led to 1) lower mgc (analysed in *Figure 3.8A-B*), and, at 5 mM, 2) higher G' and 3) higher resistance to stress than the LDL stereoconfiguration.

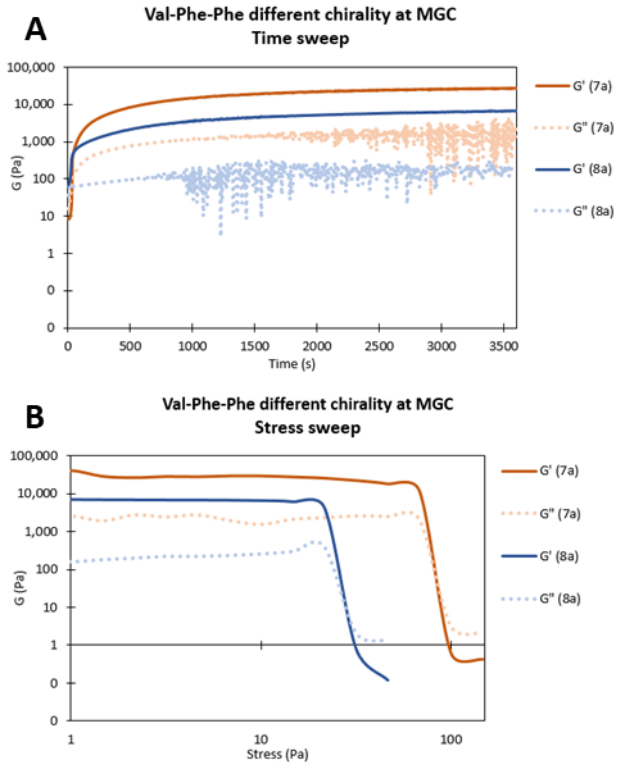

Figures 3.7 A-B Strain and stress sweep of Val-Phe-Phe different chirality at MGC

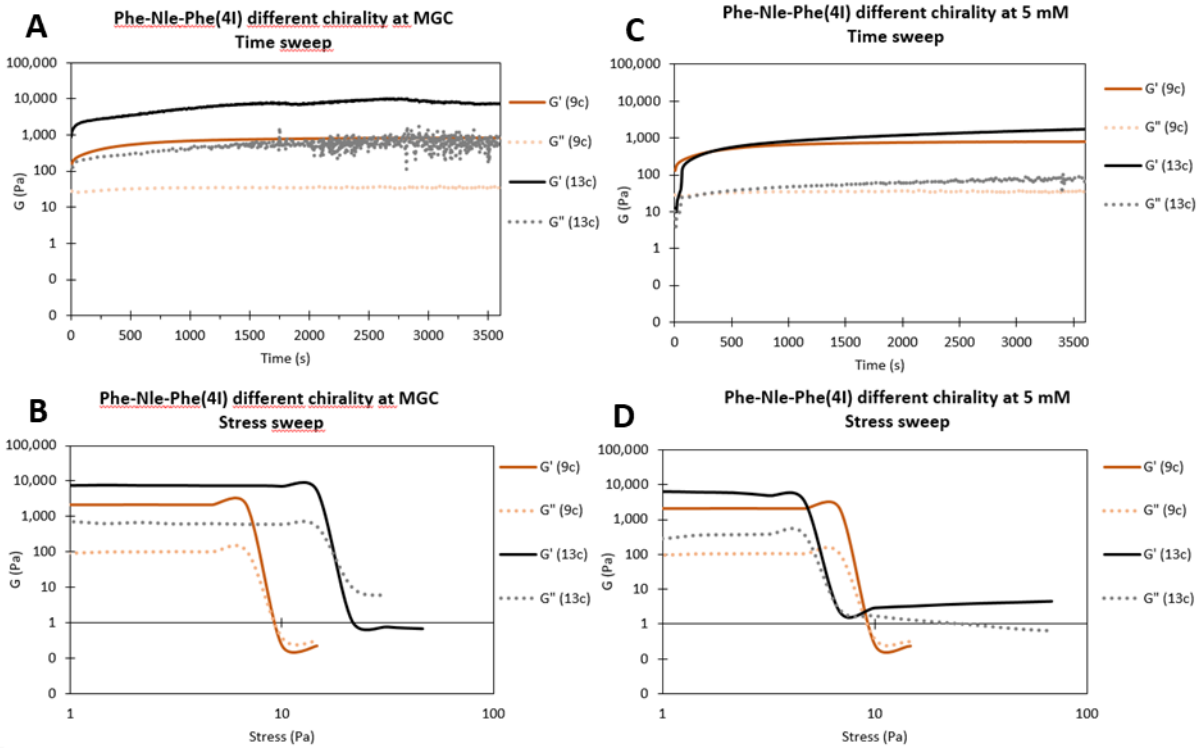

Figures 3.8 A-D Strain and stress sweep of Phe-Nle-Phe(4I) different chirality at MGC and at 5 mM

For Xaa-Phe-Phe sequences it was possible to observe that all compounds are forming a stable hydrogel with different viscoelastic properties that is not surprising due to the different mgc at which they were tested (*Figure 3.9A-B*). Moreover, only peptides containing Leu or Nle formed stable hydrogels at 5 mM (*Figure 3.9 C-D*).

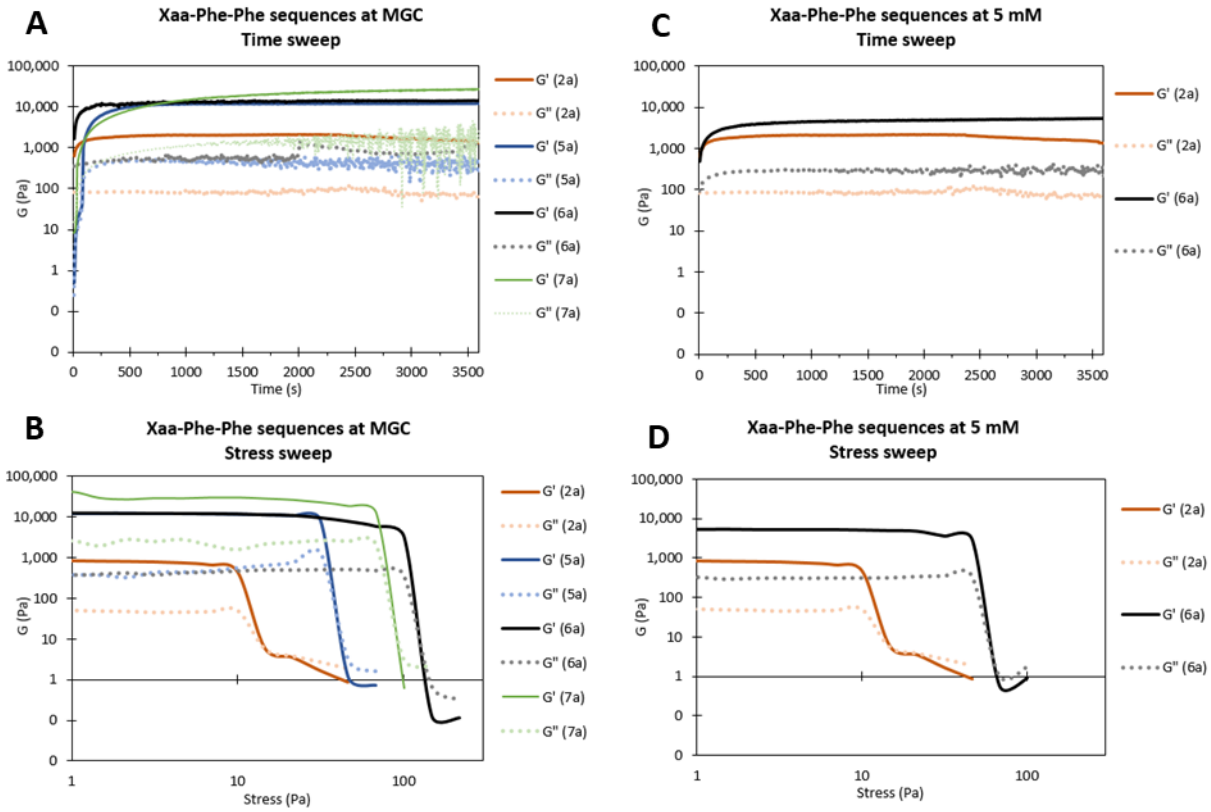

Figures 3.9 A-D Strain and stress sweep of Xaa-Phe-Phe peptides at MGC and at 5 Mm.

Halogenation of Leu-Phe-Phe (DLL or LDD) yielded peptides **2b-f**, which not only were more difficult to dissolve prior to self-assembly, but also displayed higher mgc than the parent compound **2a**. *Figure 3.10* reports only the analyses at mgc, which corresponds to 5 mM for **2b**, because the other compounds of this set did not gel at 5 mM. In general, we can conclude that for this set of peptides, halogenation did not favour self-assembly, with the extreme case of **2d** with a fluorine at the N-terminus that did not gel at all (*Table 3.5*).

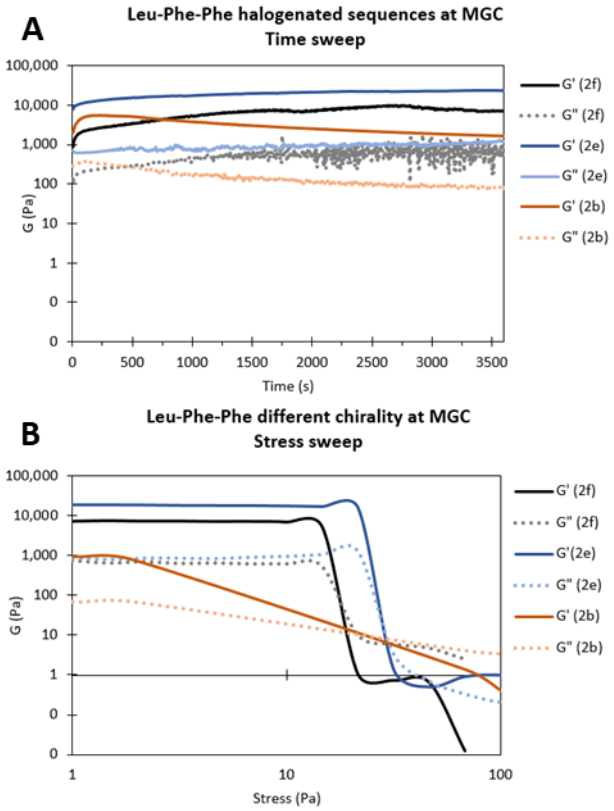

Figures 3.10 A-B Strain and stress sweep of Leu-Phe-Phe halogenated peptides at MGC.

Phe-Xaa-Phe peptides **10a**, **11a**, and **12a** were recently reported to gel at 5 mM, 8 mM, and 5 mM, respectively.[56] In the latter case, halogenation to **13b-f** did not favour self-assembly, since overall lower G' and lower resistance (than the non-halogenated parent compound **12a)** were noted as a result, with the extreme case of **13d**, which displayed a fluorine at the N-terminus, and which also displayed the slowest gelation kinetics (*Figure 3.11C*). Interestingly, monohalogenation to **13b-e** also increased mgc from 5 mM to 7.5 mM in all cases (*Table 3.5*), and in particular iodination at the N-terminus (as opposed to the C-terminus) and fluorination at the C-terminus (as opposed to the N-terminus) led to increased resistance against applied stress (*Figure 3.11D*). For this reason, both modifications were chosen for peptide **13f**, which did display the lowest mgc of 2.5 mM, but whose rheometric behaviour confirmed these effects were unfortunately not additive, once again highlighting the complexity of the self-assembly process (*Figure 3.11D*).

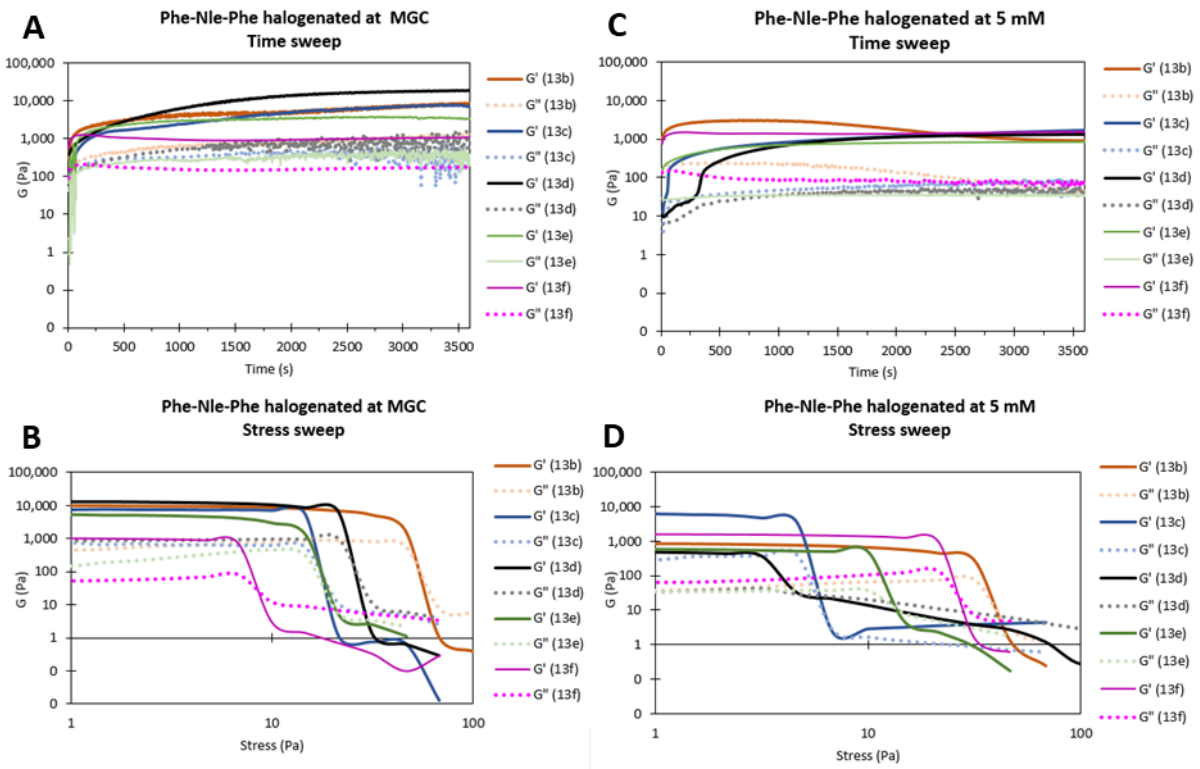

Figures 3.11 A-D Strain and stress sweep of Phe-Nle-Phe halogenated peptides at MGC and at 5 mM

3.2.3.2. Self-assembled nanostructure morphology assessed by TEM

Peptide nanostructured morphology was investigated by transmission electron microscopy (TEM) analysis (images were collected by Dr. Slavko Kralj, Jozef Stefan Institute, Ljubljana, Slovenia). TEM imaging uses high electrons (100-300 Kv) that are transmitted through the sample to form an image reproduced by apposite software. Hydrogel samples were pipetted onto a TEM support grid and subsequently examined after water evaporation. TEM imaging of nanostructures formed by organic molecules is very challenging due to sample decomposition during beam action. Peptides **10a**, **11a**, and **12a** were already reported, respectively, to form 11±2 nm-wide (**10a**) supramolecular fibreils that over time tend to bundle into stiffer fibres, 8±2 nm-wide fibrils (**11a**), and large bundles as thick as hundreds of nanometers(**12a)**, therefore they were not analysed in this work.[56]

The collected images and the size distribution of fibres are reported in *Figure 3.12.* Interestingly, Xaa-Phe-Phe sequences that display aliphatic amino acids without β-branching (*i.e.*, Leu, Nle) formed a dense network with high level of interconnectivity between fibres. On the contrary, presence of β-branched Ile led to the formation of thick and rigid bundles. This trend is exactly opposite as to what observed for Phe-Xaa-Phe peptides.[56] In addition, it is possible to observe that the presence of iodine in peptide sequences is associated with the formation of thinner supramolecular fibres in all

sequences, while the presence of fluorine is associated with the formation of thicker fibres. Interestingly, peptide **13d** samples also displayed the presence of unusual helical structures, although further investigation is needed to elucidate better the occurrence of this type of organisation. For example, cryo-TEM and atomic force microscopy (AFM) analyses may provide further insights.[106]

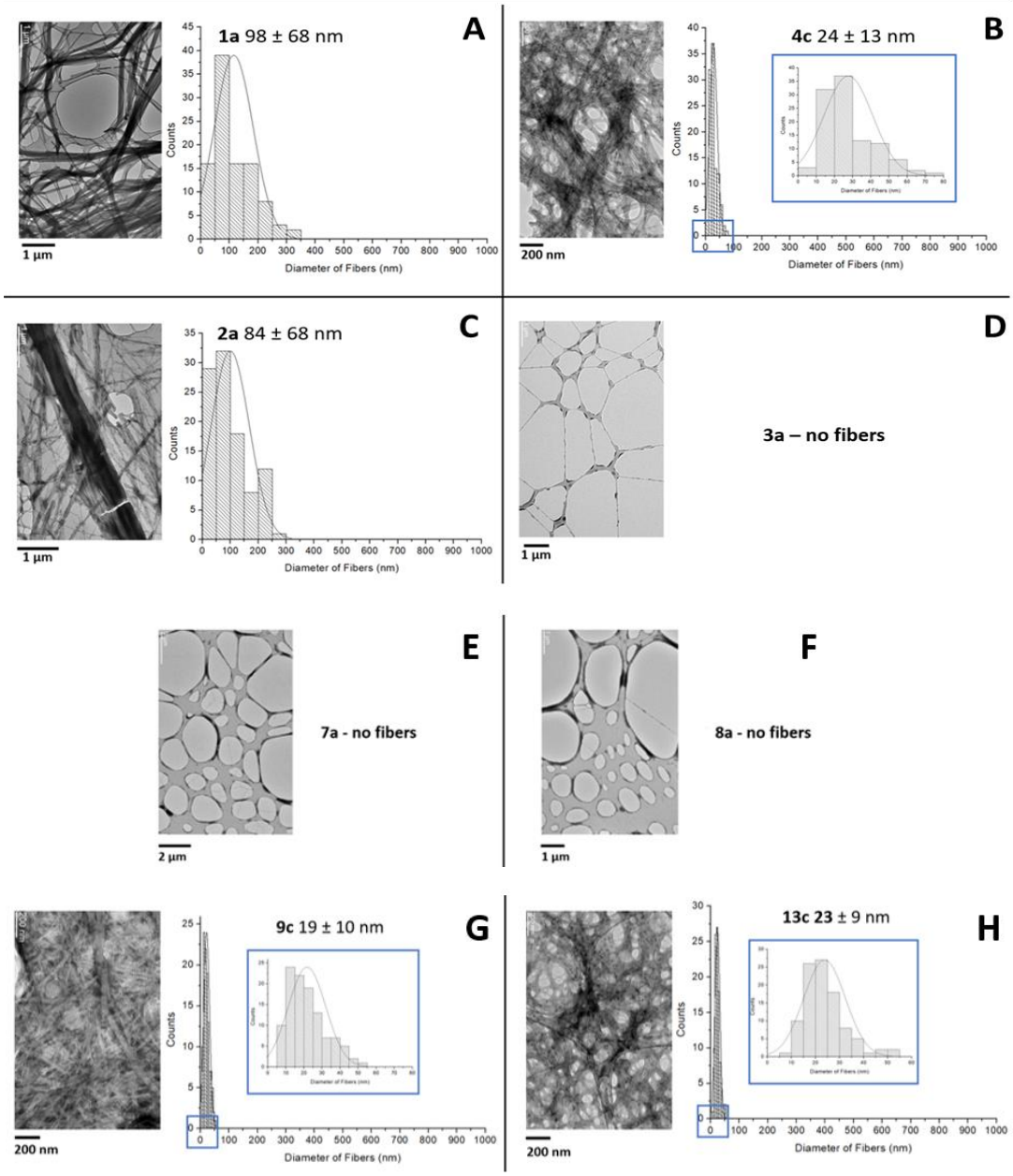

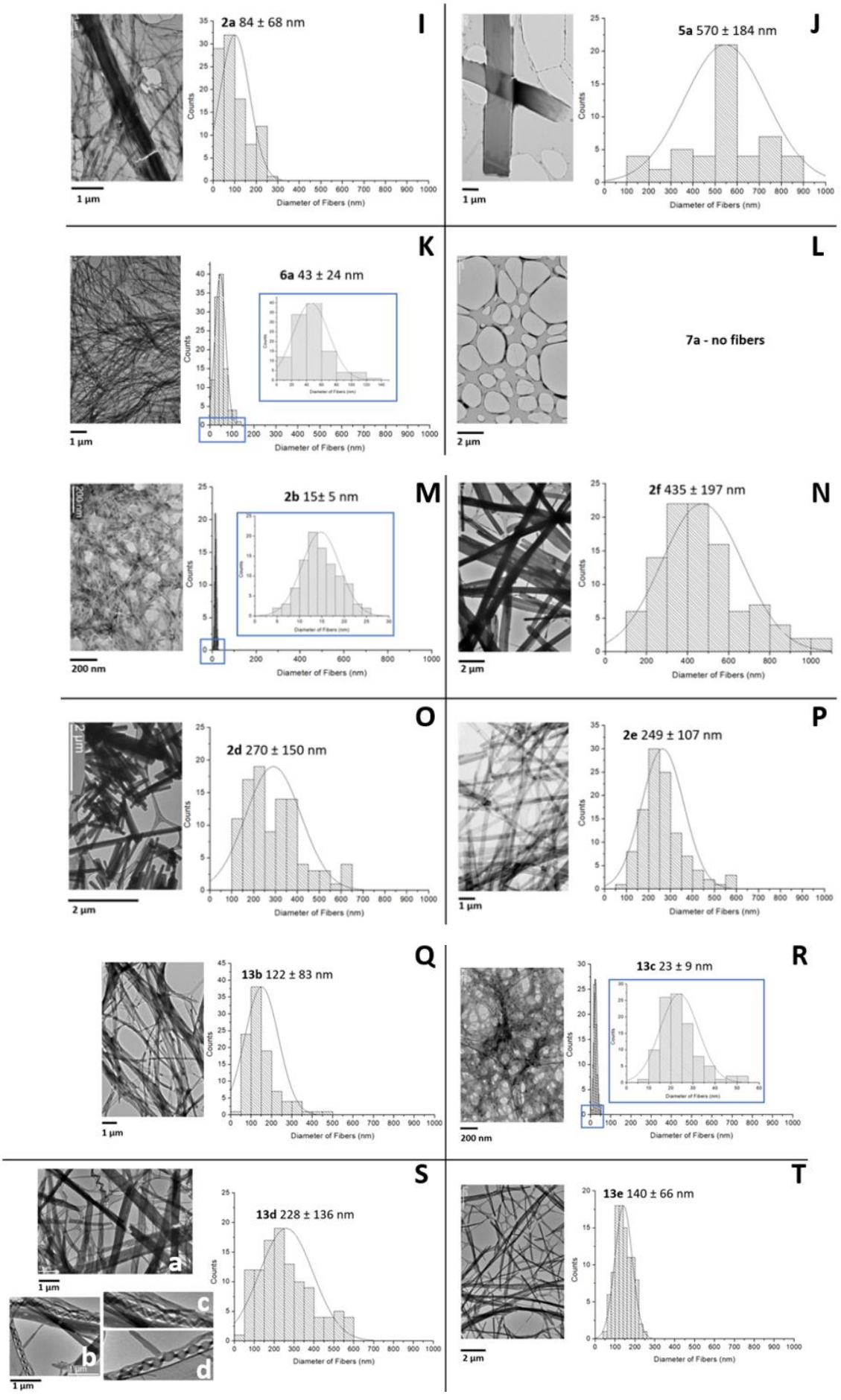
I
2a 84 ± 68 nm
1 µm
Counts
Diameter of Fibers (nm)
J
5a 570 ± 184 nm
1 µm
Counts
Diameter of Fibers (nm)
K
6a 43 ± 24 nm
1 µm
Counts
Diameter of Fibers (nm)
L
7a - no fibers
2 µm
M
2b 15± 5 nm
200 nm
Counts
Diameter of Fibers (nm)
N
2f 435 ± 197 nm
2 µm
Counts
Diameter of Fibers (nm)
O
2d 270 ± 150 nm
2 µm
Counts
Diameter of Fibers (nm)
P
2e 249 ± 107 nm
1 µm
Counts
Diameter of Fibers (nm)
Q
13b 122 ± 83 nm
1 µm
Counts
Diameter of Fibers (nm)
R
13c 23 ± 9 nm
200 nm
Counts
Diameter of Fibers (nm)
S
13d 228 ± 136 nm
a
b
c
d
1 µm
Counts
Diameter of Fibers (nm)
T
13e 140 ± 66 nm
2 µm
Counts
Diameter of Fibers (nm)

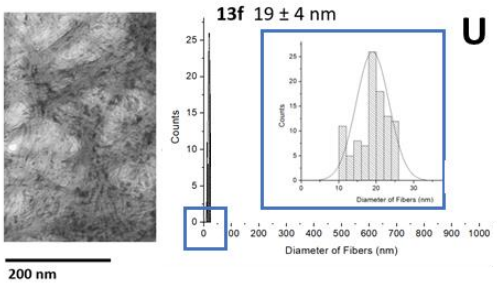

Figure 3.12 A-U TEM images and Gaussian distribution for peptide fibre diameter (nm)

3.2.3.3. Presence of amyloid-like structures

As described in Chapter 1, amyloid fibrils are ordered, β-sheet rich forms of aggregated peptides and proteins that are associated with a variety of pathological human disorders, including Alzheimer's and Parkinson's diseases. However, amyloid fibril-forming peptides may have a functional role as antimicrobial peptides, as evidenced in new theories that associated microbial infections in Alzheimer's disease and possibly a dysregulation of the innate immune system response.[79] Moreover, some antimicrobial and amyloid peptides have been identified to have dual amyloid and antimicrobial properties, suggesting a potential link between amyloid and antimicrobial peptides. Indeed, the majority of self-assembling peptides have an amyloid character defined in supramolecular organisation.[61] Currently, the criteria to be adopted to assess the presence of amyloid fibrils are quite controversial. However, characteristic fibril nanomorphology and ability to bind amyloid markers, such as Thioflavin T that leads to fluorescence, are largely used for amyloid fibers detection.[61,113] A number of experimental data and quantum mechanical predictions suggest that ThT act as a "molecular rotor".[113] In solution, a low energy barrier allows the benzylamine and benzathiole rings of ThT to rotate freely about their shared carbon-carbon bond. (*Figure 3.13*) This rotation rapidly quenches excited states generated by photon excitation, causing low fluorescence emission for free ThT. In contrast, rotational immobilization of ThT preserves the excited state, resulting in a high quantum yield of fluorescence (*Figure 3.14*). Indeed, amyloid fibrils are likely to present a ThT-binding site that sterically blocks the bound dye leading to an enhancement of ThT fluorescence.[113]

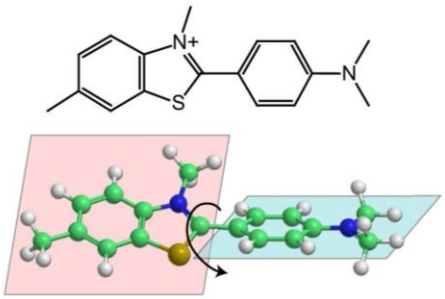

Figure 3.13 Structure of ThT (top). The two planer segments of ThT (bottom)

Reproduces with permission from ref.[113] *© 2010 Elsevier Ltd.*

ThT assay of peptides is performed at different peptide concentrations. The first set of analysis is performed at common concentration below the MGC (1 mM) in which the peptide molecules are expected to be present in solution. The second set of analysis is performed at 4 mM, that correspond to concentration below MGC but at which most of peptides are forming supramolecular structures (confirmed by TEM analysis). The third set was performed at 15 mM (7.5 mM for peptides not soluble at 15 mM, *i.e.*, **9c, 13b**, **13c**, **13d**, **13e**, **13f**) for each compound. As expected, peptides at 1 Mm are not presenting any signal due to interaction of peptides with ThT and data are reported in supporting information. Moreover, also for peptides not forming fibers at 4 Mm (TEM data) any signal is observed by ThT confirming absence of fibers. Although, not all peptides that are forming fibers, observed by TEM, are giving ThT signal. Moreover, observed signal for peptides at 4 mM and 15 mM can not be correlated neither with fibers length nor antimicrobial activity that will be discussed later. (*Figure 3.14*).

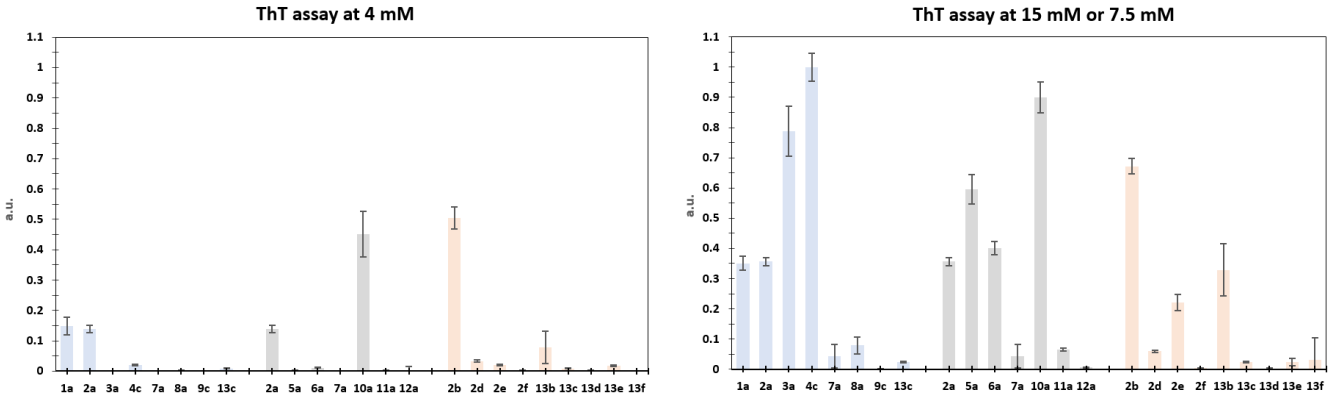

Figure 3.14 ThT assay results of peptides at 4 and 15/7.5 mM.

3.2.3.4. Secondary structure assessed by Dichroism spectroscopy

CD is a widely used technique to study the interaction between circularly polarized light and an asymmetric molecule. Subsequent differential absorption of left and right circularly polarized light components leads to elliptically polarised light (*Figure 3.15*).[114,115] The subsequent "ellipticity" at different wavelengths is measured by CD and has been widely used to assess the secondary structures of peptides and proteins, since they are associated with characteristic spectral signatures in the UV region. [115]

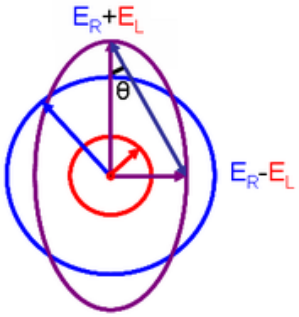

Figure 3.15 Elliptically polarised light composed of right (blue) and left (red) circularly polarised light.

In the literature, there are not many examples of CD studies on short peptides, since they are not expected to form a distinctive secondary structure.[116] However, when peptides self-organise in supramolecular structures, it is possible to observe changes in their CD signatures that can be used to monitor self-assembly and disassembly.[56,57]

It is rather challenging to predict the exact concentration at which a peptide will self-organise into fibrils or other supramolecular structures, therefore CD analyses were performed at different concentrations, *i.e.*, at 1 mM (at which peptides are expected to be in a non-assembled state), and at 4 mM (at which the majority of peptides assemble into fibrils as confirmed by TEM) (*Figure 3.19-3.25 A-B*). Higher concentrations typically lead to sub-optimal conditions for CD spectra acquisition that result in low-quality data and artefacts due to scattering, nevertheless, all compounds were analysed by CD also at mgc (see Appendix). Since this project aims at developing self-assembling peptides with antimicrobial properties, CD spectra were also acquired in the presence of sodium dodecyl sulfate (SDS) as a membrane-mimicking media (*Figure 3.19-3.25 C-D*). SDS is often used in CD analysis of antimicrobial peptides to verify presence of a bioactive conformation in a membrane-mimicking environment, since typically the bioactivity is exerted by means of membrane disruption.[117]

At 1 mM, Leu-Phe-Phe and Xaa-Phe-Phe peptides displayed a CD signature analogous to what recently reported for Phe-Xaa-Phe peptides, in which molecules visit a population of conformations in solution (*Figure 3.19, 3.20, 3.22* and *3.23*) The two maxima/minima (depending on chirality) present at 200 and 220 nm could be assigned to π-π*and n-π* transitions of peptide bonds respectively and the relative dipole orientations of the two amides could reveal an analogous statistic distribution according to CD signatures..[56] Halogenation alters CD signatures leading to spectra that are difficult to interpret (*Figure 3.21, 3.24, 3.25*).

When the concentration was increased to 4 mM, significant changes in CD spectra were observed in most, but not all, cases of peptide self-assembly. Previous studies on **10a**, **11a**, and **12a** already attempted at analysing the reasons for such spectral changes, but no correlation was found, suggesting that subtle differences in peptide conformations were amplified through the cooperative process of self-assembly in ways that were not possible to predict. [56] In the presence of SDS, regardless of peptide concentration, CD spectra changed in most cases to new signatures that were also difficult to interpret. Unfortunately, we could not find any correlation between peptide antimicrobial activity (discussed in *Section 3.3*) and CD spectral changes in the presence of SDS, thus leading us to the conclusion that this test was ineffective in monitoring peptide self-organization ability in SDS as a membrane model. Further studies will be needed using different membrane models to get more insights into peptide organisation changes and their effects on membrane integrity. Finally, spectra at mgc displayed analogous signatures compared to those observed at 4 mM, except for reduced intensity due to light scattering from the hydrogel, thus suggesting that peptide organisation at concentrations above 4 mM was preserved, as expected (*see Appendix*).

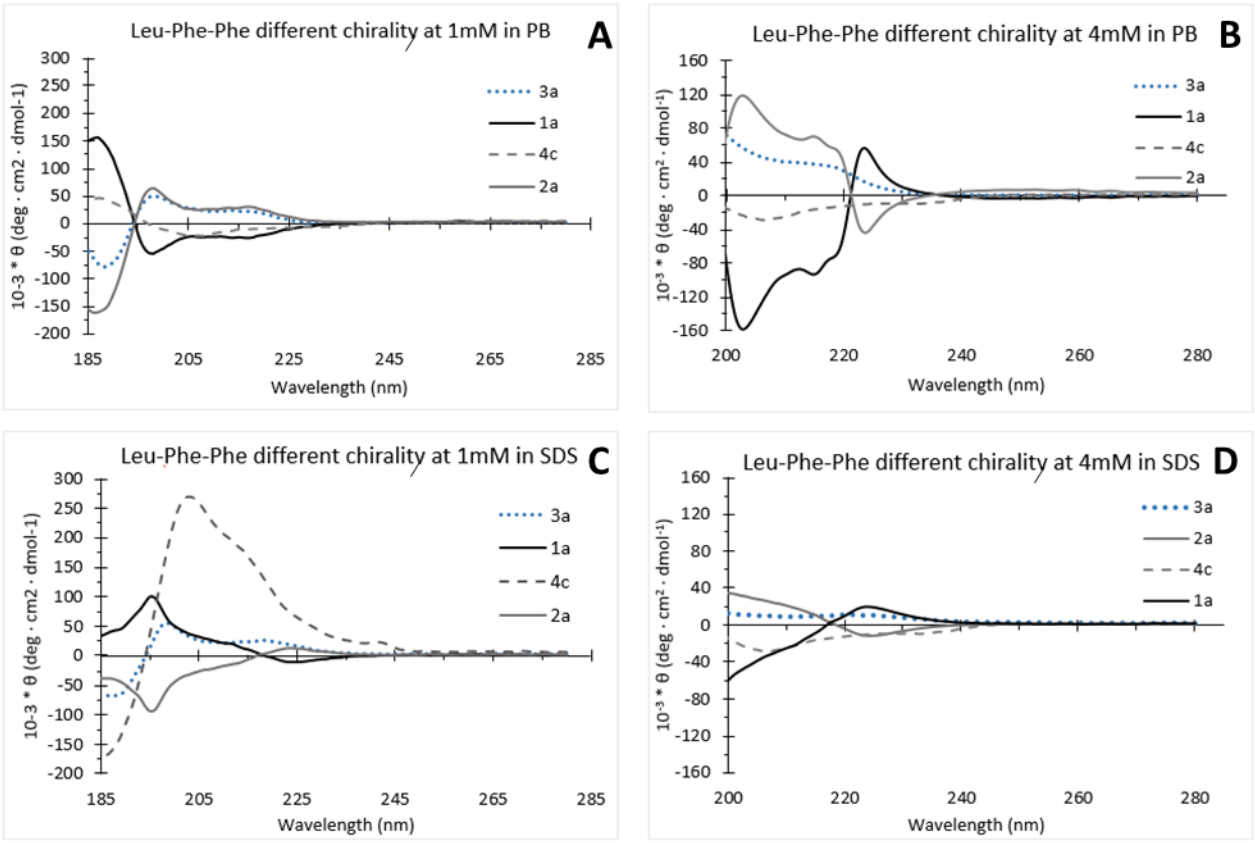

Figure 3.19 CD spectra of peptides at 1 and 4 mM in PB (left) and SDS (right).

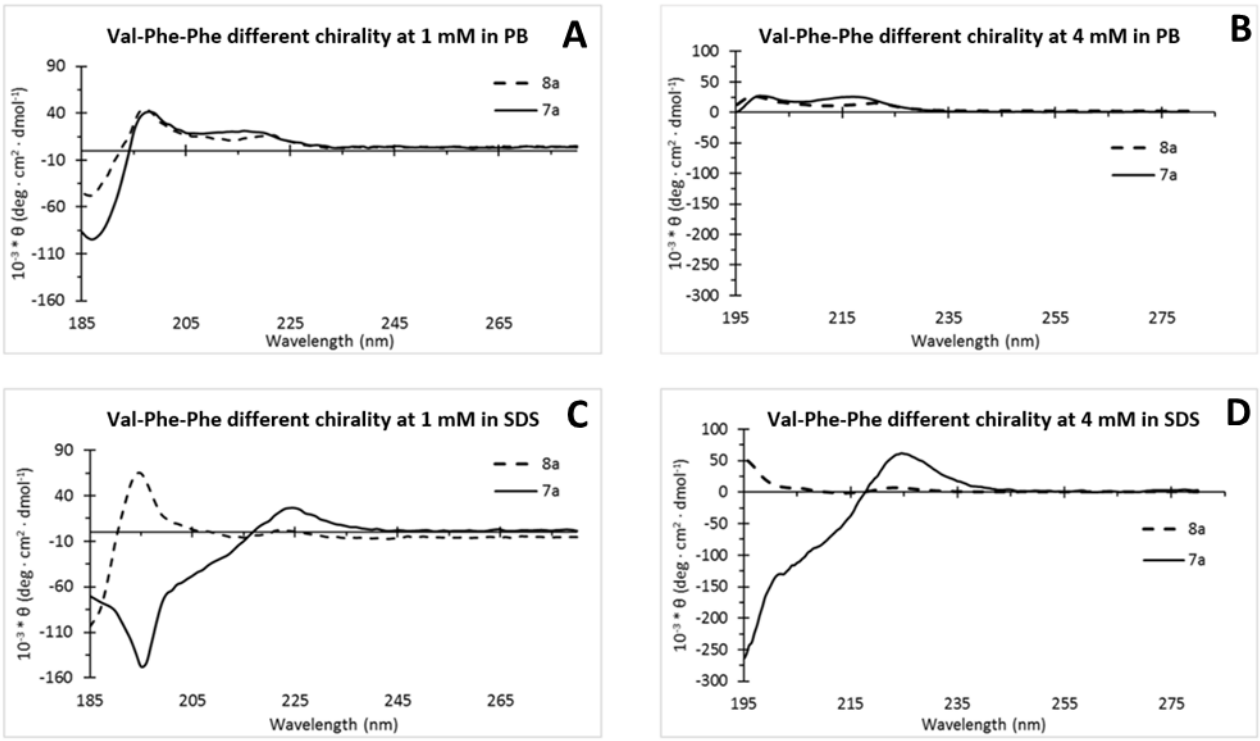

Figure 3.20 CD spectra of peptides at 1 and 4 mM in PB (left) and SDS (right).

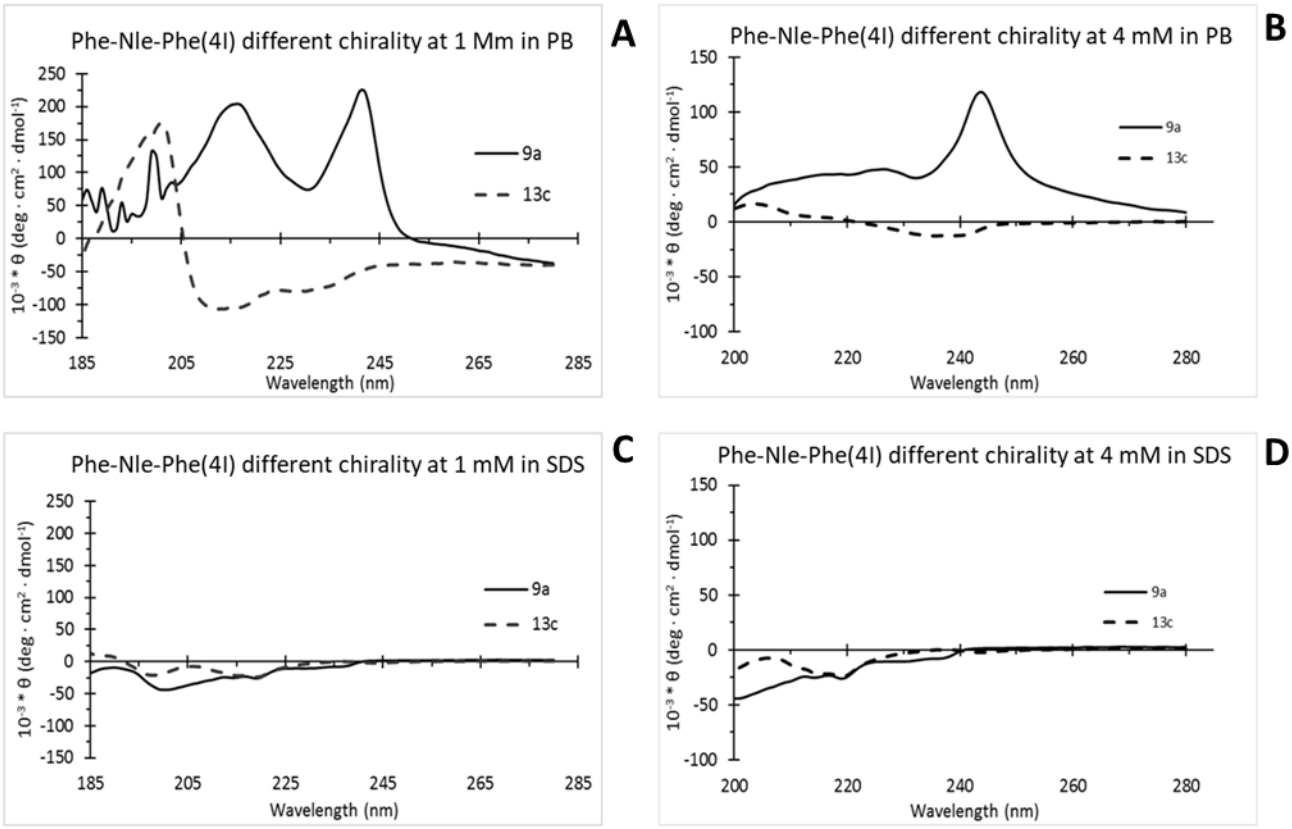

Figure 3.21 CD spectra of peptides at 1 and 4 mM in PB (left) and SDS (right).

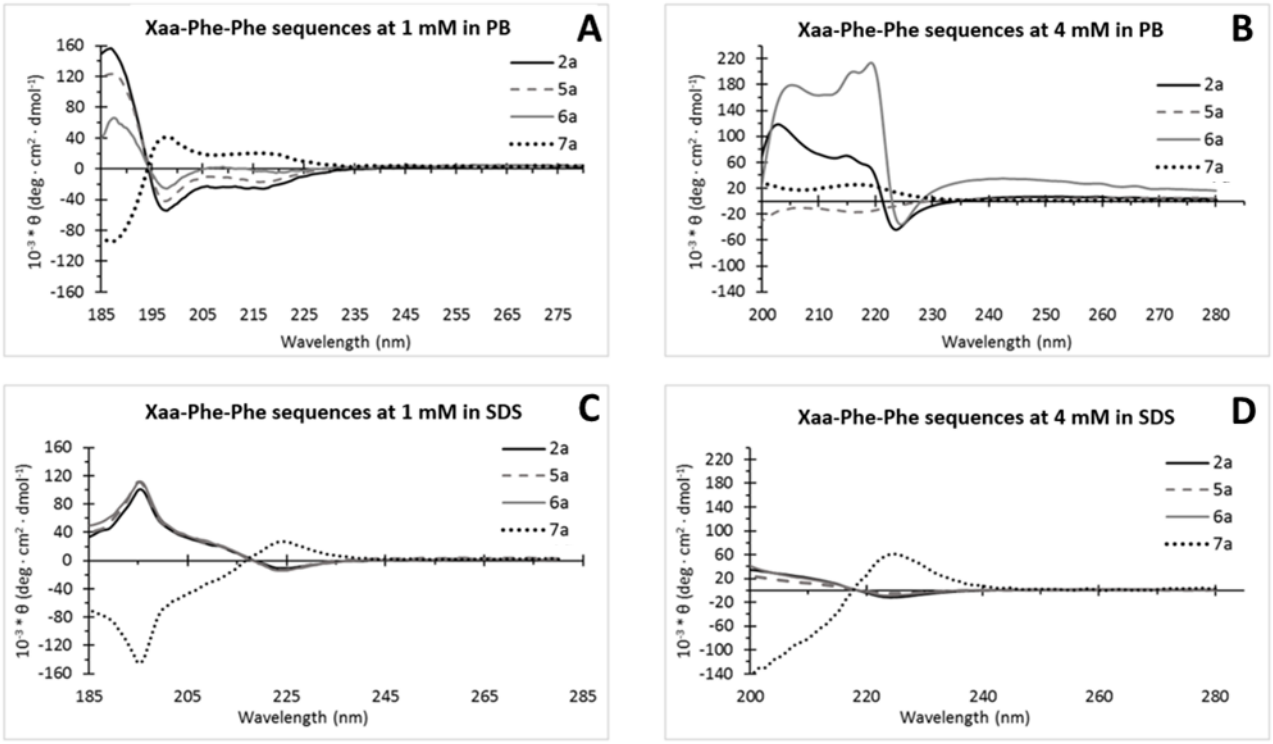

Figure 3.22 CD spectra of peptides at 1 and 4 mM in PB (left) and SDS (right).

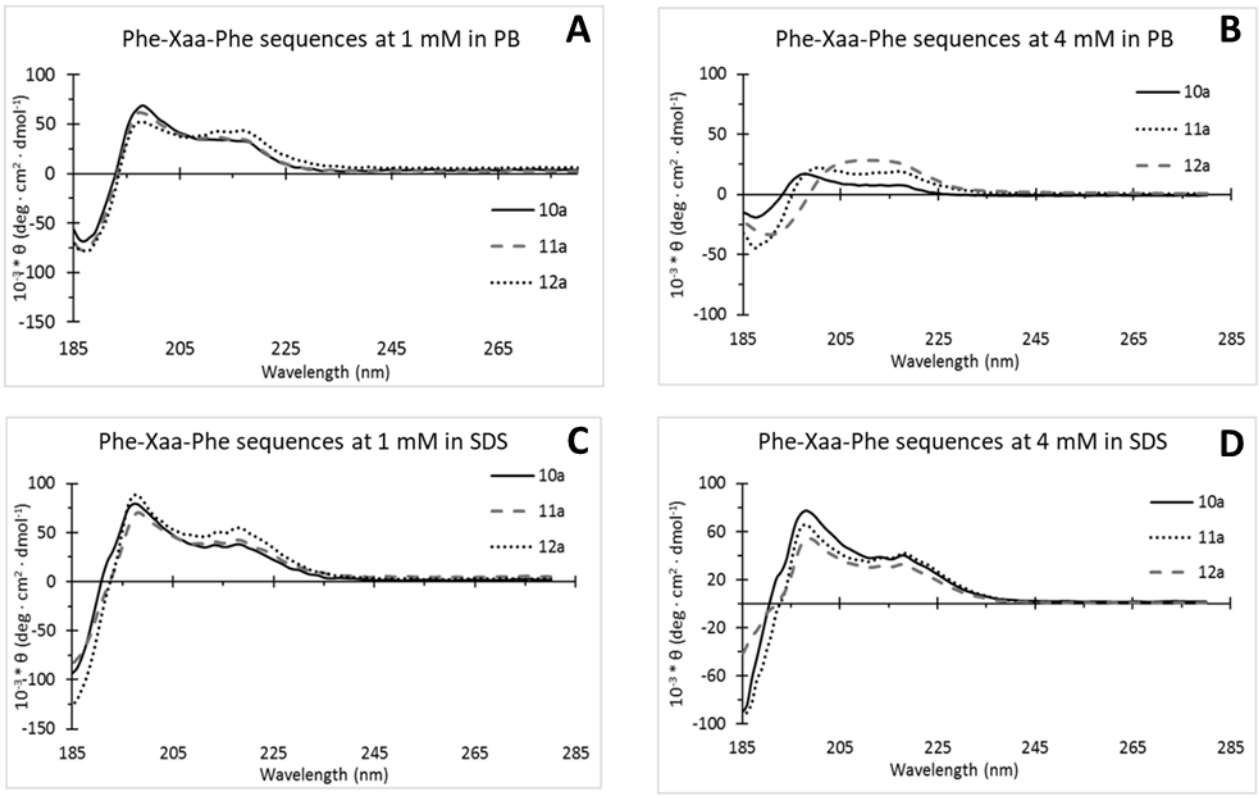

Figure 3.23 CD spectra of peptides at 1 and 4 mM in PB (left) and SDS (right).

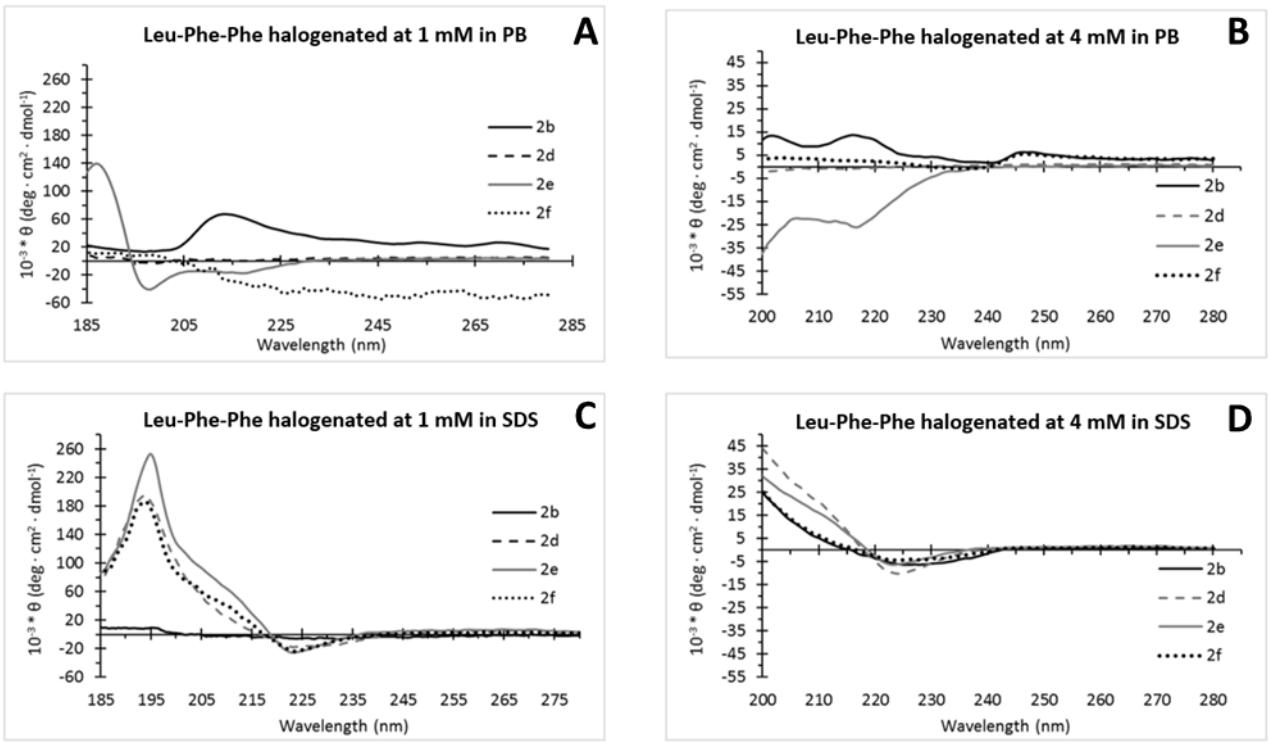

Figure 3.24 CD spectra of peptides at 1 and 4 mM in PB (left) and SDS (right).

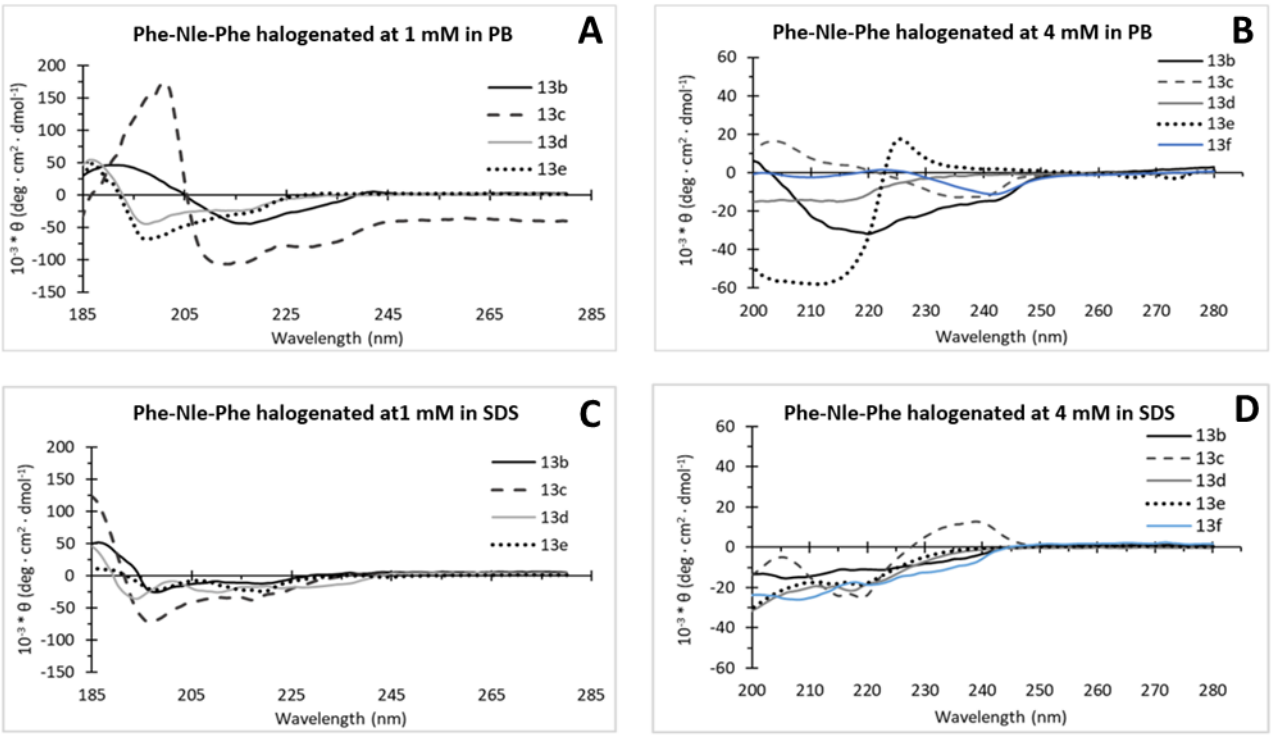

Figure 3.25 CD spectra of peptides at 1 and 4 mM in PB (left) and SDS (right).

3.2.4. Single crystal X-ray diffraction analysis

Single-crystal X-ray Diffraction is a non-destructive analytical technique which provides detailed information about the structure of crystalline substance including unit cell dimensions, bond-lengths, bond-angles, and details of site-ordering. As all diffraction methods are based on generation of X-rays of synchrotron radiation. Generated X-rays are then directed at the sample, and finally the diffracted rays are collected. Directly related is single-crystal refinement procedure, where the data generated from the X-ray analysis is interpreted and refined to obtain the crystal structure.

After several trials of conditions, some of the peptides were able to form crystals that were then solved by the group of Prof. Rita De Zorzi.

In this section are reported the description of unit cell of each solved peptide, the crystal packing, the weak interactions involved in the supramolecular organisation, and the Ramachandran plot reporting the torsion angles of the central residues of tripeptides. Moreover, for 2b and 4c peptides crystals suitable for X-ray diffraction were obtained both by vapor diffusion and by aging of the corresponding hydrogels. In both cases crystals were characterised and the crystal structures determined allowing to

evaluate if the peptide organisation was the same in both conditions (*Table 3.9*). Indeed, an indication of low energetic barrier between hydrogel and crystal organisation was crystal formation in supramolecular gel. However, for heterochiral peptide **2b** crystals were forming inside the gel (10-14 days) and these two forms were present together. Instead of homochiral peptide in which was possible observe complete hydrogel conversion in crystals (20-24 hours), confirming the importance of presence of both chirality of amino acids in peptide sequence for stable hydrogel formation.

	Compound name	Space group in solution	Space group in hydrogel
Xaa-Phe-Phe	**1a**	$P2_12_12_1$	n.a.
	3a	*P1*	not gelling
	4c	$P2_1$	$P2_1$
	2b	$P2_12_12_1$	$P2_12_12_1$
	2f	$P2_12_12_1$	n.a.
	5a	*P1*	n.a.
Phe-Xaa-Phe	**9c**	$P2_1$	n.a.
	13e	$P6_3$	n.a.

Table 3.9 Peptide solved single crystal XRD structure and space group.

3.2.4.1. XRD structures of Xaa-Phe-Phe group sequence

1a – ^{D}Leu-^{L}Phe-^{L}Phe

The asymmetric unit contains a single molecule of the peptide in its zwitterion form and a molecule of methanol, used as solvent in the crystallization experiment. A total of 4 molecules of peptide, related by symmetry operators of the $\boldsymbol{P2_12_12_1}$ space group, were present in the unit cell (*Figure 3.26*).

The crystal packing showed a separation between regions with prevalence of hydrophobic groups, i.e. the phenyl moieties and the leucine side chain, and regions with hydrophilic interactions involving the backbone of the peptides and a methanol molecule (*Figure 3.27*). Hydrophilic interactions were present between the peptides, namely hydrogen bonds between the carbonyl and the amide moieties along the *a* crystallographic direction (*Figure 3.28,* black dashes) and salt bridges between the N-

terminus and the C-terminus of different peptides, forming chains of peptides along the *b* crystallographic direction (*Figure 3.28*, blue dashes). In addition, a weaker hydrogen bonding interaction was present between the carbonyl moieties and the hydrogens of the Cα (*Figure 3.28*, cyan dashes). Notably, hydrophilic interactions were formed between a single solvent molecule (methanol) and both the N- and C- termini of a peptide molecule (*Figure 3.29*, black dashes). Only weak hydrophobic interactions were present between the phenyl moieties and the leucine side chain.

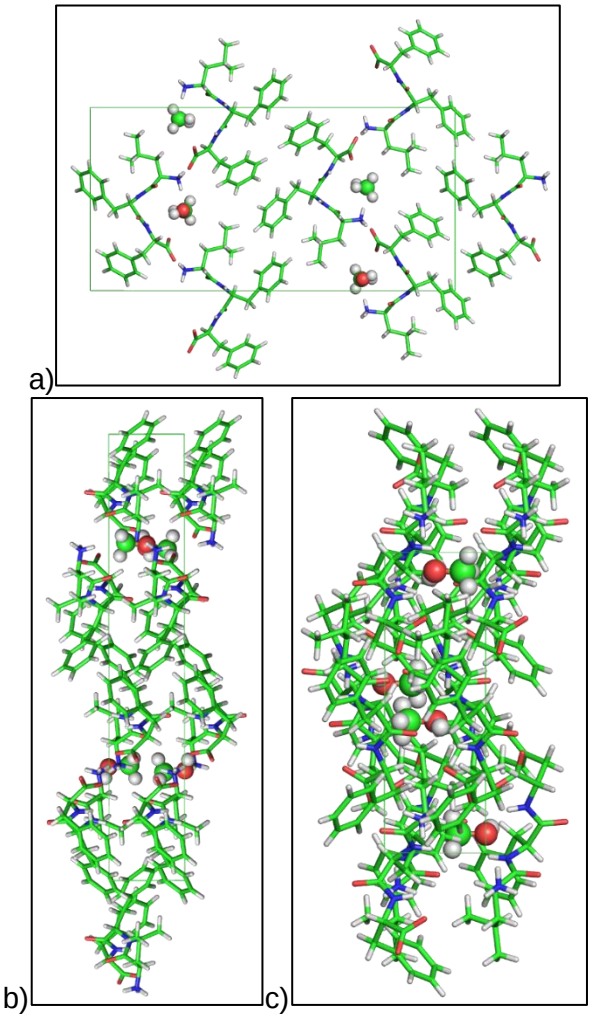

Figure 3.26 Unit cell of crystals of 1a.
Crystal packing in the crystal of the peptide **1a**, grown in methanol and water. Views along the *a* crystallographic axis (a), the *b* crystallographic axis (b) and the *c* crystallographic axis (c). Peptide molecules are shown as sticks, methanol molecules are shown as spheres. Carbon atoms are shown in green, oxygen atoms in red, nitrogen atoms in blue, hydrogen atoms in white.

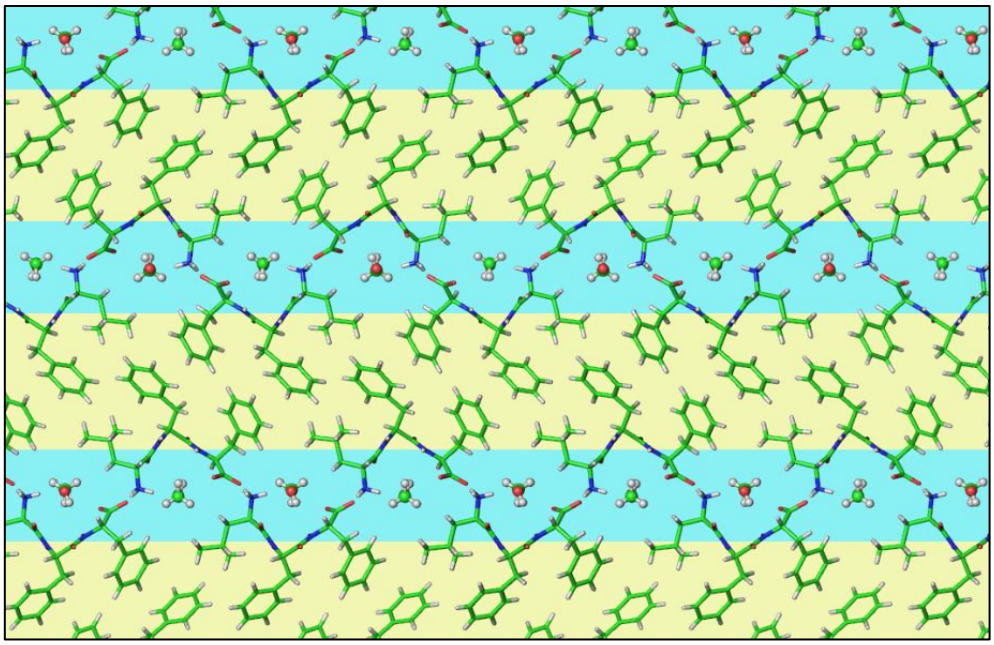

Figure 3.27 Crystal packing with alternating hydrophilic and hydrophobic regions in peptide 1a.
Hydrophilic and hydrophobic layers in the crystal of **1a**. Hydrophobic layers are shown with a yellow background, hydrophilic layers with a blue background. Crystal packing is shown in the plane perpendicular to the *a* crystallographic direction.

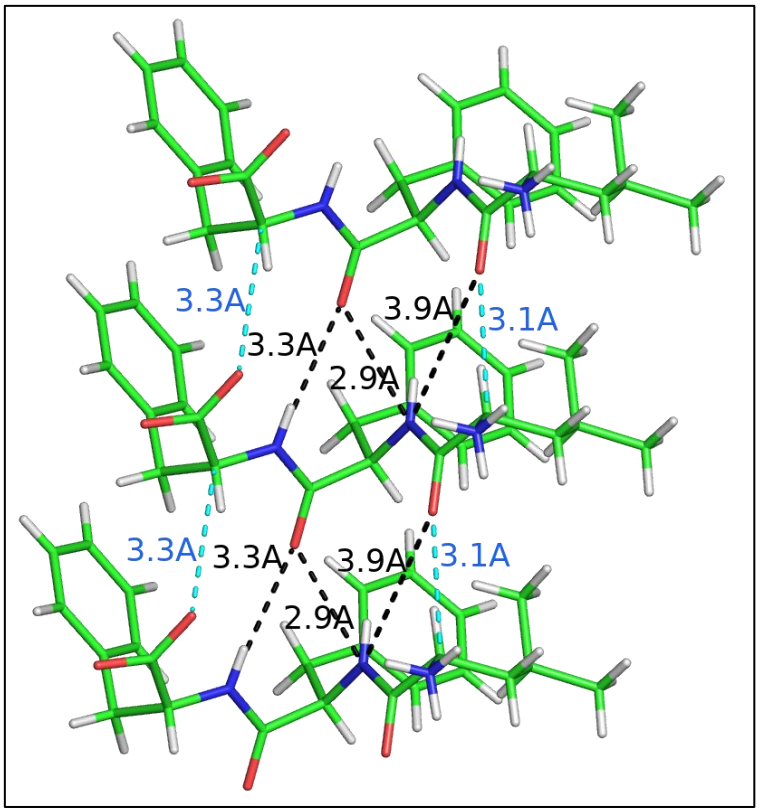

Figure 3.28 Hydrophilic interactions connecting peptides 1a along the *a* crystallographic direction.
Hydrogen bonding interactions are marked with black dashes and donor-acceptor distances are reported. Interactions between a Cα and a carbonyl moiety can be described as weak hydrogen bonding interactions; these are marked with cyan dashes and the Cα - O distances are reported.

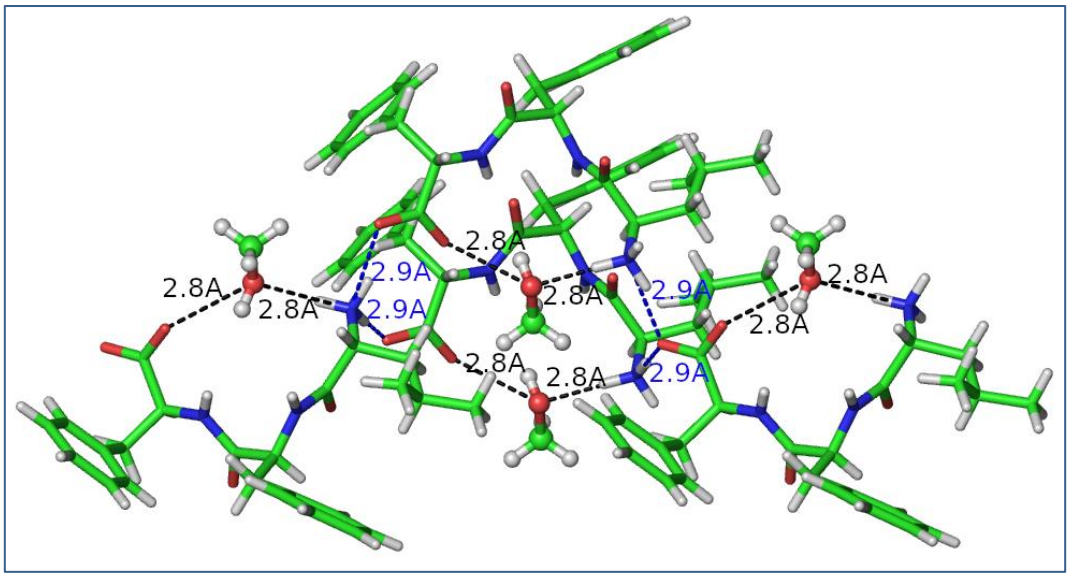

Figure 3.29 Salt bridges interactions between adjacent peptides 1a and solvent molecules.
Salt bridges interactions involving the N- and C- termini of the peptides. Blue dashes represent interactions between adjacent peptides, while black dashes show peptide-solvent (methanol) interactions. Distances between carbon and nitrogen atoms are shown.

Crystallographic details.

A stick-shaped single crystal of the peptide was collected with a loop, cryoprotected by dipping the crystal in an oil-based cryoprotectant, namely Parabar 10312 (previously known as Paratone N, from Hampton Research), and stored frozen in liquid nitrogen. A total of 180 images were collected. Reflections were indexed and integrated using the XDS package, space group $\boldsymbol{P2_12_12_1}$ was determined using POINTLESS and the resulting data set was scaled using AIMLESS.[118–120] *Table 3.10* lists the unit cell parameters and the scaling statitics.[121,122] The asymmetric unit contained a molecule of the peptide and a molecule of methanol. Hydrogen atoms of the peptide and of the methyl moiety of the alcohol molecule were added at geometrically calculated positions and refined isotropically, with thermal parameters dependent on those of the attached atom. All the atoms, except the hydrogen atoms, within the asymmetric unit have been refined with anisotropic thermal parameters. During refinement, no restraints were applied on distances, angles or thermal parameters of non-hydrogen atoms. Refinement statistics are reported in *Table 3.9*.

3a – ᴸLeu-ᴸPhe-ᴸPhe

The asymmetric unit contains six molecules of the peptide. The additional electron densities present in the asymmetric unit were recognized as two trifluoroacetic acid anions, used during the purification, and 4 molecules of acetonitrile, solvent used during the purification. The presence of two negatively charged ions suggests that not all the peptide molecules are in their zwitterionic form, but only 4 of the crystallographically independent peptide molecules had both the N-terminal group in its protonated form (charge: +1) and the C-terminal group in its deprotonated form (charge: -1). The other two peptide molecules had a net charge of +1, with both the N- and the C- terminal groups in their protonated forms. Considering the absence of symmetry elements in the ***P1*** space group, only 6 peptide molecules were present in the cell (*Figure 3.30*).

The crystal packing showed that in the *b* crystallographic direction peptide molecules were piled through hydrophilic interactions, while in the perpendicular direction mainly hydrophobic interactions were responsible for the packing of side chains. This arrangement formed hydrophilic regions corresponding to the peptide backbones and to the counterions (*Figure 3.31*, in blue), and large hydrophobic regions corresponding to the side chains of residues (in yellow). Hydrophilic interactions holding together peptides were: a) hydrogen bonding interactions between the backbone groups (*Figure 3.33*, black dashes), having a donor-acceptor distance ranging between 2.86 and 3.31 Å, with an average value of 3.0 Å; b) salt bridge interactions between the terminal groups (*Figures 3.32* and *3.33*, blue dashes). An additional, strong hydrogen bond interaction was present between the C-terminal group of a positively charged peptide (protonated carboxylic group) and the C-terminal group of a zwitterionic peptide. The strong hydrogen bonding interaction did not allow to locate the hydrogen atom on one or the other oxygen atoms involved in the interaction, therefore it was not possible to define which one of the peptide molecules had a net positive charge. The same hydrogen bond interaction was observed for both the protonated peptides. In the structure, therefore, 2 types of peptides could be recognized: (i) couples of peptides involved in strong hydrogen bonding interactions with their C-terminal group (grey and yellow peptides in *Figure 3.32*) and (ii) peptides whose C-terminal group was involved only in salt bridges interactions with the N-terminal group with a symmetry-related peptide (orange peptides in *Figure 3.32*). Of the 6 crystallographically independent peptide molecules present in the crystal structure of **3a**, 4 belong to type (i), while 2 belong to type (ii). Besides peptide-peptide interactions, hydrophilic contacts present in the structure involved also the trifluoroacetate counterions that form strong salt bridge interactions with the protonated amino terminal groups of the peptides, with donor-acceptor distances of 2.75 Å (*Figure 3.32*, magenta dashes). Hydrophobic interactions observed in the structure of **3a** are fewer in number

compared to the hydrophilic interactions. They involved the aromatic groups of the phenylalanine and are mainly CH-π interactions.

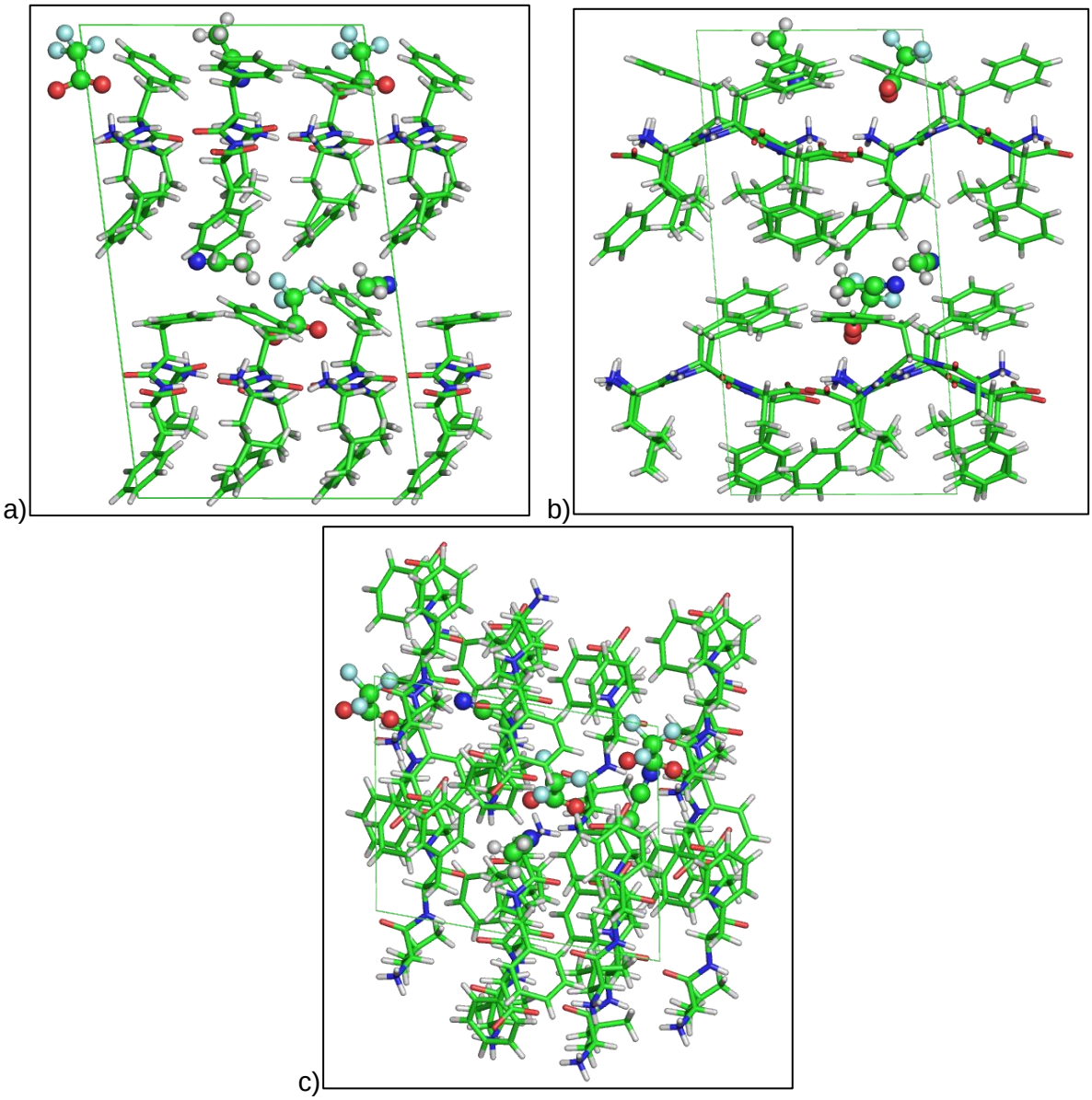

Figure 3.30 Unit cell of crystals of the peptide 3a.
Views along the *a* crystallographic axis (a), the *b* crystallographic axis (b) and the *c* crystallographic axis (c). Peptide molecules are shown as sticks, trifluoroacetate ions and acetonitrile molecules are shown as spheres.

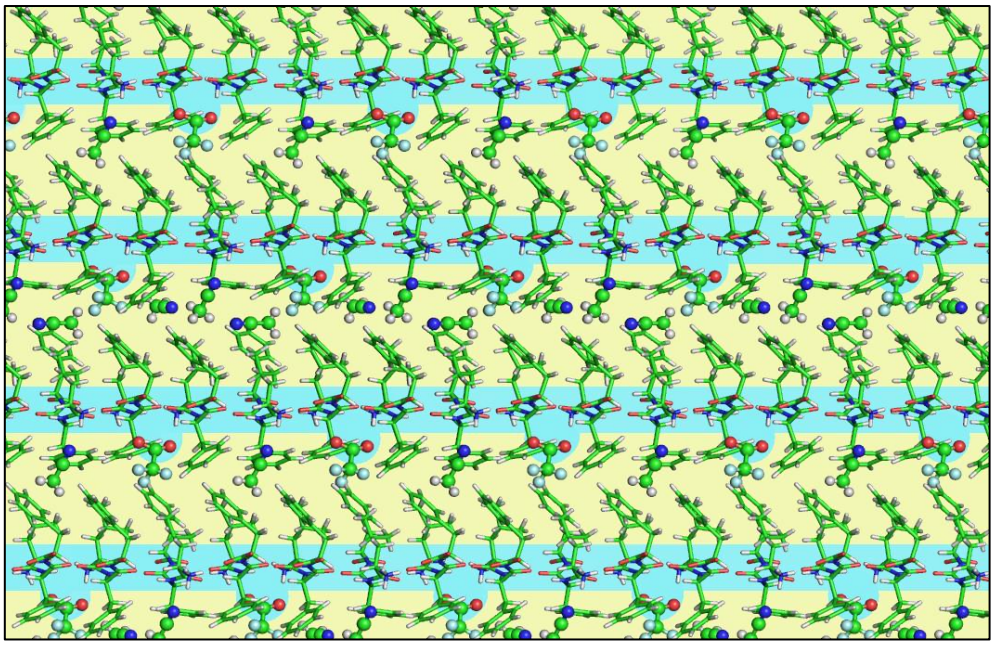

Figure 3.31 Crystal packing of 3a.
Peptide molecules form piles along the *b* crystallographic direction (horizontal direction) through hydrophilic interactions, in blue. The side chains of the residues of each pile face those of the neighboring piles (vertical direction), interacting through hydrophobic contacts, in yellow.

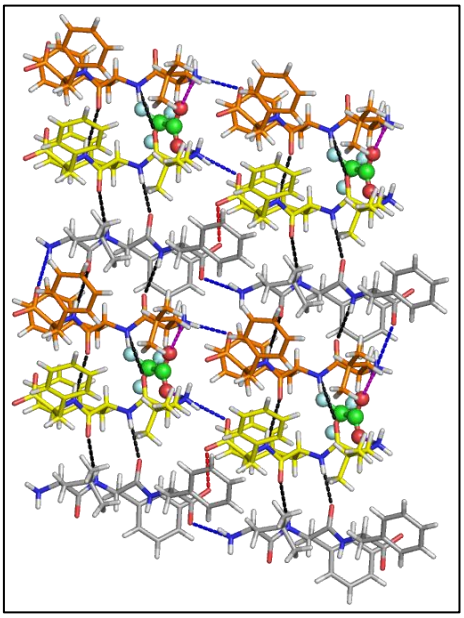

Figure 3.32 Hydrophilic interactions involving peptide 3a molecules and trifluoroacetate ions.
Pattern of hydrophilic interactions in the crystal involving peptide molecules (depicted as sticks) and trifluoroacetic ions (depicted as spheres). Peptide-peptide hydrogen-bonding interactions are represented as black dashes, salt bridge interactions between the charged terminal groups of the peptide molecules are depicted as blue dashes, a strong hydrogen bonding interaction between a deprotonated and a protonated C-terminal group are represented as red dashes, and magenta dashes show peptide-counterion interactions. Crystallographically independent molecules are shown with different colors. Only three crystallographic independent molecules are reported in the figure, for clarity reasons

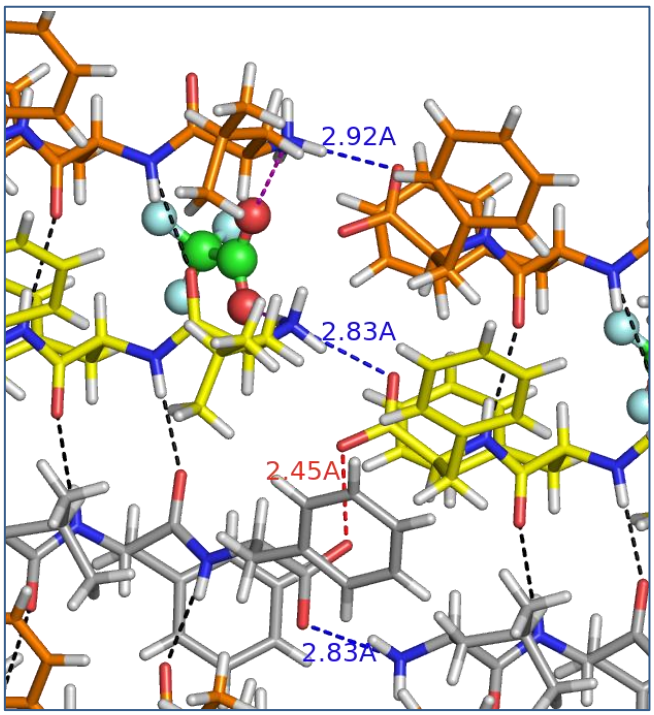

Figure 3.33 Detail of the hydrophilic interactions involving terminal groups of the peptide 3a molecules. N- and C-terminal groups of the peptide molecules are involved in salt bridge interactions with other peptide molecules, in blue, and with trifluoroacetic ions, in magenta. In addition, a particular hydrogen bond interaction is formed between the C-terminal group of positively charged peptide (protonated state of the C-terminus) and another C-terminal group of a crystallographically independent zwitterionic peptide, represented as red dashes.

Crystallographic details.

A plate-shaped single crystal of the peptide was collected with a loop, cryoprotected by dipping the crystal in glycerol and stored frozen in liquid nitrogen. A total of 360 images were collected. Reflections were indexed and integrated using the MOSFLM software, space group ***P1*** was determined using POINTLESS and the resulting data set was scaled using AIMLESS.[119,120,123] Unit cell parameters and scaling statistics are reported in *Table 3.9.*[122] The asymmetric unit contained 6 molecules of the peptide, 2 trifluoroacetic ions and 4 acetonitrile molecules. All the atoms within the asymmetric unit, except the hydrogen atoms, have been refined with anisotropic thermal parameters. Hydrogen atoms were added at geometrically calculated positions and refined isotropically, with thermal parameters dependent on those of the attached atom, except for the hydrogen atoms on the carboxylic group of the 2 cationic peptides that could not be located. Refinement statistics are reported in *Table 3.9.*

5a – ^{L}Ile-^{D}Phe-^{D}Phe

The asymmetric unit of the crystal contains three molecules of the peptide in its zwitterion form. The additional electron densities present in the asymmetric unit were recognized as 7 molecules of water, used as precipitant in the crystallization experiment, one of them in two positions with a 50% and 40% occupancy factor, respectively. The three crystallographically independent molecules of the peptide had the same backbone conformation and a similar rotamer for residues 2 and 3 (phenylalanine residues), but show small differences in the conformation of the leucine residues (*Figure 3.34*). Considering that the space group of the crystal is ***P1***, the asymmetric unit coincided with the whole unit cell (*Figure 3.35*). However, the arrangement of the peptide molecules allowed to identify a pseudosymmetry axis of third order (*Figure 3.36*), as confirmed by the angles of the unit cell, two of which are about 90° and one about 120°, closely resembling a trigonal cell.

In the crystal packing (*Figure 3.37*), mainly hydrophobic and mainly hydrophilic regions were separated, with hydrophilic moieties of the peptides forming channels filled with solvent molecules. Many hydrophilic interactions, hydrogen bonds and salt bridges, were present in the structure and involved both peptide molecules and water molecules (*Figure 3.38*). Some water molecules had interactions with two different peptides, bridging together the molecules. In the solvent filled channel, water molecules were surrounded by 4 hydrogen bonding interactions, with a nearly tetrahedral geometry. In addition, a pattern of hydrophobic interactions, mainly of the CH-π type, contributed to the crystal packing (*Figure 3.39*). The main hydrophobic interactions involved the phenyl ring of the phenylalanine residues and hydrogen atoms of the leucine residues, of the Cβ carbon of the phenylalanine residues, or of the aromatic moieties.

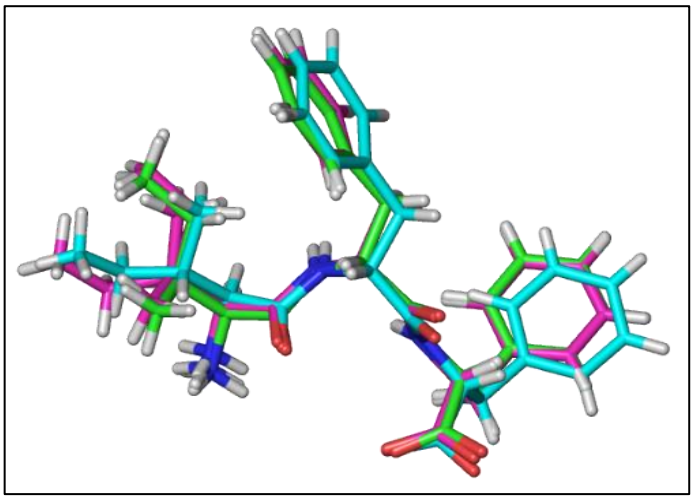

Figure 3.34 Conformations of 3 crystallographically independent peptides 5a. The three crystallographically independent molecules of the peptide present in the unit cell of crystals of **5a** share the same backbone conformation and side chain conformation, except for the side chain of the first residue (leucine), that shows different torsion angles. In the figure, the three independent molecules are superimposed and their carbon atoms are colored with different colors.

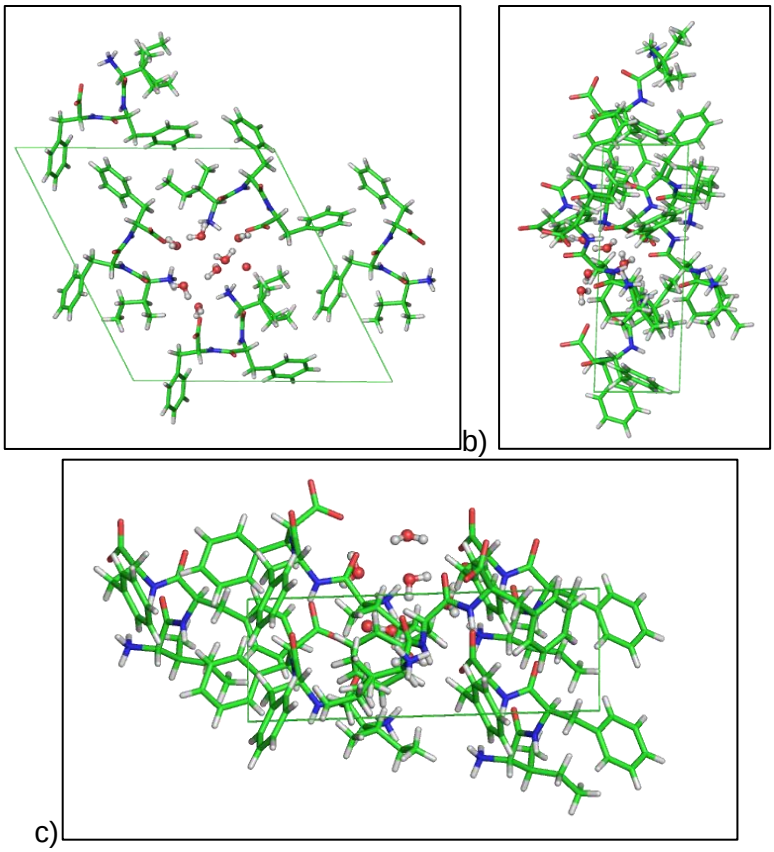

Figure 3.35 Unit cell of crystal of the peptide 5a.
Crystal of the peptide **5a**, grown in methanol and water. Views along the *a* crystallographic axis (a), the *b* crystallographic axis (b) and the *c* crystallographic axis (c). Peptide molecules are shown as sticks, water molecules are shown as spheres.

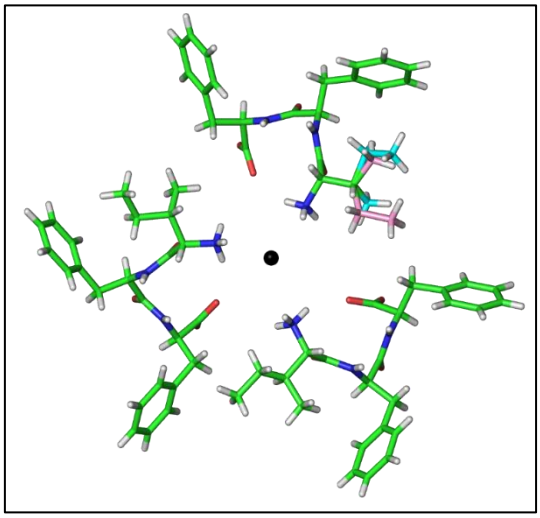

Figure 3.36 Pseudosymmetry in the crystal structure of 5a.
The arrangement of the peptide molecules in the crystal structure shows the presence of a psudosymmetry axis of third order. The figure shows the view of the three crystallographically independent peptides along the pseudosymmetry axis, represented as a black dot. The two conformations of the leucine residue at partial occupancy are represented with different colors.

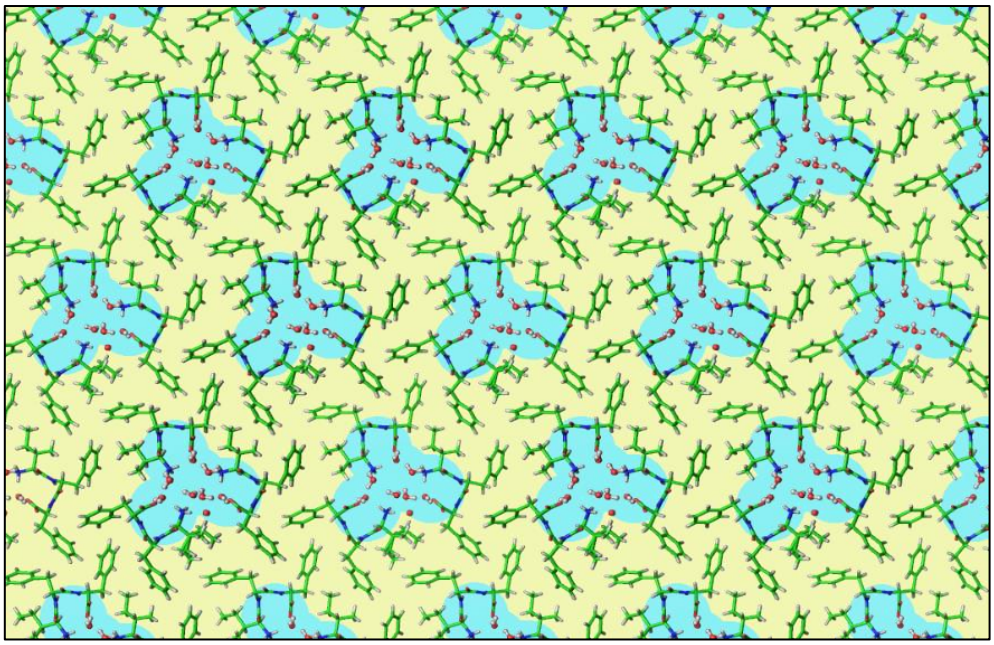

Figure 3.37 Crystal packing of 5a, forming solvent-filled channels.
The crystal packing of the structure of **5a** allows the formation of solvent channels filled with water molecules. In the figure, regions with prevalent hydrophobic character are shown in yellow, regions with hydrophilic character are shown in blue, including the solvent-filled channels.

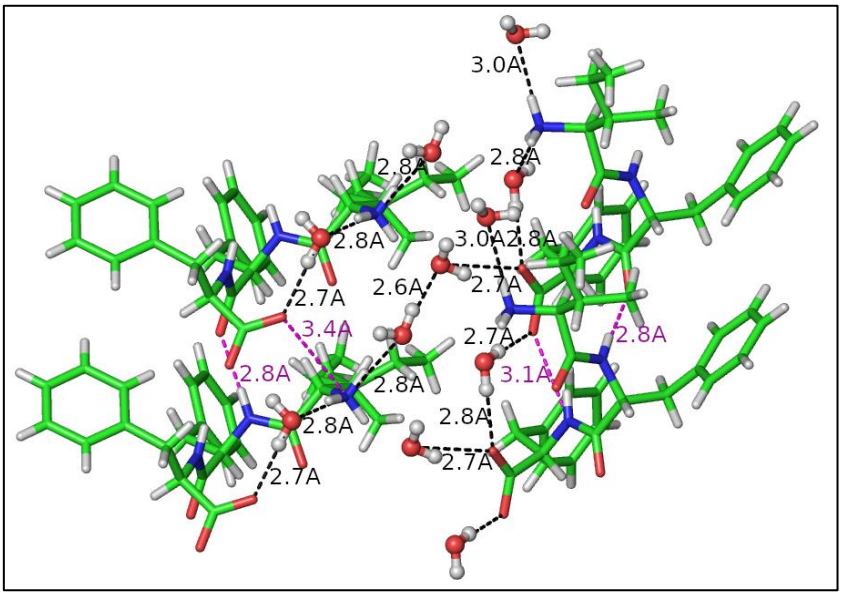

Figure 3.38 Hydrophilic interactions involving peptide 5a and water molecules.
Pattern of hydrophilic interactions in the crystal involving peptide molecules and water molecules. Peptide-water and water-water Interactions are marked with black dashes, peptide-peptide interactions are shown in magenta. Distances between donor and acceptor atoms are reported.

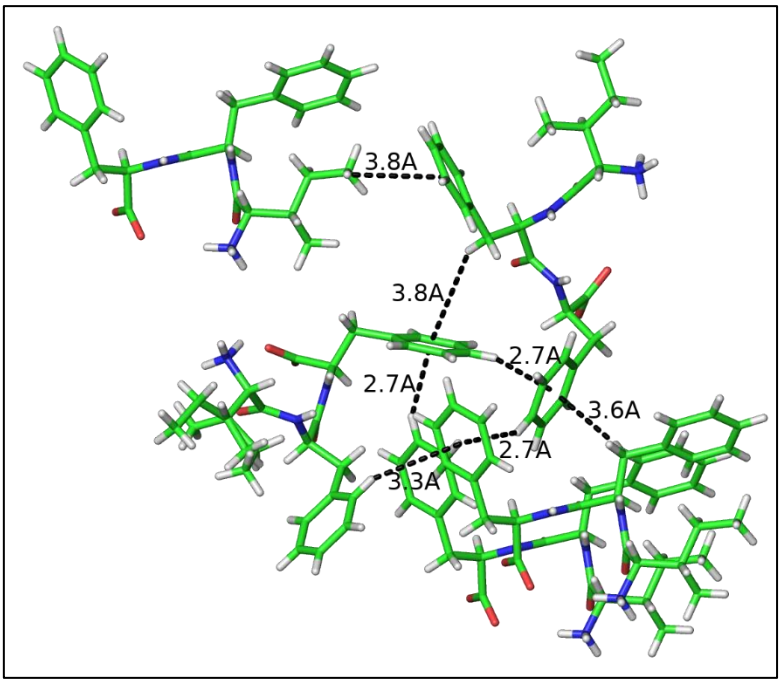

Figure 3.39 CH-π hydrophobic interactions of 5a.
The main hydrophobic interactions present in the crystal structure of **5a** are CH-π interactions involving the phenyl rings of the phenylalanine residues and both aliphatic and aromatic hydrogen atoms. Distances from the center of the phenyl ring to the hydrogen atom are reported.

Crystallographic details.

A needle-shaped single crystal of the peptide was collected with a loop, cryoprotected by dipping the crystal in glycerol and stored frozen in liquid nitrogen. Reflections were indexed and integrated using the XDS package, space group ***P1*** was determined using POINTLESS and the resulting data set was scaled using AIMLESS.[119,120,124] Unit cell parameters and scaling statistics are reported in *Table 3.10*.[121,122] The asymmetric unit contained three molecules of the peptide and 7 molecules of water, 2 of them in positions at 50% and 40% occupancy, respectively. All the atoms, except the hydrogen atoms, within the asymmetric unit have been refined with anisotropic thermal parameters. Hydrogen atoms of the peptide molecule were added at geometrically calculated positions and refined isotropically. Hydrogen atoms of the water molecules were added with restrains on bond lengths and bond angle, using the DFIX and DANG cards of SHELXL-14, respectively, except for the water molecule in a 40% occupancy position, for which hydrogen atoms could not be located. Refinement statistics are reported in *Table 3.10*.[121]

	1a	3a	5a
Formula	$C_{24}H_{31}N_3O_4 \cdot CH_4O$	$4C_{24}H_{31}N_3O_4 \cdot 2C_{24}H_{32}N_3O_4 \cdot 2C_2F_3O_2 \cdot 4C_2H_3N$	$3C_{24}H_{31}O_4N_3 \cdot 7H_2O$
Temperature (K)	100	100	100
Wavelength (Å)	0.7	0.7	0.7
Crystal system	Orthorhombic	Triclinic	Triclinic
Space group	*P 2₁ 2₁ 2₁*	*P 1*	*P 1*
a (Å)	5.181(1)	11.780(2)	5.820(1)
b (Å)	15.416(3)	14.550(3)	18.780(4)
c (Å)	30.759(6)	24.060(5)	19.030(4)
α (°)	90	96.53(3)	117.10(3)
β (°)	90	92.79(3)	91.60(3)
γ (°)	90	100.15(3)	90.57(3)
V (Å^3)	2456.7(8)	4023(1)	1850.3(8)
Z, ρcalc (g/cm^3)	4, 1.237	1, 1.216	1, 1.275
μ (mm^{-1})	0.078	0.069	0.059
F (000)	984	1914	764
Data collection θ range	1.304 - 28.217	1.55 - 28.34	1.185 - 28.646
Refl. Collected / unique	43163 / 6026	59206 / 18224	18026 / 18026
Rint	0.075	0.0614	0.083
Completeness (%)	96.2	88.0	94.6
Data/Restraints/Parameters	6026 / 0 / 304	18224 / 3 / 1932	18026 / 115 / 1005
GooF	1.032	1.052	1.033
R1, wR2 [I>2σ(I)]	0.0545 / 0.1621	0.0928 / 0.2476	0.0454 / 0.1147
R1, wR2 all data	0.0615 / 0.1712	0.1109 / 0.2647	0.0534 / 0.1207

Table 3.10: Crystallographic data for **1a**, **3a** and **5a**.

2b – ^{L}Leu-^{D}Phe(4I)-^{D}Phe in solution and in gel

Crystals of the peptide were obtained both from an acetonitrile/methanol solution, by addition of water as precipitant, and from a gel, after aging. The two crystal forms are isomorphous, with three molecules of the peptide in its zwitterion form in the asymmetric unit. Each crystal structure contains also some residual electron density, where 5 water molecules were fitted and refined. A total of 12 molecules were present in the unit cell of each crystal and two of them were obtained applying the symmetry elements of the ***P2₁2₁2₁*** space group (*Figure 3.40*). In the following discussion, the structure of the crystals obtained from the acetonitrile/methanol solution will be considered due to their better crystallographic statistical data. However, conclusions apply to both crystal structures, since they were isomorphous (*Figure 3.41*). The crystallographically independent peptide molecules shared the same conformation of both backbone and side chains (*Figure 3.42*).

The crystal packing showed a clear separation of hydrophobic and hydrophilic regions (Figure 3.43). Hydrophilic interactions were present between peptides and water molecules, forming piles of peptides in the *b* crystallographic direction (*Figure 3.44*). Peptides that interact were oriented in a parallel fashion. In addition, more hydrophilic interactions were responsible for the formation of a close network of peptides developing along the *a* crystallographic direction (*Figure 3.45*). For all

crystallographically independent peptides, there was a single water molecule positioned in the center of the peptide that binds through salt bridge interactions both the N- terminus and the C- terminus of the same peptide (*Figure 3.45*, blue dashes). Considering that the closest iodine-iodine distance is 5.5 Å, no significant halogen-halogen interactions were expected to drive the crystal packing.

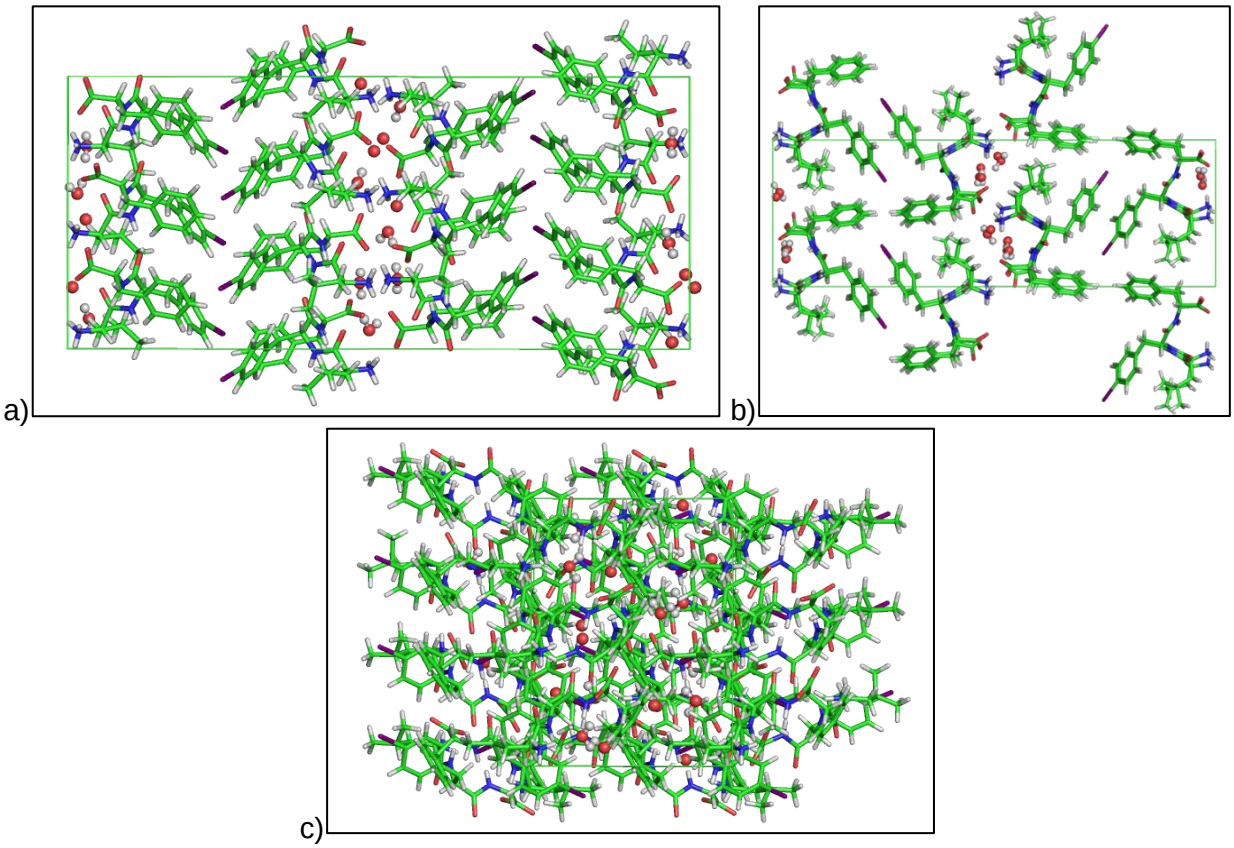

Figure 3.40 Unit cell of crystal of the peptide 2b obtained from a acetonitrile/methanol solution.
Crystal packing in the crystal of the peptide **2b**. Views along the *a* crystallographic axis (a), the *b* crystallographic axis (b) and the *c* crystallographic axis (c). Peptide molecules are shown as sticks, water molecules are shown as spheres.

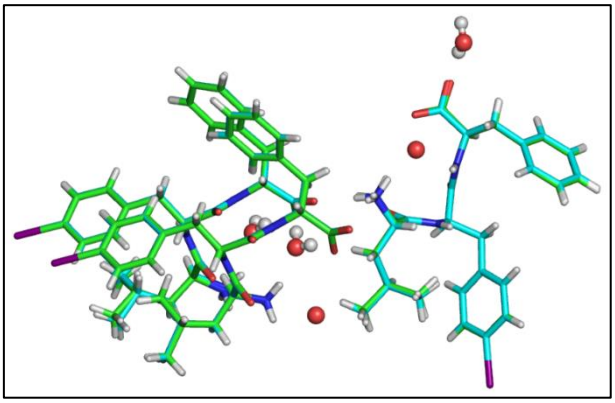

Figure 3.41 Comparison between the crystal forms of 2b obtained in solution and in gel.
The isomorphous crystals obtained from a acetonitrile/methanol solution and from an aged gel show identical conformations of the peptides, positions of peptides and water molecules. Different colors, green and cyan, represent the crystal forms obtained in the gel and in the solution, respectively.

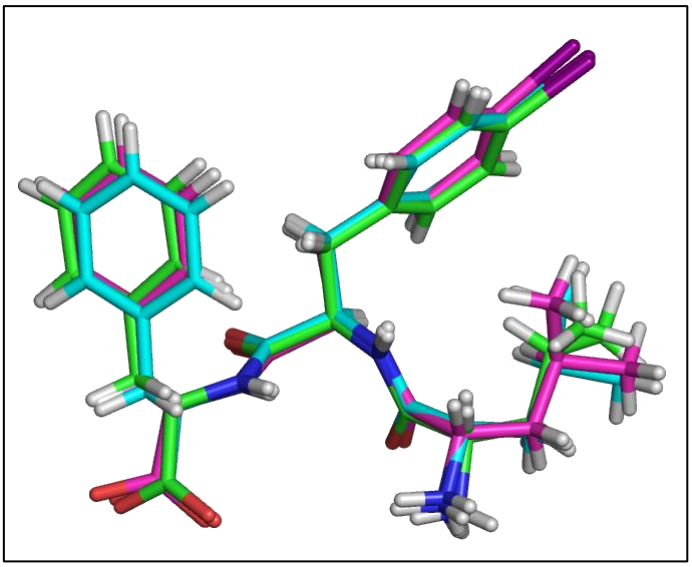

Figure 3.42 Conformation of the 3 crystallographically independent peptides 2b.
The three crystallographically independent molecules of the peptide show an identical conformation of backbone and side chains. Independent molecules are superimposed with different colors for their carbon atoms.

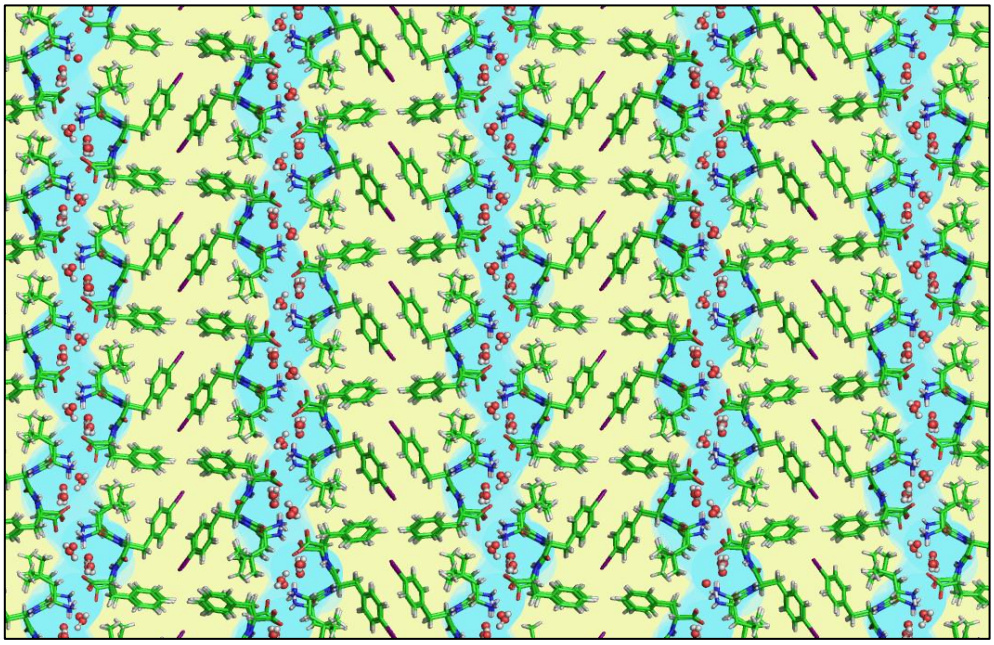

Figure 3.43 Crystal packing with alternating hydrophilic and hydrophobic regions of 2b peptide.
Hydrophilic and hydrophobic layers in the crystal of **2b**. Hydrophobic layers are shown with a yellow background, hydrophilic layers with a blue background. Crystal packing is shown in the plane perpendicular to the *b* crystallographic direction.

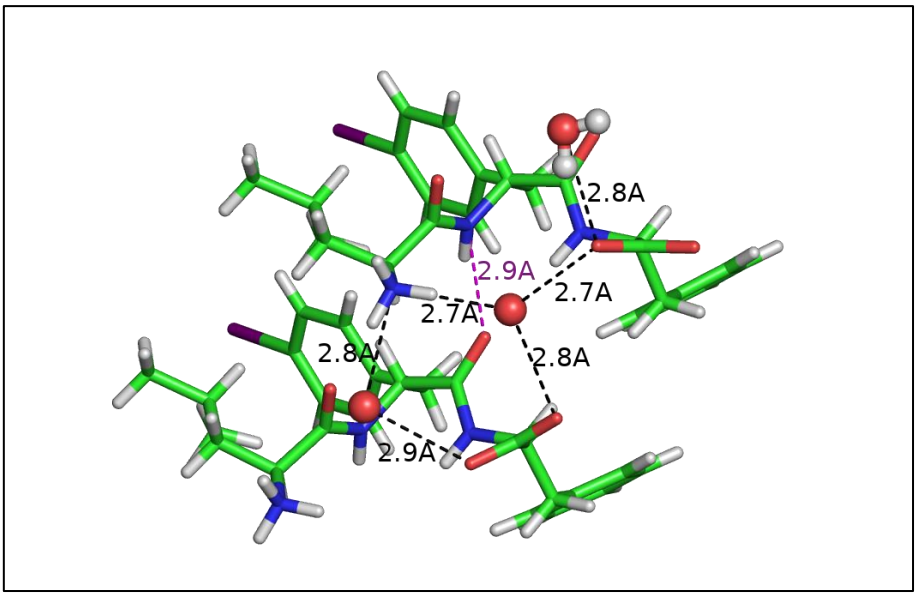

Figure 3.44 Hydrophilic interactions connecting peptides 2b along the *b* crystallographic direction.
Most of the hydrogen bond and salt bridge interactions are mediated by water molecules, connecting two different peptides (black dashes). A single direct interaction between the peptide is present, namely a hydrogen bonding interaction between the amide group of the second residue and the carboxylate of the second residue of a different peptide (magenta dashes). Peptide backbones are oriented in the same direction. Donor-acceptor distances are reported.

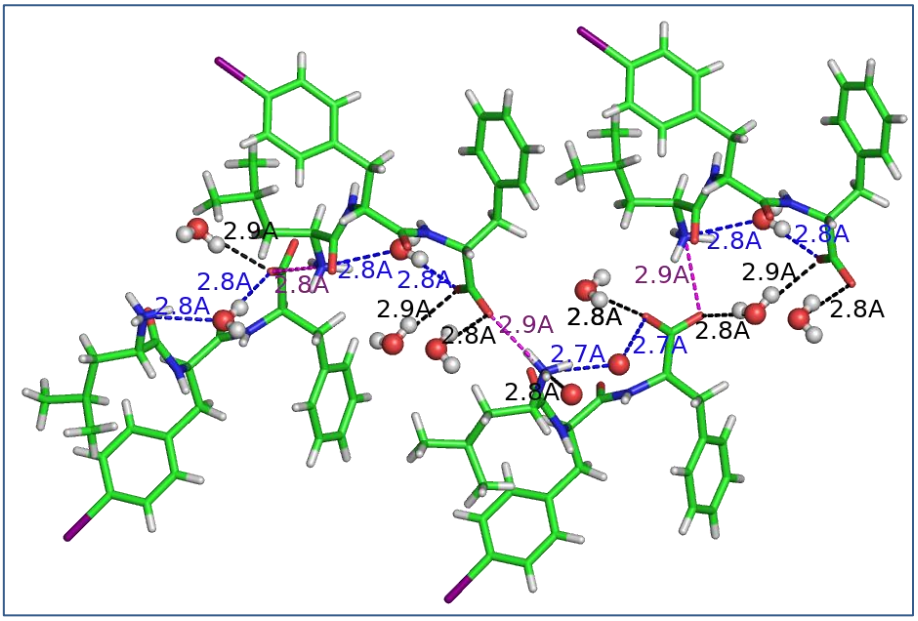

Figure 3.45 Hydrophilic interactions connecting peptides 2b along the *a* crystallographic direction.
Direct salt bridges interactions involving the N- and C- termini of different peptides (magenta dashes) and interactions between the N- and C-termini mediated by water molecules (black dashes) contribute to the formation of a close network of interactions developing along the *a* crystallographic direction. In addition, for all the crystallographically independent peptides, a single water molecule binds both the N- and the C- termini of the same peptide (blue dashes). Distances between oxygen and nitrogen atoms are shown.

Crystallographic details.

A stick-shaped single crystal of the peptide was collected from an acetonitrile/methanol solution with a loop and cryoprotected by dipping the crystal in glycerol. A similar crystal was obtained in a vial containing a gel of the peptide, after 2 weeks of aging the gel. The gel-embedded crystal was collected with a loop, the gel was coarsely removed, and the crystal was dipped in glycerol, used as cryoprotectant during data collection. A total of 360 images were collected for the crystal grown in the acetonitrile/methanol solution, while 180 images were collected for the crystal embedded in the gel. Reflections were indexed and integrated using the XDS package, space group $\boldsymbol{P2_12_12_1}$ was determined using POINTLESS and the resulting data set was scaled using AIMLESS.[119,120,124] Unit cell parameters and scaling statistics are reported in Table 2. The asymmetric unit of each structure contained 3 molecules of the peptide and 5 molecules of water. Data obtained from the crystal grown in acetonitrile/methanol solution showed higher completeness compared with data from the crystal grown in gel, therefore the former were used for the discussion. For the structure of the crystal grown in acetonitrile/methanol solution, all atoms, except the hydrogen atoms, within the asymmetric unit have been refined with anisotropic thermal parameters. Hydrogen atoms of the peptide molecules were added at geometrically calculated positions and refined isotropically, with thermal parameters dependent on those of the attached atom. Hydrogen atoms of 3 water molecules were located considering interactions with neighboring molecules and residual electron density. Hydrogen atoms of the remaining 2 water molecules could not be located. Refinement statistics are reported in *Table 3.11*.

4c – ^{D}Leu-^{D}Phe-^{D}Phe(4I) in buffer solution and in gel

Crystals of the peptide were obtained both from a phosphate buffer solution and from a gel, after aging. The two crystal forms were isomorphous, with two molecules of the peptide in its zwitterion form in the asymmetric unit. Each crystal structure contained also some residual electron density, where two water molecules were fitted and refined. A total of 4 molecules were present in the unit cell of each crystal and two of them are obtained applying the symmetry elements of the $P2_1$ space group (*Figure 3.46*). In the following discussion, the structure of the crystals obtained by aging the gel will be considered due to their better crystallographic statistical data. However, conclusions apply to both crystal structures, since they were isomorphous (*Figure 3.47*). The crystallographically independent peptide molecules showed a similar conformation of the backbone, but very different orientations of the side chains (*Figure 3.48*).

The crystal packing showed an interdigitated arrangement of hydrophobic groups and hydrophilic regions (*Figure 3.49*). Hydrophilic interactions were present between the peptides, namely hydrogen bonds between the carbonyl and the amide moieties (*Figure 3.50*, black dashes) and salt bridges between the N-terminus and the C-terminus of different peptides (*Figure 3.50*, red dashes). Such interactions allowed the formation of stacked piles of peptides along the *a* crystallographic direction. The backbones of adjacent stacked peptides pointed in opposite directions, allowing for the formation of couples of peptides with 2 strong salt bridge interactions involving the N- and C- termini of both the peptides. The structure showed also the presence of hydrophobic interactions, mainly CH-π interactions involving the phenyl moieties of the phenylalanine residues (*Figure 3.51*, black dashes). The presence of the iodine atoms allowed the formation of a cation-dipole interaction with a prevalent electrostatic character, formed between the amino-terminal charged group of a peptide and the iodine atom of another peptide (*Figure 3.51*, red dashes).

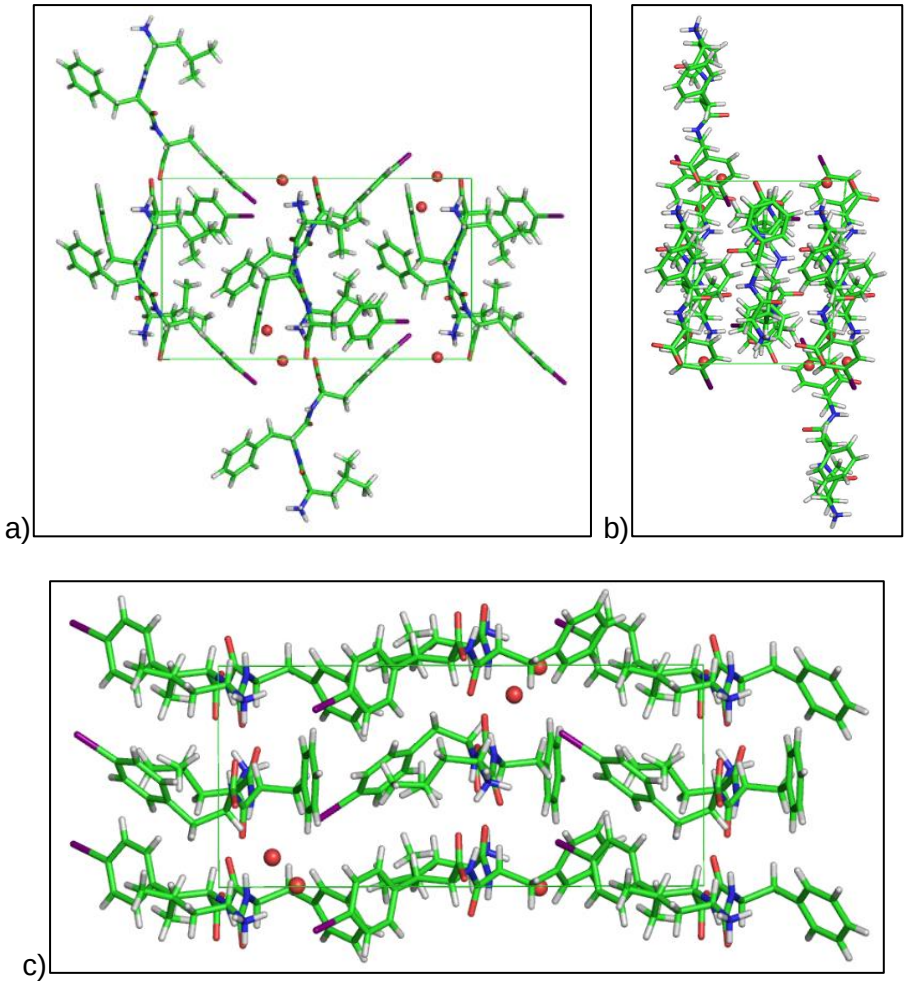

Figure 3.46 Unit cell of crystal of the peptide 4c obtained by aging a gel.
Crystal packing in the crystal of the peptide **4c**, grown in an aged gel. Views along the *a* crystallographic axis (a), the *b* crystallographic axis (b) and the *c* crystallographic axis (c). Peptide molecules are shown as sticks, water molecules are shown as spheres.

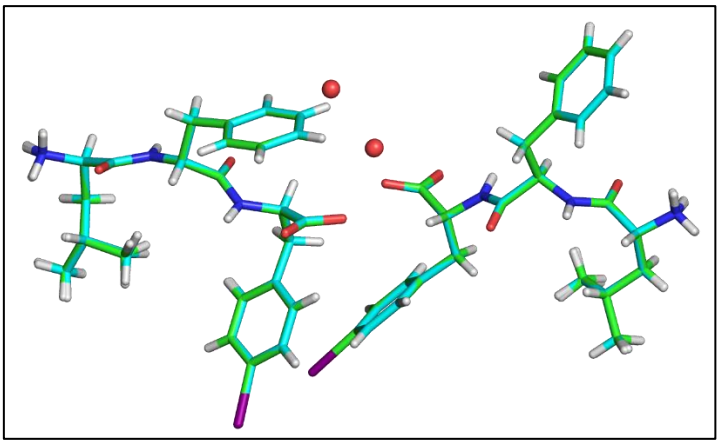

Figure 3.47 Comparison between the crystal forms obtained in buffer solution and by aging a 4c gel.
The conformation of the peptides, their position and the position of the water molecules are identical in the crystals of **4c** obtained from the buffer solution and from the gel. Different colors, green and cyan, represent the crystal forms obtained in the gel and in the solution, respectively.

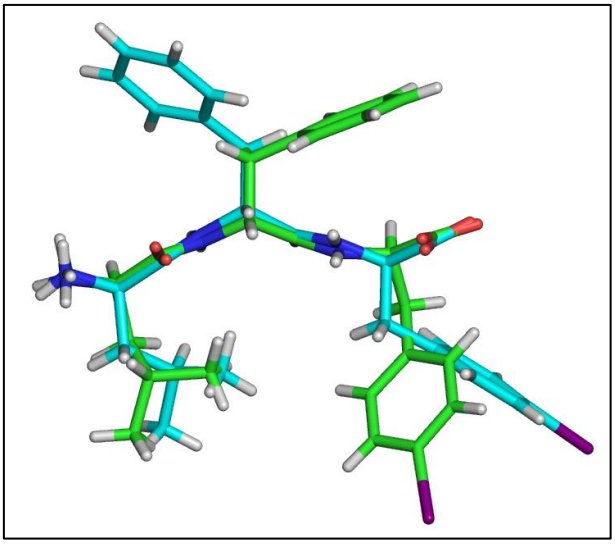

Figure 3.48 Conformation of the 2 crystallographically independent peptides 4c.
The two crystallographically independent molecules of the peptide show an identical conformation of the backbone, but very different torsion angles in the side chains, particularly regarding the phenylalanine residues. The independent molecules are superimposed and their carbon atoms are colored with different colors.

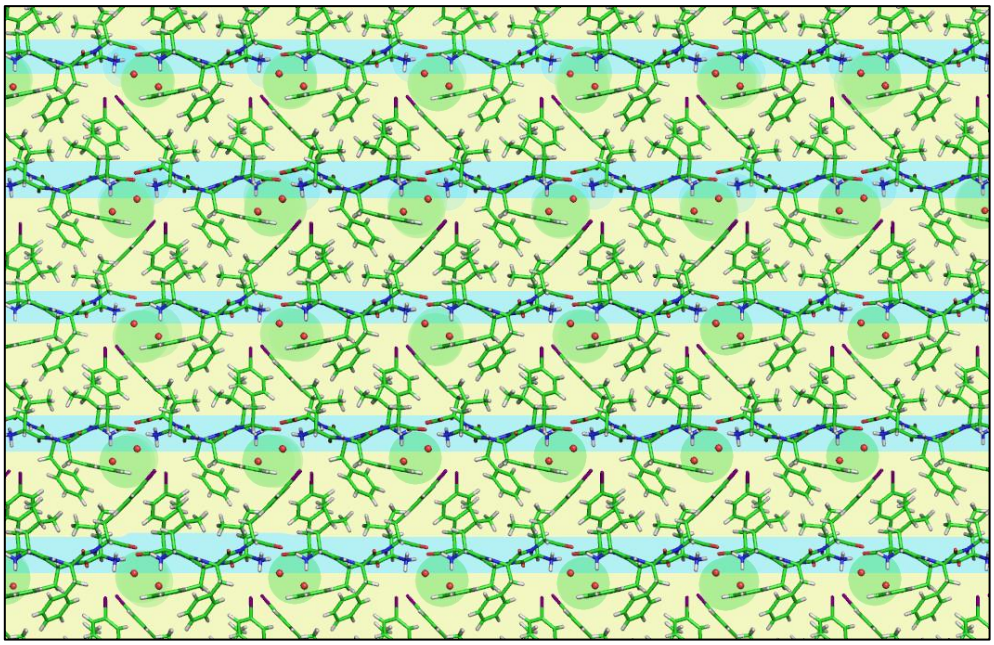

Figure 3.49 Crystal packing of the 4c peptide.
In the crystal packing, hydrophilic and hydrophobic groups are interdigitated, forming an amphipathic structure. Regions with a prevalent hydrophilic character are depicted with a blue background, regions with a prevalent hydrophobic character are shown with a yellow background. The presence of water molecules between the hydrophilic groups and the hydrophobic regions is highlighted with a green background.

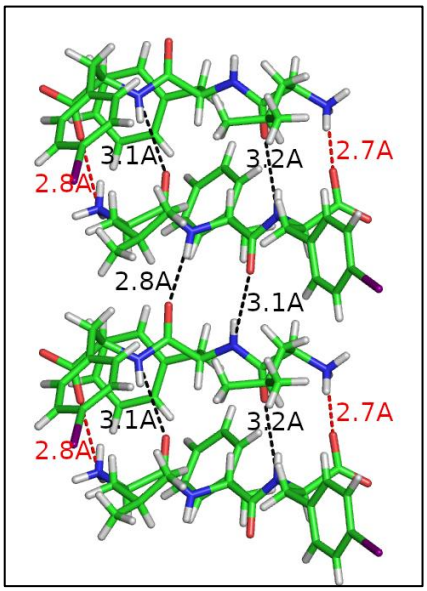

Figure 3.50 Hydrophilic interactions of peptides 4c forming antiparallel stacks of peptides.
Stacks of peptides are present in the *a* crystallographic direction and held together by hydrophilic interactions, with an antiparallel arrangement of the backbones. Salt bridges interactions involving the N- and C- termini of the peptides are shown as red dashes, hydrogen bonding interactions as black dashes. Distances between carbon and nitrogen atoms involved in the salt bridge or hydrogen bond interactions are reported.

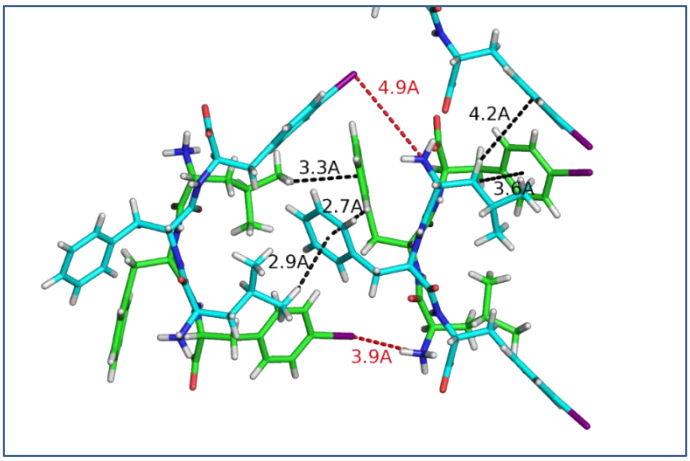

Figure 3.51 Hydrophobic CH-π and electrostatic I-NH$^+$ interactions of peptide 4c.
Besides hydrogen bonds and salt bridges, further interactions are observed in the structure of **4c**, namely CH-π interactions involving the phenyl ring of phenylalanine residues (black dashes), with a prevalent hydrophobic character, and cation-dipole interactions between the N-terminal positive group and the iodine atom (red dashes), with a significant electrostatic character. Distances from the hydrogen atom to the center of the phenyl ring are reported for the CH-π interactions, and between the nitrogen to the iodine atoms for the cation-dipole interactions.

Crystallographic details.

A plate-shaped single crystal of the peptide was collected from a phosphate buffer solution at pH7 with a loop and cryoprotected by dipping the crystal in glycerol. A similar crystal was obtained in a vial containing a gel of the peptide, after 12-24 hours of aging the gel. The gel-embedded crystal was collected with a loop, the gel was coarsely removed and the crystal was dipped in glycerol, used as cryoprotectant during the data collection. A total of 360 images were collected for each of the crystals. Reflections were indexed and integrated using the XDS package, space group ***P2₁*** was determined using POINTLESS and the resulting data set was scaled using AIMLESS.[119,120,124] The unit cells of the two different crystals were isomorphous. Phase information were obtained for both crystals separately by direct methods using the software SHELXT.[121] Refinements cycles were conducted with SHELXL-14, operating through the WinGX GUI, by full-matrix least-squares methods on F^2. Unit cell parameters and scaling statistics are reported in *Table 3.11*.[121,122] The asymmetric unit of each structure contained 2 molecules of the peptide and 2 molecules of water. Data obtained from the crystal grown in gel showed higher completeness compared with data from the crystal grown in buffer solution, therefore the former were used for the discussion. For the structure of the crystal grown in gel, all the atoms, except the hydrogen atoms, within the asymmetric unit have been refined with anisotropic thermal parameters. Hydrogen atoms of the peptide molecules were added at geometrically calculated positions and refined isotropically, with thermal parameters dependent on those of the attached atom. Hydrogen atoms of the water molecules could not be located. Refinement statistics are reported in *Table 3.11*.

	2b in solution	**2b** in gel	**4c** in solution	**4c** in gel
Formula	$3C_{24}H_{30}IN_3O_4 \cdot 5H_2O$	$3C_{24}H_{30}IN_3O_4 \cdot 5H_2O$	$C_{24}H_{30}IN_3O_4 \cdot H_2O$	$C_{24}H_{30}IN_3O_4 \cdot H_2O$
Temperature (K)	100	100	100	100
Wavelength (Å)	0.7	0.7	0.7	0.7
Crystal system	Orthorhombic	Orthorhombic	Monoclinic	Monoclinic
Space group	*P 2₁ 2₁ 2₁*	*P 2₁ 2₁ 2₁*	*P 2₁*	*P 2₁*
a (Å)	12.506(3)	12.545(2)	9.670(2)	9.680(2)
b (Å)	16.549(3)	16.534(3)	21.166(4)	21.196(4)
c (Å)	37.856(8)	37.844(4)	12.390(3)	12.402(3)
α (°)	90	90	90	90
β (°)	90	90	95.47(3)	95.50(3)
γ (°)	90	90	90	90
V (Å^3)	7835(3)	7850(2)	2524.4(9)	2532.9(9)
Z, ρcalc (g/cm^3)	4, 1.479	4, 1.476	4, 1.493	4, 1.493
μ (mm^{-1})	1.267	1.264	1.307	1.090
F (000)	3544	3520	1125	1125
Data collection θ range	1.06 - 29.99	1.06 - 28.219	1.626 - 28.244	1.625 - 28.221
Refl. Collected / unique	93679 / 23219	62841 / 18873	41662 / 12040	41619 / 12789
Rint	0.0959	0.0854	0.0412	0.0592
Completeness (%)	98.7	95.0	93.9	99.1
Data/Restraints/Parameters	23219 / 48 / 943	18873 / 0 / 919	12040 / 1 / 281	12789 / 1 / 601
GooF	0.983	1.097	1.233	1.076
R1, wR2 [I>2σ(I)]	0.0474 / 0.1268	0.0718 / 0.2096	0.0444 / 0.1111	0.0883 / 0.2121
R1, wR2 all data	0.0539 / 0.1301	0.0831 / 0.2166	0.0448 / 0.1112	0.091 / 0.2163

Table 3.11 Crystallographic data for **2b** crystals, grown in solution and in gel, and **4c** crystals, grown in solution and in gel.

2f – ^{L}Leu-^{D}Phe(4I)-^{D}Phe(4F)

The asymmetric unit of the crystal contains a single molecule of the peptide in its zwitterion form. The additional electron densities present in the asymmetric unit were recognized as 2 molecules of water, present in the buffer solution from which the crystals grew. Both the water molecules were refined with occupancy factors of 90%, taking into account the large thermal parameters observed. Considering that the space group of the crystal is ***P2₁2₁2₁,*** the unit cell of crystals of **2f** obtained from a phosphate buffer solution at pH 7 contains a total of 4 molecules of peptide and 8 molecules of water (*Figure 3.52*).

In the crystal packing (*Figure 3.53*), mainly hydrophobic and mainly hydrophilic regions were separated. In addition, the segregation of the halogen atoms in a specific region (with a purple background in *Figure 3.53*) was visible. Many hydrophilic interactions, hydrogen bonds and salt bridges, were present in the structure and involved both peptide molecules and water molecules (*Figures 3.54* and *3.55*). For each peptide, a single water molecule interacted with both the N- and C-termini (blue dashes in *Figure 3.54*). Hydrogen bonding and salt bridge interactions developed in two main directions, i.e. the crystallographic directions *a* (*Figure 3.55*) and *b* (*Figure 3.54*). Hydrophilic interactions are assisted by other types of interactions, among which hydrophobic interactions

involving the π-system of phenyl moieties. In addition, the short distances between the halogen atoms suggested an involvement of halogen-halogen interactions in the crystal packing (*Figure 3.56*).

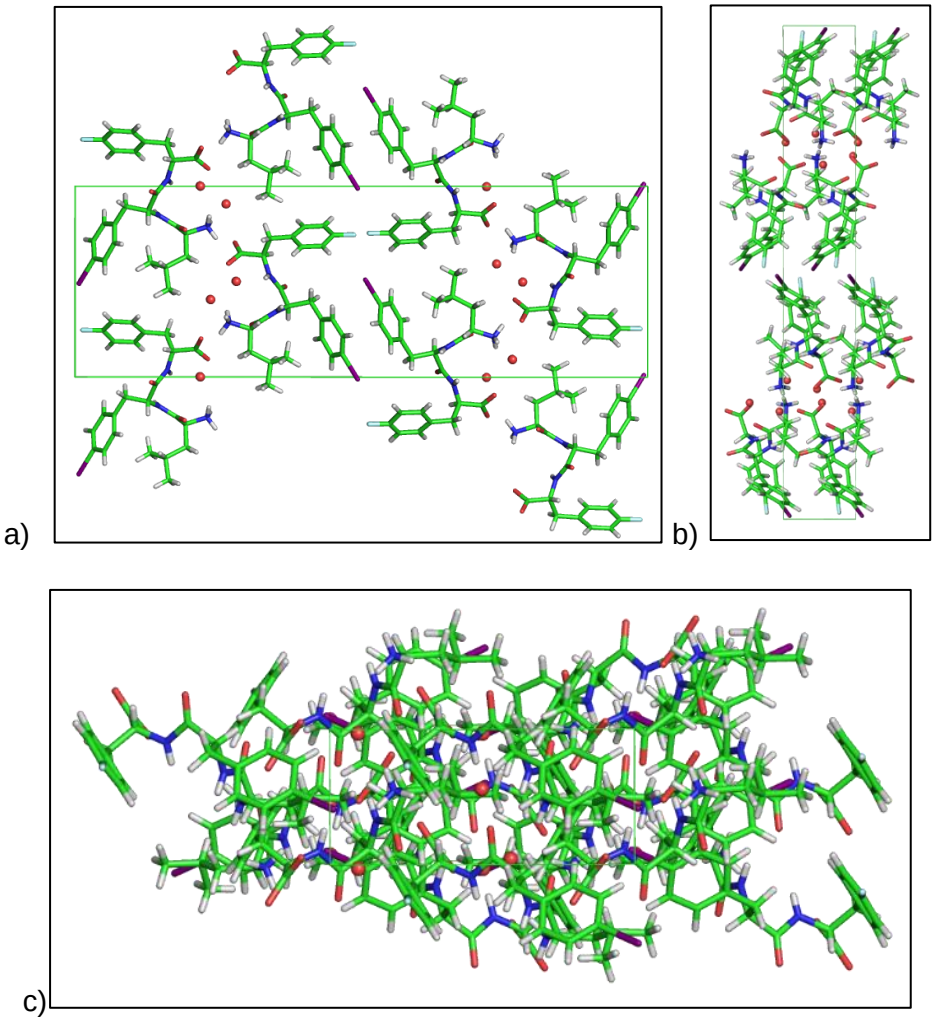

Figure 3.52 Unit cell of crystal of the peptide 2f.
Crystal of the peptide **2f**, obtained from a phosphate buffer solution. Views along the *a* crystallographic axis (a), the *b* crystallographic axis (b) and the *c* crystallographic axis (c). Peptide molecules are shown as sticks, water molecules are shown as spheres.

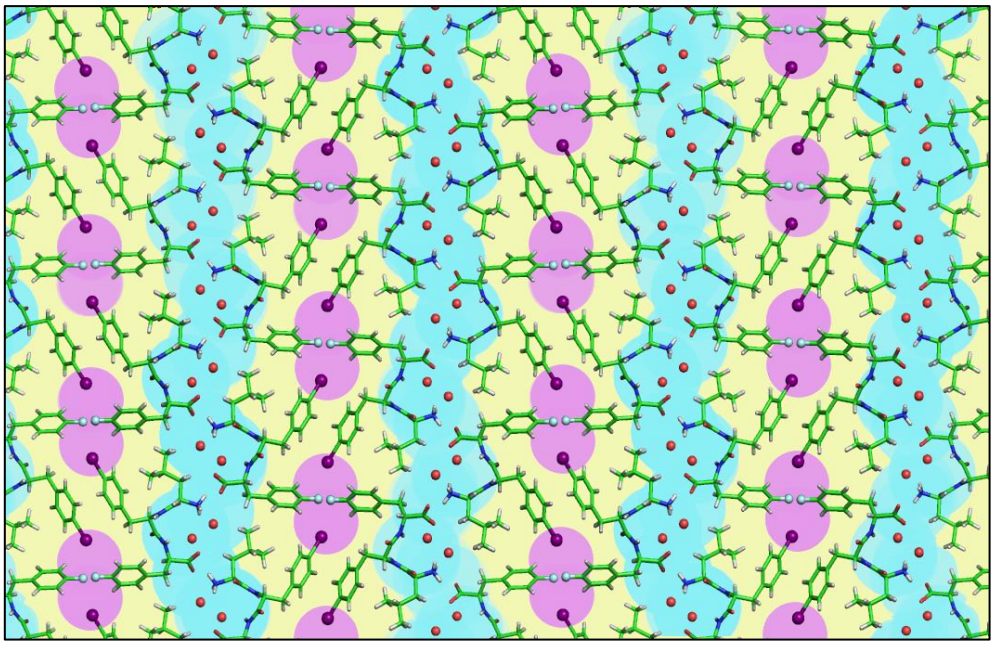

Figure 3.53 Crystal packing of 2f.
The crystal packing of the structure of **2f** shows alternating hydrophilic (blue background) and hydrophobic (yellow background) regions. Within the hydrophobic regions, a segregation of regions with halogen atoms is resent, highlighted with a purple background.

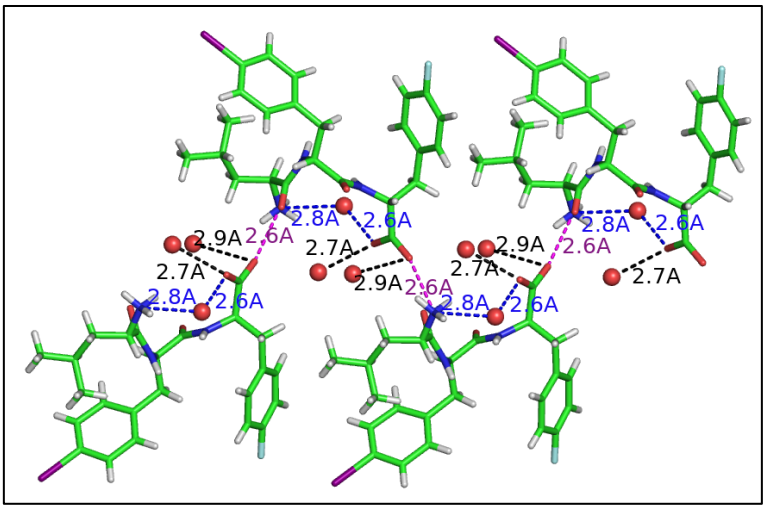

Figure 3.54 Hydrophilic interactions along the *b* crystallographic direction of peptide 2f.
In the hydrophilic regions, salt bridges (in magenta) hold together peptide molecules along the *b* crystallographic direction. Interactions with water molecules contribute to the formation of a hydrophilic environment (in black). A water molecule bridges together the N- and C-terminal groups of the same peptide (in blue). Donor-acceptor distances are reported.

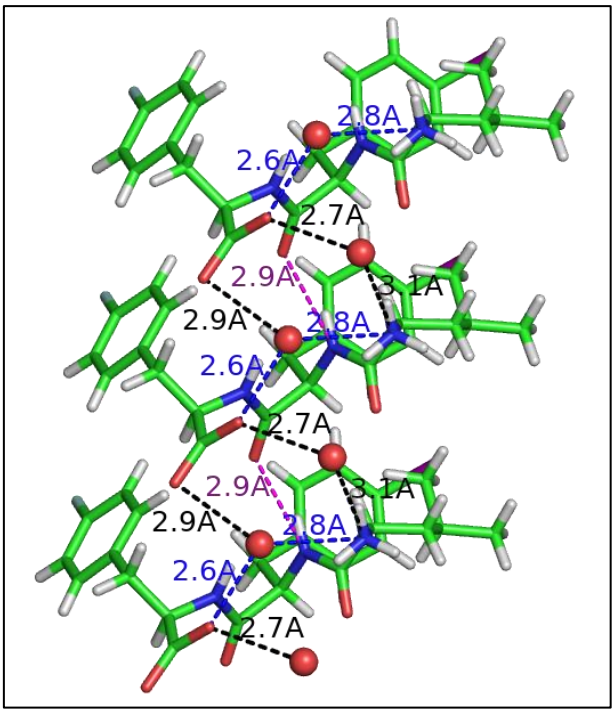

Figure 3.55 Hydrophilic interactions along the *a* crystallographic direction of 2f peptide.
Hydrophilic interactions contributing to crystal contacts in the a crystallographic direction can be divided in peptide-peptide direct interactions (magenta dashes) and peptide-water-peptide interactions (black dashes). In addition, blue dashes show the interactions of a single water molecule with the C- and N-termini of a single peptide. Donor-acceptor distances are reported.

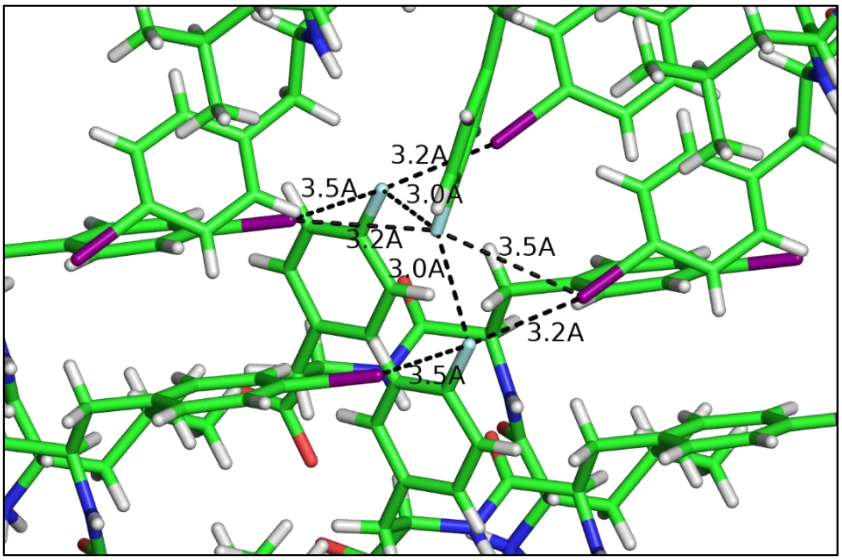

Figure 3.56 Halogen-halogen interactions and distances in the structure of 2f.
Short distances between halogen atoms (iodine atoms in magenta, fluorine atoms in cyan) suggest the presence of halogen-halogen interactions in the structure of **2f**.

Crystallographic details.

A needle-shaped single crystal of the peptide was collected with a loop, cryoprotected by dipping the crystal in glycerol and stored frozen in liquid nitrogen. A total of 270 images were collected. Reflections were indexed and integrated using the XDS package, space group ***$P2_12_12_1$*** was determined using POINTLESS and the resulting data set was scaled using AIMLESS.[119,120,124] Unit cell parameters and scaling statistics are reported in *Table 3.12*.[121,122] The asymmetric united a molecule of the peptide and 2 molecules of water, both of them at 90% occupancy. All the atoms, except the hydrogen atoms, within the asymmetric unit have been refined with anisotropic thermal parameters. Hydrogen atoms of the peptide molecule were added at geometrically calculated positions and refined isotropically. Hydrogen atoms of the water molecules could not be located. In the final refinement, restraints were applied on distances between the Cα carbon atom and the carboxylic carbon of the last residue, and between the same carboxylic carbon and the oxygen atoms, using the DFIX card of the software SHELXL-14.[121] The C-terminal group had higher refined thermal parameters and a lower density in the electron density maps, possibly due to a partial decarboxylation induced by the strong synchrotron radiation during analysis. Refinement statistics are reported in *Table 3.12*.

	2f
Formula	$C_{24}H_{29}FIN_3O_4 \cdot 2H_2O$
Temperature (K)	100
Wavelength (Å)	0.7
Crystal system	Orthorhombic
Space group	*P 2₁ 2₁ 2₁*
a (Å)	5.560(1)
b (Å)	12.585(3)
c (Å)	37.819(8)
α (°)	90
β (°)	90
γ (°)	90
V (Å^3)	2646.3(9)
Z, ρcalc (g/cm^3)	4, 1.502
μ (mm^{-1})	1.192
F (000)	1210
Data collection θ range	1.914 - 21.265
Refl. Collected / unique	5945 / 2893
Rint	0.0906
Completeness (%)	96.6
Data/Restraints/Parameters	2893 / 28 / 318
GooF	1.059
R1, wR2 [I>2σ(I)]	0.066 / 0.1679
R1, wR2 all data	0.1027 / 0.1959

Table 3.12 Crystallographic data for **2f**.

Comparison of the backbone conformation

The backbone conformation of peptides **1a**, **3a**, **5a**, **2b**, **4c** and **2f** was compared using the Ramachandran plot (*Figure 3.57*) to highlight differences between torsion angles of the second residue (phenylalanine) in the different diastereoisomeric peptides (*Table 3.13*). For peptides with chirality D of the second residue, torsion angles of the enantiomer were reported in the Ramachandran plot.

The analysis of the torsion angles of peptides Xaa-Phe-Phe showed that peptides with a opposite chirality of the first residue (D-L-L or L-D-D) have torsion angles compatible with an α-helical secondary structure (or its enantiomer), and such conformation was independent from the nature of the first residue (Leu or Ile) and the presence of substituents in position 4 on the phenylalanine aromatic moieties. On the contrary, both the structures of homochiral Xaa-Phe-Phe peptides showed a conformation compatible with a β-sheet secondary structure.

Figure 3.57 Ramachandran plot reporting the torsion angles of the central residues of tripeptides. For peptides with chirality D of the central residue, i.e. peptides **5a, 2b, 4c** and **2f**, the torsion angles of the enantiomer were reported. For the peptide DLeu-LPhe-LPhe (**1a**), the enantiomer of peptide LIle-DPhe-DPhe (**5a**), the enantiomer of peptide LLeu-DPhe(4I)-DPhe (**2b**), and the enantiomer of peptide LLeu-DPhe(4I)-DPhe(4F) (**2f**), torsion angles are compatible with a secondary structure of an α-helical secondary structure. The torsion angles of peptide LLeu-LPhe-LPhe (**3a**) and the enantiomer of peptide DLeu-DPhe(4I)-DPhe (**4c**) are compatible with a β-sheet secondary structure

	n=1	n=2		n=3
Compound name	ψ:N_n-Cα_n-C_n-N_{n+1}	φ:C_{n-1}-N_n-Cα_n-C_n	ψ:N_n-Cα_n-C_n-N_{n+1}	φ:C_{n-1}-N_n-Cα_n-C_n
1a	-136,55	-68,9	-46,56	-162,08
3a	140.91	-129.85	125.08	-121.53
	124.23	-128.9	135.15	-150.36
	125.34	-122.75	130.24	-149.85
	140.05	-130.96	120.9	-125.48
	124.04	-118.49	134.53	-150.63
	124.56	-130.13	134.07	-152.26
5a	141.55	74	27.04	69.88
	134.88	76.17	34.58	63.69
	138.26	78.31	27.44	71.2
2b	136.68	76.29	30.01	110.69
	125.8	74.9	24.06	102.89
	129.65	77.32	27.95	102.48
4c	-158.65	146.31	-139.65	145.73
	-131.83	122.9	-138.57	152.66
2f	127.66	77.83	25.66	101.72

Table 3.13 Torsion angles in the structures of **1a**, **3a**, **5a**,**2b**, **4c** and **2f**.

3.2.4.2. XRD structures of Phe-Xaa-Phe group sequence

13e – ^{D}Phe-^{L}Nle-^{D}Phe(4F)

The asymmetric unit contains a single molecule of the peptide in its zwitterionic form and three molecules of water, recognized in the residual electron density. However, the presence of large channels along the *c* crystallographic direction (*Figure 3.58*) indicated that more solvent is present in the unit cell, albeit the position of the additional solvent is not fixed in each asymmetric unit and, therefore, cannot be recognized in the crystal structure. A total of 6 molecules of peptide, related by symmetry operators of the $P6_3$ space group, are present in the unit cell (*Figure 3.59*). A similar structure was obtained for the Phe-Nva-Phe peptide, with opposite chirality compared to **13e** (L-D-L).[56] A superimposition of the two structures of the ^{L}Phe-^{D}Nva-^{L}Phe and of the enantiomer of **13e**, the peptide ^{L}Phe-^{D}Nle-^{L}Phe(4F), revealed the high degree of similarity (*Figure 3.60*).

The crystal packing showed a separation between regions with prevalence of hydrophobic groups, i.e. the phenyl moieties and the nor-leucine side chains, and the large channels filled with disordered solvent molecules and surrounded by the hydrophilic groups of the peptides (*Figure 3.58*). Channel diameter was of about 20 Å. Smaller channels were present in the hydrophobic regions of the structure, formed by the side chain groups of the peptide, with a triangular shape and a dimension of about 6 Å (*Figure 3.58*). Despite the lack of electron density observed in these smaller channels, it is likely that their space is filled with disordered solvent molecules. The main hydrophilic interactions observed in the crystal are salt bridges between the N- and C-terminal moieties of adjacent peptides (*Figure 3.61, blue dashes*), and hydrogen bond that connect peptides along the *c* crystallographic direction (*Figure 3.56*, black dashes). While the former was responsible for the formation of the large apertures in the crystal, the latter allowed for the stack of peptides in the perpendicular direction. Few additional hydrophilic interactions connected water molecules to the polar groups of the peptides (*Figure 3.61*, magenta dashes). Hydrophobic CH-π and π-π interactions between the side chains contributed to the crystal packing (*Figure 3.62*).

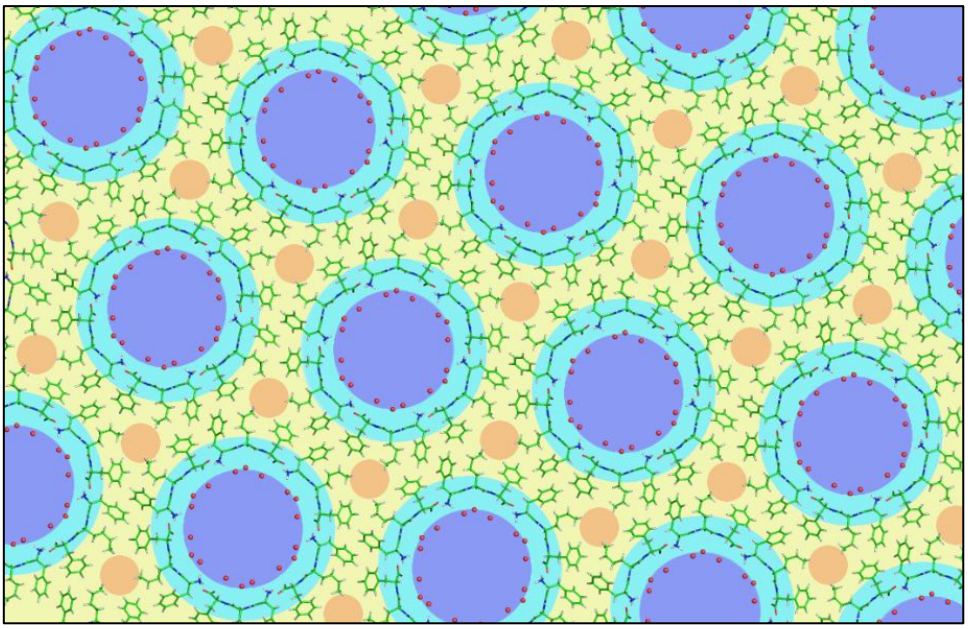

Figure 3.58 Crystal packing with large hydrophilic channels and smaller hydrophobic ones of peptide 13e.
The **13e** peptide forms crystals with large channels (dark blue areas) surrounded by the hydrophilic moieties of the peptide (light blue areas). Within the hydrophobic parts of the structure (yellow areas), smaller channels are formed (orange areas), with highly hydrophobic surroundings.

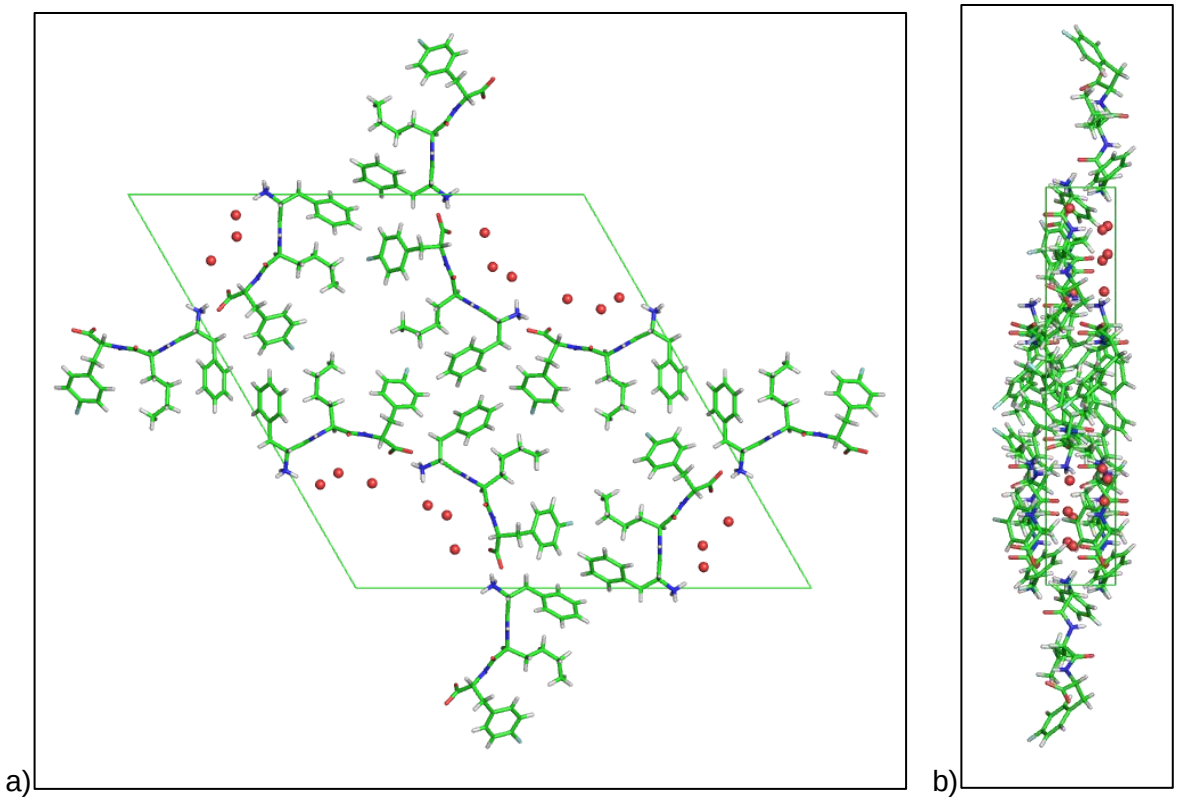

Figure 3.59 Unit cell of crystals of 13e.
Crystal packing in the crystal of the peptide **13e**. Views along the *a* crystallographic axis (a) and the *b* crystallographic axis (b). Peptide molecules are shown as sticks, water molecules are shown as spheres. Carbon atoms are shown in green, oxygen atoms in red, nitrogen atoms in blue, hydrogen atoms in white, and fluorine atoms in light blue.

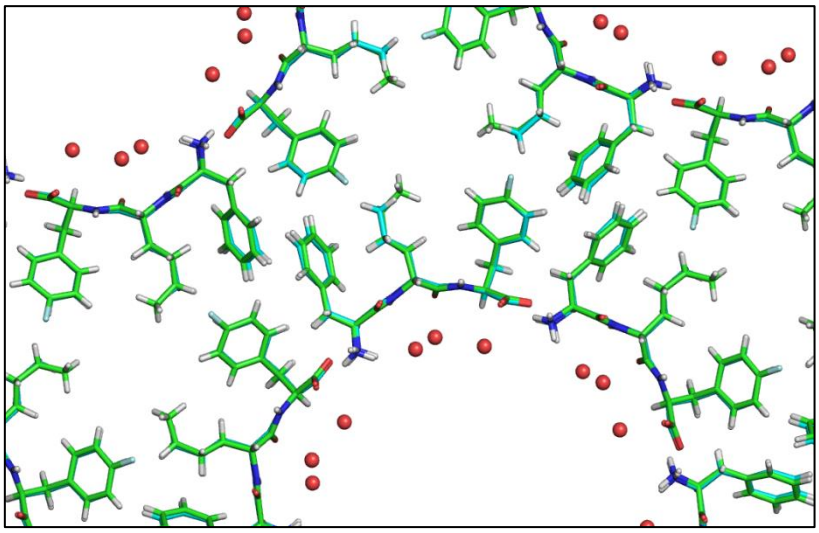

Figure 3.60 Comparison between the structures of ^{L}Phe-^{D}Nle-^{L}Phe(4F) and ^{L}Phe-^{D}Nva-^{L}Phe (from [1]).
Superimposition between the model structure of ^{L}Phe-^{D}Nle-^{L}Phe(4F) (in cyan), obtained from the crystal structure of its enantiomer **13e**, and the crystal structure of the ^{L}Phe-^{D}Nva-^{L}Phe peptide (from ref. [1]) reveals the high degree of similarity, both regarding the peptide conformation and the crystal packing.

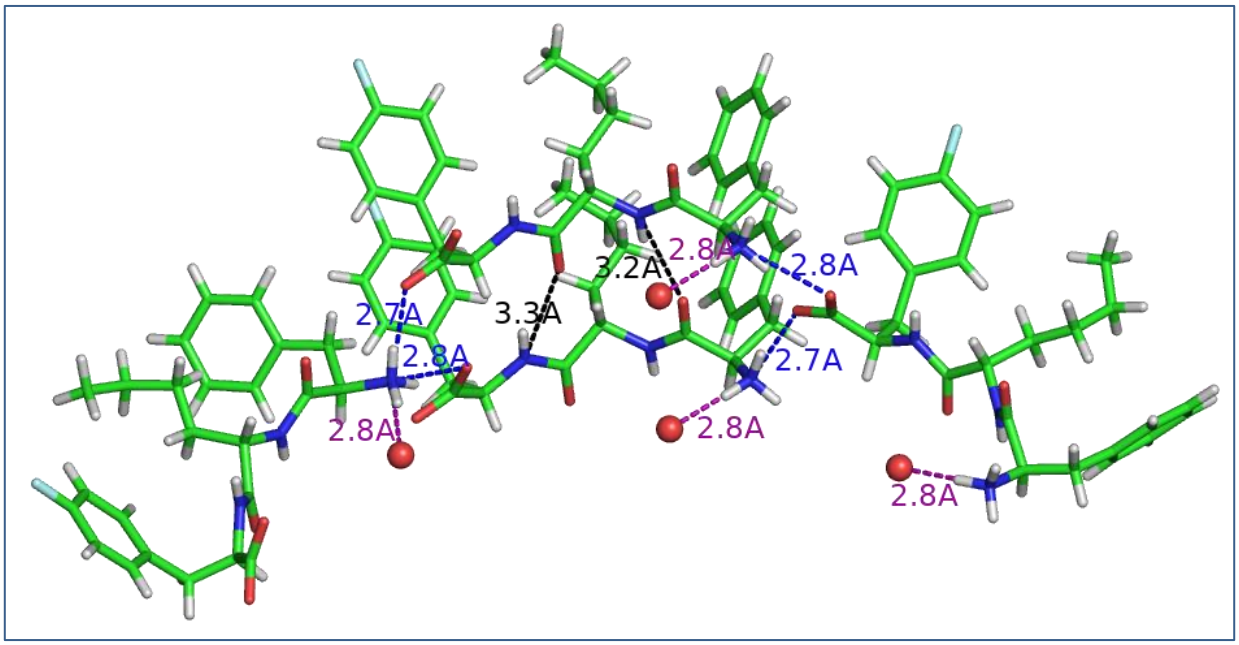

Figure 3.61 Hydrophilic interactions in the structure of 13e.
Salt bridges are the strongest interactions observed in this structure and involve N-terminal and C-terminal moieties of peptides (blue dashes). Their geometry allows the formation of the large solvent-filled channels present in the structure. In addition, weaker hydrogen bond interactions connect peptides along the *c* crystallographic direction (black dashes). Another hydrophilic interaction involves the N-terminal group of the peptide and a water molecule (magenta dashes).

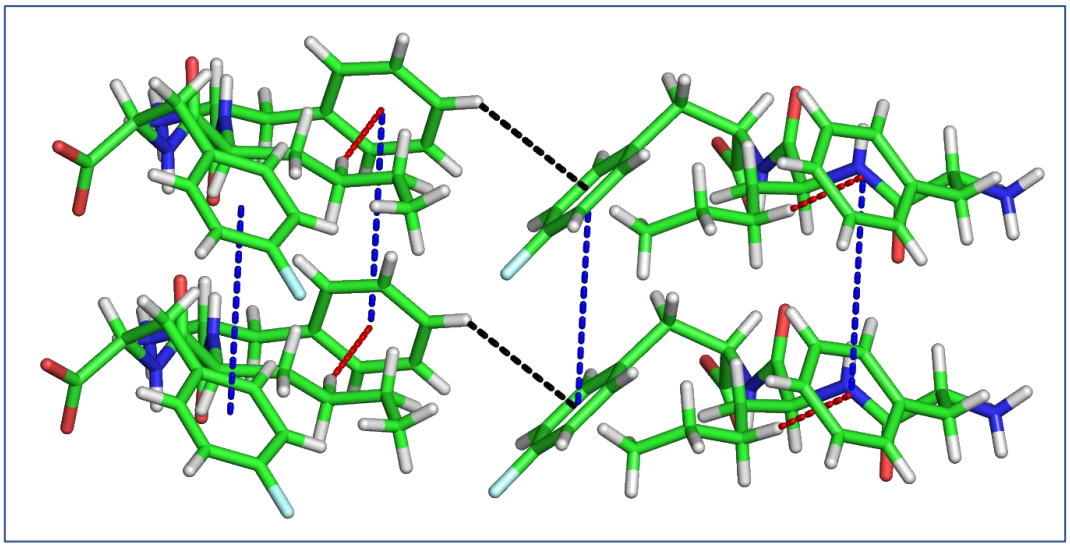

Figure 3.62 Hydrophobic interactions in the structure of 13e.
Strong CH-π intramolecular interactions are formed between the nor-leucine side chain (second residue) and the phenylalanine side chain (first residue), shown as red dashes, with a distance between the hydrogen atom and the center of the phenyl ring of 2.8 Å. Additional CH-π interactions involve an aromatic hydrogen of the first residue and the 4-fluorophenylalanine residue of a different peptide (black dashes), at a distance of 3.6 Å (hydrogen atom-center of the phenyl ring). π-π interactions between the aromatic rings of the phenylalanine and 4-fluorophenylalanine residues along the c crystallographic direction are shown as blue dashes and have a phenyl center-phenyl center distance of 5.0 Å

Crystallographic details.

A needle-shaped single crystal of the peptide was collected with a loop, cryoprotected by dipping the crystal in glycerol, and stored frozen in liquid nitrogen. Reflections were indexed and integrated using the XDS package, space group $P6_3$ was determined using POINTLESS and the resulting data set was scaled using AIMLESS.[118–120] Unit cell parameters and scaling statistics are reported in *Table 3.14*. In the asymmetric unit a single molecule of the peptide and 3 molecules of water were recognized in the electron density. Hydrogen atoms of the peptide molecule were added at geometrically calculated positions and refined isotropically, with thermal parameters dependent on those of the attached atom. Hydrogen atoms of the water molecules could not be located. All the atoms, except the hydrogen atoms, within the asymmetric unit have been refined with anisotropic thermal parameters. Restrains on the distances between carbon atoms in the nor-leucine side chain were applied during refinement using the DFIX card of the software SHELXL-14.[121] Disordered solvent molecules present in the large cavities of the structure were too difficult to be modelled, but their contribution was taken into account using the SQUEEZE/PLATON procedure.[125] Residual electron densities corresponding to 261 electrons/cell were found in the voids of the structure, corresponding to 25% of the cell volume. Refinements using reflections modified by the SQUEEZE procedure behaved well and R-factors were reduced from 11% to 8%. Refinement statistics are reported in *Table 3.14*.

9c – ^{D}Phe-^{L}Nle-^{L}Phe(4I)

The asymmetric unit of the crystal contains a molecule of the peptide in its zwitterion form. The additional electron densities present in the asymmetric unit were recognized as a molecule of 2-propanol and 2 molecules of water, used in the crystallization experiment. Considering that the space group of the crystal is ***P2$_1$***, the unit cell contained two molecules of the peptide, related by a 2-fold screw axis (*Figure 3.63*). In the crystal packing (*Figure 3.64*), mainly hydrophobic and mainly hydrophilic regions were separated, with hydrophilic moieties of the peptides and of the alcohol molecules forming small hydrophilic channels. Hydrophilic groups of the peptide interacted with the solvent molecules in the channels through hydrogen bonds and salt bridges (*Figure 3.65*), but interestingly no peptide-peptide interaction was involved in the formation of the channel between peptides facing each other. Peptide-peptide interactions were, instead, important for crystal formation along the *b* crystallographic direction (*Figure 3.66*). Considering the absence of peptide-peptide interactions in the perpendicular direction, the crystal packing relies markedly on the interplay between peptide and solvent molecules. The main hydrophobic interactions involved the phenyl ring of the phenylalanine and 4-iodophenylalanine residues and hydrogen atoms of the nor-leucine residues or of methyl groups of the 2-propanol molecules present in the structure (*Figure 3.67*). Another important hydrophobic interaction involved the halogen atom (iodine) of one 4-iodophenylalanine residue and the aromatic ring of a symmetry-related 4-iodophenylalanine residue. Halogen-halogen contacts were very weak, considering that distances between iodine atoms are in the range of 5-6 Å (*Figure 3.68*).

a)

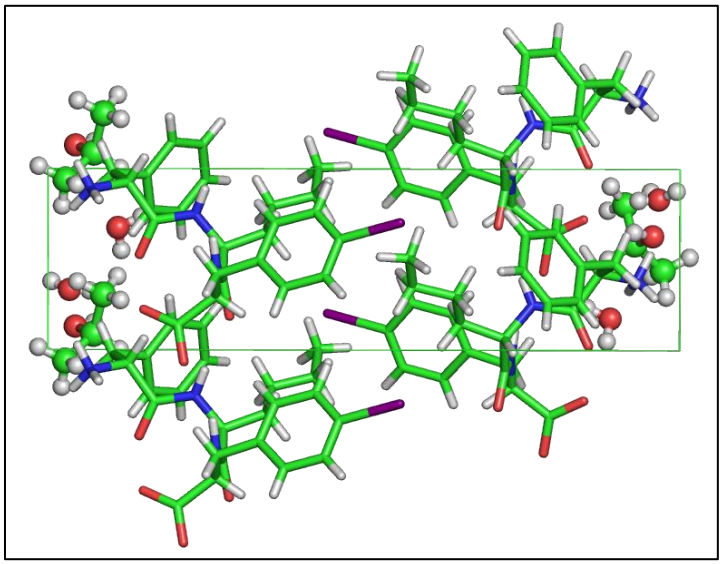

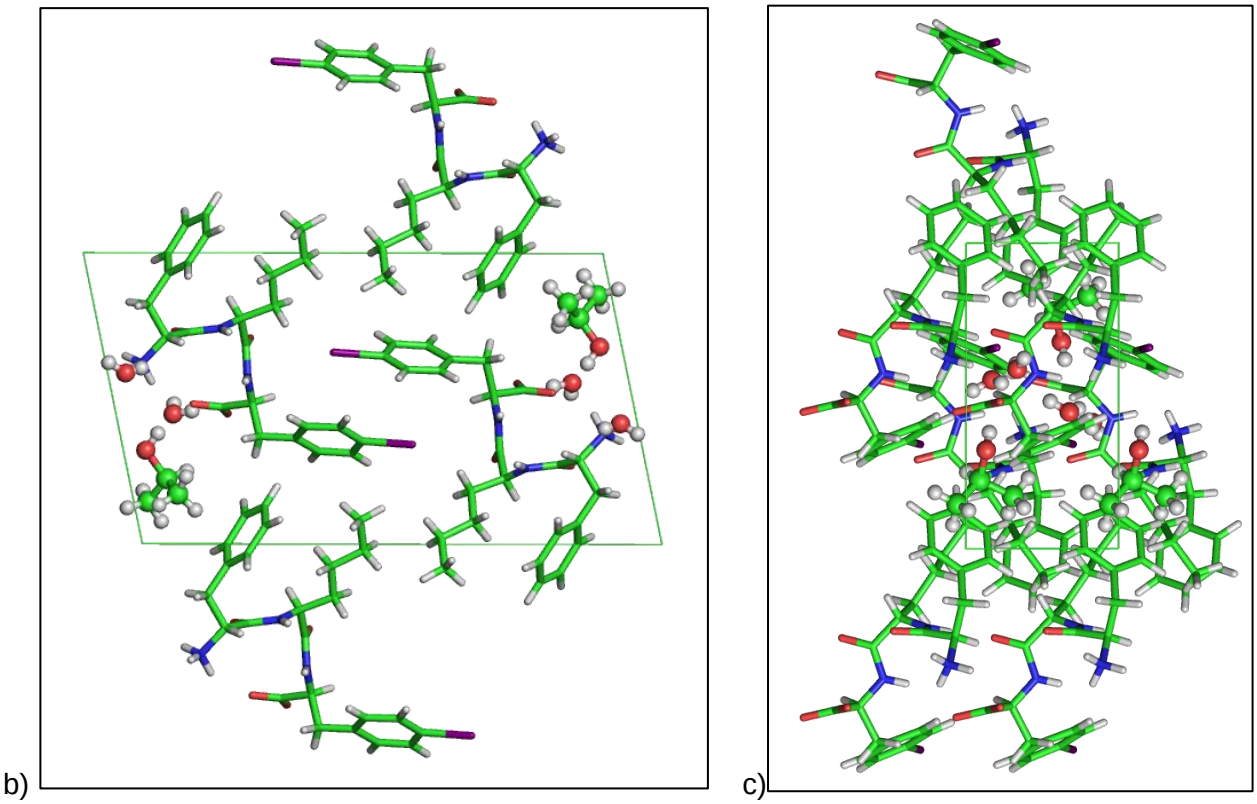

Figure 3.63 Unit cell of crystal of the peptide 9c.

Crystal of the peptide **9c**, grown in 2-propanol and water. Views along the *a* crystallographic axis (a), the *b* crystallographic axis (b) and the *c* crystallographic axis (c). Peptide molecules are shown as sticks, 2-propanol and water molecules are shown as spheres.

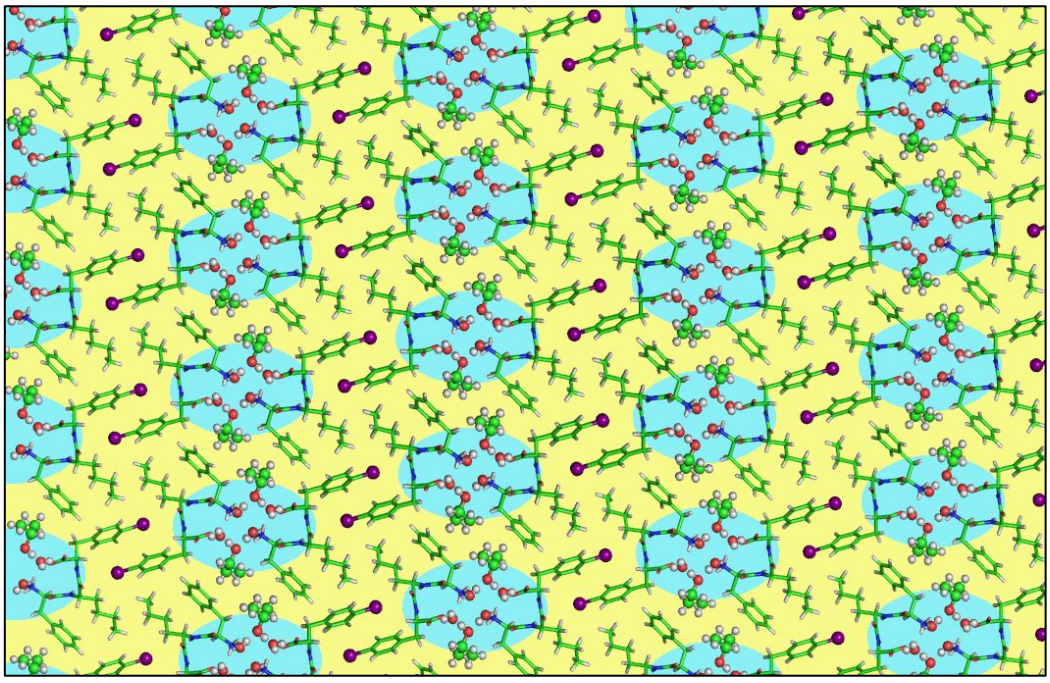

Figure 3.64 Crystal packing of 9c, forming small hydrophilic channels.

The crystal packing of the structure of **9c** shows the formation of small channels along the *b* crystallographic direction, surrounded by the hydrophilic moieties of the peptide and alcohol molecules. In the figure, regions with prevalent hydrophobic character are shown in yellow, regions with hydrophilic character are shown in blue, including the solvent-filled channels. Alcohol and water molecules and iodine atoms are shown as spheres.

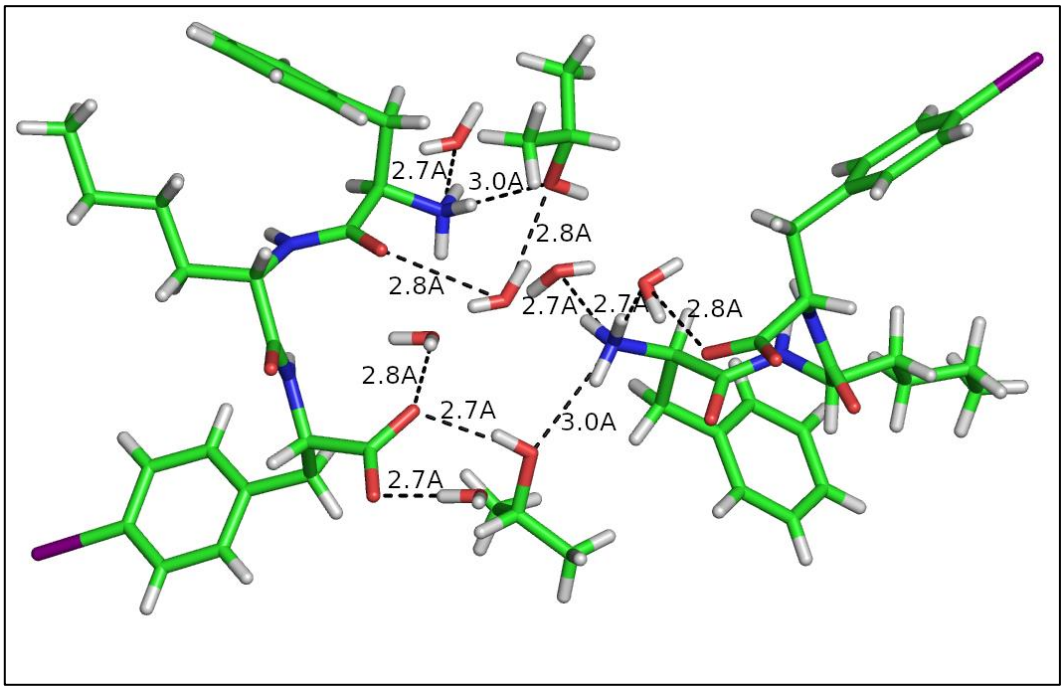

Figure 3.65 Hydrophilic interactions involving peptide 9c and solvent molecules in the *ac* crystallographic plane. Multiple hydrophilic interactions connect peptide and solvent molecules forming the small channels present in the structure of **9c**. Among the interactions, hydrogen bonds and salt bridges are formed between peptide and solvent, but no direct peptide-peptide interactions could be observed in the *ac* crystallographic plane.

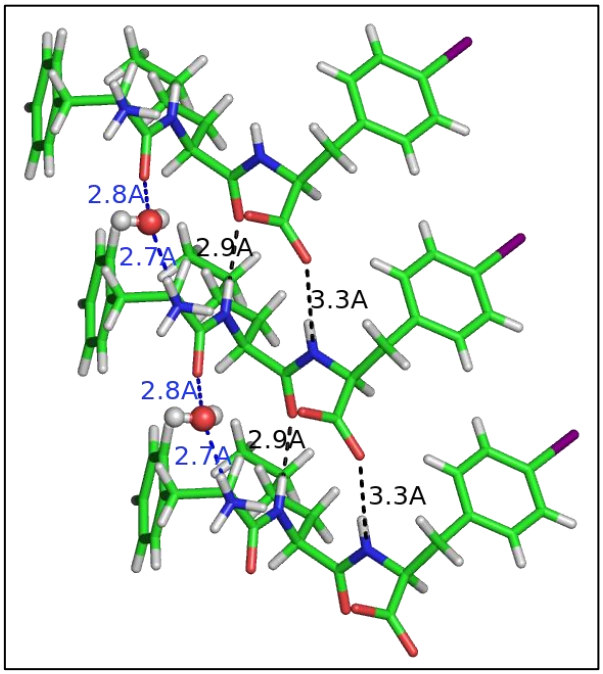

Figure 3.66 Hydrophilic interactions involving peptide 9c and solvent molecules along the *b* crystallographic direction.
Few hydrophilic interactions connect peptide molecules along the *b* crystallographic direction and are either direct peptide-peptide interactions (black dashes) or mediated by the presence of a water molecule (blue dashes).

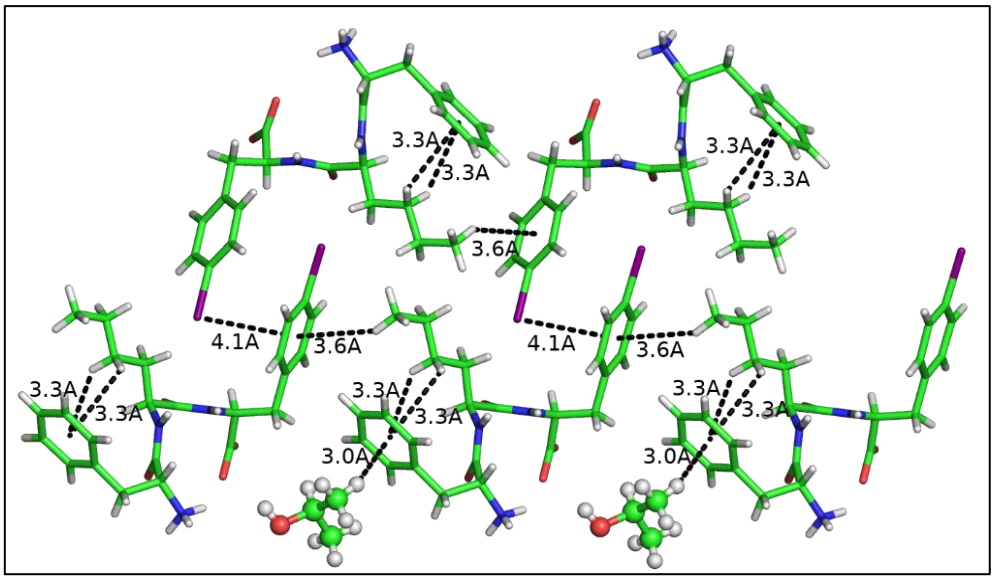

Figure 3.67 Hydrophobic interactions observed in the structure of 9c.
Among the hydrophobic interactions, CH-π interactions involve the side chain of the second residue (nor-leucine) of the methyl groups of the 2-propanol molecules, as donor group, and the aromatic moieties of the first and third residue (phenylalanine and 4-iodophenylalanine), as acceptor group. In addition, halogen-π interactions are present in the crystal packing.

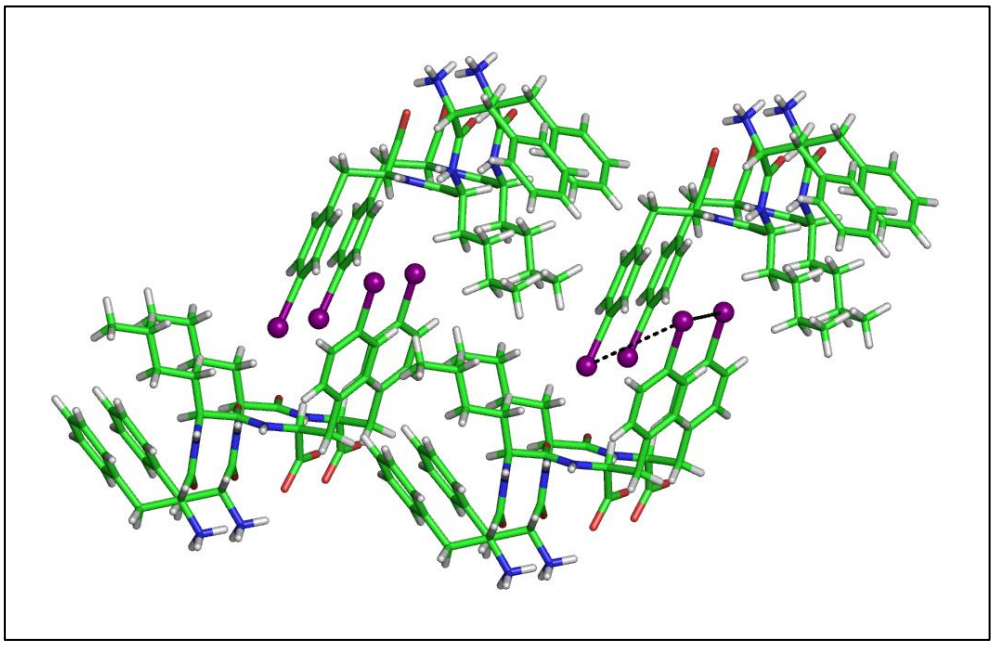

Figure 3.68 Packing of the iodine atoms in the crystal structure of peptide 9c.
Distances between the iodine atoms (purple spheres) in the structure are in the range between 5 and 6 Å, indicating only a weak interaction between the halogen atoms.

Crystallographic details.

A needle-shaped single crystal of the peptide was collected with a loop, cryoprotected by dipping the crystal in glycerol and stored frozen in liquid nitrogen. A total of 180 images were collected. Reflections were indexed and integrated using the XDS package, space group ***P2₁*** was determined using POINTLESS and the resulting data set was scaled using AIMLESS.[118–120] Phase information were obtained by direct methods using the software SHELXS.[121] Refinements cycles were conducted with SHELXL-14, operating through the WinGX GUI, by full-matrix least-squares methods on F^2.

Unit cell parameters and scaling statistics are reported in *Table 3.13*.[122,125] The asymmetric unit contained a molecule of the peptide, a molecule of 2-propanol and 2 molecules of water. All the atoms, except the hydrogen atoms, within the asymmetric unit have been refined with anisotropic thermal parameters. Hydrogen atoms of the peptide and alcohol molecules were added at geometrically calculated positions and refined isotropically. Hydrogen atoms of the water molecules were added with restrains on bond lengths and bond angle, using the DFIX and DANG cards of SHELXL-14 [6], respectively. Refinement statistics are reported in *Table 3.13*.

	13e	**9c**
Formula	$C_{24}H_{30}FN_3O_4 \cdot 3H_2O$	$C_{24}H_{30}IN_3O_4 \cdot C_3H_8O \cdot 2H_2O$
Temperature (K)	100	100
Wavelength (Å)	0.7	0.7
Crystal system	Hexagonal	Monoclinic
Space group	*P 6₃*	*P 2₁*
a (Å)	33.402(5)	12.005(2)
b (Å)	33.402(5)	5.887(1)
c (Å)	5.034(1)	20.988(4)
α (°)	90	90
β (°)	90	101.58(3)
γ (°)	120	90
V (Å^3)	4864(2)	1453.1(5)
Z, ρcalc (g/cm^3)	6, 1.007	2, 1.48
μ (mm^{-1})	0.075	1.002
F (000)	1560	665
Data collection θ range	1.201 - 21.557	0.975 – 25.935
Refl. Collected / unique	8738 / 3645	6841 / 4536
Rint	0.0815	0.0978
Completeness (%)	95.4	93.9
Data/Restraints/Parameters	3645 / 16 / 319	4536 / 6 / 365
GooF	0.897	0.962
R1, wR2 [I>2σ(I)]	0.0829 / 0.2071	0.0641 / 0.1517
R1, wR2 all data	0.1289 / 0.2384	0.0863 / 0.1677

Table 3.13 Crystallographic data for **13e** and **9c**.

Comparison of the backbone conformation

The backbone conformation of peptides **13e** and **9c** was compared using the Ramachandran plot (*Figure 3.69*) with already published peptide ^{L}Phe-^{D}Nva-^{L}Phe, to highlight differences between torsion angles of the second, aliphatic residue in the different diastereoisomeric peptides (*Table 3.14*).[56] For peptide ^{L}Phe-^{D}Nva-^{L}Phe, torsion angles of the enantiomer were reported in the Ramachandran plot, due to the inverted chirality of the central residue.[56]

The analysis of the torsion angles of peptides Phe-Xaa-Phe, with Xaa being an aliphatic residue, showed a strong similarity for peptides with the same chirality (or their enantiomers). In particular, the Ramachandran plot confirmed the observation that the conformations of ^{L}Phe-^{D}Nva-^{L}Phe and ^{D}Phe-^{L}Nle-^{D}Phe(4F) (**13e**) were similar, indicating that the presence of a fluorine atom in position 4 of the phenyl moiety of the third residue and the presence of a longer aliphatic chain in the second residue (Nle instead of Nva) did not hamper the formation of large channels. On the contrary, the different chirality of the ^{D}Phe-^{L}Nle-^{L}Phe(4I) (**9c**) peptide and/or the presence of an iodine atom in position 4 of the phenyl moiety of the third residue, a larger atom compared to fluorine, induced a different backbone

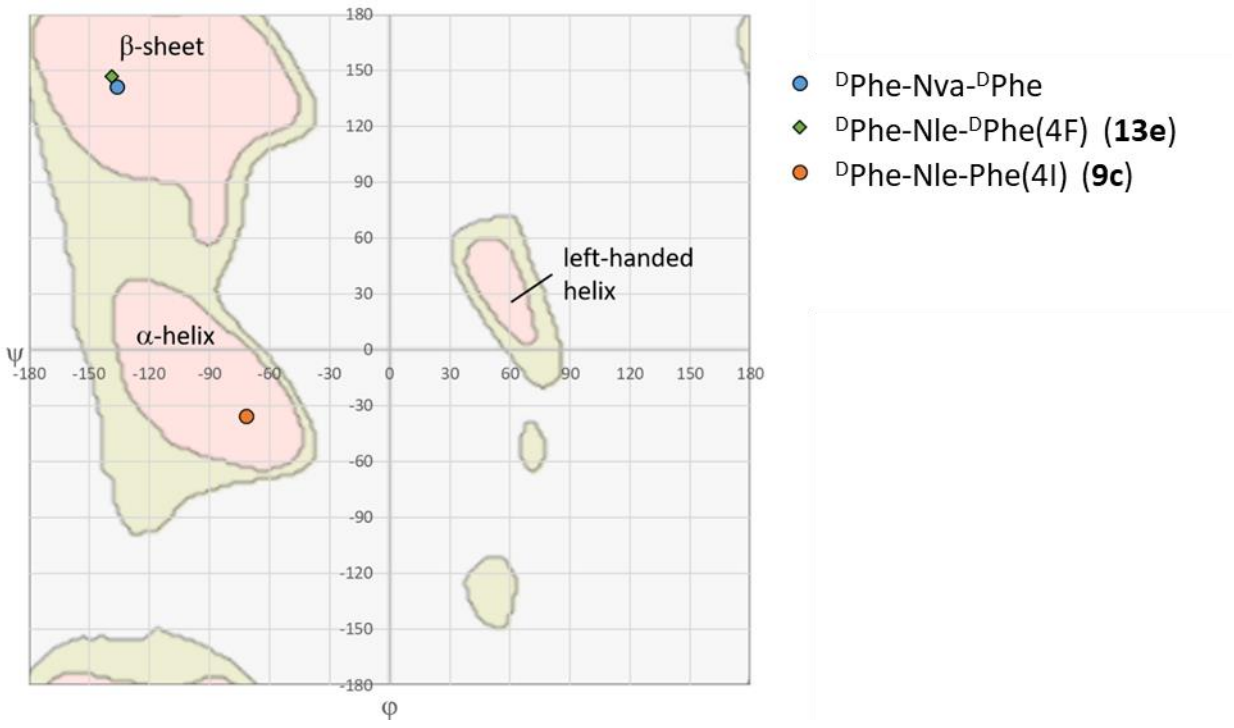

Figure 3.69 Ramachandran plot reporting the torsion angles of the central residues of tripeptides.
For the peptide Phe-^{D}Nva-Phe already reported, the torsion angles of the enantiomer were reported considering that the central residue has chirality D. For the peptides ^{D}Phe-Nle-^{D}Phe(4F) (**13e**) and Phe-^{D}Nva-Phe torsion angles are compatible with a secondary structure of a β-sheet.[56] The torsion angles of peptide ^{D}Leu-^{L}Phe-Phe(4I) (**9c**), torsion angles are compatible with an α-helical secondary structure.

	n=1	n=2		n=3
Compound name	ψ:N_n-Cα_n-C_n-N_{n+1}	φ:C_{n-1}-N_n-Cα_n-C_n	ψ:N_n-Cα_n-C_n-N_{n+1}	φ:C_{n-1}-N_n-Cα_n-C_n
Phe-^{D}Nva-Phe [REF.56]	123.75	136.32	-141.18	-154.80
13e	-127.13	-138.91	146.81	154.07
9c	-137.15	-71.75	-35.37	-66.85

Table 3.14 Torsion angles in the structures of ^{L}Phe-^{D}Nva-^{L}Phe, **13e** and **9c.** [56]

3.3 Antimicrobial activity evaluation

In recent years, the advancement of antimicrobial supramolecular hydrogels has required the development of new methods for the evaluation of antimicrobial properties. Typically, antimicrobial assays are designed for molecules in solution and it is very challenging to adapt such tests to solids, such as hydrogel materials. Here are reported the results obtained by using different antimicrobial assays on synthesised peptide supramolecular hydrogel and the respective issues encountered.

3.3.1. Antimicrobial activity evaluation of peptide in solution

3.3.1.1 Minimum Inhibitory Concentration (MIC) assay

Minimum Inhibitory Concentration (MIC) assays determine the lowest concentration of an antimicrobial agent that prevents visible growth of a microorganism. MIC test was performed to evaluate peptide antimicrobial activity in solution, and as we can observe from *Figure 3.70*, no significant activity was detected for all analysed compounds.

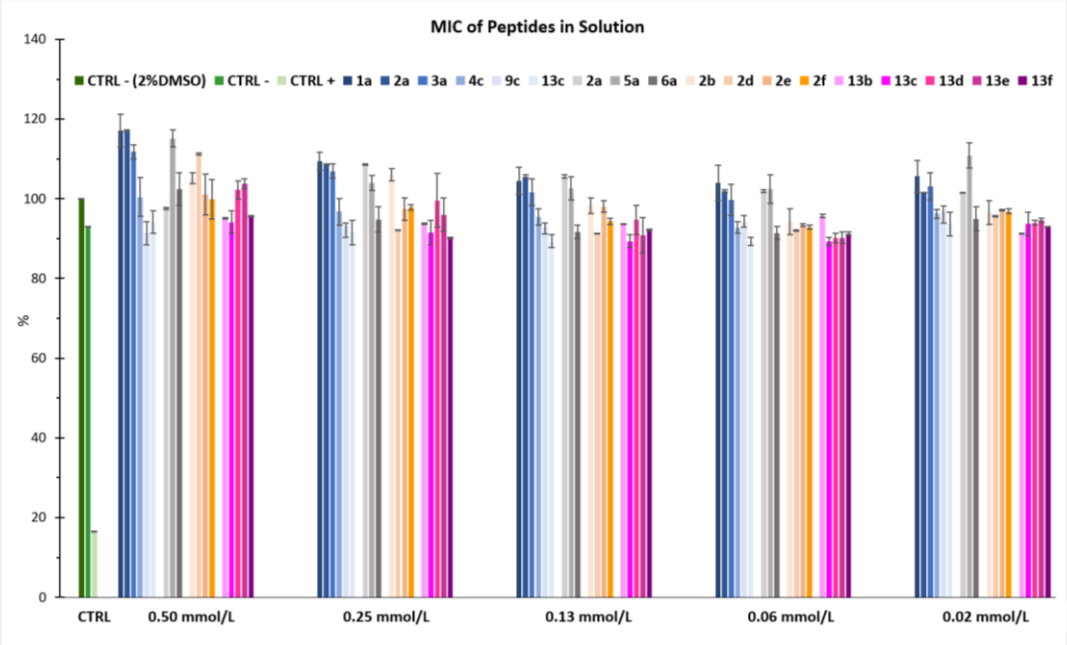

Figure 3.70 MIC test performed on peptides in solution at different concentrations.

3.3.2. Antimicrobial activity evaluation of peptide supramolecular fibres

3.3.2.1. Micro-well gel diffusion assay

Agar disk-diffusion testing is the official method used in many clinical microbiology laboratories for routine antimicrobial susceptibility testing. In this well-known procedure, agar plates are inoculated with a standardised inoculum of *E.coli*. Then, a microtome is used to cut out a disk of agar gel and obtain a 6 mm-wide well, which is subsequently filled with the peptide hydrogel (*Figure 3.71*). The Petri dishes are incubated in a humid chamber to prevent undesired drying of the hydrogel. Generally, the antimicrobial agent diffuses into the agar and inhibits germination and growth of the microorganism. Next, the diameter of the inhibition growth zone is measured (*Figure 3.74*). However, this test with peptide hydrogels is challenging due to the fact that peptide fibres may not diffuse correctly from the solid hydrogel through the agar matrix, especially those of larger size. To reduce this issue, peptides were tested at the concentration of 4 mM, a concentration below the mgc (except for peptide **13f** that gels at 2.5 mM). At these conditions, peptide fibres are dispered in a solution. Moreover, the presence of supramolecular fibres at this concentration were confirmed by TEM analysis for most compounds (except for negative controls **7a, 8a** and non-gelling peptide **3a**). Below are reported also the tests for peptides **1a** and **2a** at 15 mM, which clearly show that increasing the concentration form 4 mM to 15 mM leads to a smaller diameter of inhibition, hence an apparent reduced antimicrobial activity, likely because of reduced diffusion from the hydrogel solid relative to the solution (*Figure 3.72*).

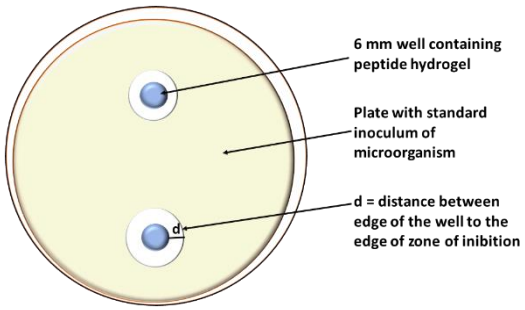

Figure 3.71 Micro-well gel diffusion assay plate.

From data obtained in this test we could make the following observations (*Figure 3.74*):

1. Peptide supramolecular fibres are required to exert antimicrobial activity (peptides not forming fibres at 4 mM, *i.e.*, **3a**,**7a**, and **8a,** do not inhibit bacterial growth).

2. Antimicrobial activity of heterochiral peptides Xaa-Phe-Phe appears slightly higher for **5a** than **2a** and **6a**. Val-Phe-Phe peptide was not considered because it does not form fibres at 4 mM. No correlation was found between fibre size and activity.
3. Antimicrobial activity of heterochiral peptides Phe-Xaa-Phe appears aslightly higher for **12a** than **10a** and **11a**
4. Halogenation of Leu-Phe-Phe leads to an increase in activity only in the case of Leu-Phe(4I)-Phe **2b**, which becomes less active in the case of concomitant presence of fluorine.
5. Halogenation of Phe-Nle-Phe leads to an increase in activity especially in the case of Phe(4I)-Nle-Phe **13b**, which becomes less active in the case of concomitant presence of fluorine.
6. Similarly active is halogenated homochiral peptide **4c**, but this peptide tends to undergo a transition from hydrogel to crystal, leading to polymorphic samples that consequently display large variability.

Figure 3.72 Plate with standard inoculum of microorganism with 6 mm well containing **1a** (up) and **1b** (down) peptide at 15 mM.

Compound name	Diam. of inibition (mm) (n=60)
1a	22 ± 7
2a	21 ± 7
3a	✕
4c	38 ± 20
7a	✕
8a	✕
9c	19 ± 10
13c	33 ± 14

Compound name	Diam. of inibition (mm) (n=60)
2a	21 ± 7
5a	25 ± 12
6a	22 ± 10
7a	✕
10a	17 ± 8
11a	18 ± 6
12a	24 ± 8

Compound name	Diam. of inibition (mm) (n=60)
2b	36 ± 12
2d	15 ± 7
2e	15 ± 6
2f	20 ± 9
13b	37 ±12
13c	33 ± 14
13d	35 ± 12
13e	35 ± 10
13f	20 ± 9

Figure 3.73 Inhibition distance d obtained by micro-well gel diffusion assay.

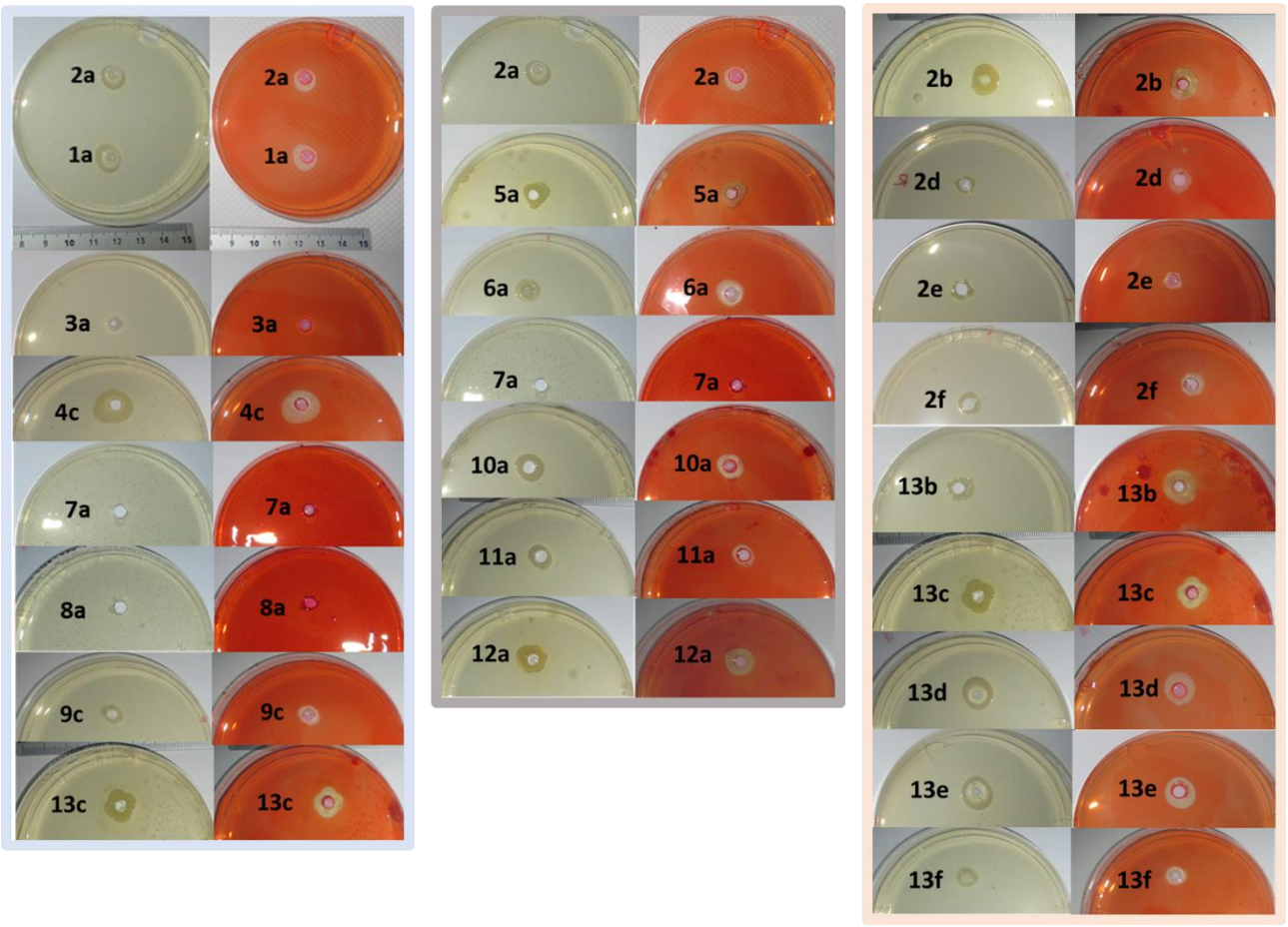

Figure 3.74 Plate with standard inoculum of microorganism with 6 mm well containing peptide hydrogel and respective inhibition of bacterial growth.

3.3.2.2 Fluorescent Microscopy LIVE/DEAD assay

Fluorescence microscopy-based live-dead assays were used to evaluate the viability of bacterial cells. Simultaneous use of two fluorescent dyes allowed a two-color discrimination of the population of living cells from the dead-cell population. In this work were used acridinium orange (AO) and propidium iodide (PI), which stained viable (green) and dead (red) cells, respectively.

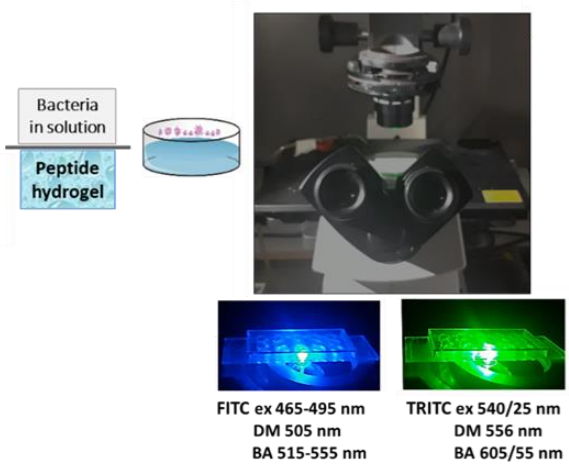

Figure 3.75 Fluorescent microscopy live/dead assay.

The images obtained by fluorescence microscopy displayed a certain level of variability between samples. Lack of activity was confirmed for samples **3a**, **7a** and **8a**, as noted by micro-well gel diffusion assay. The other peptides displayed mild antimicrobial activity that overall were quite in agreement with the results of the gel diffusion assay described above. Exceptions were **2b** and **5a** that appeared more active with this assay. It is possible that these peptides, which form large fibres, do not diffuse well in the previous assay, thus leading to an apparent minor activity than revealed by microscopy.

In addition, as it regards halogenation of Phe-Nle-Phe, the presence of iodine at the N-terminus increased the activity more than when it was at the C-terminus. On the contrary, fluorine led to higher activity when it was present on the C-terminus. To verify additive or even synergic effect of iodine (on the N-terminal Phe) and fluorine (on the C-terminal Phe), the compound **13f** was tested. Unfortunately, the resulting antimicrobial activity was decreased, confirming once again the complexity of the phenomenon under study, for which it is difficult to predict activity based on chemical structure.

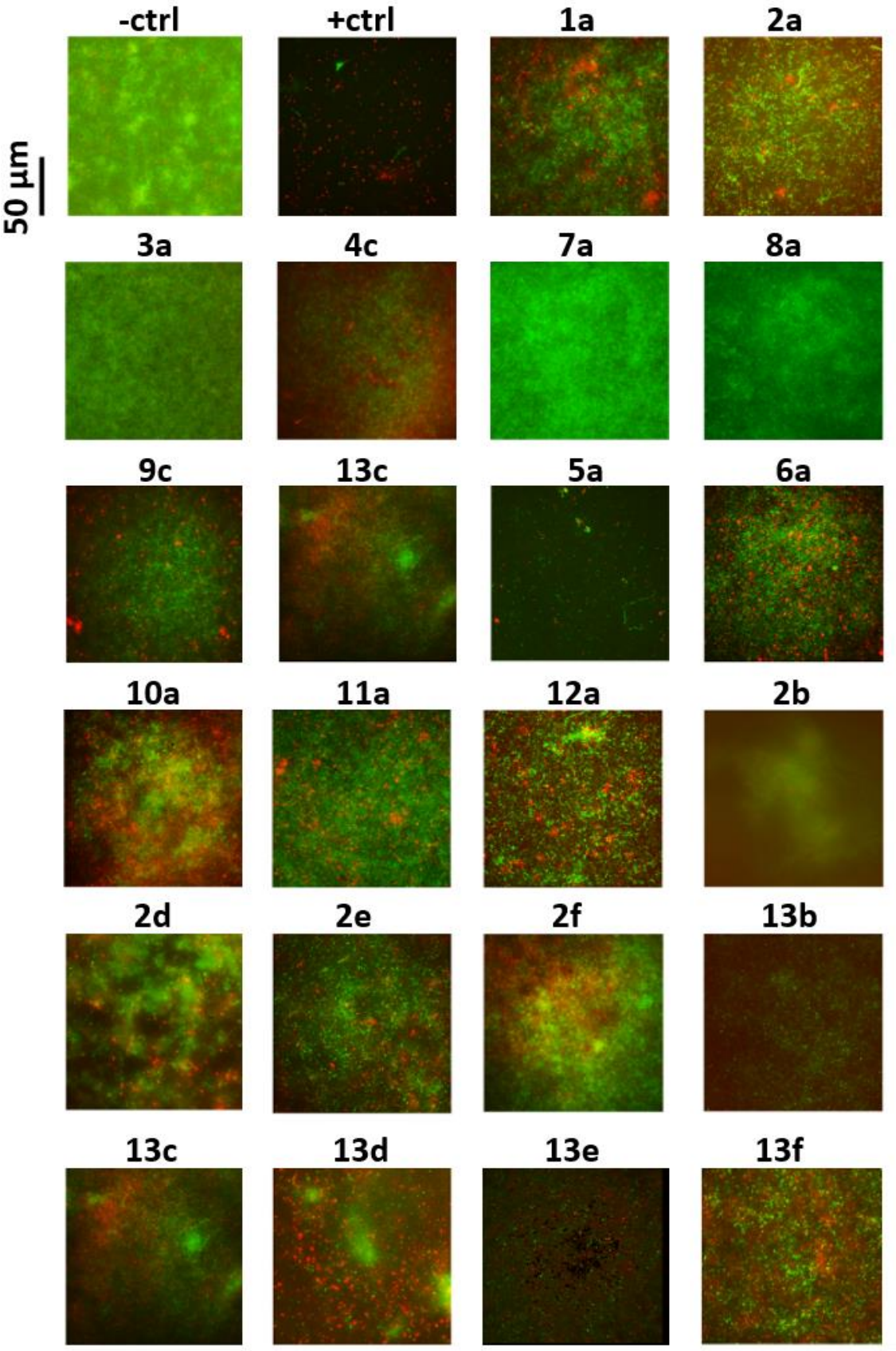

Figure 3.76 Data obtained by fluorescence microscopy live/dead assay. -ctrl was the buffer, +ctrl was polymyxin E 10 µg/ml. Scale bar = 50 µm.

3.3.2.3. Outer membrane (OM) permeability assay

Measurement of the permeability alterations of the Gram negative bacterial OM serves many purposes in the study and development of antimicrobial agents. Permeabilizers lacking inherent toxicity can sensitize bacteria to other agents, which alone are unable to penetrate into bacterial targets. Uptake of the fluorescent probe 1-N-phenylnaphthylamine (NPN), as adapted to an automated spectrofluorometer enabling multiwell reading of microtitre plates, was applied to determine permeability changes in *Gram negative* bacteria (*E.coli*). An intact OM is a permeability barrier, and excludes hydrophobic substances such as NPN but, once damaged, it can allow the entry of NPN to the phospholipid layer, resulting in prominent fluorescence. Fluorescence was recorded as a function of time until no further increase in fluorescence was observed. Values were converted to % NPN uptake using the equation (1) % NPN uptake$=(F_{obs}-F_o)/(F_{100}-F_o)\times 100$, where F_{obs} was the observed fluorescence at a given peptide concentration, F_0 was the initial fluorescence of NPN with *E. coli* cells in the absence of peptide, and F_{100} was the fluorescence of NPN with *E. coli* cells upon addition of 10 μg/ml Polymyxin E (Sigma). Polymyxin E was used as a positive control because of its strong OM permeabilizing properties. Results are shown in *Figure 3.77.*

Unfortunately this assay, which is typically employed to peptides in solution, was unreliable in the present case. In particular, significant scattering was noted due to the presence of hydrogels, and it varied over time as self-assembly proceeded. Additionally, fluorescence fluctuations suggested that peptide assemblies may interfere with the fluorescence of NPN. This is not too surprising considering that hydrophobic fluorescent dyes are known to bind to peptide assemblies (for instance, ThT), leading to increased or decreased fluorescence, depending on the peptide tested. Therefore, since the evolution of fluorescence over time is a sum of different phenomena that occurred during measurements, the obtained results were deemed unreliable. Additionally, fluorescence saturation was observed. In conclusion, this assay was not useful to study the antimicrobial activity of peptide hydrogels.

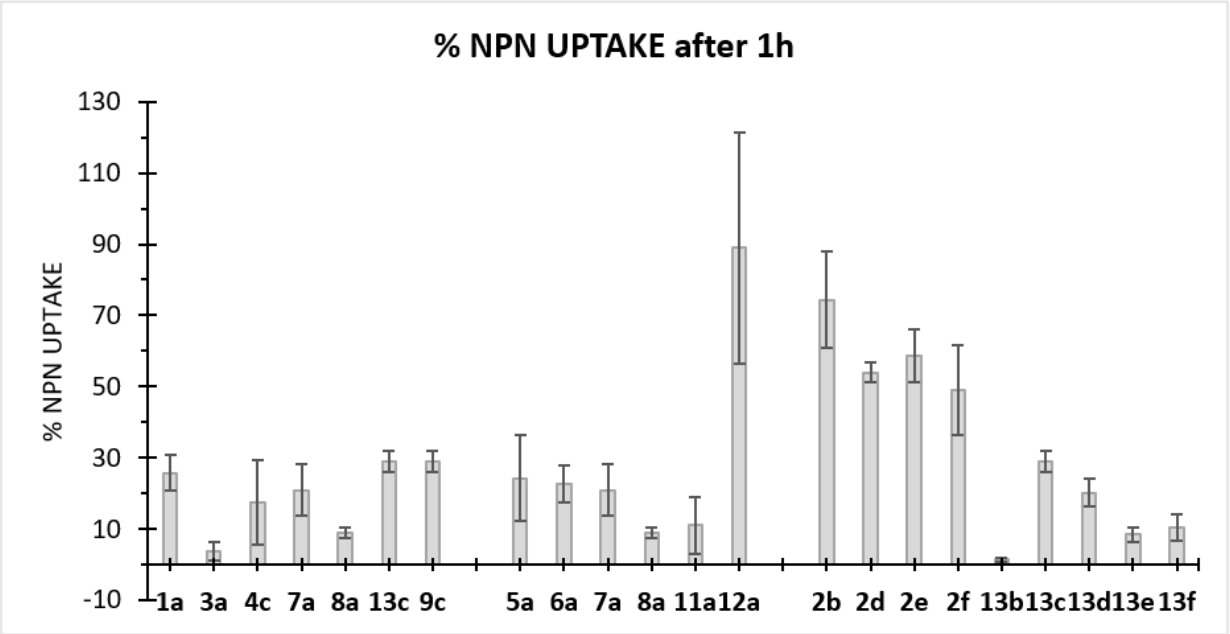

Figure 3.77 % NPN uptake in 1 hour for analysed peptides in contact with bacterial cells.

3.3.2.4. SFG spectroscopy studies of peptide interaction with lipid bilayer

The mode of action of antimicrobial peptides (AMPs) in disrupting cell membrane bilayers is of fundamental importance to understand the efficiency of different AMPs, which is crucial to design antimicrobial compounds with improved properties. Recent developments in the field of sum frequency generation (SFG) spectroscopy have made it a powerful biophysical technique to investigate the interactions between AMPs and a single substrate supported planar lipid bilayer. Sum frequency generation spectroscopy (SFG) is a non-linear laser spectroscopy technique used to analyse surfaces and interfaces. In a typical SFG setup, two laser beams mix at an interface and generate an output beam with a frequency equal to the sum of the two input frequencies, traveling in a direction given by the sum of the incident beams wave vectors (*Figure 3.78 - left*).

In collaboration with the Max Planck Institute for Polymer Research - Mainz (group of Dr. Grazia Gonella), sum frequency generation vibrational spectroscopy was employed to study *in situ* the interactions between peptides and a single lipid bilayer in real time (*Figure 3.78 - right*). Using peptides at 4 mM and a dipalmitoyl phosphatidylglycerol bilayer as a model system, the C-H and C-D stretching signals from isotopically symmetric or asymmetric dipalmitoyl phosphatidylglycerol bilayers were monitored during their interaction with peptide fibres. Bilayer was deposited on CaF_2 right angle prisms via the Langmuir–Blodgett technique.

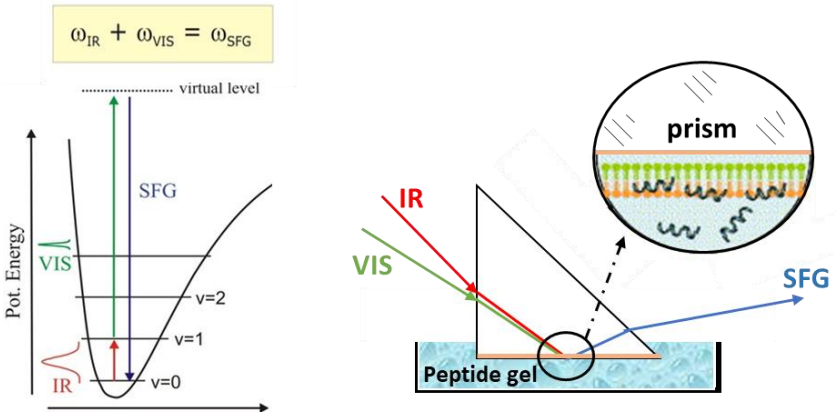

Figure 3.78 SFG spectroscopy

Comparison of membrane organisation without (black) and with peptide **1a** (red) revealed an altered signal due to membrane disorganisation in the presence of self-assembling fibres (*Figure 3.79*). Unfortunately, use of **7a** as negative control (not active peptide fibres) also led to an altering membrane signal. These results suggested an alteration of membrane due to mechanical interference of heterogeneous systems as opposed to peptides in solution. Therefore, this type of technique could not be successfully used to study self-assembling peptide interaction with membranes.

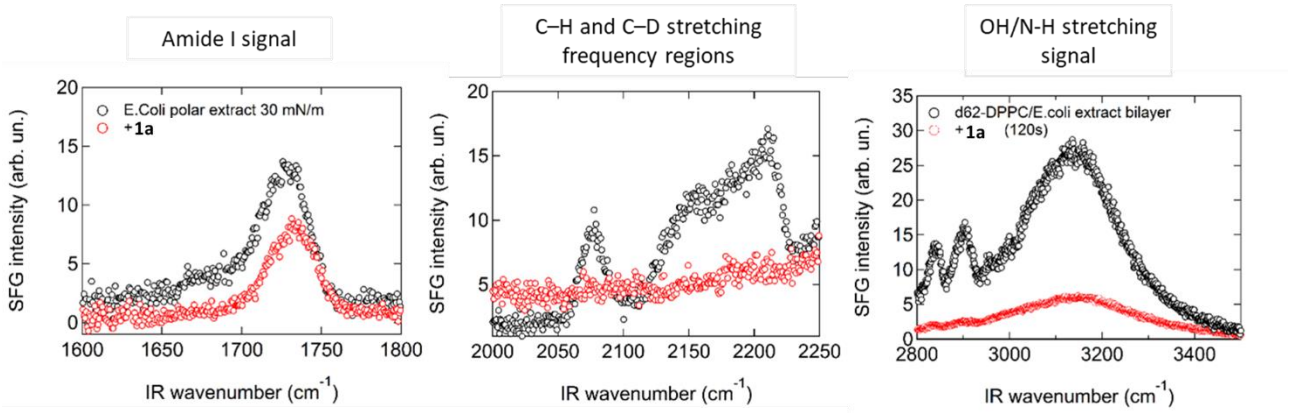

Figure 3.79 SFG spectroscopical studies on peptide supramolecular fibres.

3.4. Biological performance of peptide hydrogels

Peptide benefits as bioactive agents include high target specificity, strong binding affinity, low immunogenicity, broad range of potential targets, and high stability, tolerability, and safety, whilst only a small concentration of peptide is needed to give effective therapeutic outcomes.[126] In the case of AMPs, biocompatibility assessment starts with evaluation of haemolysis of red blood cells. This is due to the fact that often AMPs display hemolysis as a side effect due to the undesired disruption of red blood cell membranes. It is one of the most commonly used techniques to study the effects that materials have on the blood and its components, since, in this case, these *in vitro* results usually correlate quite well with *in vivo* results.[127] Another concern is the reduced bioavailability of peptide therapeutics. In many cases, proteolytic enzymes are responsible for this observation.[126] Peptide stability toward protease-mediated degradation was thus assayed below and above peptide supramolecular structure formation, as described further below.

3.4.1. *In vitro* haemolysis assays

In vitro haemolysis assay was performed by Dr. Yue Qu (Monash University, Melbourne, Australia). Haemolytic assay evaluates haemoglobin release in the plasma (as an indicator of red blood cell lysis) (*Figure 3.80*).

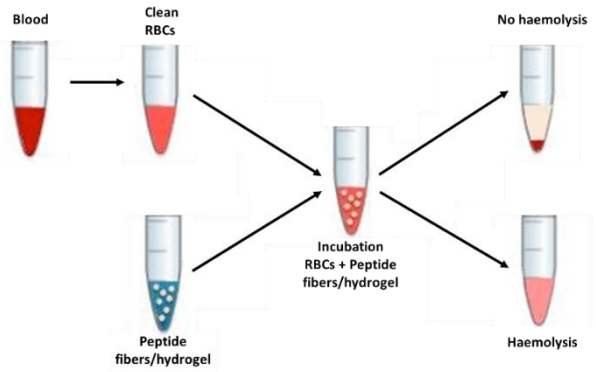

Figure 3.80 Haemolysis assay on RBCs with peptide supramolecular fibres.

Adapted with permission from ref.[127] *© 2016 MDPI.*

To measure the produced haemolysis, spectroscopic measures were performed after peptide fibre incubation with erythrocytes. In this work, the eventual release of the haemoglobin was evaluated under two different conditions. The first test was performed under dynamic flow conditions, which mimick human bloodstream. The second test was performed in static conditions to assess the contact - mediated (adhesion)between peptide hydrogel surface and red blood cells.

3.4.2.1. *In vitro* dynamic flow haemolysis assay

Results obtained under dynamic conditions were really promising. Homochiral peptide **4c,** containing all D-amino acids presented higher haemolysis (*i.e.* 20±15 %), followed by **11a** (*i.e.* 9±12 %) and **10a** (*i.e.* 3±5 %). By contrast, all other compounds presented a haemolysis lower than 1 % (*Figure 3.81*).

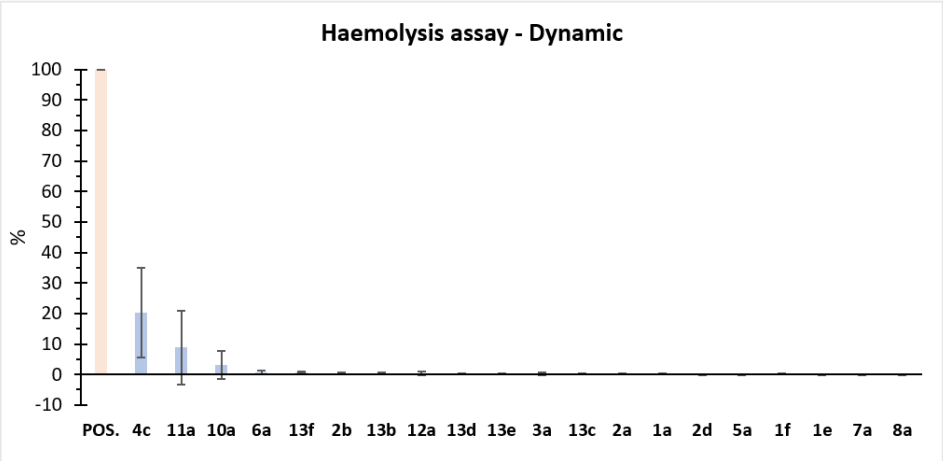

Figure 3.81 Peptide performance under red cell culture in dynamic conditions.

3.4.2.2. *In vitro* contact-mediated (adhesion) haemolysis assays

Static conditions revealed higher toxicity for some peptides (**4c, 9c, 13e, 2b, 10a, 13d, 11a, 12a, 13c, 2f**) (*Figure 3.82*). To our delight, the most active **5a** and **13b** did not display any haemolytic effect.

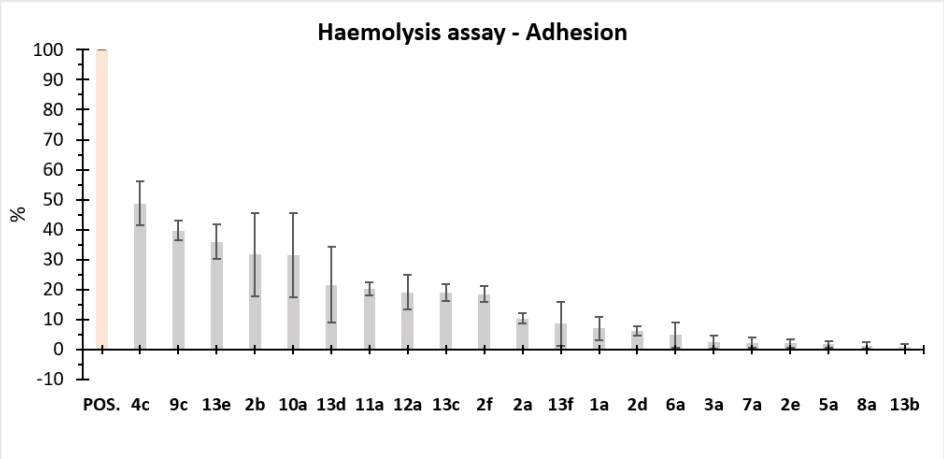

Figure 3.82 Peptide performance under red cell culture in adhesion conditions.

3.4.3. *In vitro* peptide stability to protease degradation

Protease degradation test consisted of incubation of peptide in solution or hydrogel state for 24 hours with a large excess of protease and consequent analysis of samples by HPLC.

3.4.3.1. Peptide stability in solution

Stability of peptides solution against protease degradation was assayed *in vitro* based on three independent experiments. All heterochiral peptides resisted hydrolysis for more than 50%, except for **2a** and **8a** that were less resistant, while non-assembling L-peptide analogues were completely digested within 24 hours (*Figure 3.83*). Variations in stability across samples could be due to specific affinity for the enzyme tested, thus different enzymes should be tested before generalizing any observed trend.

It should also be noted that handling of samples **2d** and **2e**, containing fluorine, was challenging due to their fibrillisation in solution.

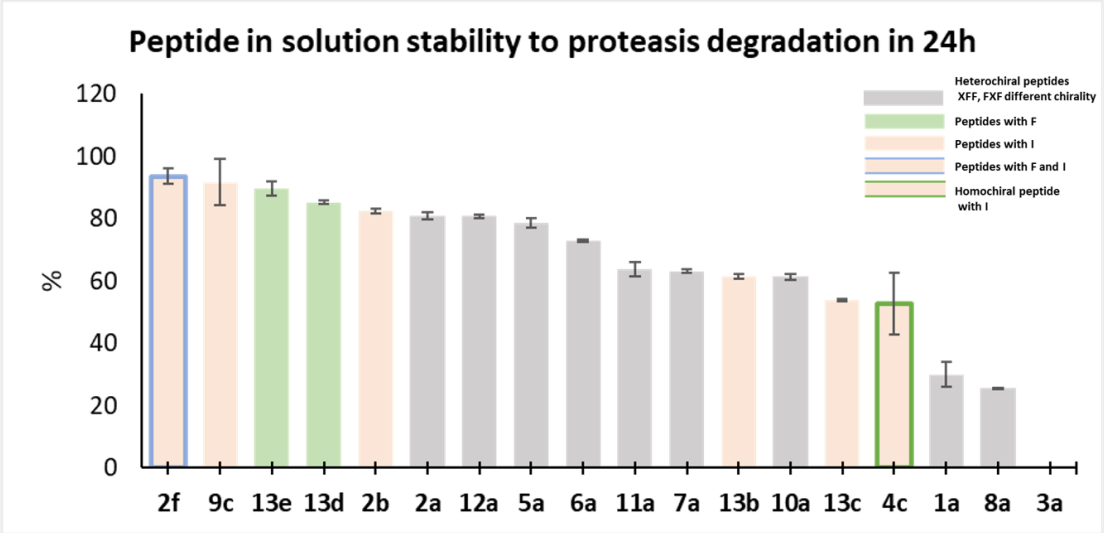

Figure 3.83 Peptide in solution performance under proteases degradation assay.

3.4.3.2. Peptide stability in hydrogel state

The same trend observed in solution was confirmed in hydrogel state, although in the latter case the resistance to protease was increased of approximately 10% for all peptides forming supramolecular hydrogels (*Figure 3.84*). Data for 13f are not reported because peptide fibrillisation occurred in the HPLC sample also at low concentration, thus hampering accurate analysis.

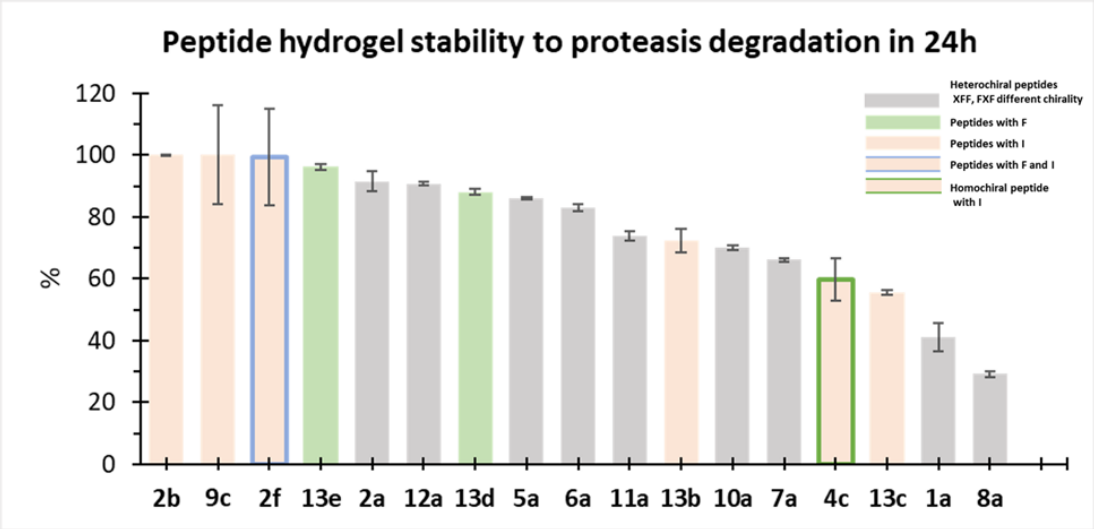

Figure 3.84 Peptide in solution performance under proteases degradation assay.

4. CONCLUSIONS AND FUTURE PERSPECTIVES

This project was aimed to get the first insights into the structure-activity relationship for the design of biocompatible peptide hydrogels. Moreover, optimisation towards a lead compound with increased antimicrobial activity and biocompatibility compared to previously reported molecules could provide important insights into the antibacterial capabilities of minimal self-assembling building blocks and their future investigations towards a realistic application. To this end, 22 hydrophobic tripeptides were designed, containing two Phe residues and an aliphatic amino acid, with structural variations in terms of aliphatic side chains, halogenation, chirality and amino acid sequence.

All the 22 target compounds were successfully synthetized by standard Fmoc solid phase synthesis and purified by RP-HPLC. Moreover, all peptides were characterised at molecular level by ^{1}H-NMR, and LC-MS analyses. Self-assembly into nanostructured hydrogels was successful in all cases by design, except for the negative control **3a**. Therefore, this study confirmed the emerging rules for the design of self-assembling hydrophobic tripeptides based on heterochirality.[56,59,100] The supramolecular structures were assessed by the inverted test tube method and oscillatory rheology. Leu-Phe-Phe peptides displayed irreversible disassembly upon heating, while all the other hydrogels were thermoreversible. It should be noted though that all halogenated Leu-Phe-Phe peptides were difficult to handle and dissolve.

Nanostructured morphology of peptide hydrogels was observed by TEM analysis and it confirmed the presence of supramolecular fibers for all compounds presenting antimicrobial activity. Interestingly, Xaa-Phe-Phe peptides formed thinner fibrils in the presence of amino acids without β-branching (*i.e.*, Leu, Nle) with a high level of interconnectivity between fibers; this trend is opposite compared to peptides Phe-Xaa-Phe. Moreover, presence of iodine was associated with thinner fibrils relative to non-halogenated analogues, while this effect was not observed for peptides containing fluorine.

The presence of amyloid-like fibers was evaluated by means of Thioflavin T fluorescence, an established assay for amyloids. However, the assay demonstrated large variability and no trend could be found between fluorescence and nanomorphology or antimicrobial activity. We inferred that, since fluorescence is the result of the dye binding onto hydrophobic grooves on the surface of peptide fibrils, it is possible that different peptide sequences led to a different fibril surface topography in a way that could not be predicted.

The secondary structure of molecules was evaluated by CD spectroscopy below and above supramolecular fibre formation. Obtained data were of difficult interpretation, however, significant changes were observed upon assembly suggesting that CD could be used to monitor assembly kinetics. Further analysis by FT-IR will be useful to better assess presence of secondary conformations.

Single-crystal XRD data were obtained for **1a**, **3a**, **5a**, **4c** (in solution and gel), **2b** (in solution and gel), **2f**, **9c** and **13e**. For Xaa-Phe-Phe (**1a**, **3a**, **5a**, **4c**, **2b** and **2f**) was observed that peptides with D-L-L or L-D-D stereoconfiguration had torsion angles compatible with an α-helical secondary structure. Such conformation was independent from the nature of the first residue (Leu or Ile) and the presence of substituents in position 4 on the phenylalanine aromatic moieties (*i.e.,* **1a**, **5a**, **2b**, **2f**). On the contrary, both the structures of homochiral Xaa-Phe-Phe peptides showed a conformation compatible with a β-sheet secondary structure (*i.e.,* **3a**, **4c**). The analysis of the torsion angles of peptides Phe-Xaa-Phe (**9c** and **13e**) showed a strong similarity for peptides with the same chirality (or their enantiomers). In particular, the Ramachandran plot confirmed that the conformations of Phe-^{D}Nva-Phe and **13e** were similar, indicating that the presence of a fluorine atom in position 4 of the phenyl moiety of the third residue and the presence of a longer aliphatic chain in the second residue (Nle instead of Nva) did not hamper the formation of large water channels. On the contrary, the different chirality of the peptide **9c** and/or the presence of an iodine atom in position 4 of the phenyl moiety of the third residue, a larger atom compared to fluorine, induced a different backbone. Moreover, heterochiral peptides formed overall structures in which better separation of hydrophobic and hydrophilic regions was observed compared to homochiral peptides. Therefore, the importance of this type of organisation for self-assembling procedure towards hydrogel formation, based on unprotected heterochiral tripeptides, is confirmed as reported previously.[56] In addition, for peptides crystals obtained both from solution and hydrogel state it was possible to observe that the conformation of the peptides, their position and the position of the water molecules were identical, indicating a low energy gap between peptide organisation in hydrogel state and crystals.

In the second part of the project, antimicrobial activity *in vitro* against *E.coli* cultures was assessed with peptides in solution and supramolecular fibre state by different assays. The key role of supramolecular structures for antimicrobial activity was determined, thus giving the possibility to switch on/off the activity *on demand*. Moreover, the same activity for enantiomers was observed, excluding in this way the interaction with any receptor present on the bacterial membrane. Variations in antimicrobial activity were noted, with higher activity for **2b**, **5a**, and **13b**. A general structure-activity relationship was not found that could relate peptide sequence and/or nanomorphology and/or

crystal structure with antimicrobial activity. Other assays (*i.e.*, outer membrane permeabilisation fluorescence assay and non-linear optical spectroscopy) were employed to elucidate the mechanism of activity. Unfortunately, these assays were not compatible with these systems due to artefacts related to the presence of fibrils and a hydrogel state.

Reduced bioavailability due to enzymatic degradation is a major concern in effective use of peptide therapeutics. Therefore, peptide stability to enzymatic degradation was assessed both in solution and hydrogel state. The vast majority of heterochiral peptides remained stable (> 50%) over 24 hours, and stability was generally increased of a further 10% by self-assembly.

Finally, cytocompatibility was assessed by means of haemolytic assays both in static and dynamic conditions. The former revealed minor haemolytic effect for some peptides, but not for **13b**, and **5a**, which were confirmed as the best candidates of the library.

As new information is gathered, the following steps will attempt at improving the activity, for instance by the rationalisation of the relationship between small structural modifications on compound **13b** and the effect on antimicrobial activity, as well on compound **5a.** Further biological studies will also be crucial to address the technical challenges that arose in this work and better delineate the possible mechanism(s) of action. Further studies could also be aimed at testing the reversibility of assembly under different conditions (*e.g.*, pH change, ionic strength, etc.) to allow the switching on/off of the antimicrobial activity as needed *on demand*, and potentially even for the *in situ* activation at a target site.

The potential use of these self-assembling peptide materials as antimicrobials is envisaged for instance for topical applications, such as in the case of extended burned skin to avoid infections as well as for wound hydration that can help skin cell healing procedure. Additional applications include the coating of medical devises; moreover, it was demonstrated how the incorporation of similar nano-assemblies into dental resin composite was useful for the antibacterial activity.[97]

5. MATERIALS AND METHODS

5.1. Peptide synthesis

5.1.1. Peptide synthesis procedure

All the peptides in this work were synthesized using standard Fmoc-based solid phase peptide synthesis (SPPS) using 2-Chlorotrityl chloride resin as solid support and activation via uronium salt of O-(Benzotriazol-1-yl)-N,N,N′,N′-tetramethyluronium hexafluorophosphate (HBTU) and 1-Hydroxy-7-azabenzotriazole (HOAt).

5.1.2. Loading of the first amino acid on the resin

1 g of 2-Chlorotrityl chloride resin were swelled for 5 minutes using DCM in a plastic reaction vessel. After the swelling, the resin was treated with 0.1 ml of thionyl chloride $SOCl_2$ in DCM and leave to react, mild stirring for 1h at room temperature. After 1 h the solution was removed and the resin was washed with DCM and DMF twice. Fmoc-amino acid (2.0 mmol) solution in DCM and half part of DMF was prepared and added to the activated resin, followed by the addition of 0.9 mL of N,N-Diisopropylethylamine (DIPEA) and left to stir for 1.5 h at room temperature. After this reaction time, without remove the mixture, 0.5 mL of methanol was added, and the vessel was spinned for 5 min. After that, the resin was dripped and washed with DCM and DMF twice. Fmoc protecting group was removed after two deprotection steps of 5-10 min each using a solution of 20 % piperidine in DMF. After that, the resin was newly dripped and washed with DCM and DMF twice.

5.1.3. Calculation of the first amino acid loading on the resin

Before to perform the Fmoc deprotection step after the loading of the first amino acid, triplicate samples of 5 to 10 mg of loaded resin were weighed and stored in Eppendorf tubes. To each sample 1.00 mL of deprotection solution of 20% piperidine in DMF was added and left to mild shake for 20 min. After that time, each Eppendorf tube containing the resin were centrifuged for 5 min at 12.000 rpm and 100 μL were transferred into a vial glass tube containing 10 ml DMF and mixed well. The absorbance at λ=301 nm was measured in triplicate samples, considering DMF solvent for baseline and calculating the average substitution, according to the formula below:

$$\text{Substitution (mmol/g)} = (101 * A301) / (7.8 * w)$$

where A301 is the absorbance at λ=301 nm, w = exact mass weighted of resin sample (mg), and considering the initial Lambert-Beer law formula: $A = C*l*\varepsilon$, where C is the concentration of the solution, l is the optical pathway (1 cm) and ε is the molar extinction coefficient.

5.1.4. Colorimetric tests

Before and after every Fmoc deprotection step, few beads of loaded resin in Eppendorf tubes were transfered to perform the colorimetric tests.

5.1.4.1. Chloranil test

This test was developed to detect secondary amino group, indeed it is very specific and used not only for primary amine detection. In case of positive test, few beads of resin placed in a small test tube will be colored, after the addition of two solutions, appropriately prepared: solution 1 (2% acetaldehyde in DMF) and solution 2 (2% chloranil in DMF), left to react for 5 min at room temperature.

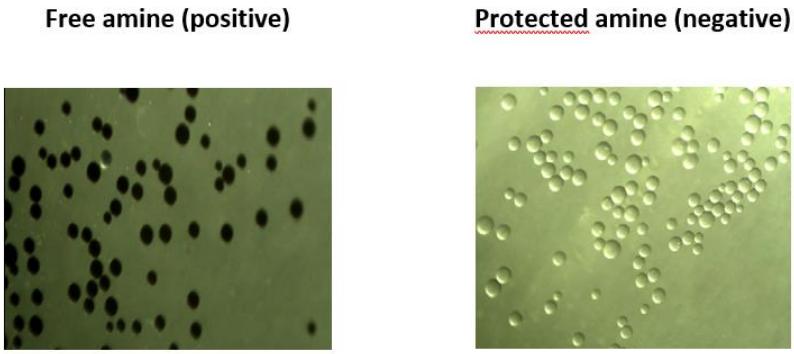

Figure 5.1 Chloranil test

5.1.4.2. Bromophenol Blue test

Bromophenol blue test is an immediate test to detect all types of amines, but it has to be performed carefully because traces of acid can provide false negative results. Few beads of the resin were placed in a small test tube and few drops of reagent solution were added.

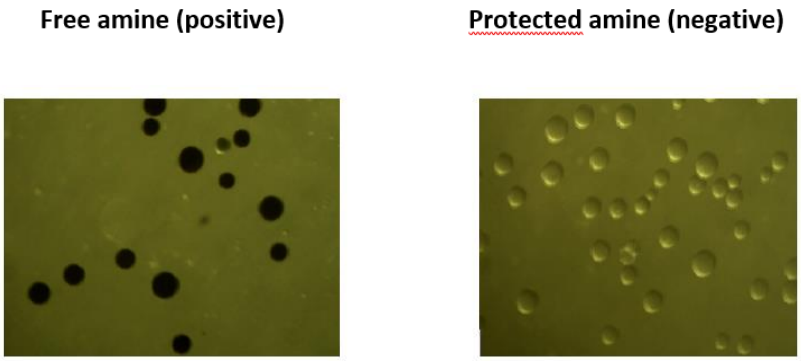

Figure 5.2 Bromophenol Blue test

5.1.5. Cleavage of peptide from the resin

Considering the use of 2-chlorotrityl chloride resin, the cleavage solution of the peptides was prepared using 49.5% TFA, 49.5% DCM with 0.5% TIPS and 0.5% H2O as scavengers after the last Fmoc group removal and a proper dehydration of the resin. A fresh prepared cleavage solution was added to the resin and left to react under mild shaking for 2 hours (1.5 hours for W-containing peptides, to reduce the side reactions of the electronic doublet of the indole nitrogen, once that the Boc orthogonal protection has been removed). After the reaction time, the resin was washed with DCM and well dried. The peptide cleaved from resin was collected and leave under evaporation in a flask under air. The obtained oil after the completion of the evaporation was then dissolved in the HPLC mixture for purification (MeCN/ H2O with 0.05% TFA).

5.1.6. Peptide purification

Each peptide was purified using reverse-phase HPLC (1260 Agilent Infinity system) equipped with a preparative gradient pump (G1311B), semipreparative C-18 column (Kinetex, 5 μm, 100 Å, 250 x 10 mm, Phenomenex) and Photodiode Array detector (G1315C). The gradient used consisted of acetonitrile (MeCN)/ H2O with 0.05% TFA with the following program: t = 0–2 min, 30 % MeCN; t = 16 min, 95 % MeCN; t = 18 min, 95% MeCN. Collected solvent containing peptides was then freeze-dried to yield the corresponding peptide as a white fluffy powder.

5.1.7. Peptide characterisation

All the synthesised peptides were characterised by ESI-MS (Electrospray Ionisation Mass Spectroscopy) and ^{1}H-NMR (Nuclear Magnetic Resonance Spectroscopy). The ESI-MS spectra were

recorded in MeCN/ H_2O 1:1 with 0.1% of Formic acid, using am analytic C-18 column (Luna, 5 μm, 100 Å, 150 x 2 mm, Phenomenex) and Quadrupole LC/MS (6120). The ^{1}H-NMR spectra were recorded in deuterated dimethyl sulfoxide (DMSO-*d6*), with tetramethylsilane (TMS) as internal standard at the frequency of 400MHz, using a Varian Innova Instrument Spectrometer.

5.2. Peptide hydrogel preparation

Peptides were dissolved in an alkaline saline buffer (sodium phosphate 0.1M pH=12) in ultrasonic bath, at 50 °C, then the peptide solution was diluted 1:1 using a mild acid saline buffer (0.1 M sodium phosphate, pH~5.8). The pH trigger was used to drive the self-assembly of peptide zwitterions, to achieve final supramolecular hydrogel at neutral pH (~7).

5.3. Hydrogel characterisation

Hydrogel nature of the peptide was confirmed by Oscillatory Rheometry measurements whereas secondary structures of the heterochiral tripeptides were determined by Circular Dichroism (CD) Spectroscopy. Morphology of the nanostructures were assessed by Transmission Electron Microscopy (TEM).

5.3.1. Oscillatory Rheometry

Dynamic time sweep rheological analyses were conducted on a Malvern Kinexus Ultra Plus Rheometer (Alfatest) with a 20 mm stainless steel parallel plate geometry, at fix temperature of 25°C using a Peltier temperature controller. All the samples were prepared in situ, and immediately analysed with a gap of 1.00 mm. Time sweeps were recorded for 1 hour, using 1.00 Hz frequency and 1.00 or 2.00 Pa (depending from the sequence) controlled stress conditions. After 1h, frequency sweeps were recorded using a 1.00 or 2.00 (depending from the sequence) Pa controlled stress and final stress sweeps were recorded using 1.00 Hz frequency.

5.3.2. Transmission Electron Microscopy (TEM)

Nanostructure morphology of each peptide was assessed by TEM analyses. Small aliquot of gels prepared 24 hours before were deposited on a TEM grid (carbon-coated 300 mesh copper grid), dried opportunely and contrasted by aqueous tungsten phosphate solution (pH ~7.3±0.1). Grids were

maintained air-dried until their examination using Jeol, JEM 2100 instrument at 100 kV. The average size of the nanostructures was determined by considering 100 measurements.

5.3.3. Circular Dichroism (CD) Spectroscopy

The secondary structure of peptides was analysed using a 0.1 mm quartz cell on a Jasco J815 Spectropolarimeter, with 1 s integrations, one accumulation and a step size of 1 nm with a bandwidth of 1 nm over a range of wavelengths from 185 to 285 nm at 25°C. All the samples were freshly prepared in situ, mixing the peptide dissolved in alkaline buffer, after the addition of the second mild acid buffer directly in the CD cell. Analysis of peptides in presence of SDS were performed dissolving peptides in 30 mM SDS (prepared in PB at pH=7.2).

5.4. X-Ray Diffraction (XRD) single crystal structures

Crystals of heterochiral and homochiral tripeptides were grown using the sitting-drop vapour diffusion method. Each peptide was dissolved in a specific organic solvent at very low concentration. 1.5 mL were deposited and put in vapour diffusion with a reservoir containing 3 mL a mixture at different ratio of the solvents in which the peptide was dissolved and another solvent or MilliQ water. Single crystals were grown upon a range of few weeks or even 6 months period, depending from the sequence.

A single crystal of the peptides was collected with a loop, cryoprotected and stored frozen in liquid nitrogen. The crystals were mounted on the diffractometer at the synchrotron Elettra, Trieste (Italy), beamline XRD1, using the robot present at the facility. Temperature was kept at 100 K by a stream of nitrogen on the crystals. Diffraction data were collected by the rotating crystal method using synchrotron radiation, wavelength 0.70 Å, rotation interval 1°/image, crystal-to-detector distance of 85 mm. Reflections were indexed and integrated using the XDS package, space group was determined using POINTLESS and the resulting data set was scaled using AIMLESS.[119,120,124] Phase information were obtained by direct methods using the software SHELXT.[128] Refinements cycles were conducted with SHELXL-14, operating through the WinGX GUI, by full-matrix least-squares methods on F^2. Moreover, more information can be found in description of crystallographic details for each peptide crystal structure.

5.5 Antimicrobial assays

5.5.1. Preparation of MH broth

Suspend 21 grams in 1000 ml distilled water. Heat to boiling to dissolve the medium completely. Mix well and dispense into tubes as desired. Sterilize by autoclaving at 15 lbs pressure (121°C) for 15 minutes. Cool to 45-50°C.

5.5.2. Preparation of Inoculum

Inocula of E. coli (ATCC 25922) was prepared by growing cells overnight in MH broth. The suspension was diluted with MH and put growing cells to a log phase (1-2 h) to final optical density (OD) readings of 0.5-0.7 with a spectrophotometer at 600 nm. The bacteria suspension was diluted to $2*10^5$ CFU*ml^{-1} with MH broth for MIC and Micro well gel diffusion assay and to $1*10^3$ CFU*ml^{-1} for microscopy live/dead assay.

5.5.3. Preparation of Colistin Sulfate salt solution (Positive Control)

Colistine sulfate salt (Polymyxin E) (Sigma Aldrich - C4461) was dissolved in sodium phosphate buffer (10 mM, pH = 7.8) at concentration of 0.5 mg/ml as stock solution. All buffer solutions were filtered (0.2 μm) prior to use.

5.5.4 The minimum inhibitory concentration (MIC)

The minimum inhibitory concentration (MIC) is the lowest concentration of a peptide that prevents visible growth of bacteria. Minimal inhibitory concentration was determined by a standard microtiter dilution method. Cells were grown overnight at 37 °C, 140 RPM in MH broth and were diluted in the same medium. Peptide solution is prepared in buffer PB (0.1 M) at concentration of 500 μM by adding 2 % of DMSO to help peptide dissolution. Serial dilutions of the peptides were added into 96-well microtiter plates in a volume of 90 μl/well (500 μM, 250 μM, 125 μM, 63 μM, 125 μM, 32 μM, 16 μM), followed by the addition of 10μl of bacteria to give final inoculums of 2×10^5 colony-forming units(CFU)/ml. As positive control was used colistine sulfat salt prepared in PBS (10 mM) at concentration of 10 μM, and as a negative control were used both PB and also PB containing 2 % of DMSO. All buffer solutions were filtered (0.2 μm) prior to use. The plates were incubated at 37 °C for 24 h and the optical density (OD) was measured with a spectrophotometer at 600 nm. Finally, CFU/ml was calculated by following equation.

$$CFU/ml = Absorbance\ (600\ nm) * 4.6 * 10^7 : 0.31$$

5.5.5 Micro-gel well diffusion assay

Bacteria inoculate was prepared as mentioned above. 20 mL of MH agar were melted, then cooled to 55 °C and finally inoculated with the bacteria. The inoculated agar was poured into the Petri dish plate, and allowed to cool down on a levelled surface. Once the medium has solidified, 2 wells of 6 mm in each dish were made. 30 µl of peptide at 8 mM dissolved in buffer 1 (pH 12.0) were put in every well and after that 30 µl of second buffer were added in order to form supramolecular structures and reach final concentration of 4 mM (as describe in *Section 5.3*.) The plates were incubated in a humid chamber for 20 h at 37 °C. The bacteria were distributed over the plate achieving uniformly circular inhibition zones. The plates with inhibition zone of bacterial growth were imaged and the measurements of inhibition diameter were performed by Fiji, at least 60 measures on 6 plates (3 independent measurements).

5.5.6 Live/Dead Microscopy Assay

Peptide self-assembled hydrogels were prepared as described above (*Section 5.3*) and added to each microwell of a µ-slide Angiogenesis uncoated (Ibidi) in a laminar-flow cabinet. In each well 20 µl of solution/hydrogel of peptide were placed and self-assembled for 24 h, then in each well 10 µl of bacteria suspension ($1*10^3$ $CFU*ml^{-1}$) were added and incubated for 24 h. After 24 h of incubation staining for live/dead bacteria were added (acridine orange (AO) 20 µM in PBS 50 mM and propidium iodide (PI) 30 µM in PBS 50 mM). Analysis of the samples permits determination of cell viability using two common microscope filters (FITC and TRITC) (*Figure 3.75*). The images are performed using Microscopy instruments, in reverse phase, 60x. Finally, all data are processed using *Adobe Photoshop C26*.

5.5.7 Outer membrane permeability Assay

Measurements were performed using the 1-N-Phenylnaphthylamine (NPN) uptake assay. Peptide supramolecular structures were prepared as mentioned above (at 4 mM) and self-assembled for 24 h before adding bacterial suspension. *E. coli* bacteria (ATCC 25922) were grown overnight in MH media and diluted (1:100) in MH and grown for 1 h at 37 °C until an OD_{600} of 0.5-0.7. Bacteria were then washed with 10 mM Tris HCl, 150 mM NaCl buffer (pH 7.4) and resuspended in the same buffer

with 10 μM NPN. The resuspended bacterial samples were then transferred to 96-well plates containing peptide supramolecular structures self-assembled for 24 h. The changes in the fluorescence emission was measured between 450–600 nm with excitation at 380 nm, using TECAN M1000 Infinity microplate reader. 1% TritonX-100 was used as a positive control.

5.5.8 Sum frequency generation vibrational spectroscopy

Sum frequency generation vibrational spectroscopy was performed to study in situ the interactions between peptides and a single lipid bilayer in real time. Using peptides at 4 mM and a dipalmitoyl phosphatidylglycerol bilayer as a model system, the C-H and C-D stretching signals from isotopically symmetric or asymmetric dipalmitoyl phosphatidylglycerol bilayers was monitored during their interaction with peptide. Bilayer was deposited on CaF_2 right angle prisms via the Langmuir–Blodgett. A clean CaF_2 prism is immersed in water with the right-angle face to be coated perpendicular to the water surface. A suitable amount of lipid chloroform solution is then spread onto the water surface in a Langmuir trough. After the evaporation of chloroform, the surface area is then compressed at a rate of 5 mm/min until the surface pressure reaches 34 mN/m. The prism is vertically lifted up at 2 mm/min, while the surface pressure is maintained at 34 mN/m by a feedback system controlling the trough surface area. The right angle face with the newly coated lipid monolayer is then faced parallel to the water surface and lowered until it contacts the lipid monolayer at the air/water interface (also with a surface pressure of 34 mN/m). After this fabrication process, the bilayer is kept under water since exposure to air will destroy the delicate bilayer structure. For SFG experiments, the bilayer is immersed in a small reservoir filled with 1.8 mL ultrapure water. An appropriate amount of peptide fibers at 4 mM were injected into the reservoir and stirred to achieve the desired solution concentration.

5.5 Biological performance of peptides

5.6.1 Haemolysis Assay

Haemolysis assay was modified from a 96-well microplate model described by Evans *et al*. (J.Vis Exp. 2013; (73): 50166). Peptide-hydrogels were formulated in a well of 96-well microplate (NUNC) by mixing up 30 µl of buffer B1 with peptide and 30 µl of buffer B2. Human red blood cells were centrifuged at 800 x g for 10 min, washed twice with PBS after moving the supernatant (plasma) and ‘buffy coat’, and then resuspended in phosphate-buffered saline (pH 7.4).

5.6.1.1 Haemolysis Assay under dynamic flow conditions

First, was examined the toxicity of peptide-hydrogels to erythrocytes under a dynamic flow condition mimicking human bloodstream. 100 µl of RBC suspension at a density of 5 $x10^9$ cells/ml were added to a microwell containing pre-formed peptide-fibers at 4 mM. The microplate was incubated at 37° C for 2 h with shaking at 75 rpm. Triton X-100 at 2% (Sigma-Aldrich) served as a positive control, and tissue culture treated polystyrene (TCPS) surface without hydrogel served as a negative control. After incubation, the microplates were centrifuged at 800 x g for 10 min. 80 µl from each well were transferred to a new microplate. The release of haemoglobin was monitored by measuring the absorbance at 540 nm and was expressed as a percentage of the value for Triton X-100-induced haemolysis.

5.6.1.2 Direct-contact mediated Haemolysis Assay

To ensure adequate contact between erythrocytes and hydrogels, an issue often encountered in the dynamic haemolysis assay, a direct-contact-mediated haemolysis assay was also carried out. After peptide hydrogels were prepared in the 96-well microplate, 100 uL of RBC suspension containing 5 $x10^6$ cells were added to a microwell containing pre-formed peptide-hydrogel. The microplate was centrifuged at 500x g for 5 mins to allow erythrocytes to evenly form monolayers on the hydrogel surface. The microplate was then incubated at 37° C for 2 h without shaking. Quantification of haemolysis was as described in the dynamic flow model.

5.6.2 *In vitro* peptide stability to proteases degradation

5.6.2.1 Peptide stability in solution

The peptide was dissolved in 250 µl of DMSO and 4.75 ml of 50 mM sodium phosphate buffer (pH 7.5) containing a large excess (5 mg) of proteinase K (Sigma Aldrich) in 15 ml Falcon tubes. The tubes were incubated at 37 °C, 60 rpm. After 24 h of incubation with proteases 2 ml of NaOH 1 mM were added to the solution to stop enzyme reaction. Then 500 µl of samples were filtred (0.4 µm filter) and analysed by HPLC (Abs 254 nm, same program as described above for peptide purification). Peptide final concentration is calculated from equation obtained from peptide calibration (analysis at known concentration *i.e.*, 1.00, 0.75, 0.50, 0.25, 0.125 mg/ml). All data are obtained from 3 independent analysis.

5.6.2.2 Peptide stability in hydrogel state

The assay on gel was performed by preparing 250 µl of peptide hydrogel at minimum gelation concentration in 15 ml-Falcon tubes. The gel was left to self-assemble overnight. The following morning, 4.75 ml of 50 mM sodium phosphate buffer (pH 7.5) containing a large excess (5 mg) of protease were added on top. The tubes were incubated at 37°C, 60 rpm, and after 24 hours, 2 ml of NaOH 1M were added to completely dissolve the gel and slow-down protease activity prior to HPLC analysis as described above. Average and standard deviation values (n=3) were calculated and plotted with Excel.

6. APPENDIX

6.1 Peptides spectroscopic data

1a - ^{D}Leu-^{L}Phe-^{L}Phe

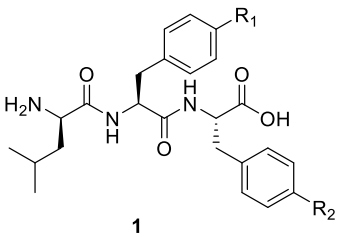

1

Chemical Formula: $C_{24}H_{31}N_3O_4$
Exact Mass: 425.23
Molecular Weight: 425.53
m/z: 425.23 (100.0%), 426.23 (26.0%), 427.24 (2.7%), 426.23 (1.1%)
Elemental Analysis: C, 67.74; H, 7.34; N, 9.88; O, 15.04

^{1}H-NMR (500 MHz, DMSO):δ (ppm) 8.70 ppm (d, *J* = 8.8 Hz, 1H, **NH**), 8.60 ppm (d, *J* = 7.8 Hz, 1H, **NH**), 7.40-7.08 ppm(m, 10H, **Ar**), 4.78-4.63 ppm (m, 1H, **αCH**), 4.45 ppm (td, *J* = 8.6, 5.1 Hz, 1H, **αCH**), 3.60 ppm (dd, *J* = 22.6, 16.2 Hz 1H, **αCH**), 3.18-3.00 ppm (m, 2H, **βCH**), 2.94 ppm (dd, 1H, J=14.0; 9.2 Hz, **βCH**), 2.65 ppm (dd, *J* = 13.7; 11.5 Hz, 1H, **βCH**), 1.26-0.92 ppm (m, 3H, **β and γ CH**), 0.68 ppm (dd, *J* = 9.2, 6.2 Hz, 6H, **δCH3**).

MS (ESI): m/z 426.2 (M+H), C24H31N3O4 requires 425.2.

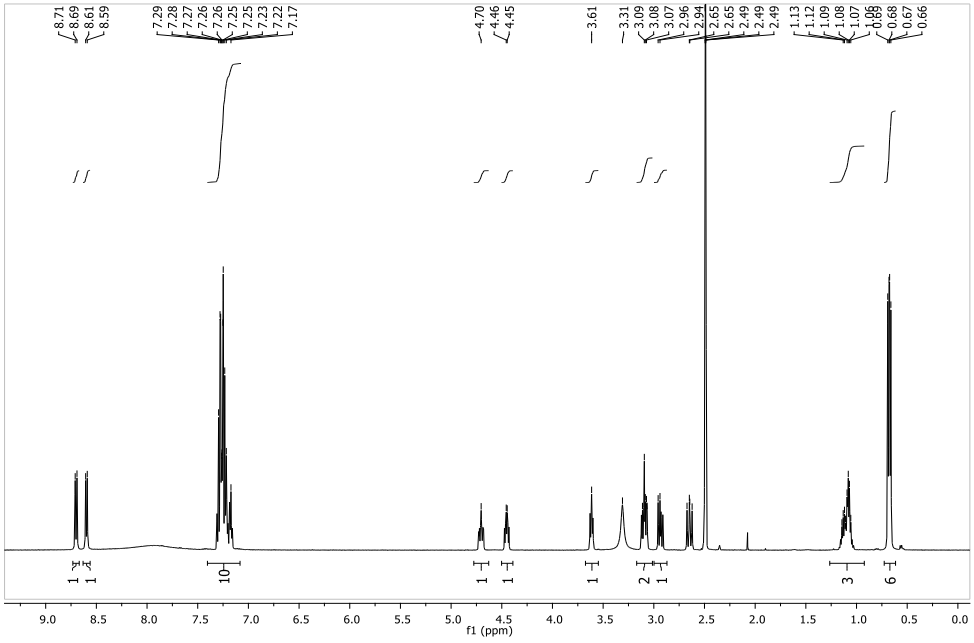

Figure 6.1 ^{1}H-NMR spectrum of ^{D}Leu-^{L}Phe-^{L}Phe.

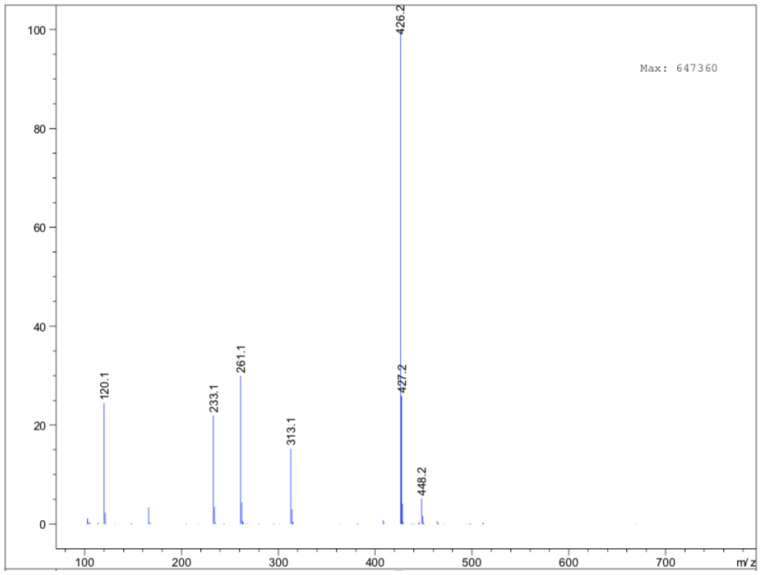

Figure 6.2 ESI-MS spectrum of ^{D}Leu-^{L}Phe-^{L}Phe.

2a - ^{L}Leu-^{D}Phe-^{D}Phe

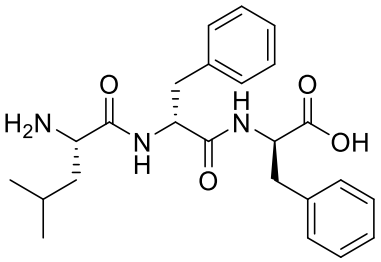

Chemical Formula: $C_{24}H_{31}N_3O_4$
Exact Mass: 425.23
Molecular Weight: 425.53
m/z: 425.23 (100.0%), 426.23 (26.0%), 427.24 (2.7%), 426.23 (1.1%)
Elemental Analysis: C, 67.74; H, 7.34; N, 9.88; O, 15.04

^{1}H-NMR (400 MHz, DMSO):δ (ppm) 8.61 ppm (d, *J* = 8.3 Hz, 1H, **NH**), 8.45 ppm (d, *J* = 7.9 Hz, 1H, **NH**), 7.51-6.79 ppm(m, 10H, **Ar**), 4.60 ppm (m, 1H, **αCH**), 4.44 ppm (m, 1H, **αCH**), 3.68 ppm (m, 1H, **αCH**), 3.14-3.04 ppm (m, 2H, **βCH**), 2.95-2.83 ppm (m, 1H, **βCH**), 2.65 ppm (dd, *J* = 13.7; 11.5 Hz, 1H, **βCH**), 1.10 ppm (m, 3H, **β and γ CH**), 0.67 ppm (m, 6H, **δCH3**).

MS (ESI): m/z 426.2 (M+H), C24H31N3O4 requires 425.2.

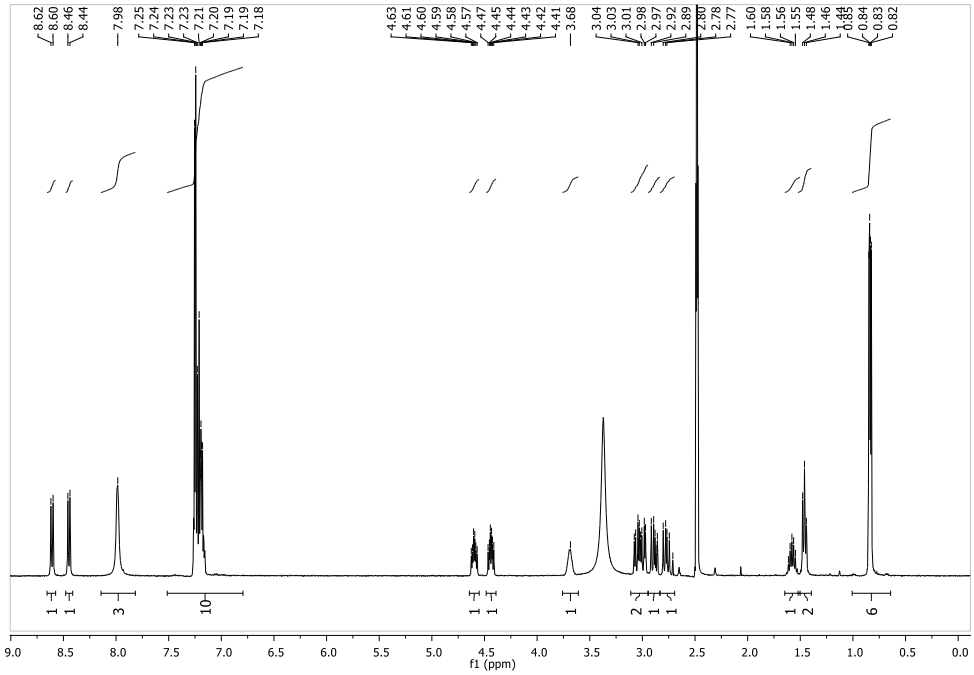

Figure 6.3 ^{1}H-NMR spectrum of ^{L}Leu-^{D}Phe-^{D}Phe.

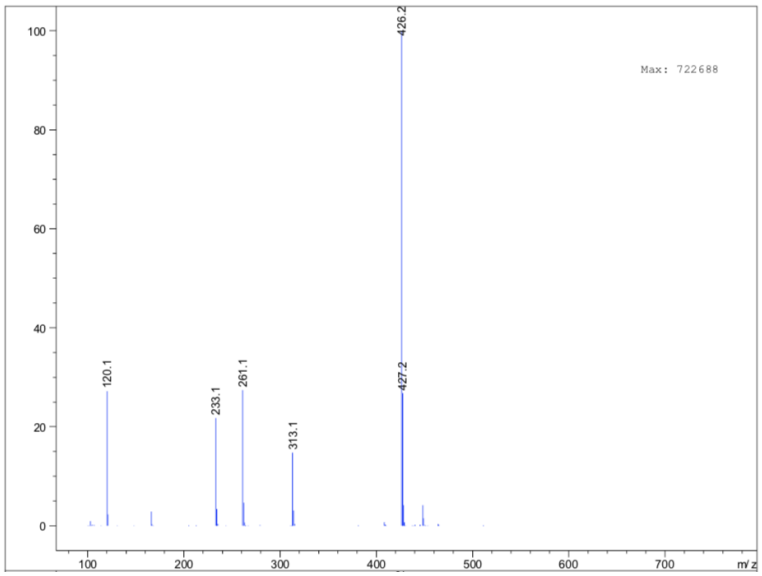

Figure 6.4 ESI-MS spectrum of ^{L}Leu-^{D}Phe-^{D}Phe.

3a - ^{L}Leu-^{L}Phe-^{L}Phe

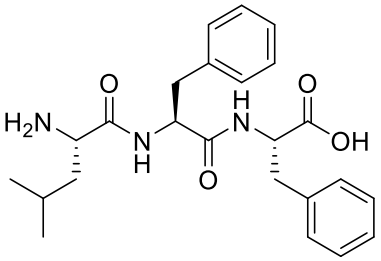

Chemical Formula: $C_{24}H_{31}N_3O_4$
Exact Mass: 425.23
Molecular Weight: 425.53
m/z: 425.23 (100.0%), 426.23 (26.0%), 427.24 (2.7%), 426.23 (1.1%)
Elemental Analysis: C, 67.74; H, 7.34; N, 9.88; O, 15.04

^{1}H-NMR (400 MHz, DMSO):δ (ppm) 8.62 ppm (d, *J* = 8.3 Hz, 1H, **NH**), 8.44 ppm (d, *J* = 7.9 Hz, 1H, **NH**), 7.30-7.12 ppm (m, 10H, **Ar**), 4.60 ppm (td, *J*=8.9, 4.7 Hz, 1H, **αCH**), 4.44 ppm (td, *J*=8.7, 5.1 Hz, 1H, **αCH**), 3.69 ppm (t, *J*=7.1 Hz, 1H, **αCH**), 3.02 ppm (ddd, *J*=25.0, 14.0, 4.9, 2H, **βCH**), 2.95-2.83 ppm (m, 1H, **βCH**), 2.78 ppm (dd, *J* = 14.0, 9.1 Hz, 1H, **βCH**), 2.78 ppm (dd, *J*= 14.1; 9.2, 1 H, **βCH**), 1.65-1.51 ppm (m, 1 H, **γCH**) 1.52-1.40 ppm (m, 2H, **βCH**), 0.84 ppm (dd, *J* = 6.4, 3.5 Hz, 6H, **δCH3**).

MS (ESI): m/z 426.2 (M+H), C24H31N3O4 requires 425.2.

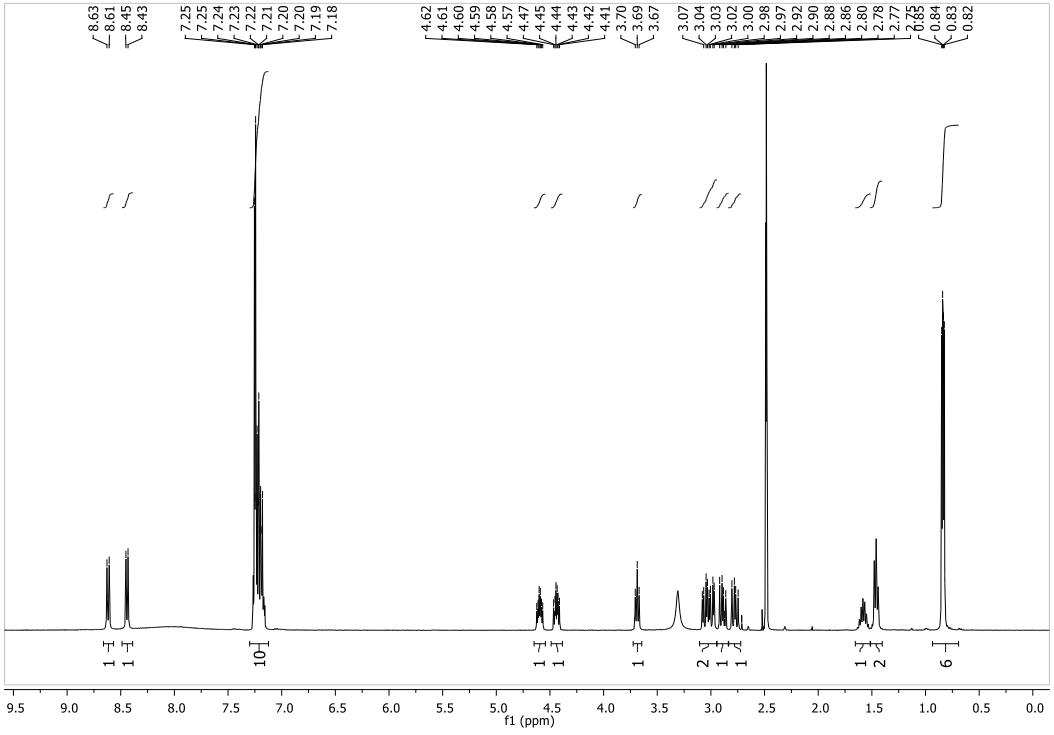

Figure 6.5 ^{1}H-NMR spectrum of ^{L}Leu-^{L}Phe-^{L}Phe.

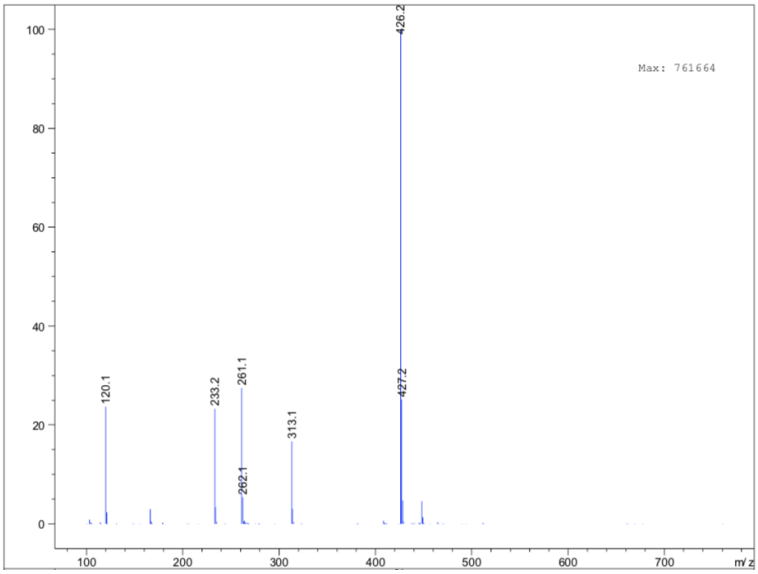

Figure 6.12 ESI-MS spectrum of ^{L}Leu-^{L}Phe-^{L}Phe.

5a - ^{L}Ile-^{D}Phe-^{D}Phe

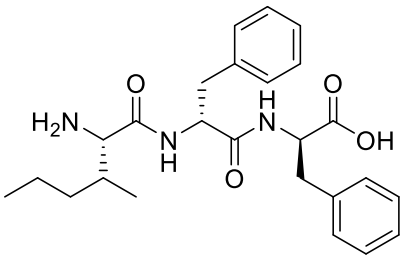

Chemical Formula: $C_{24}H_{31}N_3O_4$
Exact Mass: 425.23
Molecular Weight: 425.53
m/z: 425.23 (100.0%), 426.23 (26.0%), 427.24 (2.7%), 426.23 (1.1%)
Elemental Analysis: C, 67.74; H, 7.34; N, 9.88; O, 15.04

^{1}H-NMR (400 MHz, DMSO, TMS):δ (ppm) 8.57 ppm (dd, *J* = 16.2; 8.2 Hz, 2H, **NH**), 7.56-6.90 ppm (m, 10H, **Ar**), 4.72 ppm (t, *J*= 9.9 Hz, 1H, **αCH**), 4.43 ppm (dd, *J= 13.4, 8.1* Hz, 1H, **αCH**), 3.53 ppm (d, *J*= 3.6 Hz, 1H, **αCH**), 3.12-3.02 ppm (m, 2H, **βCH**), 2.92 ppm (d, *J=13.9; 9.3 Hz*, 1H, **βCH**), 2.64 ppm (t, *J* = 12.8 Hz, 1H, **βCH**), 1.49 ppm (s, 1H, β**CH**), 0.88 ppm (s, 2H, **γCH**), 0.54 ppm (t, *J*=6.6 Hz, 6H, **γ and δ CH3**).

MS (ESI): m/z 426.2 (M+H), C24H31N3O4 requires 425.2.

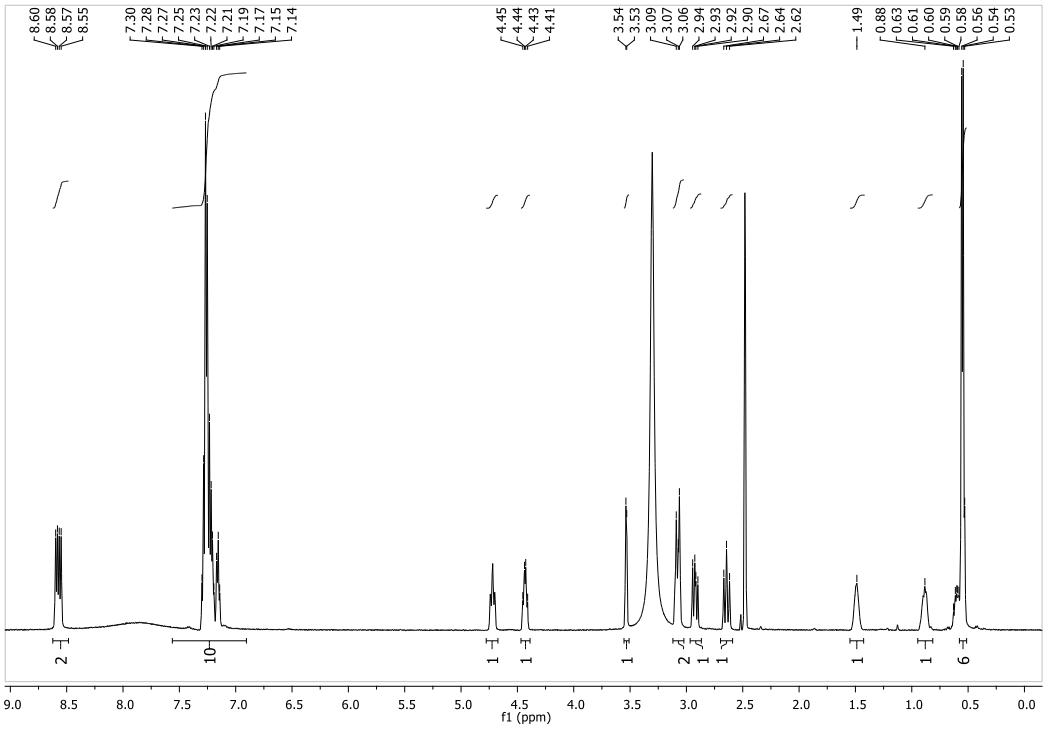

Figure 6.6 ^{1}H-NMR spectrum of ^{L}Ile-^{D}Phe-^{D}Phe.

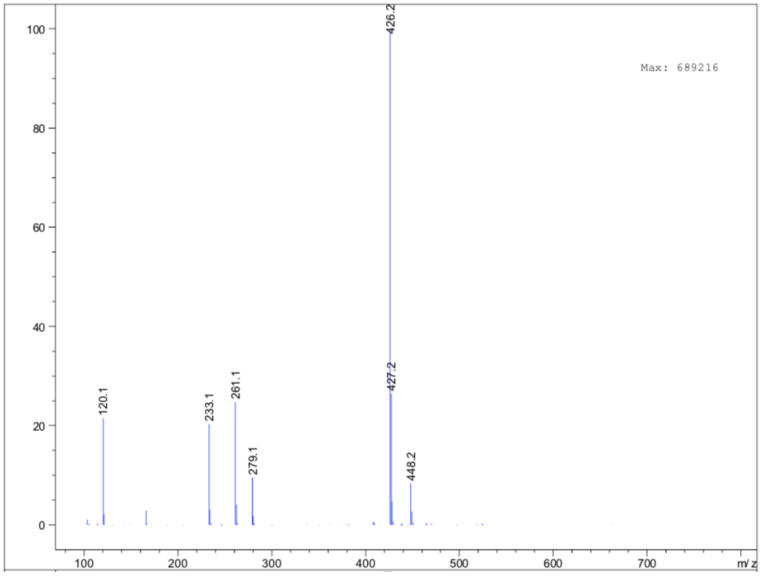

Figure 6.7 ESI-MS spectrum of ^{L}Ile-^{D}Phe-^{D}Phe.

6a - ^{L}Nle-^{D}Phe-^{D}Phe

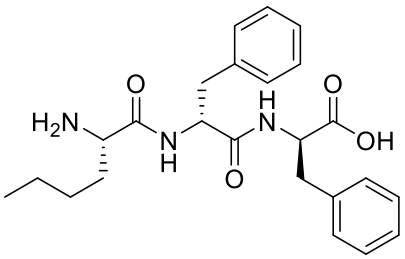

Chemical Formula: $C_{24}H_{31}N_3O_4$
Exact Mass: 425.23
Molecular Weight: 425.53
m/z: 425.23 (100.0%), 426.23 (26.0%), 427.24 (2.7%), 426.23 (1.1%)
Elemental Analysis: C, 67.74; H, 7.34; N, 9.88; O, 15.04

^{1}H-NMR (400 MHz, DMSO):δ (ppm) 8.62 ppm (dd, *J* =16.0, 8.3 Hz, 2H, **NH**), 7.30-7.14 ppm(m, 10H, **Ar**), 4.71-4.70 ppm (m, 1H, **αCH**), 4.46-4.42 ppm (m, 1H, **αCH**), 3.65 ppm (s, 1H, **αCH**), 3.12-3.05 ppm (m, 2H, **βCH**), 2.93 ppm (dd, *J*=14.0, 9.2 Hz, 2H, **βCH**), 2.64 ppm (dd, *J*=13.8, 11.4 Hz, 1H, **βCH**), 1.35-1.29 ppm (m, 2H, **βCH**), 1.03-0.98 ppm (m, 2H, **γCH**), 0.71-0.69 (m, 1H, **δCH$_3$**), 0.64-0.58 (m, 4H, **δ and ε CH**).

MS (ESI): m/z 426.2 (M+H), C24H31N3O4 requires 425.2.

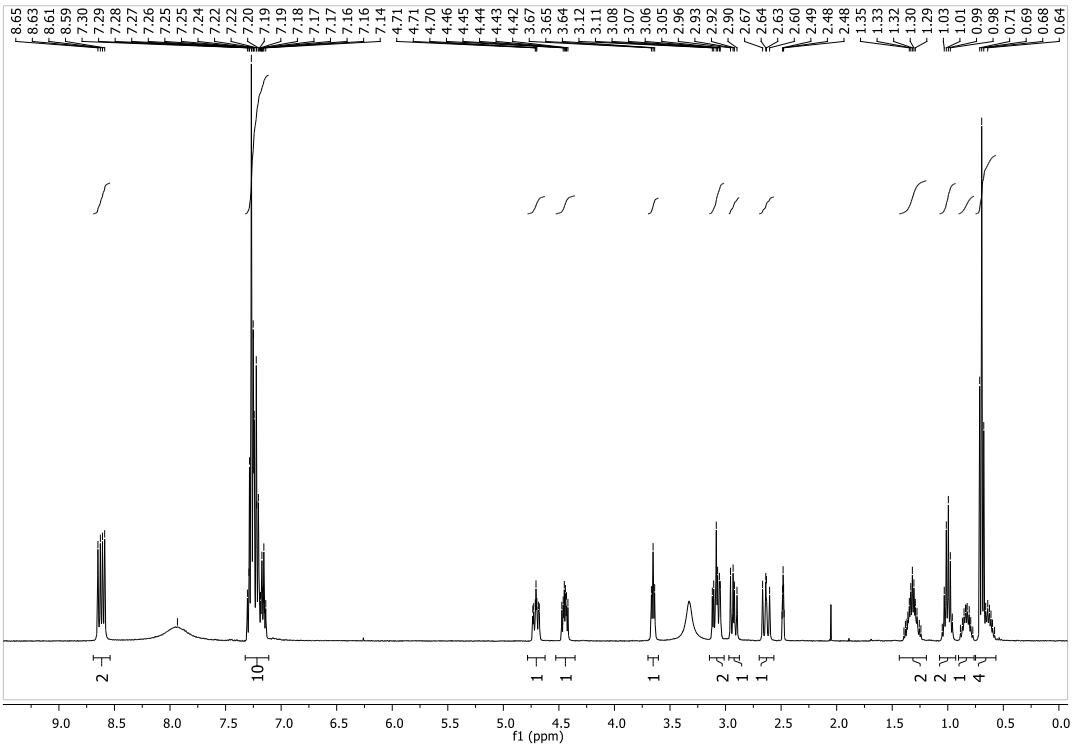

Figure 6.8 ^{1}H-NMR spectrum of ^{L}Nle-^{D}Phe-^{D}Phe.

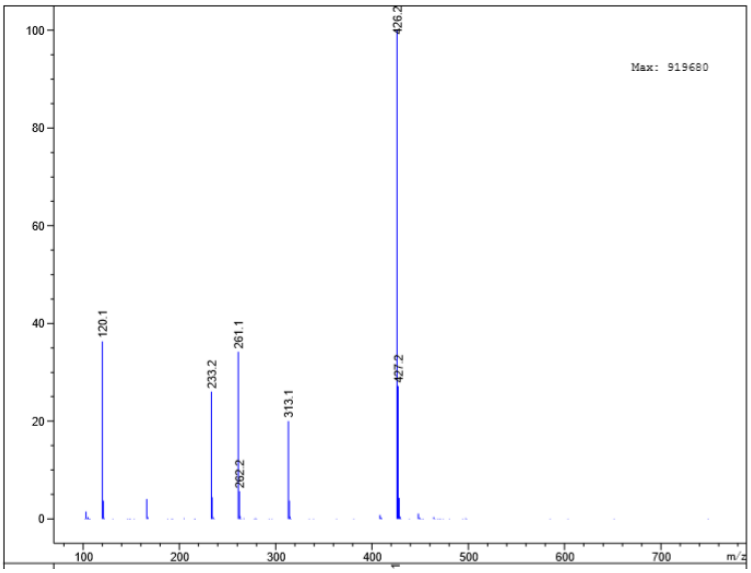

Figure 6.9 ESI-MS spectrum of ^{L}Nle-^{D}Phe-^{D}Phe.

7a - ^{D}Val-^{L}Phe-^{L}Phe

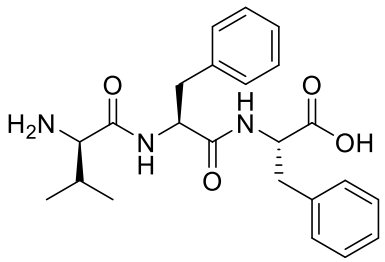

Chemical Formula: $C_{23}H_{29}N_3O_4$
Exact Mass: 411.22
Molecular Weight: 411.50
m/z: 411.22 (100.0%), 412.22 (24.9%), 413.22 (2.7%), 412.21 (1.1%)
Elemental Analysis: C, 67.13; H, 7.10; N, 10.21; O, 15.55

^{1}H-NMR (400 MHz, DMSO, TMS):δ (ppm) 8.65-8.60 ppm (m, 2H, **NH**), 7.89 ppm (s, 2H, **NH**$_2$) 7.51-6.79 ppm (m, 10H, **Ar**), 4.76-4.74 ppm (m, 1H, **αCH**), 4.44-4.41 ppm (m, 1H, **αCH**), 3.68 ppm (s, 1H, **αCH**), 3.12-3.06 ppm (m, 2H, **βCH**), 2.95-2.83 ppm (m, 1H, **βCH**), 2.83-2.69 ppm (s, 1H, **βCH**), 1.58 ppm (m, 1H, **βCH**), 0.62 ppm (d, *J* = 7.0 Hz 2H, **γCH**), 0.35 ppm (d, *J* = 7.1 Hz, 3H, **γCH**).

MS (ESI): m/z 412.2 (M+H), C24H31N3O4 requires 411.2.

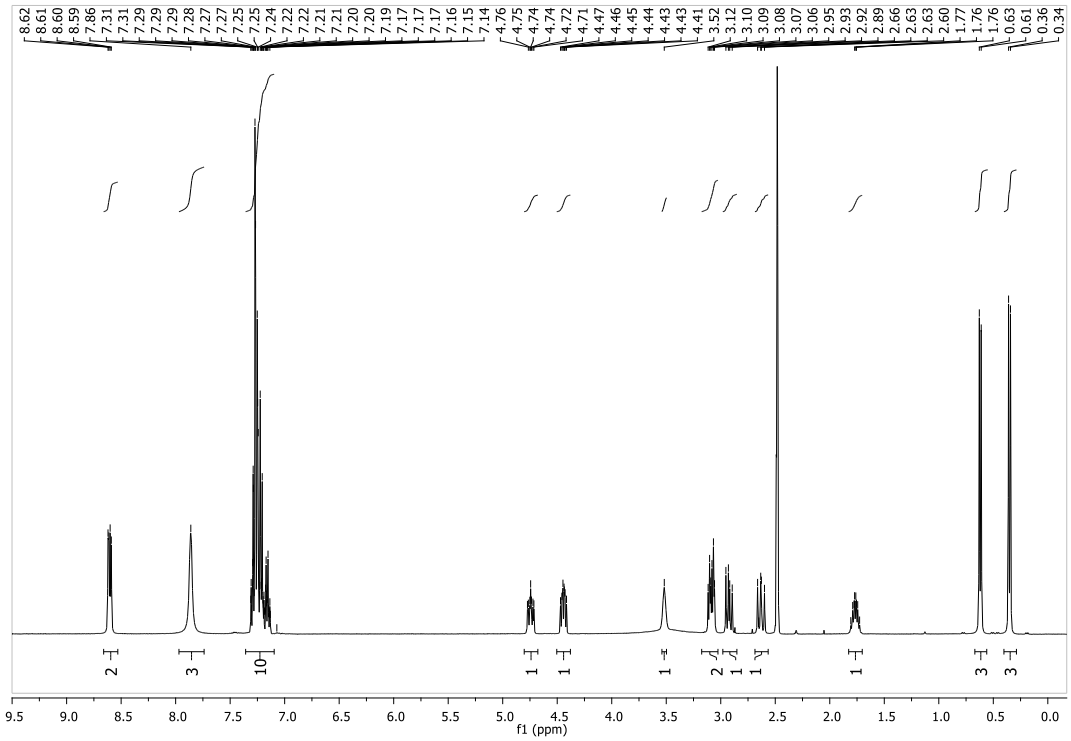

Figure 6.10 ^{1}H-NMR spectrum of ^{D}Val-^{L}Phe-^{L}Phe.

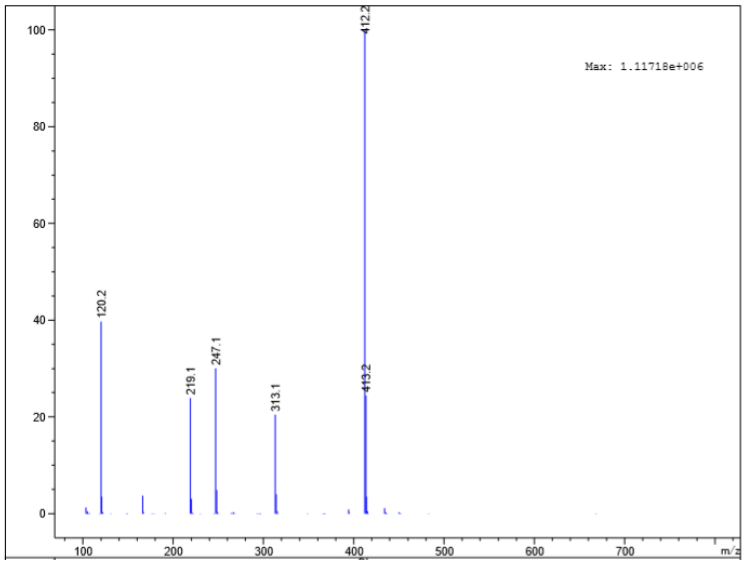

Figure 6.11 ESI-MS spectrum of ^{D}Val-^{L}Phe-^{L}Phe.

8a - ^{D}Val-^{L}Phe-^{D}Phe

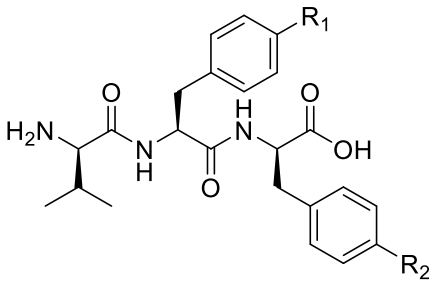

Chemical Formula: $C_{23}H_{29}N_3O_4$
Exact Mass: 411.22
Molecular Weight: 411.50
m/z: 411.22 (100.0%), 412.22 (24.9%), 413.22 (2.7%), 412.21 (1.1%)
Elemental Analysis: C, 67.13; H, 7.10; N, 10.21; O, 15.55

^{1}H-NMR (400 MHz, DMSO, TMS):δ (ppm) 8.71 ppm (d, *J* = 8.5 Hz, 1H, **NH**), 8.57 ppm (d, *J* = 8.9 Hz, 1H, **NH**), 7.29-7.07 ppm (m, 10H, **Ar**), 4.81-4.73 ppm (m, 1H, **αCH**), 4.55-4.45 ppm (m, 1H, **αCH**), 3.52 ppm (d, *J* = 4.5 Hz, 1H, **αCH**), 3.11 ppm (dd, *J* = 13.7, 4.7 Hz, 1H, **βCH**), 2.82 ppm (dd, *J* = 13.7, 10.1 Hz, 1H, **βCH**), 2.65 ppm (dd, *J* = 13.7, 3.4 Hz, 1H, **βCH**), 2.37 ppm (dd, *J* = 13.7, 11.1 Hz, 1H, **βCH**), 1.86-1.70 ppm (m, 1H, **βCH**), 0.64 ppm (d, *J* = 7.0 Hz 2H, **γCH**), 0.38 ppm (d, *J* = 7.0 Hz, 3H, **γCH**).

MS (ESI): m/z 412.2 (M+H), C24H31N3O4 requires 411.2.

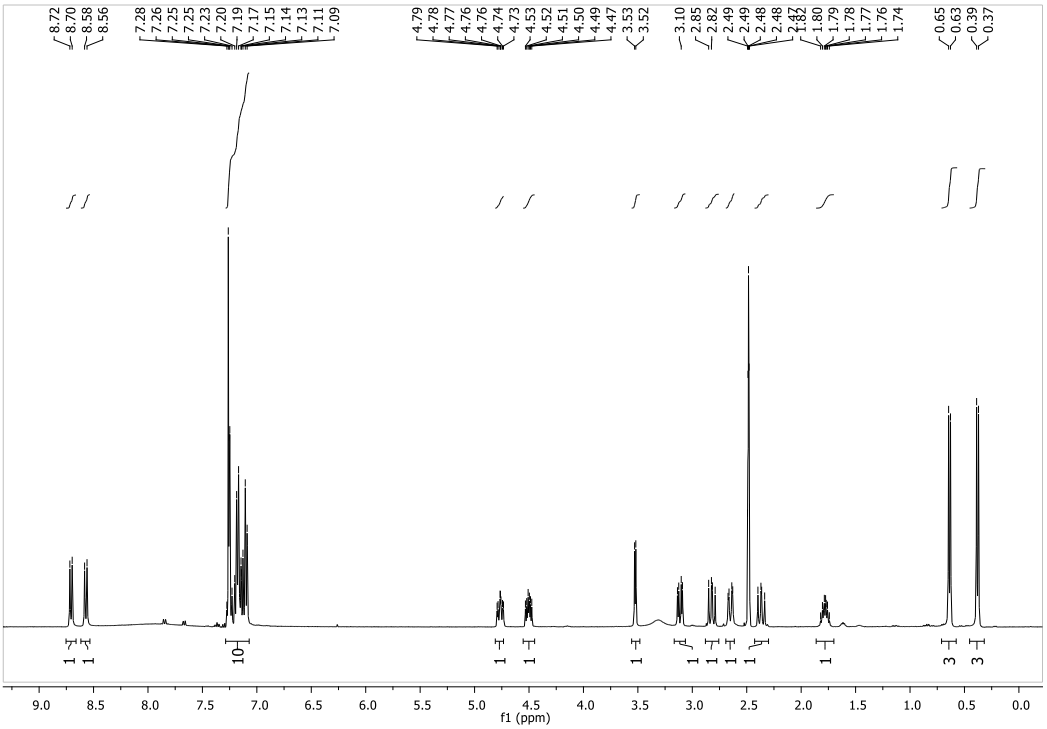

Figure 6.12 ^{1}H-NMR spectrum of ^{D}Val-^{L}Phe-^{D}Phe.

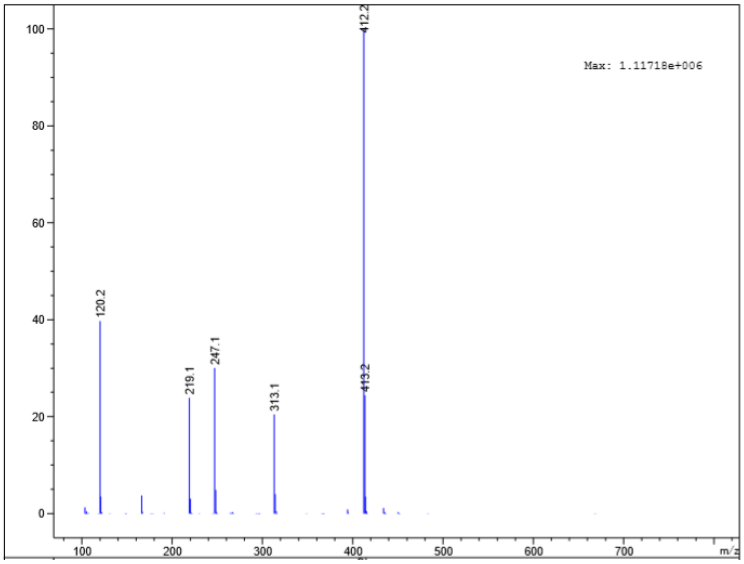

Figure 6.13 ESI-MS spectrum of ^{D}Val-^{L}Phe-^{D}Phe.

10a - ^{L}Phe-^{D}Leu -^{L}Phe

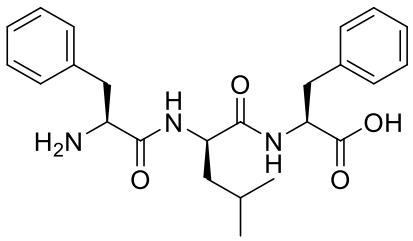

Chemical Formula: $C_{24}H_{31}N_3O_4$
Exact Mass: 425.23
Molecular Weight: 425.53
m/z: 425.23 (100.0%), 426.23 (26.0%), 427.24 (2.7%), 426.23 (1.1%)
Elemental Analysis: C, 67.74; H, 7.34; N, 9.88; O, 15.04

^{1}H-NMR (400 MHz, DMSO, TMS):δ (ppm) 8.50 ppm (d, *J* = 8.5 Hz, 1H, **NH**), 8.42 ppm (d, *J* = 8.6 Hz, 1H, **NH**), 7.36-7.06 ppm (m, 10H, **Ar**), 4.45-4.40 ppm (m, 1H, **αCH**), 4.36-4.27 ppm (m, 1H, **αCH**), 4.03 ppm (t, *J*=7.3 Hz, 1H, **αCH**), 3.08 ppm (dd, *J*=13.6, 4.4, 1H, **βCH**), 2.96-2.75 ppm (m, 2H, **βCH**), 2.78 ppm (dd, *J* = 13.6, 10.7 Hz, 1H, **βCH**), 1.01-0.83 ppm (m, 3H, **βCH** and **γCH**), 0.63 ppm (d, *J* = 5.8 Hz, 6H, **δCH3**).

MS (ESI): m/z 426.2 (M+H), C24H31N3O4 requires 425.2.

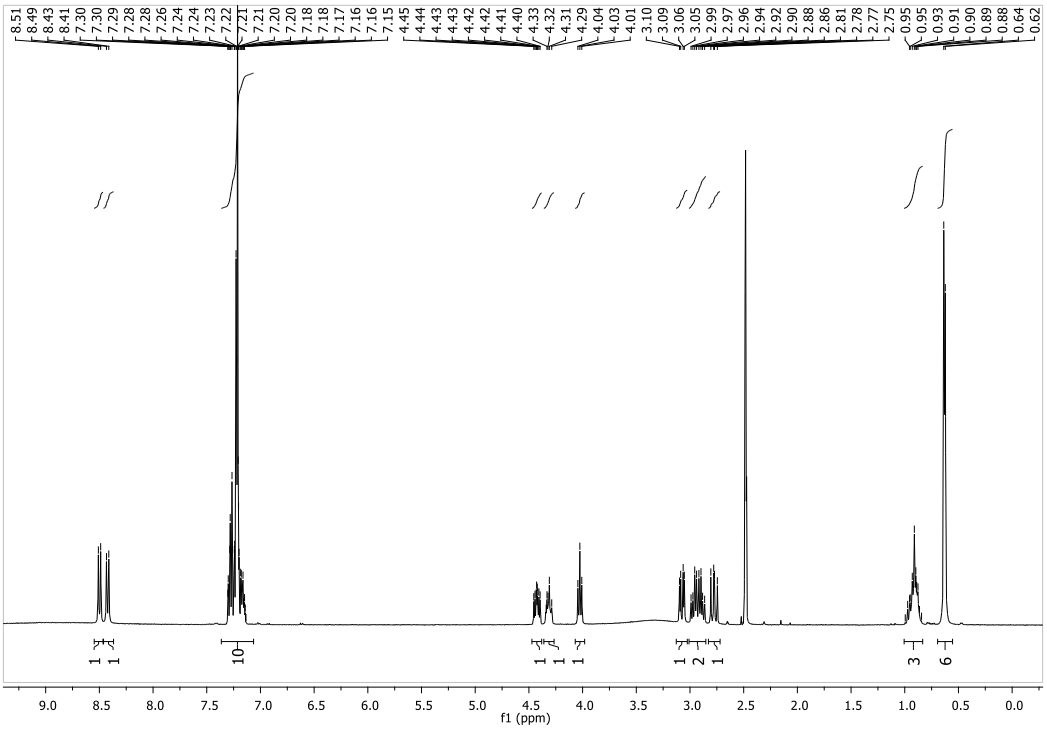

Figure 6.14 ^{1}H-NMR spectrum of ^{L}Phe-^{D}Leu-^{L}Phe.

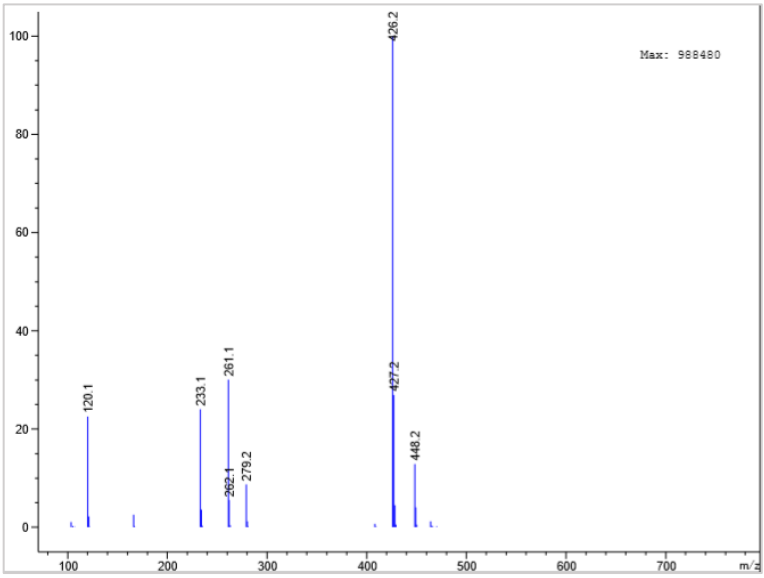

Figure 6.15 ESI-MS spectrum of ^{L}Phe-^{D}Leu^{L}Phe.

11a - ^{L}Phe-^{D}Ile -^{L}Phe

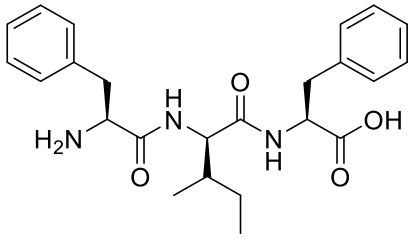

Chemical Formula: $C_{24}H_{31}N_3O_4$
Exact Mass: 425.23
Molecular Weight: 425.53
m/z: 425.23 (100.0%), 426.23 (26.0%), 427.24 (2.7%), 426.23 (1.1%)
Elemental Analysis: C, 67.74; H, 7.34; N, 9.88; O, 15.04

^{1}H-NMR (500 MHz, DMSO):δ (ppm) 8.50 ppm (d, *J* = 8.3 Hz, 1H, **NH**), 8.41 ppm (d, *J* = 9.0 Hz, 1H, **NH**), 7.35-7.14 ppm(m, 10H, **Ar**), 4.50-4.46 ppm (m, 1H, **αCH**), 4.34 ppm (dd, *J* = 8.8, 5.8 Hz, 1H, **αCH**), 4.20 ppm (t, *J* = 7.3 Hz, 1H, **αCH**), 3.08 ppm (dd, *J* = 13.8, 4.2 Hz, 1H, **βCH**), 3.01 ppm (dd, *J* = 13.7, 6.6 Hz, 1H, **βCH**), 2.91 ppm (dd, *J* = 13.7, 8.1 Hz, 1H, **βCH**), 2.78 ppm (dd, *J*=13.7, 10.8, 1H, **βCH**), 1.42-1.24 ppm (m, 1H, **βCH**), 1.01-0.80 (m, 1H, **γCH**), 0.63-0.44(m, 5H, **γCH),** 0.38 (d, *J* = 6.8 Hz, 3H, **δ CH**).

MS (ESI): m/z 426.2 (M+H), C24H31N3O4 requires 425.2.

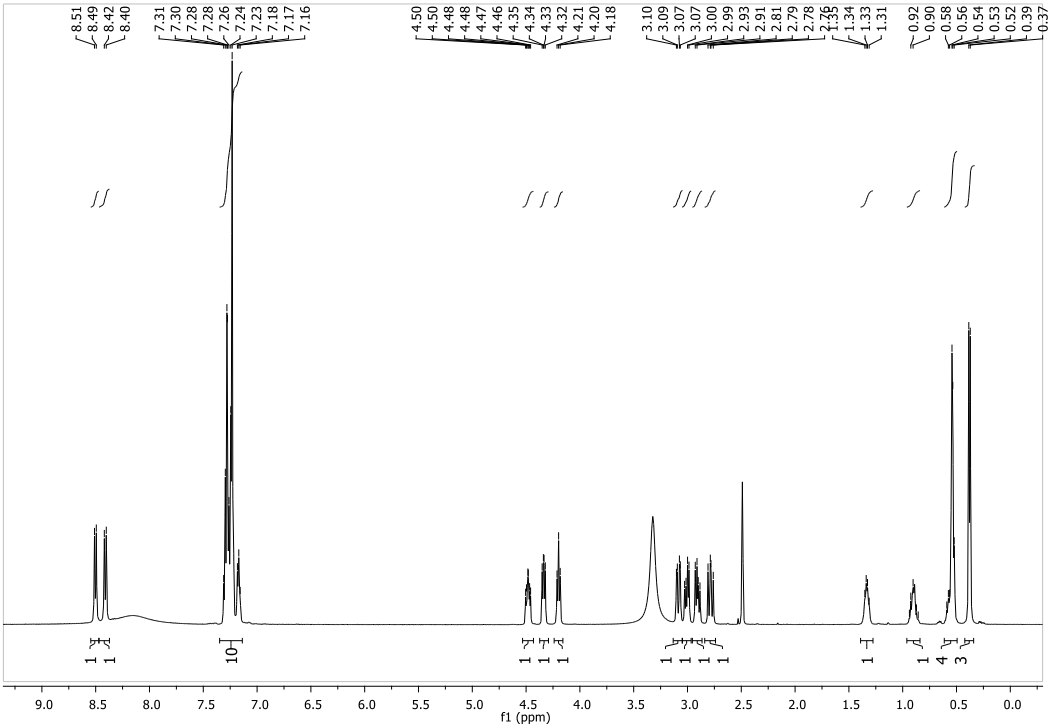

Figure 6.16 ^{1}H-NMR spectrum of ^{L}Phe-^{D}Ile-^{L}Phe.

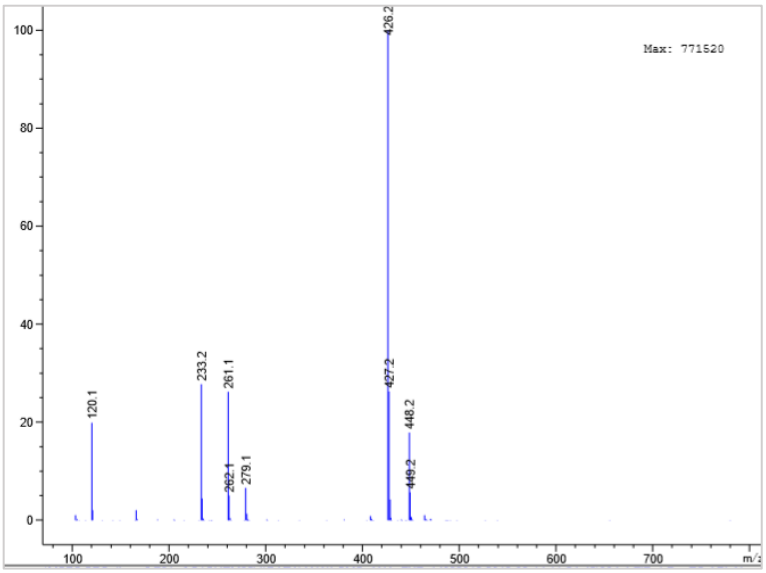

Figure 6.17 ESI-MS spectrum of ^{L}Phe-^{D}Ile-^{L}Phe.

12a - ^{L}Phe-^{D}Nle -^{L}Phe

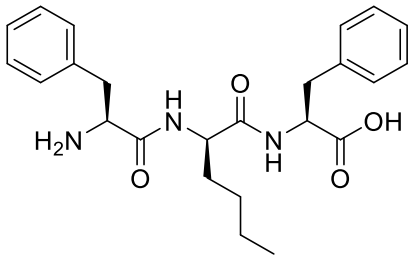

Chemical Formula: $C_{24}H_{31}N_3O_4$
Exact Mass: 425.23
Molecular Weight: 425.53
m/z: 425.23 (100.0%), 426.23 (26.0%), 427.24 (2.7%), 426.23 (1.1%)
Elemental Analysis: C, 67.74; H, 7.34; N, 9.88; O, 15.04

^{1}H-NMR (400 MHz, DMSO):δ (ppm) 8.47 ppm (d, *J* = 8.5 Hz, 1H, **NH**), 8.39 ppm (d, *J* = 8.4 Hz, 1H, **NH**), 7.36-7.11 ppm(m, 10H, **Ar**), 4.53-4.35 ppm (m, 1H, **αCH**), 4.36-4.27 ppm (m, 1H, **αCH**), 4.10 ppm (t, *J* = 7.3 Hz, 1H, **αCH**), 3.08 ppm (dd, *J* = 13.7, 4.2 Hz, 1H, **βCH**), 3.01-2.85 ppm (m, 2H, **βCH**), 2.74 ppm (dd, *J*=13.8, 11.4 Hz, 1H, **βCH**), 1.19-0.87 ppm (m, 4H, **βCH**, **γCH**), 0.90-0.76 (m, 1H, **δCH$_3$**), 0.70-0.60 (m, 5H, **δ and ε CH**).

MS (ESI): m/z 426.2 (M+H), C24H31N3O4 requires 425.2.

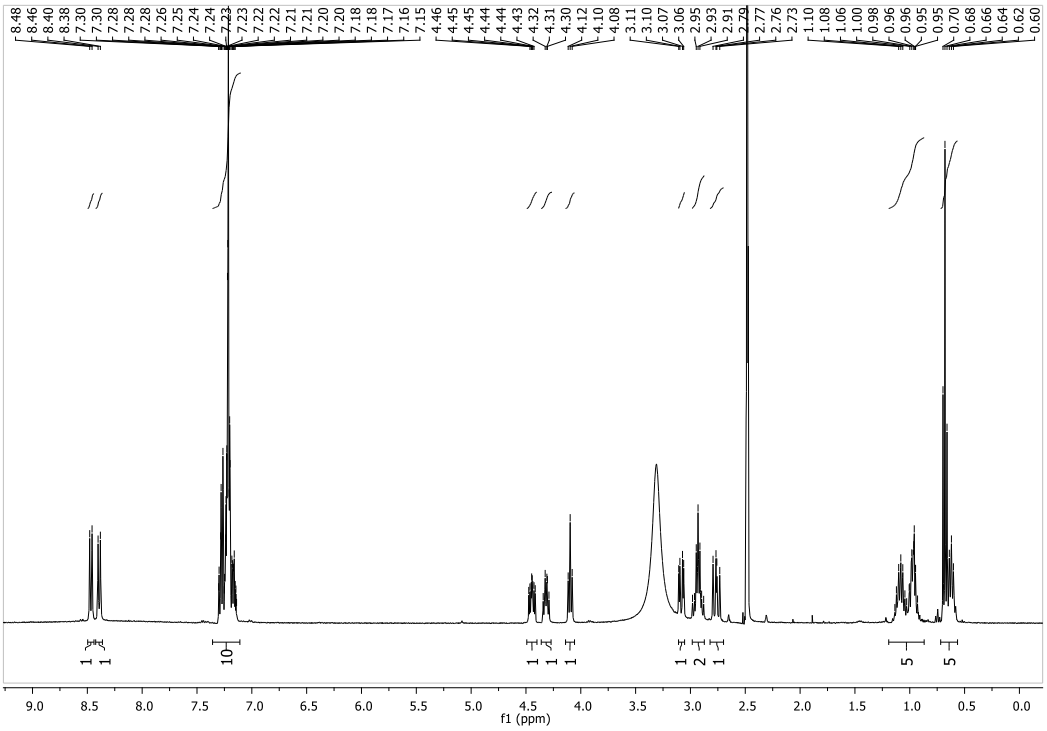

Figure 6.18 ^{1}H-NMR spectrum of ^{L}Phe-^{D}Nle-^{L}Phe.

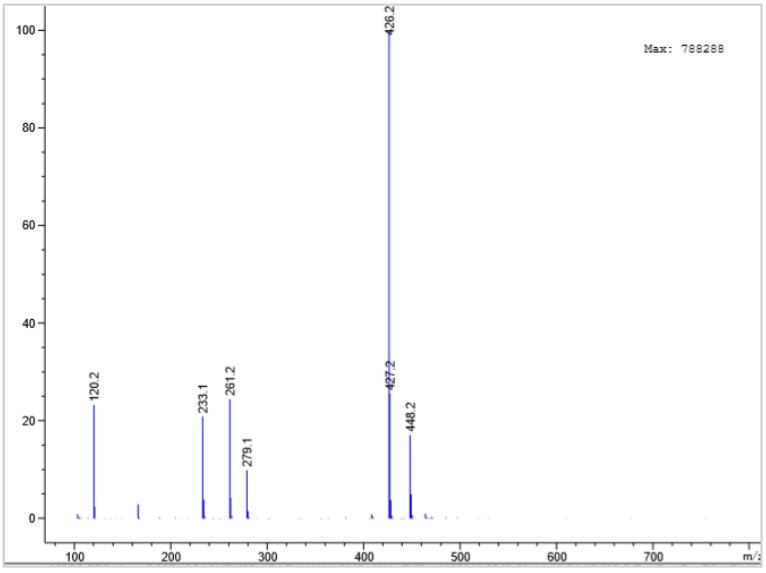

Figure 6.19 ESI-MS spectrum of ^{L}Phe-^{D}Nle-^{L}Phe.

4c - ^{D}Leu-^{D}Phe-^{D}Phe(4I)

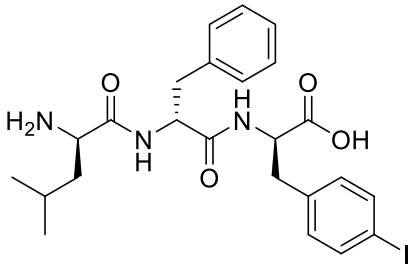

Chemical Formula: $C_{24}H_{30}IN_3O_4$
Exact Mass: 551.13
Molecular Weight: 551.43
m/z: 551.13 (100.0%), 552.13 (26.0%), 553.13 (3.2%), 552.13 (1.1%)
Elemental Analysis: C, 52.28; H, 5.48; I, 23.01; N, 7.62; O, 11.61

^{1}H-NMR (400 MHz, DMSO):δ (ppm) 8.67 ppm (d, *J* =8.2 Hz, 1H, **NH**), 8.45 ppm (d, *J* =8.0 Hz, 1H, **NH**), 8.04 ppm (s, 1H, **NH₂**), 7.63-7.55 ppm (m, 2H, **Ar**), 7.37-7.14 ppm (m, 5H, **Ar**),7.02 ppm (d, *J* = 8.3 Hz, 2H, **Ar**), 4.58 ppm (td, *J*=8.7, 4.8 Hz, 1H, **αCH**), 4.42 ppm (td, *J*=14.4, 6.4 Hz, 1H, **αCH**), 3.71 ppm (s, 1H, **αCH**), 2.99 ppm (ddd, *J*=14.1, 11.1, 4.7 Hz, 2H, **βCH**), 2.81 ppm (ddd, *J*=14.0, 9.0 Hz, 2H, **βCH**), 1.58 ppm (td, *J*=13.2, 6.6 Hz, 1H, **γ CH**), 1.47 ppm (t, *J*=7.1, 2H, **β CH**), 0.84 (t, *J*=6.4 Hz, 6H, **δCH₃**).

MS (ESI): m/z 552.2 (M+H), C24H31N3O4 requires 551.2.

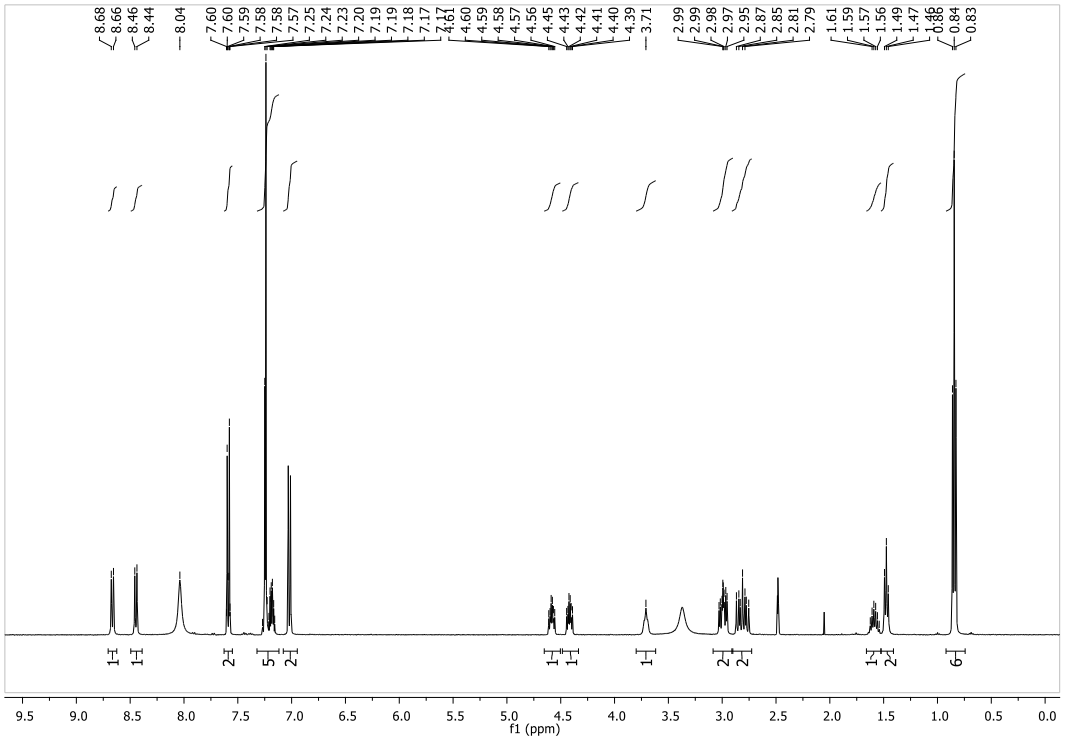

Figure 6.20 ^{1}H-NMR spectrum of ^{D}Leu-^{D}Phe-^{D}Phe(4-I).

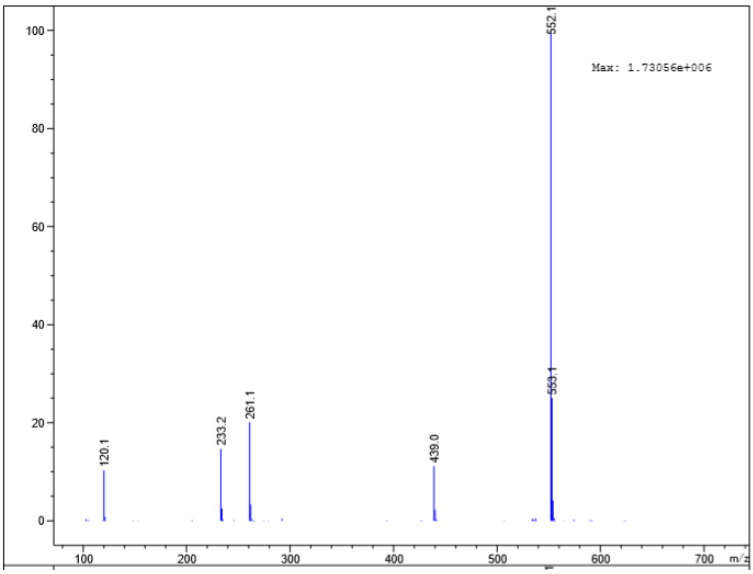

Figure 6.21 ESI-MS spectrum of ^{D}Leu-^{D}Phe-^{D}Phe(4-I).

2b - ^{L}Leu-^{D}Phe(4-I)-^{D}Phe

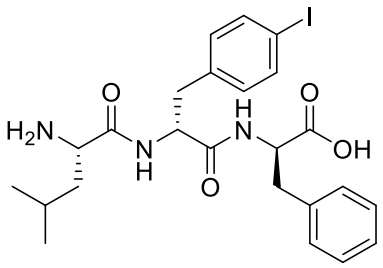

Chemical Formula: $C_{24}H_{30}IN_3O_4$
Exact Mass: 551.13
Molecular Weight: 551.43
m/z: 551.13 (100.0%), 552.13 (26.0%), 553.13 (3.2%), 552.13 (1.1%)
Elemental Analysis: C, 52.28; H, 5.48; I, 23.01; N, 7.62; O, 11.61

^{1}H-NMR (400 MHz, DMSO):δ (ppm) 8.72 ppm (d, *J* =8.9 Hz, 1H, **NH**), 8.59 ppm (d, *J* =7.8 Hz, 1H, **NH**), 7.97 ppm (s, 1H, **NH$_2$**), 7.59 ppm (d, *J* = 8.3 Hz, 2H, **Ar**), 7.37-7.14 ppm(m, 5H, **Ar**),7.07 ppm (d, *J* = 8.3 Hz, 2H, **Ar**), 4.78-4.58 ppm (m, 1H, **αCH**), 4.30 ppm (dd, *J*=14.4, 6.4 Hz, 1H, **αCH**), 3.59 ppm (s, 1H, **αCH**), 3.18-2.98 ppm (m, 2H, **βCH**), 2.92 ppm (dd, *J*=14.0, 9.2 Hz, 1H, **βCH**), 2.57 ppm (dd, *J*=13.6, 11.7 Hz, 1H, **βCH**), 1.11-0.97 ppm (m, 3H, **β and γ CH**), 0.75-0.60 (m, 6H, **δCH$_3$**).

MS (ESI): m/z 552.2 (M+H), C24H31N3O4 requires 551.2.

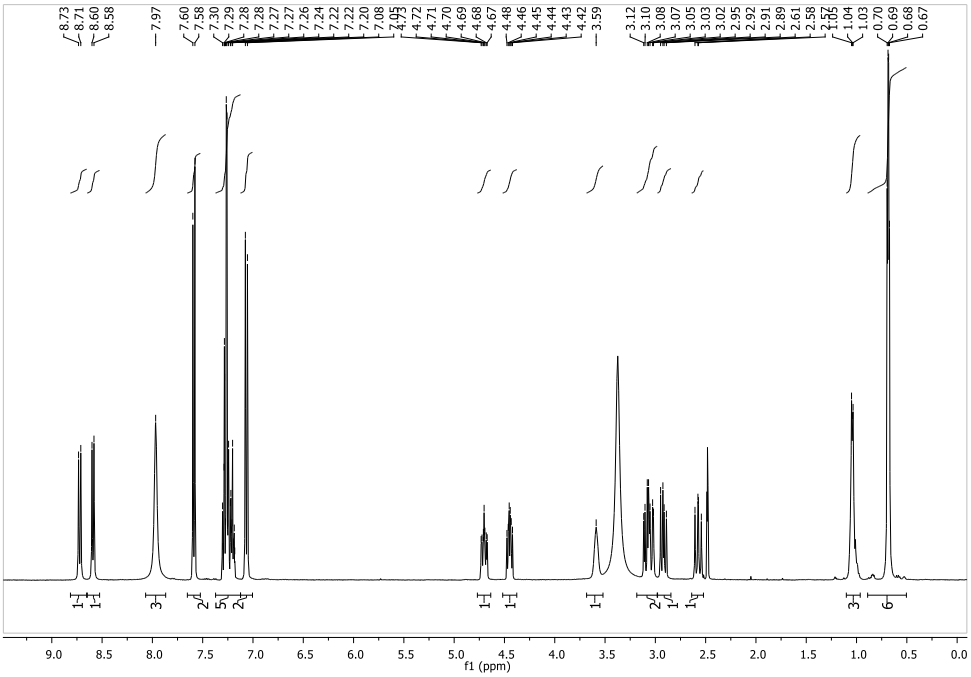

Figure 6.22 ^{1}H-NMR spectrum of ^{L}Leu-^{D}Phe(4-I)-^{D}Phe.

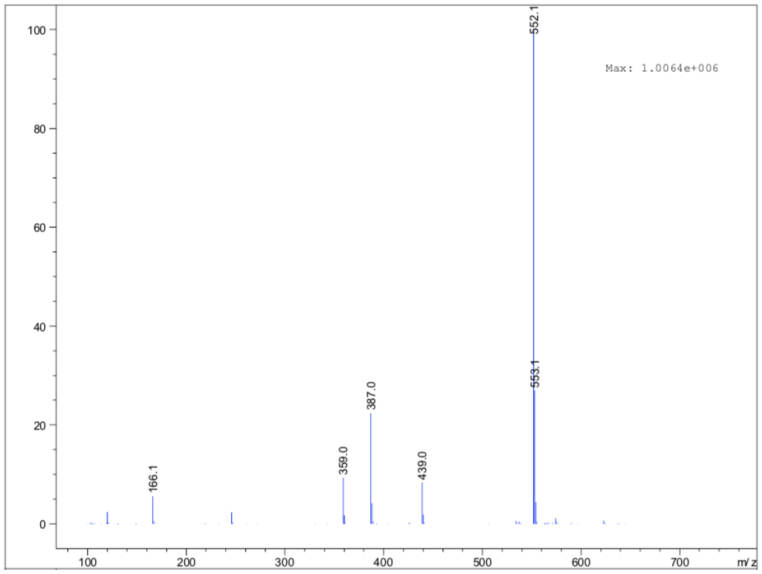

Figure 6.23 ESI-MS spectrum of ^{L}Leu-^{D}Phe(4-I)-^{D}Phe.

2d - ^{L}Leu-^{D}Phe(4-F)-^{D}Phe.

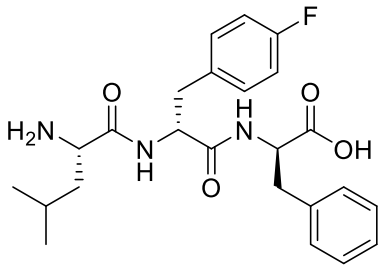

Chemical Formula: $C_{24}H_{30}FN_3O_4$
Exact Mass: 443.22
Molecular Weight: 443.52
m/z: 443.22 (100.0%), 444.23 (26.0%), 445.23 (2.7%), 444.22 (1.1%)
Elemental Analysis: C, 64.99; H, 6.82; F, 4.28; N, 9.47; O, 14.43

^{1}H-NMR (400 MHz, DMSO):δ (ppm) 8.71 ppm (d, *J* =8.9 Hz, 1H, **NH**), 8.59 ppm (d, *J* =7.9 Hz, 1H, **NH**), 7.35-7.16 ppm (m, 7H, **Ar**), 7.12-6.99 ppm (m, 2H, **Ar**), 4.78-4.58 ppm (m, 1H, **αCH**), 4.50-4.39 ppm (m, 1H, **αCH**), 3.61 ppm (t, *J* = 6.6 Hz, 1H, **αCH**), 3.14-3.00 ppm (m, 2H, **βCH**), 2.68-2.57 ppm (m, 1H, **βCH**), 2.49-2.57 ppm (m, 1H, **βCH**), 1.08 ppm (d, *J* = 4.1 Hz, 3H, **β and γ CH**), 0.68 (t, *J* = 5.6 Hz, 6H, **δCH$_3$**).

MS (ESI): m/z 444.2 (M+H), C24H31N3O4 requires 443.2.

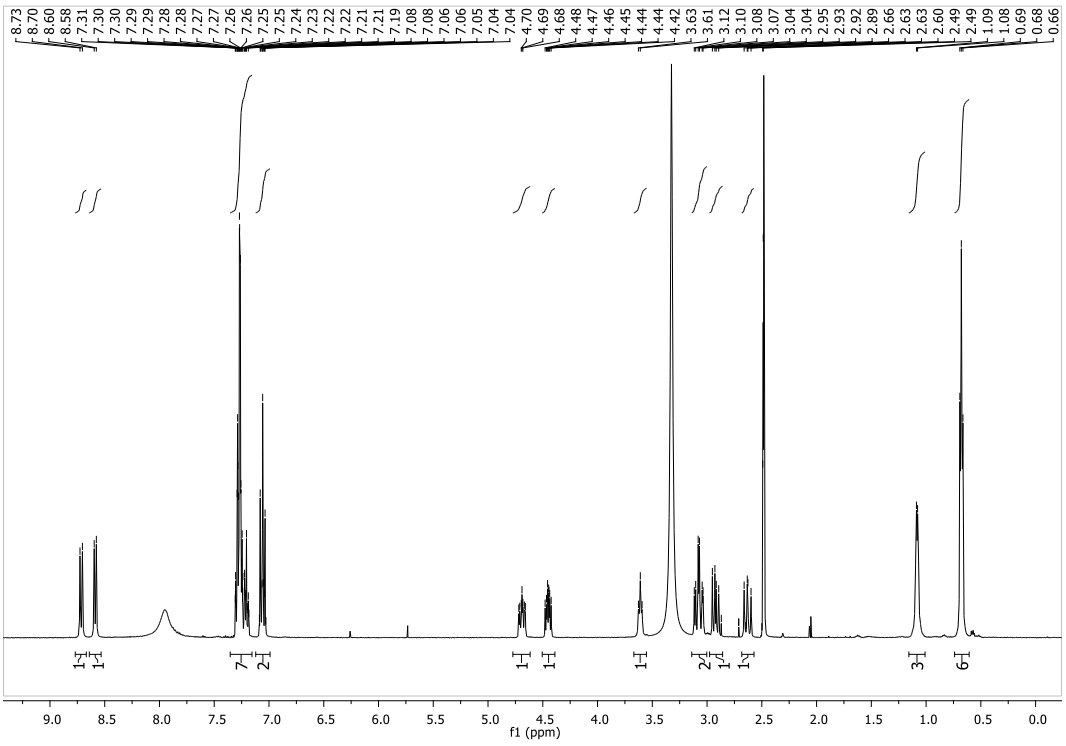

Figure 6.24 ^{1}H-NMR spectrum of ^{L}Leu-^{D}Phe(4-F)-^{D}Phe.

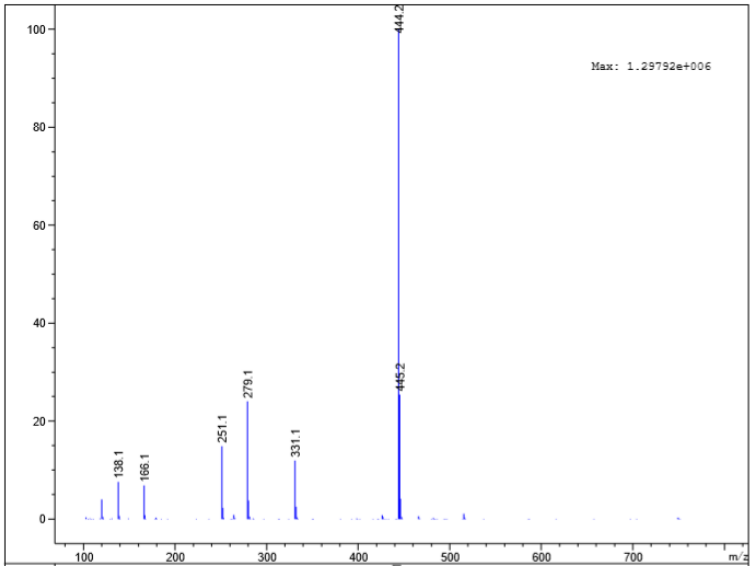

Figure 6.25 ESI-MS spectrum of ^{L}Leu-^{D}Phe(4-F)-^{D}Phe.

2e - ^{L}Leu-^{D}Phe-^{D}Phe(4-F).

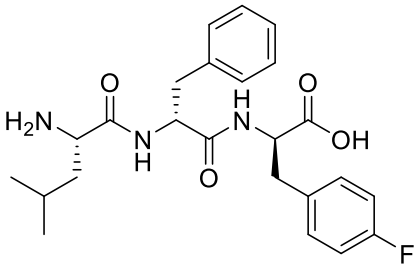

Chemical Formula: $C_{24}H_{30}FN_3O_4$
Exact Mass: 443.22
Molecular Weight: 443.52
m/z: 443.22 (100.0%), 444.23 (26.0%), 445.23 (2.7%), 444.22 (1.1%)
Elemental Analysis: C, 64.99; H, 6.82; F, 4.28; N, 9.47; O, 14.43

^{1}H-NMR (400 MHz, DMSO):δ (ppm) 8.70 ppm (d, *J* =8.7 Hz, 1H, **NH**), 8.58 ppm (d, *J* =7.89Hz, 1H, **NH**), 7.37-7.03 ppm (m, 9H, **Ar**),4.74-4.62 ppm (m, 1H, **αCH**), 4.30 ppm (dd, *J*=8.7, 5.2 Hz, 1H, **αCH**), 3.61 ppm (t, *J* = 6.9 Hz, 1H, **αCH**), 3.10-3.04 ppm (m, 2H, **βCH**), 2.92 ppm (dd, *J*=14.0, 9.0 Hz, 1H, **βCH**), 2.64 ppm (dd, *J*=13.7, 11.5 Hz, 1H, **βCH**), 1.19-1.02 ppm (m, 3H, **β and γ CH**), 0.68-0.65 (m, 6H, **δCH$_3$**).

MS (ESI): m/z 444.2 (M+H), C24H31N3O4 requires 443.2.

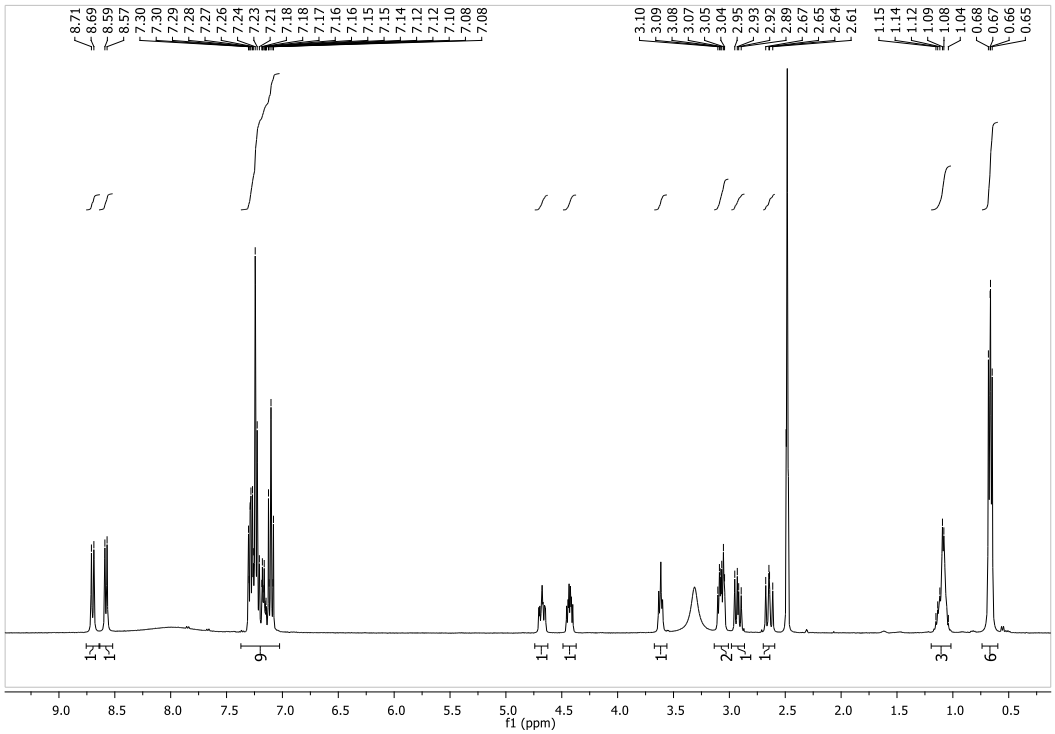

Figure 6.26 ^{1}H-NMR spectrum of ^{L}Leu-^{D}Phe-^{D}Phe(4-F).

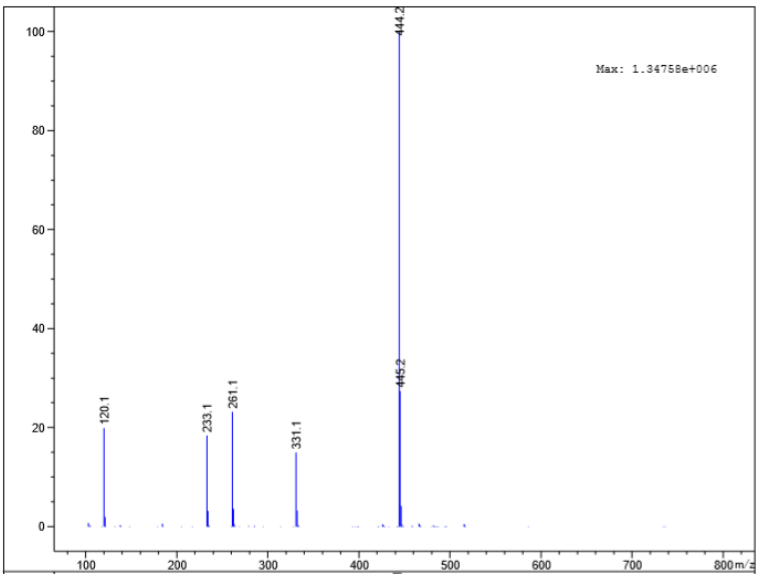

Figure 6.27 ESI-MS spectrum of ^{L}Leu-^{D}Phe-^{D}Phe(4-F).

2f - ^{L}Leu-^{D}Phe(4-I)-^{D}Phe(4-F).

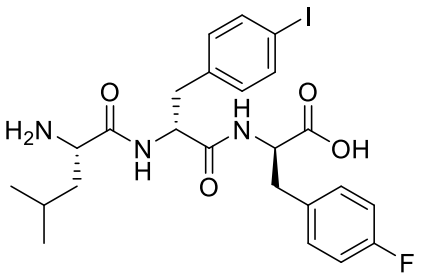

Chemical Formula: $C_{24}H_{29}FIN_3O_4$
Exact Mass: 569.12
Molecular Weight: 569.42
m/z: 569.12 (100.0%), 570.12 (26.0%), 571.13 (3.2%), 570.12 (1.1%)
Elemental Analysis: C, 50.62; H, 5.13; F, 3.34; I, 22.29; N, 7.38; O, 11.24

^{1}H-NMR (400 MHz, DMSO):δ (ppm) 8.70 ppm (d, *J* =8.9 Hz, 1H, **NH**), 8.58 ppm (d, *J* =7.9 Hz, 1H, **NH**), 7.95 ppm (s, 1H, **NH$_2$**), 7.66-7.54 ppm (m, 2H, **Ar**), 7.34-7.23 ppm (m, 2H, **Ar**), 7.15-7.02 ppm (m, 4H, **Ar**), 4.68 ppm (ddd, *J* = 12.1, 8.9, 3.6 Hz, 1H, **αCH**), 4.43 ppm (td, *J*=8.8, 5.1 Hz, 1H, **αCH**), 3.58 ppm (s, 1H, **αCH**), 3.14-2.96 ppm (m, 2H, **βCH**), 2.96-2.86 ppm (m, 1H, **βCH**), 2.58 ppm (dd, *J*=13.7, 11.7 Hz, 1H, **βCH**), 1.12-0.94 ppm (m, 3H, **β and γ CH**), 0.68 (dd, *J* = 5.9, 4.5 Hz, 6H, **δCH$_3$**).

MS (ESI): m/z 569.2 (M+H), C24H31N3O4 requires 570.2.

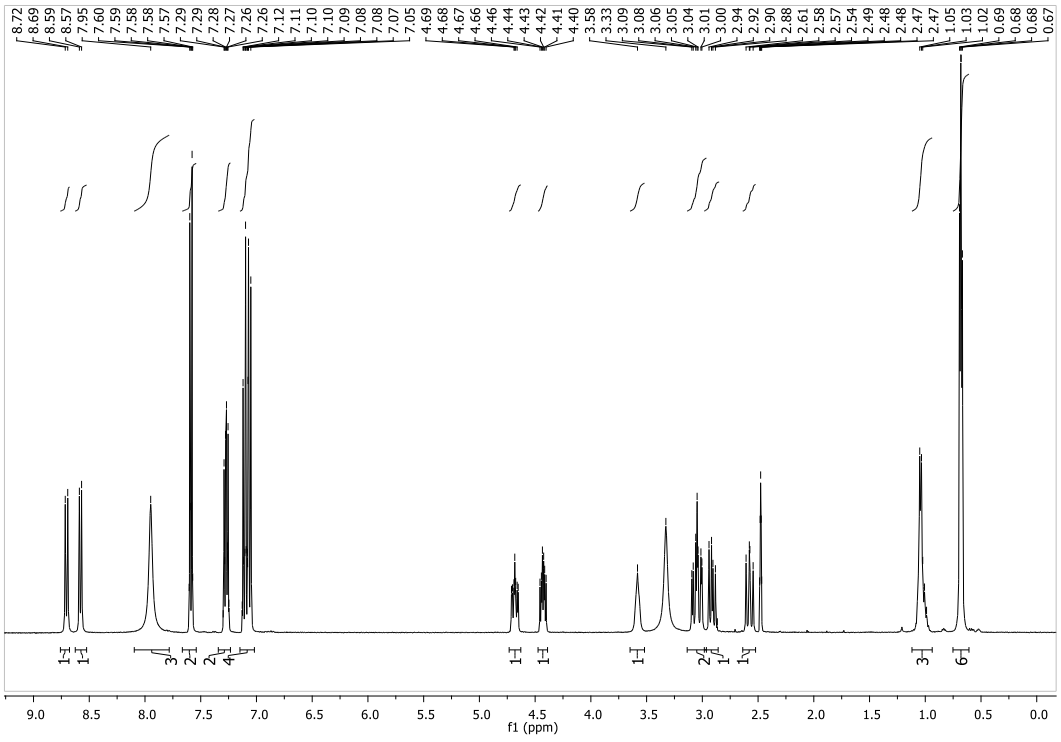

Figure 6.27 ^{1}H-NMR spectrum of ^{L}Leu-^{D}Phe(4-I)-^{D}Phe(4-F).

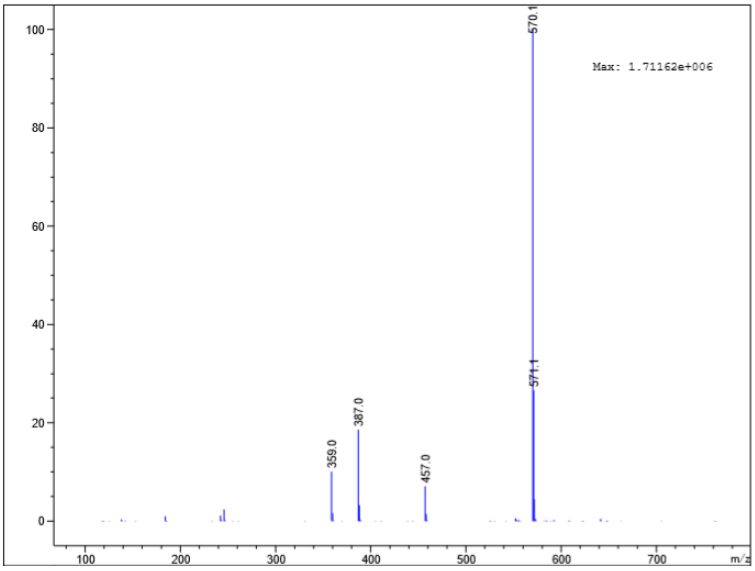

Figure 6.28 ESI-MS spectrum of ^{L}Leu-^{D}Phe(4-I)-^{D}Phe(4-F).

13b - (4-I) ^{D}Phe- ^{L}Nle -^{D}Phe

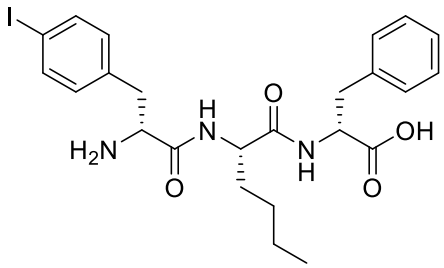

Chemical Formula: $C_{24}H_{30}IN_3O_4$
Exact Mass: 551.13
Molecular Weight: 551.43
m/z: 551.13 (100.0%), 552.13 (26.0%), 553.13 (3.2%), 552.13 (1.1%)
Elemental Analysis: C, 52.28; H, 5.48; I, 23.01; N, 7.62; O, 11.61

^{1}H-NMR (400 MHz, DMSO):δ (ppm) δ 12.82 (s, 1H, -COOH), 8.46 ppm (dd, *J* =15.8, 8.5 Hz, 2H, **NH**), 8.16 (s, 3H, -NH_2), 7.64 ppm (d, *J* = 8.3 Hz, 2H, **Ar**), 7.30-7.11 ppm(m, 5H, **Ar**),7.02 ppm (d, *J* = 8.3 Hz, 2H, **Ar**), 4.45 ppm (ddd, *J* = 10.8, 8.5, 4.3 Hz, 1H, **αCH**), 4.36-4.26 ppm (m, 1H, **αCH**), 4.09 ppm (t, *J*=7.2 Hz, 1H, **αCH**), 3.09 ppm (dd, *J* = 13.8, 10.8 Hz, 1H, **βCH**), 2.99-2.82 (m, 2H, **βCH**), 2.76 ppm (dd, *J*=13.7, 10.8 Hz, 1, **βCH**), 1.19-0.88 ppm (m, 4H, **β and γ CH**), 0.74-0.49 ppm (m, 5H, **δCH** e **εCH**).

MS (ESI): m/z 551.2 (M+H), C24H31N3O4 requires 552.2.

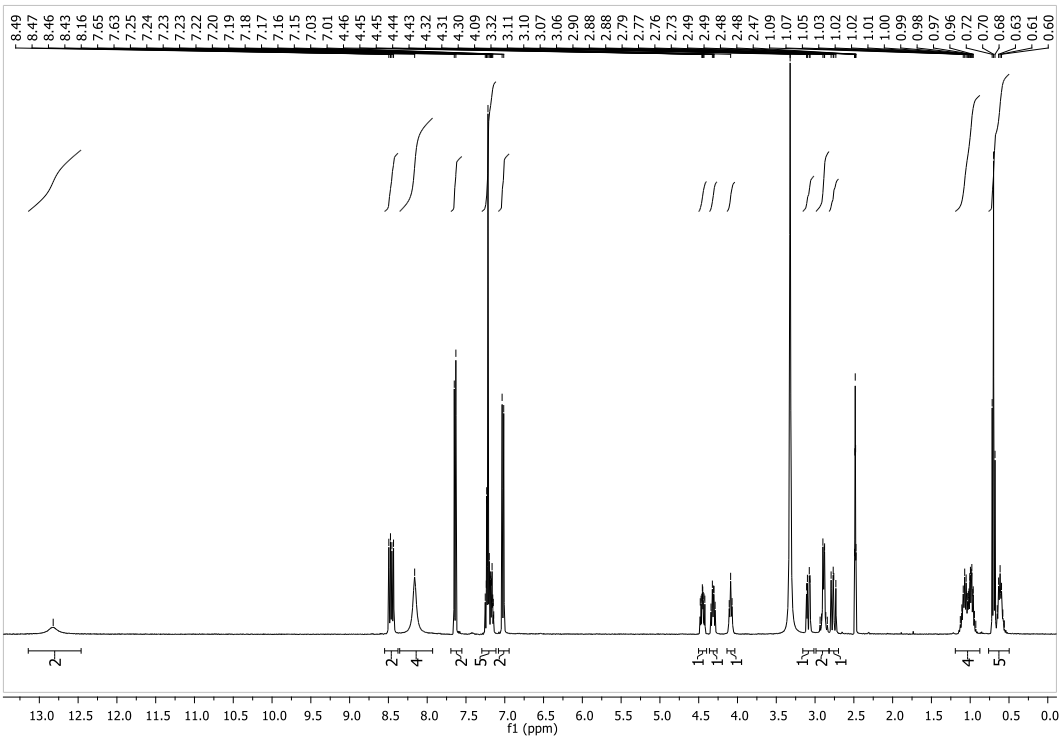

Figure 6.29 ^{1}H-NMR spectrum of (4-I)^{D}Phe-^{L}Nle-^{D}Phe.

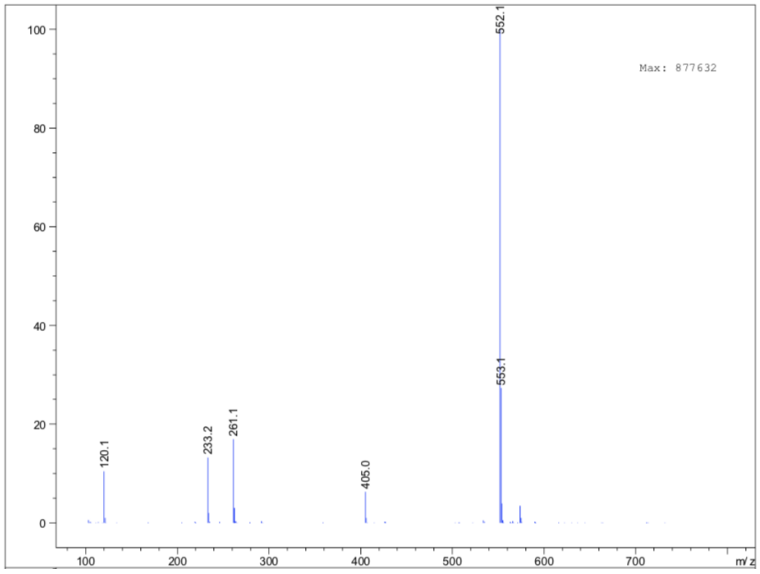

Figure 6.30 ESI-MS spectrum of (4-I)^{D}Phe-^{L}Nle-^{D}Phe.

13c - ^{D}Phe-^{L}Nle -^{D}Phe(4-I)

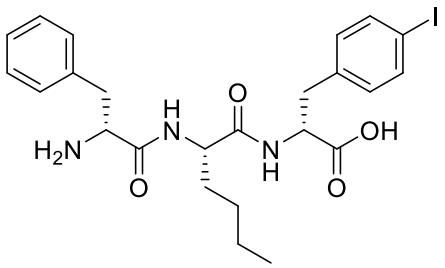

Chemical Formula: $C_{24}H_{30}IN_3O_4$
Exact Mass: 551.13
Molecular Weight: 551.43
m/z: 551.13 (100.0%), 552.13 (26.0%), 553.13 (3.2%), 552.13 (1.1%)
Elemental Analysis: C, 52.28; H, 5.48; I, 23.01; N, 7.62; O, 11.61

^{1}H-NMR (400 MHz, DMSO):δ (ppm) 8.46 ppm (d, *J* = 8.6 Hz, 1H, **NH**), 8.41 ppm (d, *J* = 8.3 Hz, 1H, **NH**), 8.16 ppm (s, 3H, **NH$_2$**), 7.62-7.53 ppm (m, 2H, **Ar**), 7.33-7.16 ppm (m, 5H, **Ar**),7.03 ppm (d, *J* = 8.3 Hz, 2H, **Ar**), 4.44 ppm (ddd, *J* = 11.1, 8.6, 4.2 Hz, 1H, **αCH**), 4.28 ppm (dd, *J*=14.4, 6.4 Hz, 1H, **αCH**), 4.12 ppm (t, *J*=7.2 Hz, 1H, **αCH**), 3.05 ppm (dd, *J*=13.8, 4.2 Hz, 1, **βCH**), 2.94 ppm (d, *J* = 7.4 Hz, 2H, **βCH**), 2.71 ppm (dd, *J* = 13.7; 11.1 Hz, 1H, **βCH**), 1.01 ppm (ddt, *J* = 29.7, 14.6, 7.5 Hz, 4H, **β and γ CH**), 0.70 ppm (t, *J*=7.3 Hz, 3H, **εCH**), 0.64-0.51 (m, 2H, **δCH**).

MS (ESI): m/z 551.1 (M+H), C24H31N3O4 requires 552.1.

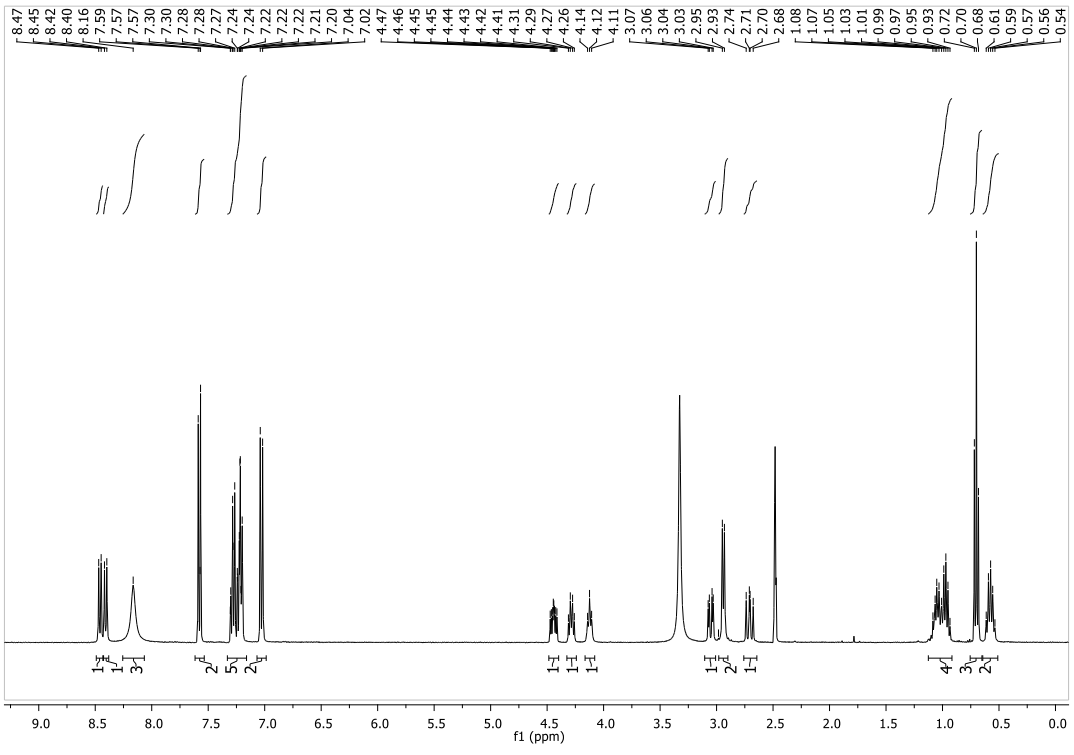

Figure 6.31 ^{1}H-NMR spectrum of ^{D}Phe-^{L}Nle-^{D}Phe(4-I).

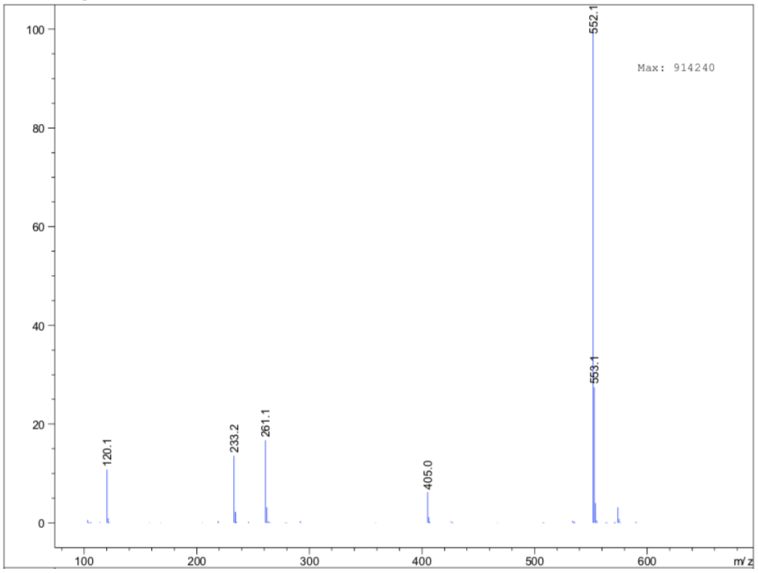

Figure 6.32 ESI-MS spectrum of ^{D}Phe-^{L}Nle-^{D}Phe(4-I).

9c - ^{D}Phe-^{L}Nle-^{L}Phe(4-I)

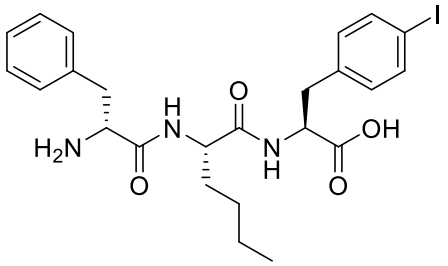

Chemical Formula: $C_{24}H_{30}IN_3O_4$
Exact Mass: 551.13
Molecular Weight: 551.43
m/z: 551.13 (100.0%), 552.13 (26.0%), 553.13 (3.2%), 552.13 (1.1%)
Elemental Analysis: C, 52.28; H, 5.48; I, 23.01; N, 7.62; O, 11.61

^{1}H-NMR (400 MHz, DMSO):δ (ppm) 8.42 ppm (d, *J* = 8.2 Hz, 1H, **NH**), 8.35 ppm (d, *J* = 7.8 Hz, 1H, **NH**), 7.68-7.54 ppm (m, 2H, **Ar**), 7.35-7.18 ppm (m, 5H, **Ar**),7.04 ppm (d, *J* = 8.3 Hz, 2H, **Ar**), 4.39-4.30 ppm (m, 1H, **αCH**), 4.30-4.22 ppm (m, 1H, **αCH**), 4.06 ppm (t, *J*=7.3 Hz, 1H, **αCH**), 3.05-2.77 ppm (m, 4,H **βCH**), 1.49-1.24 ppm (m, 2H, **βCH**), 1.20-1.06 ppm (m, 2H, **γCH**), 0.97 (dd, *J* = 15.3, 7.8 Hz, 2H, **δCH**).0.70 ppm (t, *J*=7.3 Hz, 3H, **εCH**).

MS (ESI): m/z 551.1 (M+H), C24H31N3O4 requires 552.1.

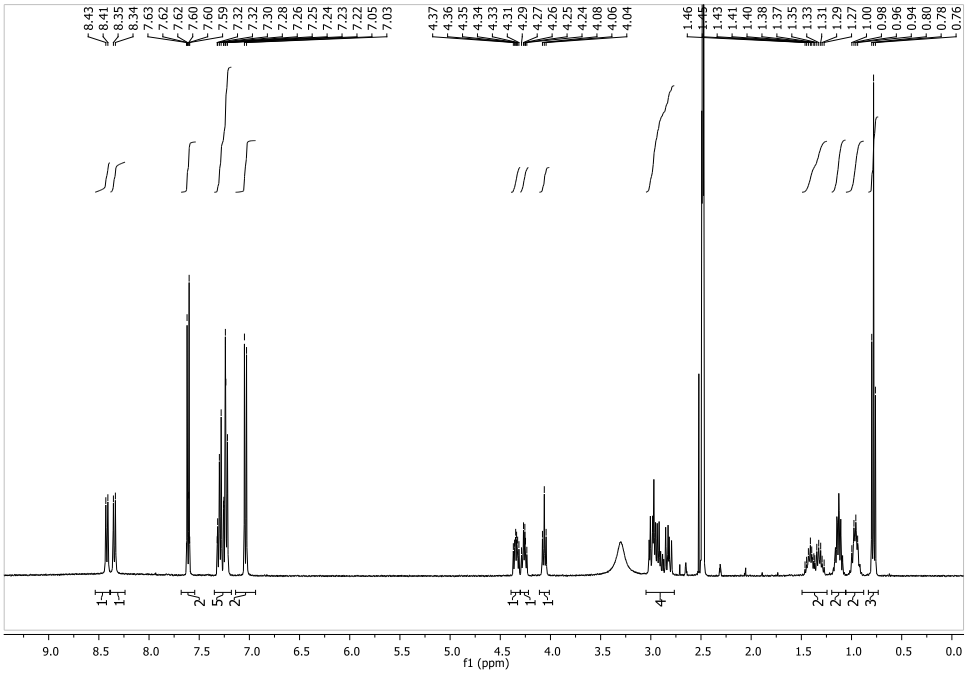

Figure 6.33 ^{1}H-NMR spectrum of ^{D}Phe-^{L}Nle-^{L}Phe(4-I).

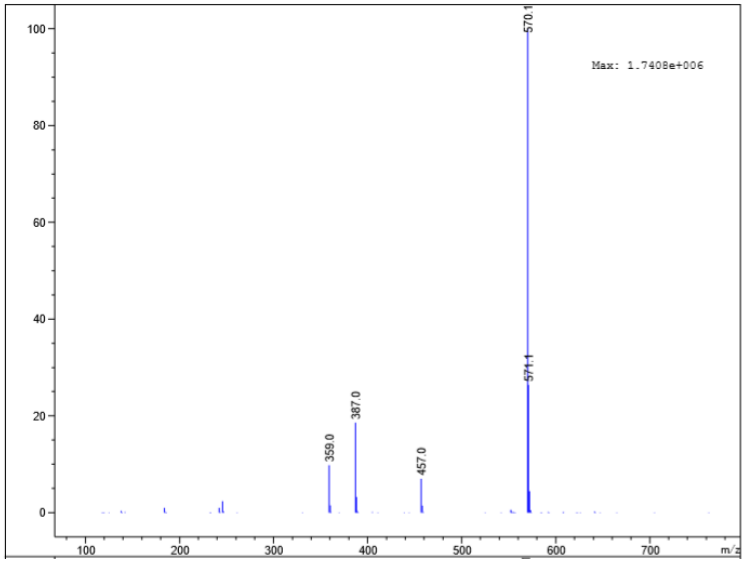

Figure 6.34 ESI-MS spectrum of ^{D}Phe-^{L}Nle-^{L}Phe(4-I).

13d - (4-F)^{D}Phe-^{L}Nle-^{D}Phe

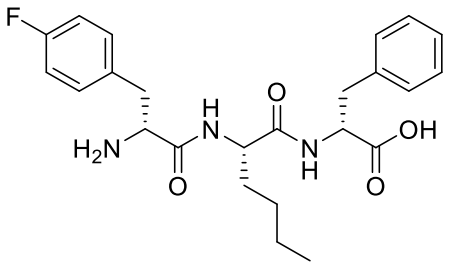

Chemical Formula: $C_{24}H_{30}FN_3O_4$
Exact Mass: 443.22
Molecular Weight: 443.52
m/z: 443.22 (100.0%), 444.23 (26.0%), 445.23 (2.7%), 444.22 (1.1%)
Elemental Analysis: C, 64.99; H, 6.82; F, 4.28; N, 9.47; O, 14.43

^{1}H-NMR (400 MHz, DMSO, TMS):δ (ppm) 8.47 ppm (d, *J* = 8.5 Hz, 1H, **NH**), 8.41 ppm (d, *J* = 8.5 Hz, 1H, **NH**), 7.36-6.98 ppm(m, 10H, **Ar**), 4.51-4.38 ppm (m, 1H, **αCH**), 4.32 ppm (dd, *J*=13.6, 7.1 Hz, 1H, **αCH**), 4.08 ppm (t, *J*=7.3 Hz 1H, **αCH**), 3.09 ppm (dd, *J*=13.7, 4.2 Hz, 1H, **βCH**), 3.00-2.85 ppm (m, 2H, **βCH**), 2.76 ppm (dd, *J* = 13.7, 10.8 Hz, 1H, **βCH**), 2.76 (dd, *J*=13.7 Hz, 1H, **βCH**), 1.17-0.90 ppm (m, 4H, **β and γ CH**), 0.68 ppm (t, *J*=7.3 Hz, 3H, **εCH**), 0.68 ppm (dd, *J*=14.7, 7.4 Hz, 2H, **δCH**).

MS (ESI): m/z 443.2 (M+H), C24H31N3O4 requires 444.2.

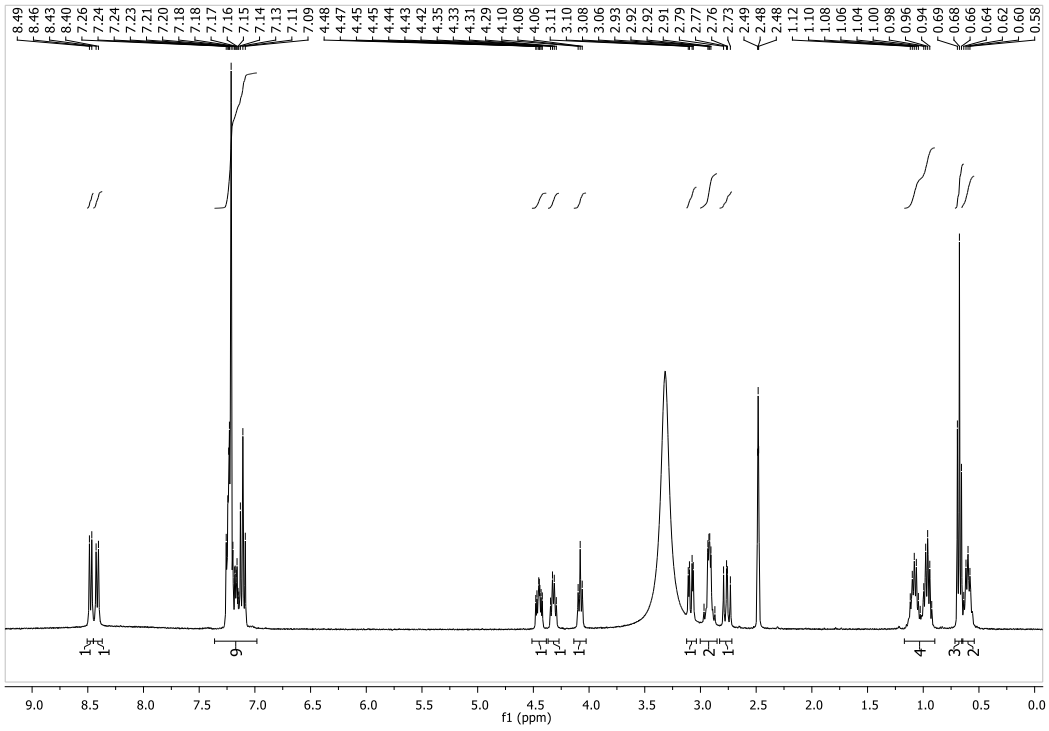

Figure 6.35 ^{1}H-NMR spectrum of (4-F)^{D}Phe-^{L}Nle-^{D}Phe.

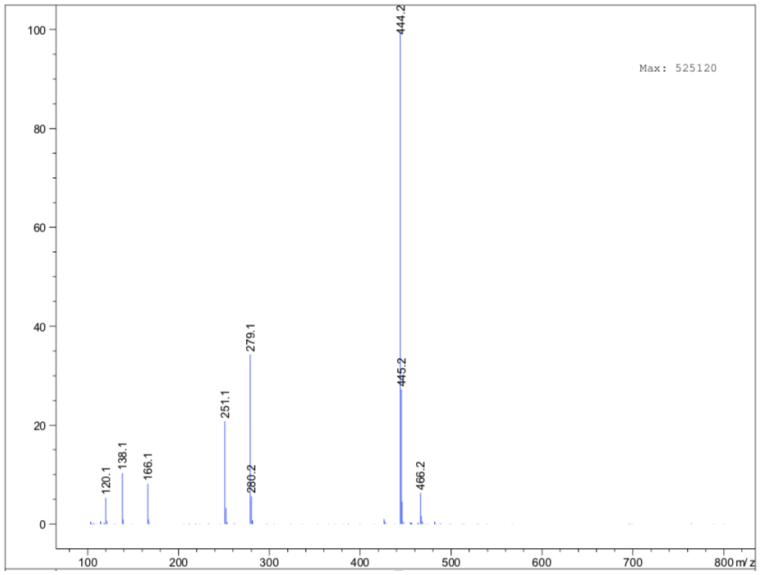

Figure 6.36 ESI-MS spectrum of (4-F)^{D}Phe-^{L}Nle-^{D}Phe.

13e - ^{D}Phe-^{L}Nle-^{D}Phe(4-F)

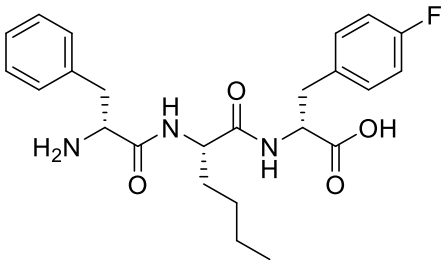

Chemical Formula: $C_{24}H_{30}FN_3O_4$
Exact Mass: 443.22
Molecular Weight: 443.52
m/z: 443.22 (100.0%), 444.23 (26.0%), 445.23 (2.7%), 444.22 (1.1%)
Elemental Analysis: C, 64.99; H, 6.82; F, 4.28; N, 9.47; O, 14.43

^{1}H-NMR (400 MHz, DMSO):δ (ppm) 8.47 ppm (d, *J* = 8.6 Hz, 1H, **NH**), 8.41 ppm (d, *J* = 8.4 Hz, 1H, **NH**), 8.17 ppm (s, -**NH**$_2$), 7.25 ppm (dtd, *J* = 11.3, 8.2, 4.0 Hz, 7H, **Ar**), 7.12-6.98 ppm (m, 2H, **Ar**), 4.44 ppm (ddd, *J* = 11.1, 8.6, 4.3 Hz, 1H, **αCH**), 4.30 ppm (dd, *J* = 14.5, 6.4 Hz, 1H, **αCH**), 4.13 ppm (s, 1H, **αCH**), 3.08 ppm (dd, *J* = 13.8, 4.2 Hz, 1H, **αCH**), 3.10-2.96 ppm (m, 1H, **βCH**), 2.94 ppm (d, *J*=7.3 Hz, 2H, **βCH**), 2.74 (dd, *J* = 13.8, 11.0 Hz, 1H, **βCH**), 1.18-0.86 ppm (m, 4H, **β, γ CH**), 0.67 (t, *J* = 7.1 Hz, 3H, **εCH**), 0.57 (dt, *J* = 15.0, 7.4 Hz, 2H, **δCH**).

MS (ESI): m/z 444.2 (M+H), C24H31N3O4 requires 443.2.

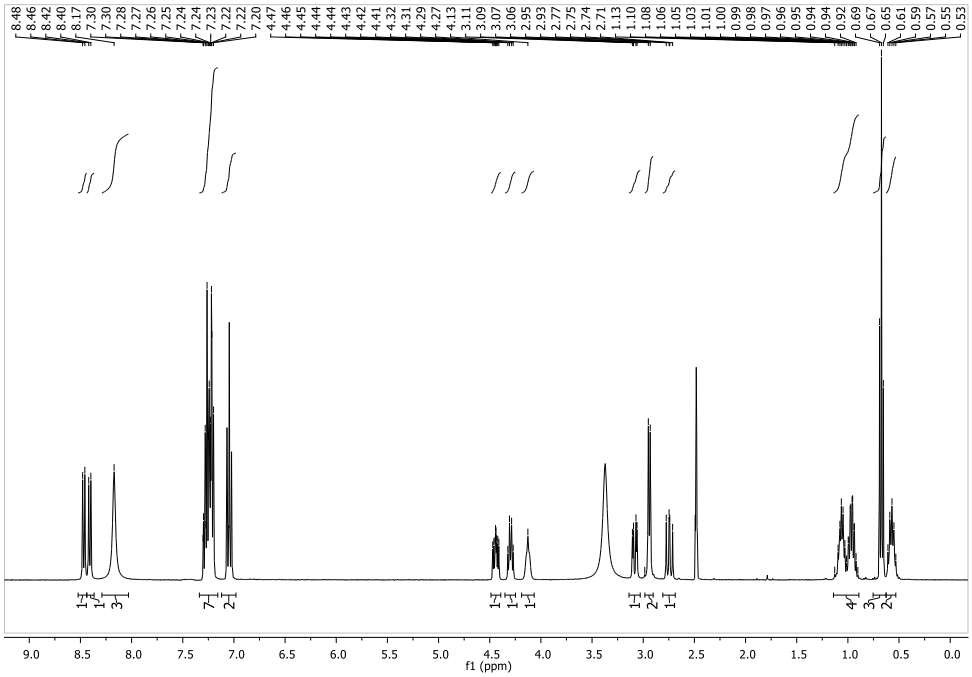

Figure 6.37 ^{1}H-NMR spectrum of ^{D}Phe-^{L}Nle-^{D}Phe(4-F).

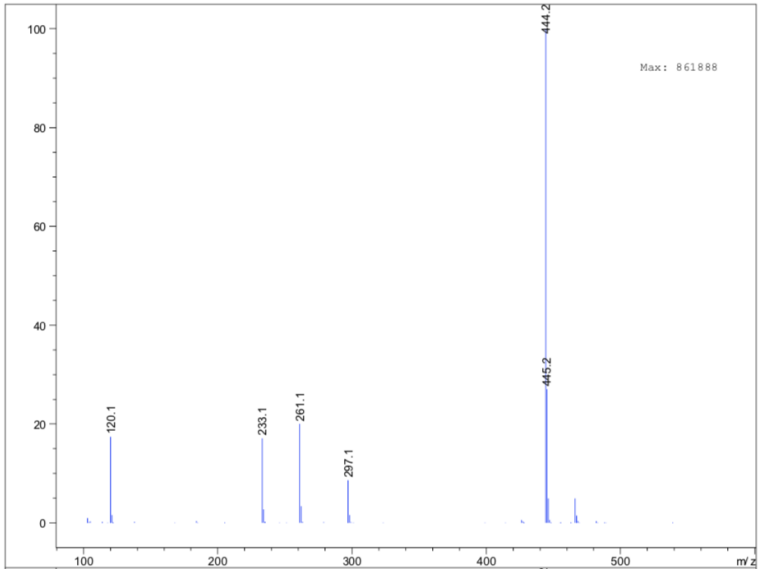

Figure 6.38 ESI-MS spectrum of ^{D}Phe-^{L}Nle-^{D}Phe(4-F).

13f - ^{D}Phe(4-I)-^{L}Nle-^{D}Phe(4-F)

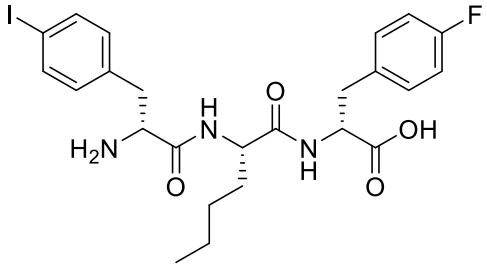

Chemical Formula: $C_{24}H_{29}FIN_3O_4$
Exact Mass: 569.12
Molecular Weight: 569.42
m/z: 569.12 (100.0%), 570.12 (26.0%), 571.13 (3.2%), 570.12 (1.1%)
Elemental Analysis: C, 50.62; H, 5.13; F, 3.34; I, 22.29; N, 7.38; O, 11.24

^{1}H-NMR (400 MHz, DMSO):δ (ppm) 8.48-8.42 ppm (dd, *J* = 16.1, 8.6 Hz, 2H, **NH**), 8.16 ppm (s, 3H, **NH_3**), 7.64 ppm(d, *J* = 8.2 Hz, 2H, **Ar**), 7.24 ppm(dd, *J* = 8.4, 5.6 Hz, 2H, **Ar**), 7.03 ppm(dd, *J* = 16.5, 8.5 Hz, 4H, **Ar**), 4.51-4.36 ppm (m, 1H, **αCH**), 4.28 ppm (dd, *J*=13.3, 6.6 Hz, 1H, **αCH**), 4.15-4.01 ppm (m, 1H ,**αCH**), 3.08 ppm (dd, *J*=13.7, 4.0 Hz, 1H, **βCH**), 2.88 ppm (d, *J* = 7.3 Hz, 2H, **βCH**), 2.74 ppm (dd, *J* = 11.7, 10.0 Hz, 1H, **βCH**), 1.06-0.96 ppm (m, 4H, **β** and **γ CH**), 0.71-0.55 ppm (m, 4H, **εCH** and **δCH)**

MS (ESI): m/z 570.1 (M+H), C24H31N3O4 requires 569.1.

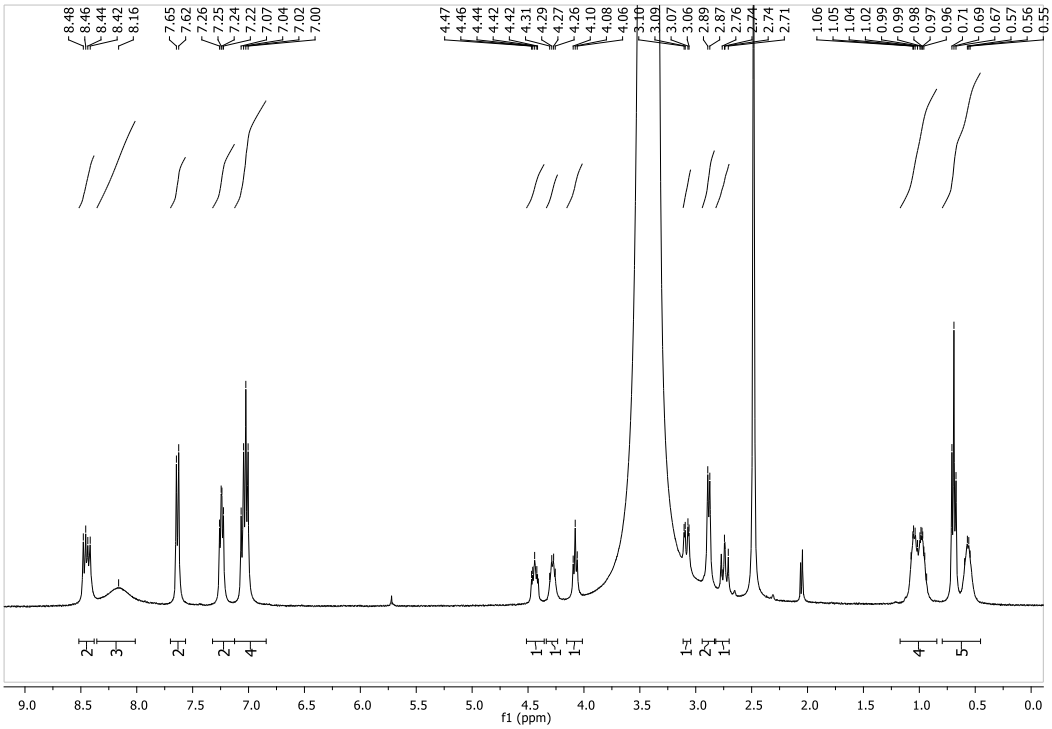

Figure 6.39 ^{1}H-NMR spectrum of (4-I) ^{D}Phe- ^{L}Nle ^{D}Phe(4-F).

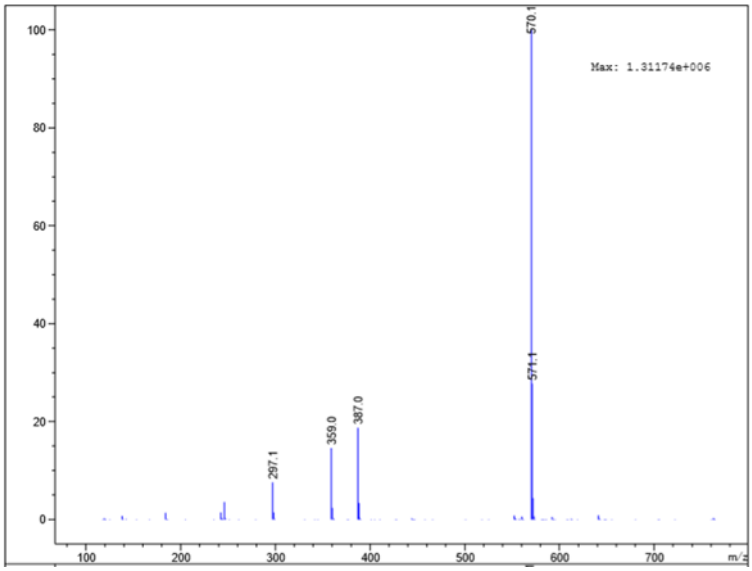

Figure 6.40 ESI-MS spectrum of (4-I) ^{D}Phe-^{L}Nle ^{D}Phe(4-F).

6.2 HPLC trace

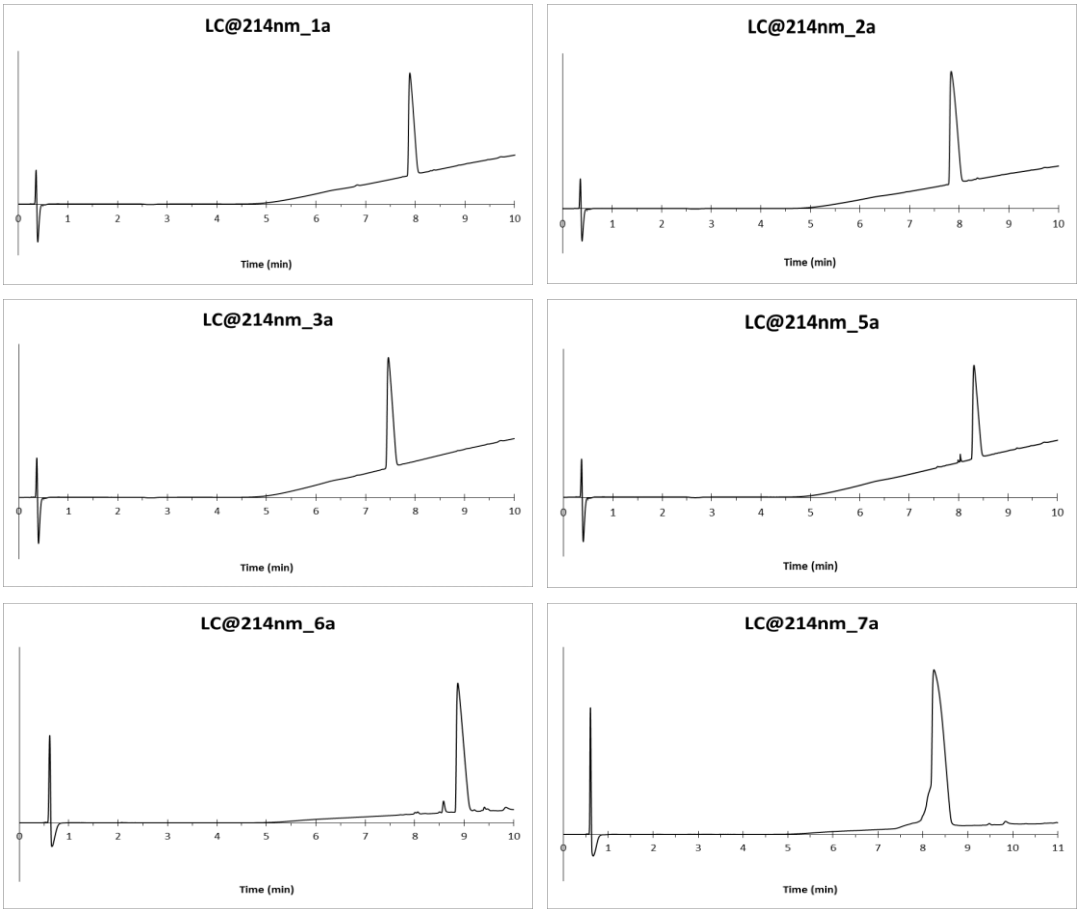

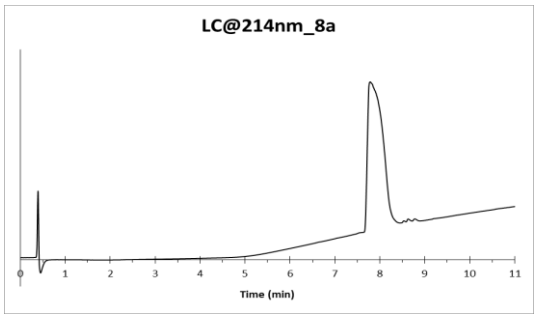
LC@214nm_8a
0 1 2 3 4 5 6 7 8 9 10 11
Time (min)

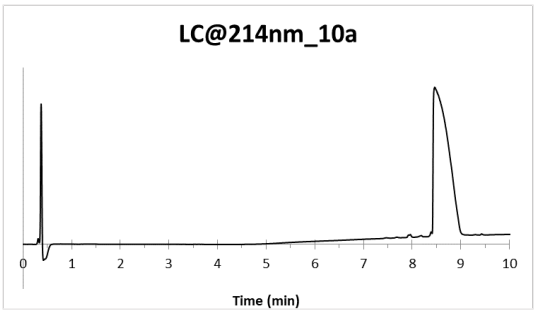
LC@214nm_10a
0 1 2 3 4 5 6 7 8 9 10
Time (min)

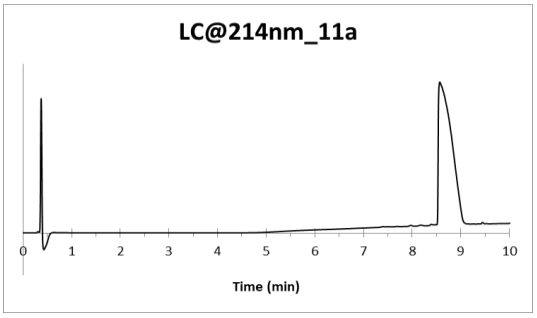
LC@214nm_11a
0 1 2 3 4 5 6 7 8 9 10
Time (min)

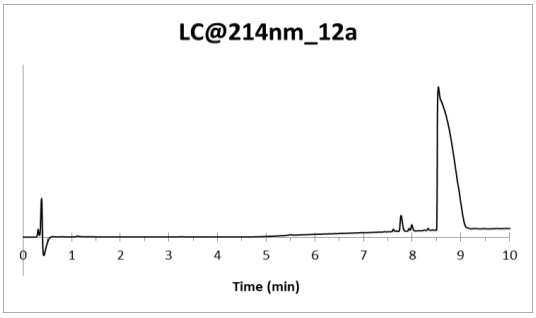
LC@214nm_12a
0 1 2 3 4 5 6 7 8 9 10
Time (min)

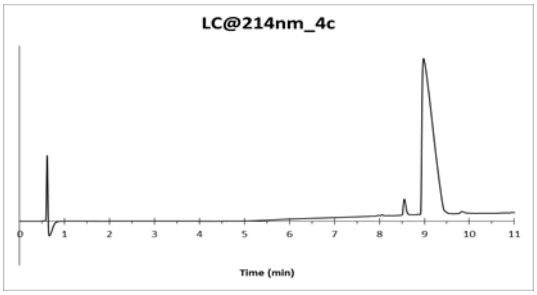
LC@214nm_4c
0 1 2 3 4 5 6 7 8 9 10 11
Time (min)

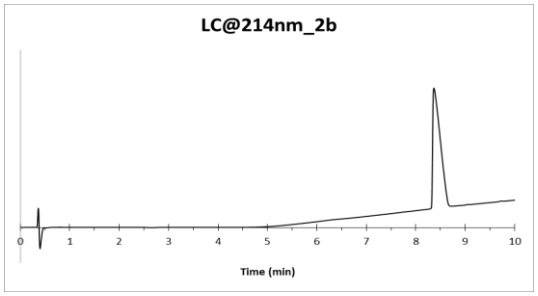
LC@214nm_2b
0 1 2 3 4 5 6 7 8 9 10
Time (min)

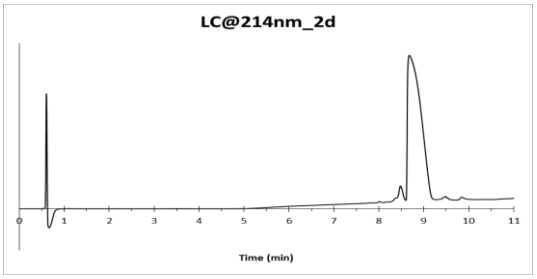
LC@214nm_2d
0 1 2 3 4 5 6 7 8 9 10 11
Time (min)

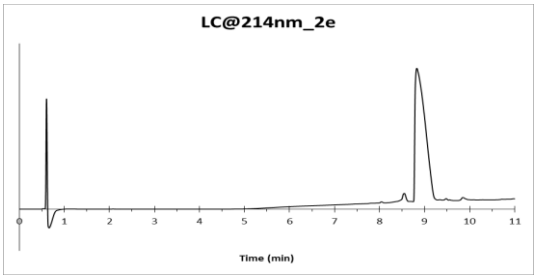
LC@214nm_2e
0 1 2 3 4 5 6 7 8 9 10 11
Time (min)

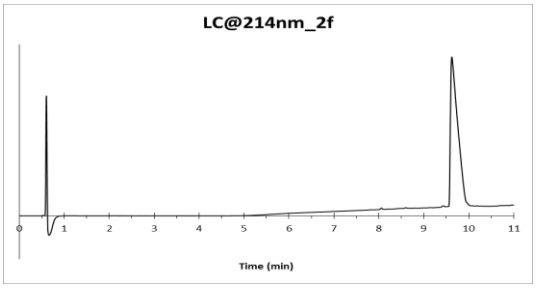
LC@214nm_2f
0 1 2 3 4 5 6 7 8 9 10 11
Time (min)

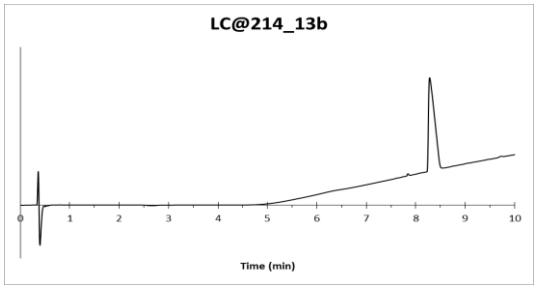
LC@214_13b
0 1 2 3 4 5 6 7 8 9 10
Time (min)

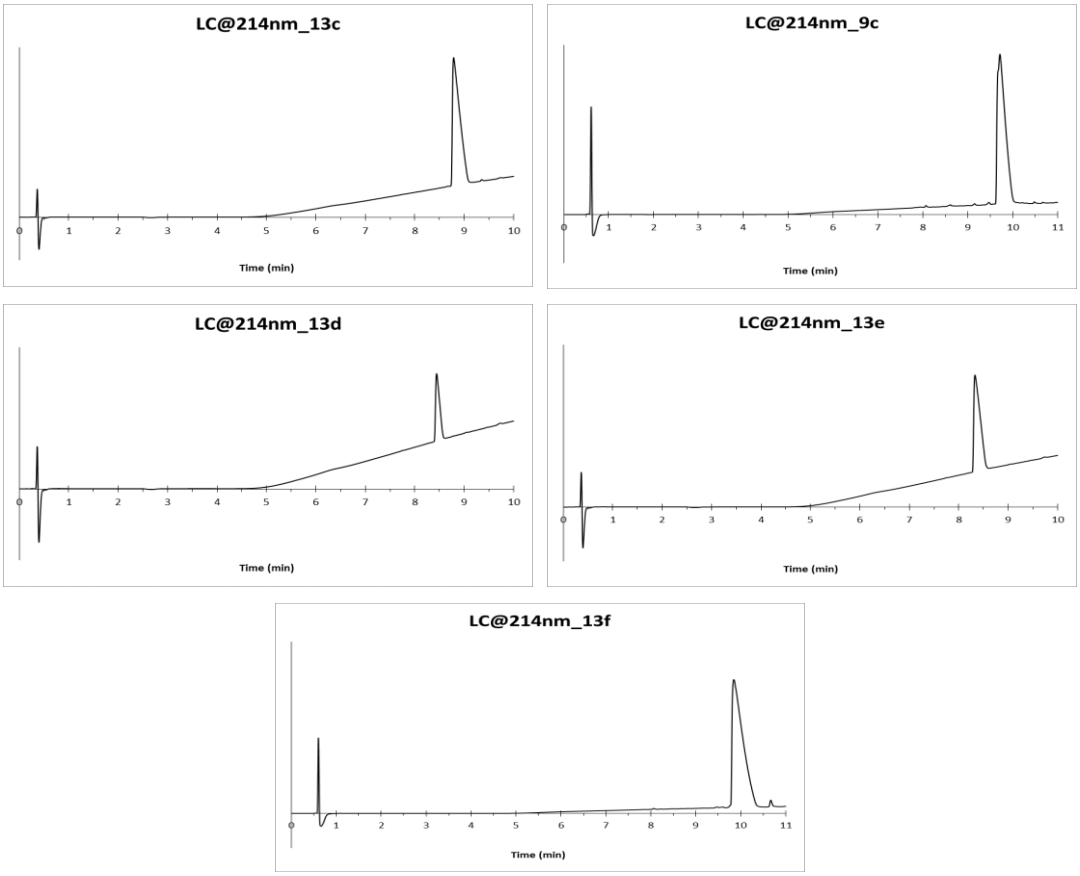

Figure 6.41 HPLC trace of peptides.

6.3 Photographs of non-assembling peptides

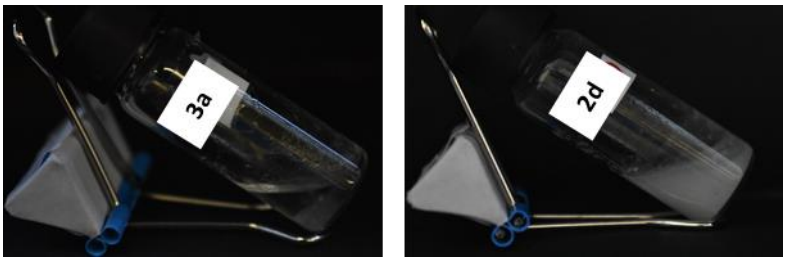

Figure 6.42 Not gelling peptides **3a** and **2d**

6.3 Rheometry data

	15 mM		
Compound name	**G' (Pa)**	**G" (Pa)**	**Stress (Pa)**
1a	6180	306	22
2a	5090	739	22

Tables 6.1 Elastic, viscous moduli and breaking point of **1a** and **2a** at 15 mM

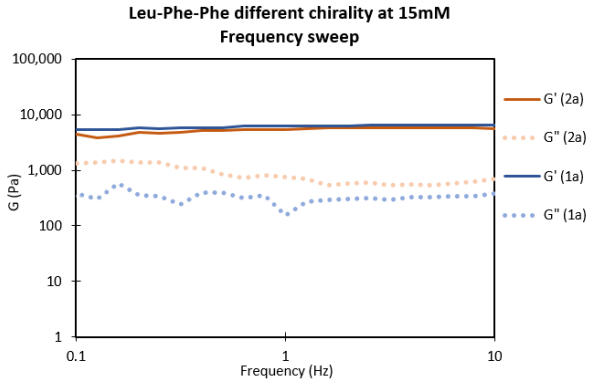

Figure 6.43 Frequence sweep of **1a** and **2a** at 15 mM.

A	**5 mM**			**MGC**		
Compound name	**G' (Pa)**	**G" (Pa)**	**Stress (Pa)**	**G' (Pa)**	**G" (Pa)**	**Stress (Pa)**
1a	1350	68	15	1350	68	15
2a	1600	57	15	1600	57	15
3a	0	0	0	0	0	0
4c	16200	811	22	16200	811	22
7a	0	0	0	27700	1660	46
8a	0	0	0	6500	173	32
9c	817	34	7	817	34	7
13c	1730	85	6	7210	276	22

Table 6.2 A Comparison between elastic, viscous moduli and breaking point of peptides having the same structure but different chirality at MGC and at 5 mM.

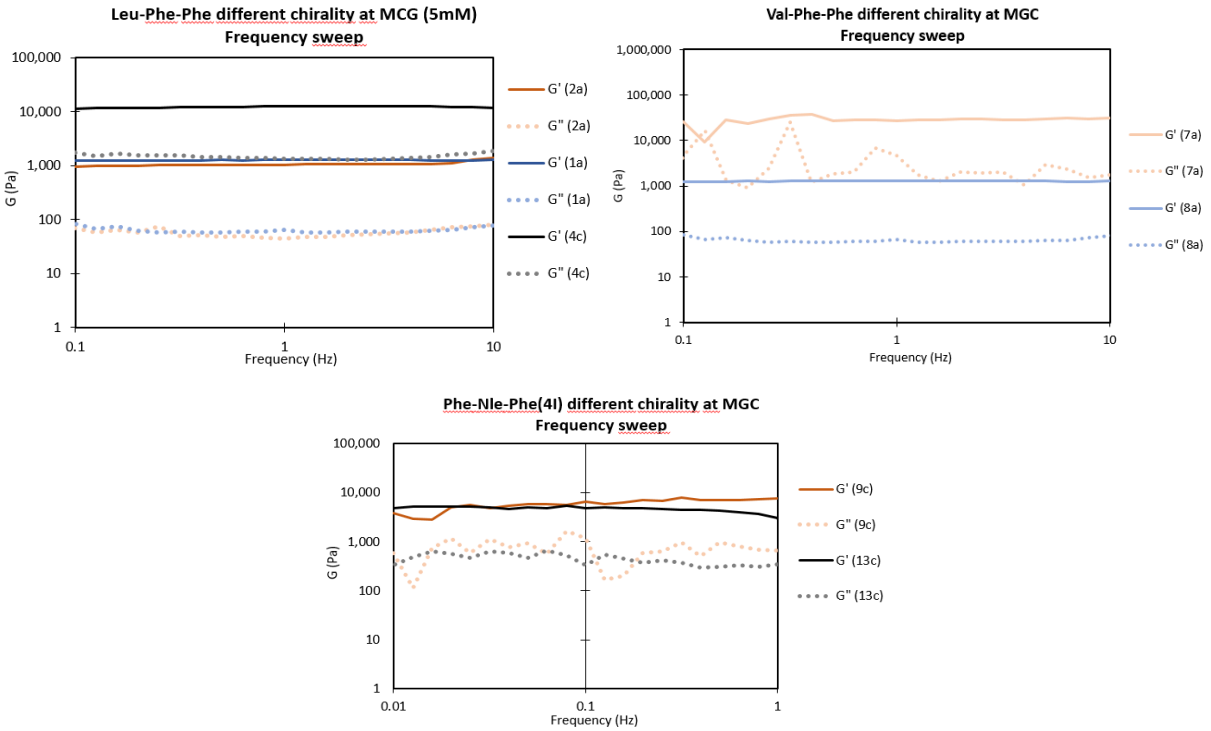

Figure 6.44 Frequence sweep of peptides with the same structure but different chirality at MGC.

B	**5 mM**			**MGC**		
Compound name	**G' (Pa)**	**G" (Pa)**	**Stress (Pa)**	**G' (Pa)**	**G" (Pa)**	**Stress (Pa)**
2a	1600	57	15	1600	57	15
5a	13	3	3	12500	288	46
6a	5330	317	68	14500	1220	147
7a	0	0	0	27700	1660	100

Table 6.2 B Comparison between elastic, viscous moduli and breaking point of Xaa-Phe-Phe peptides at MGC and at 5 mM.

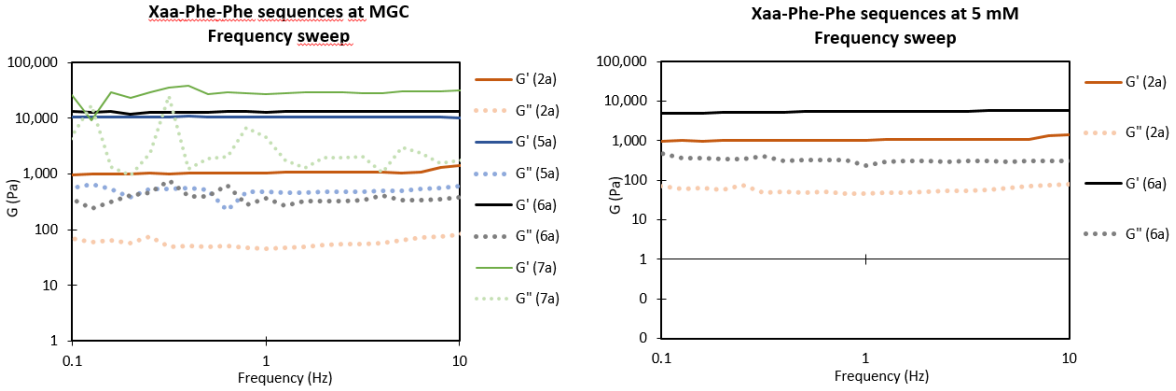

Figure 6.45 Frequence sweep of Xaa-Phe-Phe peptides at MGC and at 5 mM.

C	MGC		
Compound name	**G' (Pa)**	**G" (Pa)**	**Stress (Pa)**
10a	5874	374	36
11a	5052	271	100
12a	6075	390	34

Table 6.2 C Comparison between elastic, viscous moduli and breaking point of Phe-Xaa-Phe peptides at MGC. Ref.4

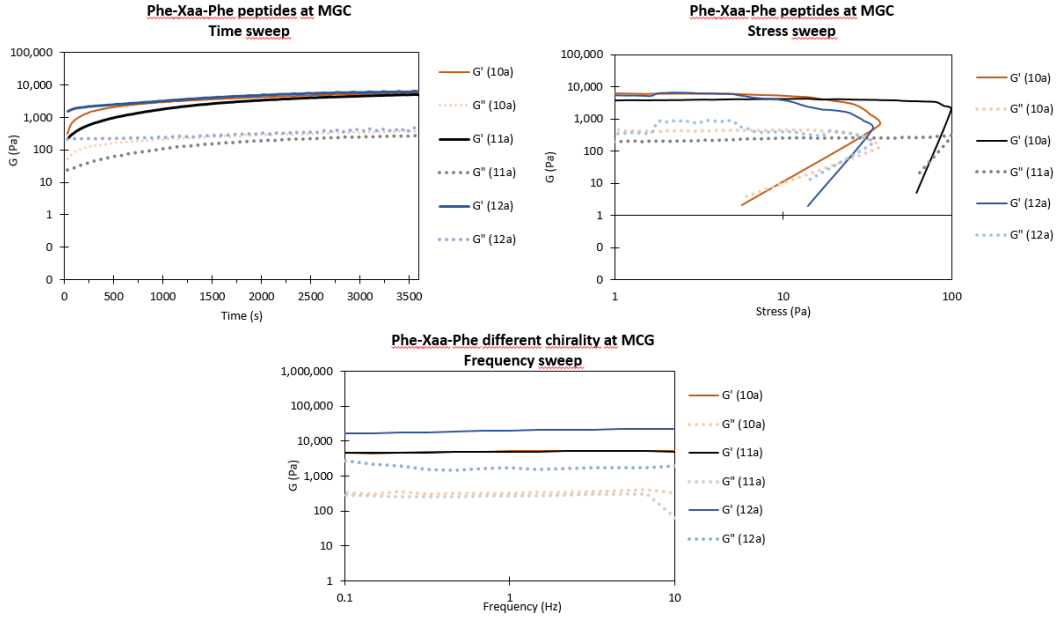

Figure 6.46 Frequence sweep of Phe-Xaa-Phe peptides at MGC. Ref.[56]

D	5 mM			MGC		
Compound name	**G' (Pa)**	**G" (Pa)**	**Stress (Pa)**	**G' (Pa)**	**G" (Pa)**	**Stress (Pa)**
2b	1690	82	70	1690	82	70
2d	0	0	0	0	0	0
2e	23	0	0	24000	1180	32
2f	30	29	2	7200	624	22
13b	911	45	46	8470	1350	68
13c	1730	85	6	7210	276	22
13d	817	48	5	18500	607	32
13e	2910	35	15	3310	278	22
13f	1540	62	32	1090	174	10

Table 6.2 D Comparison between elastic, viscous moduli and breaking point of halogenated peptides at MGC and at 5 mM

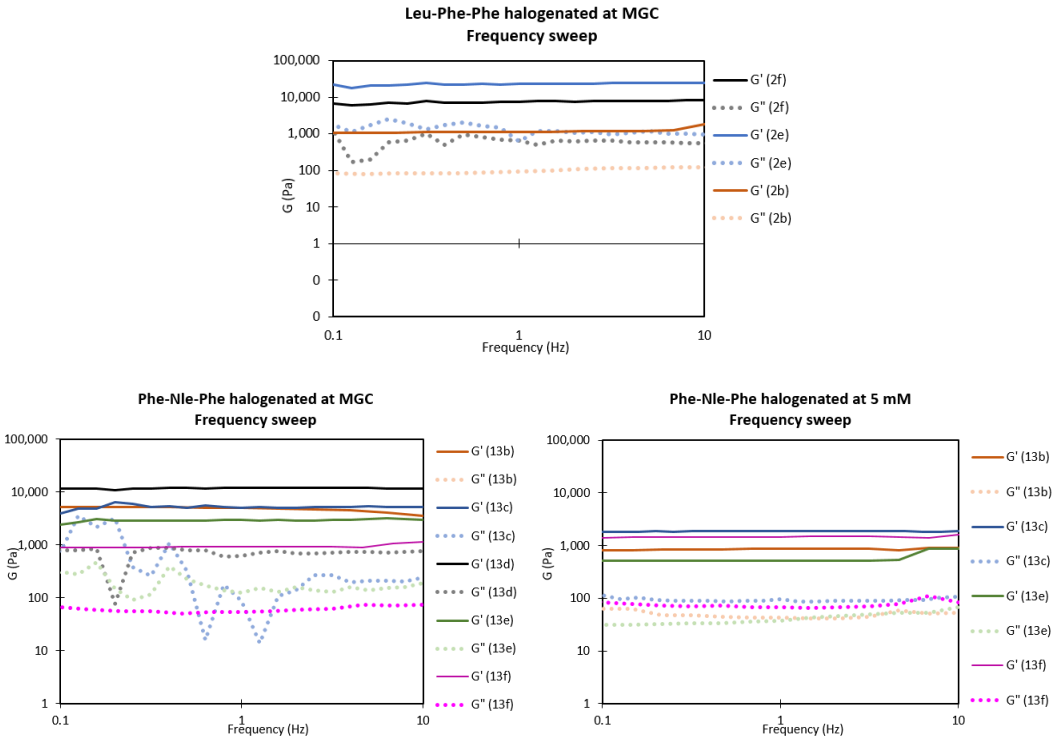

Figure 6.47 Frequence sweep of halogenated peptides at MGC and at 5 mM.

6.4 CD spectra of peptides at MGC

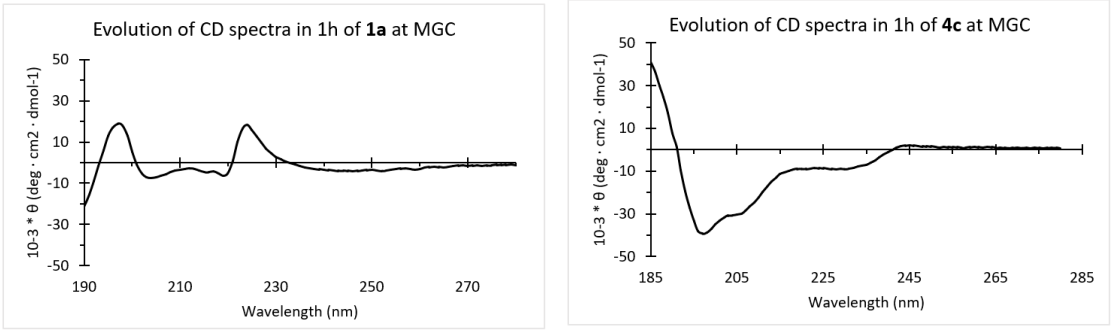

Figure 6.48 CD spectra of Leu-Phe-Phe peptides at different chirality at MGC.

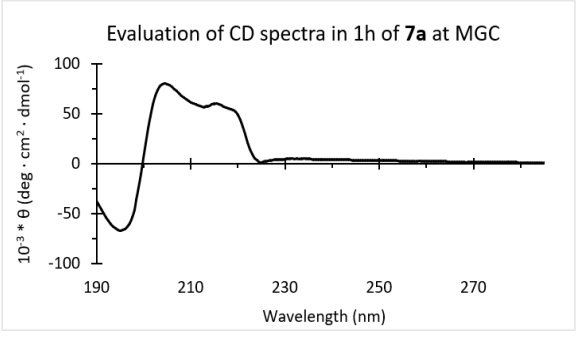

Figure 6.49 CD spectra of Val-Phe-Phe peptides at different chirality at MGC.

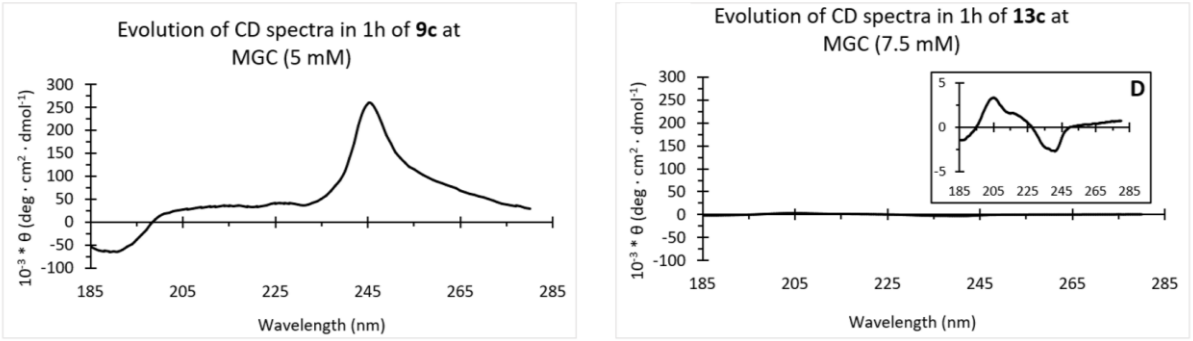

Figure 6.50 CD spectra of Phe-Nle-Phe(4I) peptides at different chirality at MGC

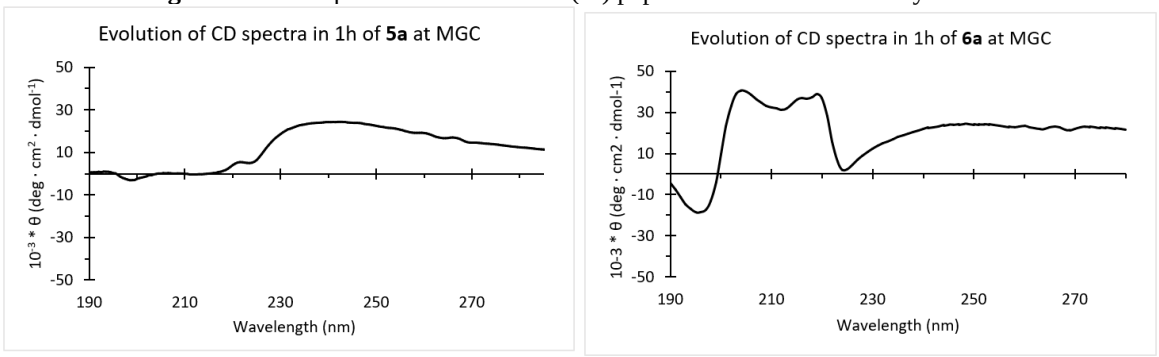

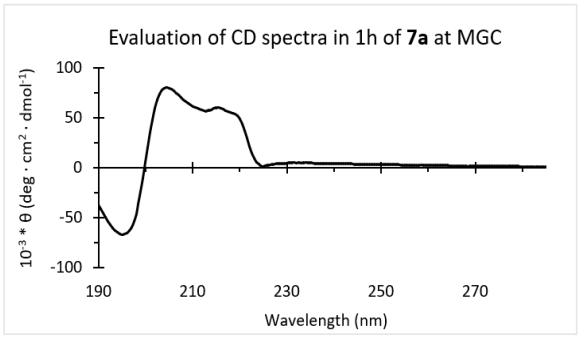

Figure 6.51 CD spectra of non Xaa-Phe-Phe peptides at MGC.

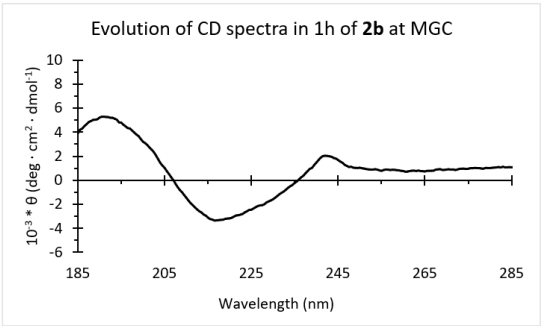

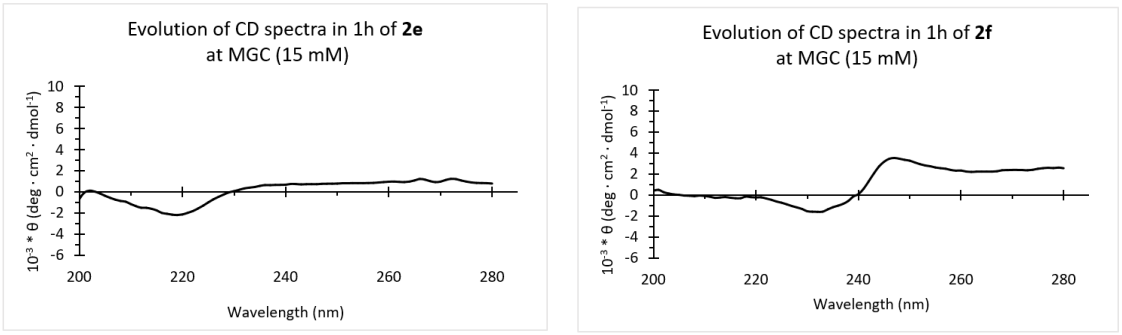

Figure 6.52 CD spectra of Leu-Phe-Phe halogenated peptides at MGC.

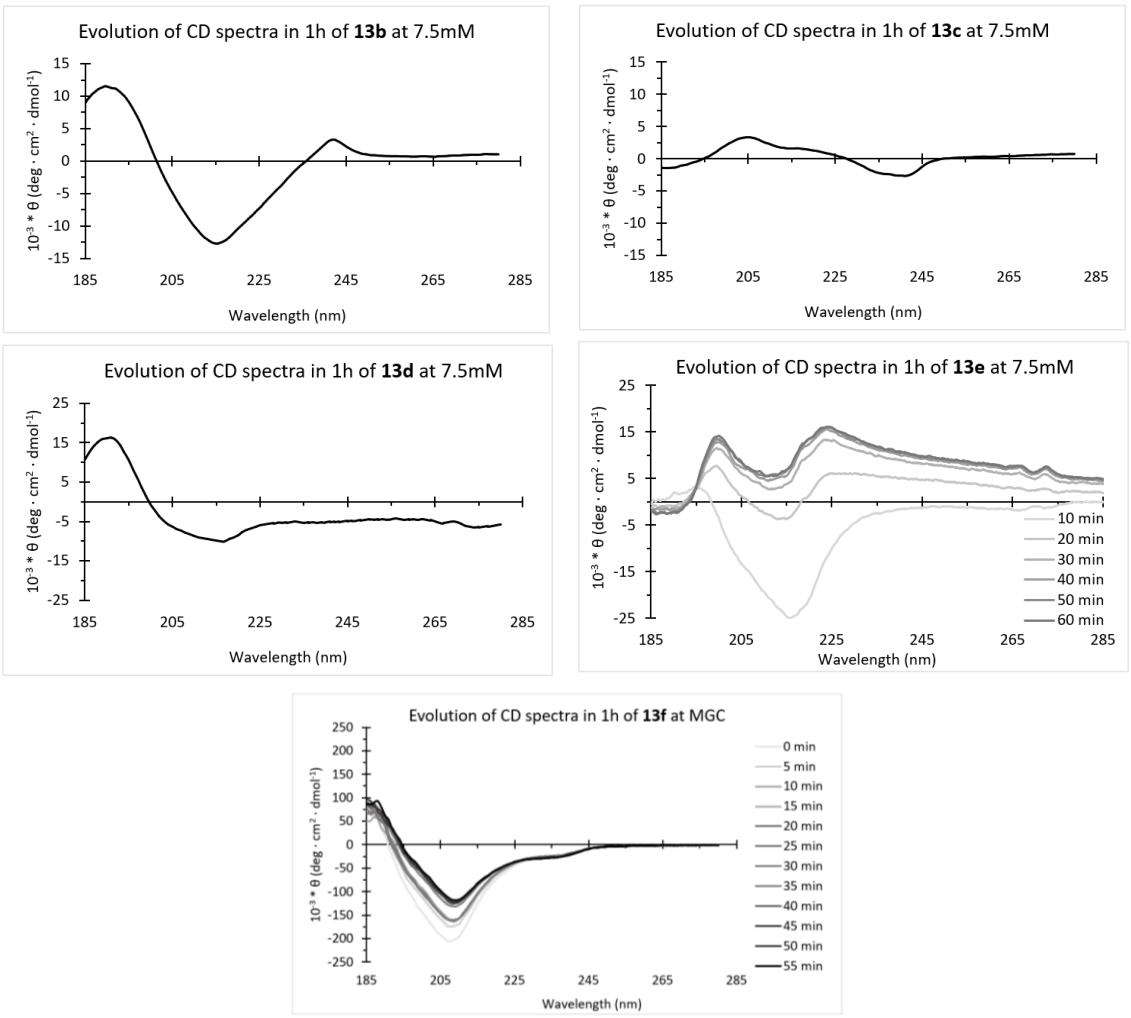

Figure 6.53 CD spectra of Phe-Nle-Phe halogenated peptides at MGC

REFERENCES

(1) Fernandes, P.; Martens, E. Antibiotics in Late Clinical Development. *Biochem. Pharmacol* **2017**, No. 133, 152–163.

(2) Antimicrobial Resistance Fact Sheet. p https://www.who.int/antimicrobial-resistance/en/ a.

(3) Mohanan, P.; Reshma, V.; Santha kumar, S.; Sruthi, S.; Cherian, R.; S, R. Engineered Nanoparticles with Antimicrobial Property. *Current Drug Metabolism* **2017**, *18*. https://doi.org/10.2174/1389200218666170925122201.

(4) Lombardi, L.; Falanga, A.; Del Genio, V.; Galdiero, S. A New Hope: Self-Assembling Peptides with Antimicrobial Activity. *Pharmaceutics* **2019**, *11* (4). https://doi.org/10.3390/pharmaceutics11040166.

(5) Sierra, J. M.; Fusté, E.; Rabanal, F.; Vinuesa, T.; Viñas, M. An Overview of Antimicrobial Peptides and the Latest Advances in Their Development. *Expert Opinion on Biological Therapy* **2017**, *17* (6), 663–676. https://doi.org/10.1080/14712598.2017.1315402.

(6) Lim, H. L.; Hwang, Y.; Kar, M.; Varghese, S. Smart Hydrogels as Functional Biomimetic Systems. *Biomater. Sci.* **2014**, *2* (5), 603–618. https://doi.org/10.1039/C3BM60288E.

(7) Gibas, I.; Janik, H. Review: Synthetic Polymer Hydrogels for Biomedical Applications. *Chem. Chem. Technol.* **2010**, *4*, 297–304.

(8) Ganguly, K.; Chaturvedi, K.; More, U.; Nadagouda, M.; Aminabhavi, T. Polysaccharide-Based Micro/Nanohydrogels for Delivering Macromolecular Therapeutics. *Journal of Controlled Release* **2014**, *193*, 162–173. https://doi.org/10.1016/j.jconrel.2014.05.014.

(9) Jonker, A.; Löwik, D.; Hest, J. Peptide- and Protein-Based Hydrogels. *Chemistry of Materials - CHEM MATER* **2012**, *24*, 759–773. https://doi.org/10.1021/cm202640w.

(10) Iglesias, D.; Bosi, S.; Melchionna, M.; Da Ros, T.; Marchesan, S. The Glitter of Carbon Nanostructures in Hybrid/Composite Hydrogels for Medicinal Use. *Current topics in medicinal chemistry* **2016**, *16* (18), 1976—1989. https://doi.org/10.2174/1568026616666160215154807.

(11) Zasloff, M. Antimicrobial Peptides of Multicellular Organisms. *Nature* **2002**, *415*, 389.

(12) Shai, Y. Mode of Action of Membrane Active Antimicrobial Peptides. *Peptide Science* **2002**, *66* (4), 236–248. https://doi.org/10.1002/bip.10260.

(13) Wade, D.; Boman, A.; Wåhlin, B.; Drain, C. M.; Andreu, D.; Boman, H. G.; Merrifield, R. B. All-D Amino Acid-Containing Channel-Forming Antibiotic Peptides. *Proceedings of the National Academy of Sciences* **1990**, *87* (12), 4761 LP – 4765.

(14) Vunnam, S.; Juvvadi, P.; Merrifield, R. B. Synthesis and Antibacterial Action of Cecropin and Proline-Arginine- Rich Peptides from Pig Intestine. *Journal of Peptide Research* **1997**, *49* (1), 59–66.

(15) Greco, I.; Hansen, E. J.; Jana, B.; Molchanova, N.; Oddo, A.; Thulstrup, W. P.; Damborg, P.; Guardabassi, L.; Hansen, R. P. Structure–Activity Study, Characterization, and Mechanism of Action of an Antimicrobial Peptoid D2 and Its d- and l-Peptide Analogues. *Molecules* . 2019. https://doi.org/10.3390/molecules24061121.

(16) Rao, A. G. Conformation and Antimicrobial Activity of Linear Derivatives of Tachyplesin Lacking Disulfide Bonds. *Archives of Biochemistry and Biophysics* **1999**, *361* (1), 127–134. https://doi.org/https://doi.org/10.1006/abbi.1998.0962.

(17) Wang, G.; Li, X.; Wang, Z. APD2: The Updated Antimicrobial Peptide Database and Its Application in Peptide Design. *Nucleic Acids Research* **2009**, *37* (Database issue), D933–D937. https://doi.org/10.1093/nar/gkn823.

(18) Kumar, P.; Kizhakkedathu, N. J.; Straus, K. S. Antimicrobial Peptides: Diversity, Mechanism of Action and Strategies to Improve the Activity and Biocompatibility In Vivo. *Biomolecules* . 2018. https://doi.org/10.3390/biom8010004.

(19) Chen, H.-C.; Brown, J. H.; Morell, J. L.; Huang, C. M. Synthetic Magainin Analogues with Improved Antimicrobial Activity. *FEBS Letters* **1988**, *236* (2), 462–466. https://doi.org/10.1016/0014-5793(88)80077-2.

(20) Brewer, D.; Hunter, H.; Lajoie, G. NMR Studies of the Antimicrobial Salivary Peptides Histatin 3 and Histatin 5 in Aqueous and Nonaqueous Solutions. *Biochemistry and Cell Biology* **1998**, *76* (2–3), 247–256. https://doi.org/10.1139/o98-066.

(21) Helmerhorst, E. J.; Breeuwer, P.; Van 't Hof, W.; Walgreen-Weterings, E.; Oomen, L. C. J. M.; Veerman, E. C. I.; Amerongen, A. V. N.; Abee, T. The Cellular Target of Histatin 5 on Candida Albicans Is the Energized Mitochondrion. *Journal of Biological Chemistry* **1999**, *274* (11), 7286–7291. https://doi.org/10.1074/jbc.274.11.7286.

(22) Persson, S.; Antoinette Killian, J.; Lindblom, G. Molecular Ordering of Interfacially Localized Tryptophan Analogs in Ester- and Ether-Lipid Bilayers Studied by 2H-NMR. *Biophysical Journal* **1998**, *75* (3), 1365–1371. https://doi.org/https://doi.org/10.1016/S0006-3495(98)74054-8.

(23) Gräfe, U. CIBA Foundation Symposium 186: Antimicrobial Peptides. VIII + 283 S., 35 Abb., 22 Tab. Chichester-New York-Brisbane-Toronto-Singapore 1994. John Wiley & Sons. £ 47.50. ISBN: 0-471-95025-4. *Journal of Basic Microbiology* **1995**, *35* (2), 72. https://doi.org/10.1002/jobm.3620350203.

(24) Montville, T. J.; Chen, Y. Mechanistic Action of Pediocin and Nisin: Recent Progress and Unresolved Questions. *Applied Microbiology and Biotechnology* **1998**, *50* (5), 511–519. https://doi.org/10.1007/s002530051328.

(25) Xhindoli, D.; Pacor, S.; Benincasa, M.; Scocchi, M.; Gennaro, R.; Tossi, A. The Human Cathelicidin LL-37 — A Pore-Forming Antibacterial Peptide and Host-Cell Modulator. *Biochimica et Biophysica*

Acta (BBA) - Biomembranes **2016**, *1858* (3), 546–566. https://doi.org/https://doi.org/10.1016/j.bbamem.2015.11.003.

(26) Lazaridis, T.; He, Y.; Prieto, L. Membrane Interactions and Pore Formation by the Antimicrobial Peptide Protegrin. *Biophysical Journal* **2013**, *104* (3), 633–642. https://doi.org/10.1016/j.bpj.2012.12.038.

(27) Zelezetsky, I.; Pontillo, A.; Puzzi, L.; Antcheva, N.; Segat, L.; Pacor, S.; Crovella, S.; Tossi, A. Evolution of the Primate Cathelicidin. *Journal of Biological Chemistry* **2006**, *281*, 19861–19871.

(28) Dathe, M.; Schümann, M.; Wieprecht, T.; Winkler, A.; Beyermann, M.; Krause, E.; Matsuzaki, K.; Murase, O.; Bienert, M. Peptide Helicity and Membrane Surface Charge Modulate the Balance of Electrostatic and Hydrophobic Interactions with Lipid Bilayers and Biological Membranes. *Biochemistry* **1996**, *35* (38), 12612–12622. https://doi.org/10.1021/bi960835f.

(29) Oren, Z.; Shai, Y. Mode of Action of Linear Amphipathic α-Helical Antimicrobial Peptides. *Peptide Science* **1998**, *47* (6), 451–463. https://doi.org/10.1002/(SICI)1097-0282(1998)47:6<451::AID-BIP4>3.0.CO;2-F.

(30) Guida, F.; Benincasa, M.; Zahariev, S.; Scocchi, M.; Berti, F.; Gennaro, R.; Tossi, A. Effect of Size and N-Terminal Residue Characteristics on Bacterial Cell Penetration and Antibacterial Activity of the Proline-Rich Peptide Bac7. *Journal of Medicinal Chemistry* **2015**, *58* (3), 1195–1204. https://doi.org/10.1021/jm501367p.

(31) Shagaghi, N.; Palombo, E.; Clayton, A.; Bhave, M. Archetypal Tryptophan-Rich Antimicrobial Peptides: Properties and Applications. *World journal of microbiology & biotechnology* **2016**, *32*, 31. https://doi.org/10.1007/s11274-015-1986-z.

(32) Lee, J. Y.; Yang, S.-T.; Lee, S. K.; Jung, H. H.; Shin, S. Y.; Hahm, K.-S.; Kim, J. I. Salt-Resistant Homodimeric Bactenecin, a Cathelicidin-Derived Antimicrobial Peptide. *The FEBS Journal* **2008**, *275* (15), 3911–3920. https://doi.org/10.1111/j.1742-4658.2008.06536.x.

(33) Blondelle, S. E.; Houghten, R. A. Design of Model Amphipathic Peptides Having Potent Antimicrobial Activities. *Biochemistry* **1992**, *31* (50), 12688–12694. https://doi.org/10.1021/bi00165a020.

(34) Hans, D.; Fairlie, P. R. Y. and D. P. Current Status Of Short Synthetic Peptides As Vaccines. *Medicinal Chemistry*. 2006, pp 627–646. https://doi.org/http://dx.doi.org/10.2174/1573406410602060627.

(35) Jiang, L.; Xu, D.; Sellati, T. J.; Dong, H. Self-Assembly of Cationic Multidomain Peptide Hydrogels: Supramolecular Nanostructure and Rheological Properties Dictate Antimicrobial Activity. *Nanoscale* **2015**, *7* (45), 19160–19169. https://doi.org/10.1039/C5NR05233E.

(36) Kagan, B. L.; Jang, H.; Capone, R.; Teran Arce, F.; Ramachandran, S.; Lal, R.; Nussinov, R.

Antimicrobial Properties of Amyloid Peptides. *Molecular Pharmaceutics* **2012**, *9* (4), 708–717. https://doi.org/10.1021/mp200419b.

(37) Zhang, M.; Zhao, J.; Zheng, J. Molecular Understanding of a Potential Functional Link between Antimicrobial and Amyloid Peptides. *Soft Matter* **2014**, *10* (38), 7425–7451. https://doi.org/10.1039/C4SM00907J.

(38) Lashuel, H. A.; Lansbury, P. T. Are Amyloid Diseases Caused by Protein Aggregates That Mimic Bacterial Pore-Forming Toxins? *Quarterly Reviews of Biophysics* **2006**, *39* (2), 167–201. https://doi.org/DOI: 10.1017/S0033583506004422.

(39) Tian, X.; Sun, F.; Zhou, X.-R.; Luo, S.-Z.; Chen, L. Role of Peptide Self-Assembly in Antimicrobial Peptides. *Journal of Peptide Science* **2015**, *21* (7), 530–539. https://doi.org/10.1002/psc.2788.

(40) Quist, A.; Doudevski, I.; Lin, H.; Azimova, R.; Ng, D.; Frangione, B.; Kagan, B.; Ghiso, J.; Lal, R. Amyloid Ion Channels: A Common Structural Link for Protein-Misfolding Disease. *Proceedings of the National Academy of Sciences of the United States of America* **2005**, *102* (30), 10427–10432. https://doi.org/10.1073/pnas.0502066102.

(41) Chen, T.; Hou, K.; Ren, Q.; Chen, G.; Wei, P.; Zhu, M. Nanoparticle–Polymer Synergies in Nanocomposite Hydrogels: From Design to Application. *Macromolecular Rapid Communications* **2018**, *39* (21), 1800337. https://doi.org/10.1002/marc.201800337.

(42) Marchesan, S.; Prato, M. Nanomaterials for (Nano)Medicine. *ACS Medicinal Chemistry Letters* **2013**, *4* (2), 147–149. https://doi.org/10.1021/ml3003742.

(43) Adams, D. J. Dipeptide and Tripeptide Conjugates as Low-Molecular-Weight Hydrogelators. *Macromolecular Bioscience* **2011**, *11* (2), 160–173. https://doi.org/10.1002/mabi.201000316.

(44) Hoque, J.; Sangaj, N.; Varghese, S. Stimuli-Responsive Supramolecular Hydrogels and Their Applications in Regenerative Medicine. *Macromolecular Bioscience* **2019**, *19* (1), 1800259. https://doi.org/10.1002/mabi.201800259.

(45) Frederix, P. W. J. M.; Scott, G. G.; Abul-Haija, Y. M.; Kalafatovic, D.; Pappas, C. G.; Javid, N.; Hunt, N. T.; Ulijn, R. V.; Tuttle, T. Exploring the Sequence Space for (Tri-)Peptide Self-Assembly to Design and Discover New Hydrogels. *Nature Chemistry* **2015**, *7* (1), 30–37. https://doi.org/10.1038/nchem.2122.

(46) Adler-Abramovich, L.; Vaks, L.; Carny, O.; Trudler, D.; Magno, A.; Caflisch, A.; Frenkel, D.; Gazit, E. Phenylalanine Assembly into Toxic Fibrils Suggests Amyloid Etiology in Phenylketonuria. *Nature Chemical Biology* **2012**, *8* (8), 701–706. https://doi.org/10.1038/nchembio.1002.

(47) Reches, M.; Gazit, E. Casting Metal Nanowires within Discrete Self-Assembled Peptide Nanotubes. *Science* **2003**, *300* (5619), 625–627. https://doi.org/10.1126/science.1082387.

(48) Conte, M. P.; Singh, N.; Sasselli, I. R.; Escuder, B.; Ulijn, R. V. Metastable Hydrogels from Aromatic Dipeptides. *Chem. Commun.* **2016**, *52* (96), 13889–13892. https://doi.org/10.1039/C6CC05821C.

(49) Kurbasic, M.; Semeraro, S.; Garcia, A. M.; Kralj, S.; Parisi, E.; Deganutti, C.; De Zorzi, R.; Marchesan, S. Microwave-Assisted Cyclization of Unprotected Dipeptides in Water to 2,5-Piperazinediones and Self-Assembly Study of Products- and Reagents. *Synthesis* **2019**, *51* (14), 2829–2838. https://doi.org/10.1055/s-0037-1612376.

(50) Marchesan, S.; Vargiu, A. V.; Styan, K. E. The Phe-Phe Motif for Peptide Self-Assembly in Nanomedicine. *Molecules*. 2015, pp 19775–19788. https://doi.org/10.3390/molecules201119658.

(51) Du, X.; Zhou, J.; Shi, J.; Xu, B. Supramolecular Hydrogelators and Hydrogels: From Soft Matter to Molecular Biomaterials. *Chemical Reviews*. 2015, pp 13165–13307. https://doi.org/10.1021/acs.chemrev.5b00299.

(52) Tao, K.; Levin, A.; Adler-Abramovich, L.; Gazit, E. Fmoc-Modified Amino Acids and Short Peptides: Simple Bio-Inspired Building Blocks for the Fabrication of Functional Materials. *Chem. Soc. Rev.* **2016**, *45*, 3935.

(53) Martin, A. D.; Wojciechowski, J. P.; Robinson, A. B.; Heu, C.; Garvey, C. J.; Ratcliffe, J.; Waddington, L. J.; Gardiner, J.; Thordarson, P. Controlling Self-Assembly of Diphenylalanine Peptides at High PH Using Heterocyclic Capping Groups. *Scientific reports* **2017**, *7*, 43947. https://doi.org/10.1038/srep43947.

(54) Wojciechowski, J. P.; Martin, A. D.; Mason, A. F.; Fife, C. M.; Sagnella, S. M.; Kavallaris, M.; Thordarson, P. Choice of Capping Group in Tripeptide Hydrogels Influences Viability in the Three-Dimensional Cell Culture of Tumor Spheroids. *ChemPlusChem* **2017**, *82* (3), 383–389. https://doi.org/10.1002/cplu.201600464.

(55) Truong, W. T.; Su, Y.; Gloria, D.; Braet, F.; Thordarson, P. Dissolution and Degradation of Fmoc-Diphenylalanine Self-Assembled Gels Results in Necrosis at High Concentrations in Vitro. *Biomater. Sci.* **2015**, *3* (2), 298–307. https://doi.org/10.1039/C4BM00244J.

(56) Garcia, A. M.; Iglesias, D.; Parisi, E.; Styan, K. E.; Waddington, L. J.; Deganutti, C.; De Zorzi, R.; Grassi, M.; Melchionna, M.; Vargiu, A. V; et al. Chirality Effects on Peptide Self-Assembly Unraveled from Molecules to Materials. *Chem* **2018**, *4* (8), 1862–1876. https://doi.org/10.1016/j.chempr.2018.05.016.

(57) Garcia, A. M.; Kurbasic, M.; Kralj, S.; Melchionna, M.; Marchesan, S. A Biocatalytic and Thermoreversible Hydrogel from a Histidine-Containing Tripeptide. *Chem. Commun.* **2017**, *53* (58), 8110–8113. https://doi.org/10.1039/C7CC03371K.

(58) Vargiu, A. V.; Iglesias, D.; Styan, K. E.; Waddington, L. J.; Easton, C. D.; Marchesan, S. Design of a

Hydrophobic Tripeptide That Self-Assembles into Amphiphilic Superstructures Forming a Hydrogel Biomaterial. *Chemical Communications* **2016**, *52* (35), 5912–5915. https://doi.org/10.1039/c5cc10531e.

(59) Melchionna, M.; E. Styan, K.; Marchesan, S. The Unexpected Advantages of Using D-Amino Acids for Peptide Self- Assembly into Nanostructured Hydrogels for Medicine. *Current Topics in Medicinal Chemistry* **2016**, *16* (18), 2009–2018. https://doi.org/10.2174/1568026616999160212120302.

(60) Marchesan, S.; Styan, K. E.; Easton, C. D.; Waddington, L.; Vargiu, A. V. Higher and Lower Supramolecular Orders for the Design of Self-Assembled Heterochiral Tripeptide Hydrogel Biomaterials. *Journal of Materials Chemistry B* **2015**, *3* (41), 8123–8132. https://doi.org/10.1039/C5TB00858A.

(61) Jahn, T. R.; Makin, O. S.; Morris, K. L.; Marshall, K. E.; Tian, P.; Sikorski, P.; Serpell, L. C. The Common Architecture of Cross-β Amyloid. *Journal of Molecular Biology* **2010**, *395* (4), 717–727. https://doi.org/https://doi.org/10.1016/j.jmb.2009.09.039.

(62) Eisenberg, D.; Jucker, M. The Amyloid State of Proteins in Human Diseases. *Cell* **2012**, *148* (6), 1188–1203. https://doi.org/10.1016/j.cell.2012.02.022.

(63) Cherny, I.; Gazit, E. Amyloids: Not Only Pathological Agents but Also Ordered Nanomaterials. *Angewandte Chemie - International Edition*. 2008, pp 4062–4069. https://doi.org/10.1002/anie.200703133.

(64) Riek, R.; Eisenberg, D. S. The Activities of Amyloids from a Structural Perspective. *Nature* **2016**, *539*, 227.

(65) Benson, M. D.; Buxbaum, J. N.; Eisenberg, D. S.; Merlini, G.; Saraiva, M. J. M.; Sekijima, Y.; Sipe, J. D.; Westermark, P. Amyloid Nomenclature 2018: Recommendations by the International Society of Amyloidosis (ISA) Nomenclature Committee. *Amyloid* **2018**, *25* (4), 215–219. https://doi.org/10.1080/13506129.2018.1549825.

(66) Greenwald, J.; Riek, R. Biology of Amyloid: Structure, Function, And Regulation. *Structure* **2010**, *18* (10), 1244–1260. https://doi.org/10.1016/j.str.2010.08.009.

(67) Seviour, T.; Hansen, S. H.; Yang, L.; Yau, Y. H.; Wang, V. B.; Stenvang, M. R.; Christiansen, G.; Marsili, E.; Givskov, M.; Chen, Y.; et al. Functional Amyloids Keep Quorum-Sensing Molecules in Check. *Journal of Biological Chemistry* **2015**, *290* (10), 6457–6469. https://doi.org/10.1074/jbc.M114.613810.

(68) Jackson, P. M.; Hewitt, W. E. Why Are Functional Amyloids Non-Toxic in Humans? *Biomolecules* . 2017. https://doi.org/10.3390/biom7040071.

(69) Shewmaker, F.; McGlinchey, R. P.; Wickner, R. B. Structural Insights into Functional and Pathological Amyloid. *Journal of Biological Chemistry*. 2011, pp 16533–16540.

https://doi.org/10.1074/jbc.R111.227108.

(70) Bieler, S.; Estrada, L.; Lagos, R.; Baeza, M.; Castilla, J.; Soto, C. Amyloid Formation Modulates the Biological Activity of a Bacterial Protein. *Journal of Biological Chemistry* **2005**, *280* (29), 26880–26885. https://doi.org/10.1074/jbc.M502031200.

(71) Blanco, L. P.; Evans, M. L.; Smith, D. R.; Badtke, M. P.; Chapman, M. R. Diversity, Biogenesis and Function of Microbial Amyloids. *Trends in Microbiology* **2012**, *20* (2), 66–73. https://doi.org/10.1016/j.tim.2011.11.005.

(72) Hengge, R. Spotlight On… Regine Hengge. *FEMS Microbiology Letters* **2019**, *366* (2). https://doi.org/10.1093/femsle/fny293.

(73) Andreasen, M.; Meisl, G.; Taylor, J. D.; Michaels, T. C. T.; Levin, A.; Otzen, D. E.; Chapman, M. R.; Dobson, C. M.; Matthews, S. J.; Knowles, T. P. J. Physical Determinants of Amyloid Assembly in Biofilm Formation. *mBio* **2019**, *10* (1). https://doi.org/10.1128/mBio.02279-18.

(74) Soscia, S. J.; Kirby, J. E.; Washicosky, K. J.; Tucker, S. M.; Ingelsson, M.; Hyman, B.; Burton, M. A.; Goldstein, L. E.; Duong, S.; Tanzi, R. E.; et al. The Alzheimer's Disease-Associated Amyloid β-Protein Is an Antimicrobial Peptide. *PLoS ONE* **2010**, *5* (3), 1–10. https://doi.org/10.1371/journal.pone.0009505.

(75) Brogden, K. A. Antimicrobial Peptides: Pore Formers or Metabolic Inhibitors in Bacteria? *Nature Reviews Microbiology* **2005**, *3* (3), 238–250. https://doi.org/10.1038/nrmicro1098.

(76) Luna, S.; Cameron, D. J.; Ethell, D. W. Amyloid-β and APP Deficiencies Cause Severe Cerebrovascular Defects: Important Work for an Old Villain. *PLOS ONE* **2013**, *8* (9), e75052.

(77) Kumar, D. K. V.; Eimer, W. A.; Tanzi, R. E.; Moir, R. D. Alzheimer's Disease: The Potential Therapeutic Role of the Natural Antibiotic Amyloid-β Peptide. *Neurodegenerative Disease Management* **2016**, *6* (5), 345–348. https://doi.org/10.2217/nmt-2016-0035.

(78) Gosztyla, M.; Brothers, H.; Robinson, S. Alzheimer's Amyloid-β Is an Antimicrobial Peptide: A Review of the Evidence. *Journal of Alzheimer's Disease* **2018**, *62*, 1–12. https://doi.org/10.3233/JAD-171133.

(79) Fulop, T.; Itzhaki, R.; Balin, B.; Miklossy, J.; Barron, A. Role of Microbes in the Development of Alzheimer's Disease: State of the Art – An International Symposium Presented at the 2017 IAGG Congress in San Francisco. *Frontiers in Genetics* **2018**, *9*, 362. https://doi.org/10.3389/fgene.2018.00362.

(80) Mitra, R. N.; Shome, A.; Paul, P.; Das, P. K. Antimicrobial Activity{,} Biocompatibility and Hydrogelation Ability of Dipeptide-Based Amphiphiles. *Org. Biomol. Chem.* **2009**, *7* (1), 94–102. https://doi.org/10.1039/B815368J.

(81) Hu, Y.; Xu, W.; Li, G.; Xu, L.; Song, A.; Hao, J. Self-Assembled Peptide Nanofibers Encapsulated with Superfine Silver Nanoparticles via Ag+ Coordination. *Langmuir* **2015**, *31* (31), 8599–8605. https://doi.org/10.1021/acs.langmuir.5b02036.

(82) Liu, Y.; Yang, Y.; Wang, C.; Zhao, X. Stimuli-Responsive Self-Assembling Peptides Made from Antibacterial Peptides. *Nanoscale* **2013**, *5* (14), 6413–6421. https://doi.org/10.1039/C3NR00225J.

(83) Schneider, A.; Garlick, J. A.; Egles, C. Self-Assembling Peptide Nanofiber Scaffolds Accelerate Wound Healing. *PLOS ONE* **2008**, *3* (1), e1410.

(84) McCloskey, A. P.; Gilmore, B. F.; Laverty, G. Evolution of Antimicrobial Peptides to Self-Assembled Peptides for Biomaterial Applications. *Pathogens* **2014**, *3* (4), 791–821. https://doi.org/10.3390/pathogens3040791.

(85) Takeuchi, O.; Hoshino, K.; Kawai, T.; Sanjo, H.; Takada, H.; Ogawa, T.; Takeda, K.; Akira, S. Differential Roles of TLR2 and TLR4 in Recognition of Gram-Negative and Gram-Positive Bacterial Cell Wall Components. *Immunity* **2018**, *11* (4), 443–451. https://doi.org/10.1016/S1074-7613(00)80119-3.

(86) Pochan, D. J.; Schneider, J. P.; Kretsinger, J.; Ozbas, B.; Rajagopal, K.; Haines, L. Thermally Reversible Hydrogels via Intramolecular Folding and Consequent Self-Assembly of a de Novo Designed Peptide. *Journal of the American Chemical Society* **2003**, *125* (39), 11802–11803. https://doi.org/10.1021/ja0353154.

(87) Tang, C.; Ulijn, R. V; Saiani, A. Effect of Glycine Substitution on Fmoc–Diphenylalanine Self-Assembly and Gelation Properties. *Langmuir* **2011**, *27* (23), 14438–14449. https://doi.org/10.1021/la202113j.

(88) Tang, C.; Ulijn, R.; Saiani, A. Self-Assembly and Gelation Properties of Glycine/Leucine Fmoc-Dipeptides. *The European physical journal. E, Soft matter* **2013**, *36*, 9925. https://doi.org/10.1140/epje/i2013-13111-3.

(89) Liu, Y.; Ma, W.; Liu, W.; Li, C.; Liu, Y.; Jiang, X.; Tang, Z. Silver(i)-Glutathione Biocoordination Polymer Hydrogel: Effective Antibacterial Activity and Improved Cytocompatibility. *J. Mater. Chem.* **2011**, *21* (48), 19214–19218. https://doi.org/10.1039/C1JM13693C.

(90) Wu, L.-Q.; Payne, G. F. Biofabrication: Using Biological Materials and Biocatalysts to Construct Nanostructured Assemblies. *Trends in Biotechnology* **2004**, *22* (11), 593–599. https://doi.org/10.1016/j.tibtech.2004.09.008.

(91) Hughes, M.; Debnath, S.; Knapp, C. W.; Ulijn, R. V. Antimicrobial Properties of Enzymatically Triggered Self-Assembling Aromatic Peptide Amphiphiles. *Biomater. Sci.* **2013**, *1*, 1138.

(92) Hughes, M.; Birchall, L. S.; Zuberi, K.; Aitken, L. A.; Debnath, S.; Javid, N.; Ulijn, R. V. Differential Supramolecular Organisation of Fmoc-Dipeptides with Hydrophilic Terminal Amino Acid Residues

by Biocatalytic Self-Assembly. *Soft Matter* **2012**, *8* (45), 11565. https://doi.org/10.1039/c2sm26092a.

(93) Baral, A.; Roy, S.; Ghosh, S.; Hermida-Merino, D.; Hamley, I. W.; Banerjee, A. A Peptide-Based Mechano-Sensitive, Proteolytically Stable Hydrogel with Remarkable Antibacterial Properties. *Langmuir* **2016**, *32* (7), 1836–1845. https://doi.org/10.1021/acs.langmuir.5b03789.

(94) Gahane, A. Y.; Ranjan, P.; Singh, V.; Sharma, R. K.; Sinha, N.; Sharma, M.; Chaudhry, R.; Thakur, A. K. Fmoc-Phenylalanine Displays Antibacterial Activity against Gram-Positive Bacteria in Gel and Solution Phases. *Soft Matter* **2018**, *14*, 2234.

(95) Debnath, S.; Shome, A.; Das, D.; Das, P. K. Hydrogelation Through Self-Assembly of Fmoc-Peptide Functionalized Cationic Amphiphiles: Potent Antibacterial Agent. *J. Phys. Chem. B* **2010**, *114*, 4407.

(96) Irwansyah, I.; Li, Y.-Q.; Shi, W.; Qi, D.; Leow, W. R.; Tang, M. B. Y.; Li, S.; Chen, X. Gram-Positive Antimicrobial Activity of Amino Acid-Based Hydrogels. *Advanced Materials* **2015**, *27* (4), 648–654. https://doi.org/10.1002/adma.201403339.

(97) Schnaider, L.; Ghosh, M.; Bychenko, D.; Grigoriants, I.; Ya'ari, S.; Shalev Antsel, T.; Matalon, S.; Sarig, R.; Brosh, T.; Pilo, R.; et al. Enhanced Nanoassembly-Incorporated Antibacterial Composite Materials. *ACS Applied Materials & Interfaces* **2019**, *11* (24), 21334–21342. https://doi.org/10.1021/acsami.9b02839.

(98) Schnaider, L.; Brahmachari, S.; Schmidt, N. W.; Mensa, B.; Shaham-Niv, S.; Bychenko, D.; Adler-Abramovich, L.; Shimon, L. J. W.; Kolusheva, S.; DeGrado, W. F.; et al. Self-Assembling Dipeptide Antibacterial Nanostructures with Membrane Disrupting Activity. *Nature Communications* **2017**, *8* (1), 1365. https://doi.org/10.1038/s41467-017-01447-x.

(99) Marchesan, S.; Waddington, L.; Easton, C. D.; Winkler, D. A.; Goodall, L.; Forsythe, J.; Hartley, P. G. Unzipping the Role of Chirality in Nanoscale Self-Assembly of Tripeptide Hydrogels. *Nanoscale* **2012**, *4* (21), 6752–6760. https://doi.org/10.1039/C2NR32006A.

(100) Marchesan, S.; Qu, Y.; Waddington, L. J.; Easton, C. D.; Glattauer, V.; Lithgow, T. J.; McLean, K. M.; Forsythe, J. S.; Hartley, P. G. Self-Assembly of Ciprofloxacin and a Tripeptide into an Antimicrobial Nanostructured Hydrogel. *Biomaterials* **2013**, *34* (14), 3678–3687. https://doi.org/https://doi.org/10.1016/j.biomaterials.2013.01.096.

(101) Kurbasic, M.; Romano, C.; Garcia, A.; Kralj, S.; Marchesan, S. Assembly of a Tripeptide and Anti-Inflammatory Drugs into Supramolecular Hydrogels for Sustained Release. *Gels* **2017**, *3* (3), 29. https://doi.org/10.3390/gels3030029.

(102) Marchesan, S.; Waddington, L.; Easton, C. D.; Kushkaki, F.; McLean, K. M.; Forsythe, J. S.; Hartley, P. G. Tripeptide Self-Assembled Hydrogels: Soft Nanomaterials for Biological Applications. *BioNanoScience* **2013**, *3* (1), 21–29. https://doi.org/10.1007/s12668-012-0074-1.

(103) Parisi, E.; Garcia, A. M.; Marson, D.; Posocco, P.; Marchesan, S. Supramolecular Tripeptide

Hydrogel Assembly with 5-Fluorouracil. *Gels* **2019**, *5* (1). https://doi.org/10.3390/gels5010005.

(104) Colquhoun, C.; Draper, E. R.; Eden, E. G. B.; Cattoz, B. N.; Morris, K. L.; Chen, L.; McDonald, T. O.; Terry, A. E.; Griffiths, P. C.; Serpell, L. C.; et al. The Effect of Self-Sorting and Co-Assembly on the Mechanical Properties of Low Molecular Weight Hydrogels. *Nanoscale* **2014**, *6* (22), 13719–13725. https://doi.org/10.1039/C4NR04039B.

(105) Draper, E. R.; Eden, E. G. B.; McDonald, T. O.; Adams, D. J. Spatially Resolved Multicomponent Gels. *Nature Chemistry* **2015**, *7*, 848.

(106) Marchesan, S.; Styan, K. E.; Easton, C. D.; Waddington, L.; Vargiu, A. V. Higher and Lower Supramolecular Orders for the Design of Self-Assembled Heterochiral Tripeptide Hydrogel Biomaterials. *Journal of Materials Chemistry B* **2015**, *3* (41), 8123–8132. https://doi.org/10.1039/c5tb00858a.

(107) Marchesan, S.; Easton, C. D.; Styan, K. E.; Waddington, L. J.; Kushkaki, F.; Goodall, L.; McLean, K. M.; Forsythe, J. S.; Hartley, P. G. Chirality Effects at Each Amino Acid Position on Tripeptide Self-Assembly into Hydrogel Biomaterials. *Nanoscale* **2014**, *6* (10), 5172–5180. https://doi.org/10.1039/c3nr06752a.

(108) Ryan, D. M.; Anderson, S. B.; Senguen, F. T.; Youngman, R. E.; Nilsson, B. L. Self-Assembly and Hydrogelation Promoted by F5 -Phenylalanine. *Soft Matter* **2010**, *6*, 475.

(109) Bertolani, A.; Pirrie, L.; Stefan, L.; Houbenov, N.; Haataja, J. S.; Catalano, L.; Terraneo, G.; Giancane, G.; Valli, L.; Milani, R.; et al. Supramolecular Amplification of Amyloid Self-Assembly by Iodination. *Nature Communications* **2015**, *6* (May), 1–9. https://doi.org/10.1038/ncomms8574.

(110) Wang, J.; Liu, K.; Xing, R.; Yan, X. Peptide Self-Assembly: Thermodynamics and Kinetics. *Chem. Soc. Rev.* **2016**, *45* (20), 5589–5604. https://doi.org/10.1039/C6CS00176A.

(111) Morel, B.; Varela, L.; Conejero-Lara, F. The Thermodynamic Stability of Amyloid Fibrils Studied by Differential Scanning Calorimetry. *The Journal of Physical Chemistry B* **2010**, *114* (11), 4010–4019. https://doi.org/10.1021/jp9102993.

(112) Jobling, A. An Introduction to Rheology H. A. Barnes, J. F. Hutton and K. Walters, Elsevier Science Publishers, Amsterdam, 1989. Pp. v + 199, Price $6050/Dfl 115.00. ISBN 0-444-87469-0. *Polymer International* **1991**, *25* (1), 61. https://doi.org/10.1002/pi.4990250112.

(113) Biancalana, M.; Koide, S. Molecular Mechanism of Thioflavin-T Binding to Amyloid Fibrils. *Biochimica et Biophysica Acta - Proteins and Proteomics*. 2010, pp 1405–1412. https://doi.org/10.1016/j.bbapap.2010.04.001.

(114) Greenfield, N. J. Using Circular Dichroism Spectra to Estimate Protein Secondary Structure. *Nature Protocols* **2007**, *1* (6), 2876–2890. https://doi.org/10.1038/nprot.2006.202.

(115) Drake, A. ~F. REVIEW ARTICLE: Polarisation Modulation-the Measurement of Linear and Circular Dichroism. *Journal of Physics E Scientific Instruments* **1986**, *19* (3), 170–181. https://doi.org/10.1088/0022-3735/19/3/002.

(116) Polavarapu, P. L.; Zhao, C. Vibrational Circular Dichroism: A New Spectroscopic Tool for Biomolecular Structural Determination. *Fresenius' Journal of Analytical Chemistry* **2000**, *366* (6), 727–734. https://doi.org/10.1007/s002160051566.

(117) Gopal, R.; Park, J. S.; Seo, C. H.; Park, Y. Applications of Circular Dichroism for Structural Analysis of Gelatin and Antimicrobial Peptides. *International Journal of Molecular Sciences* **2012**, *13* (3), 3229–3244. https://doi.org/10.3390/ijms13033229.

(118) Kabsch, W. {\it XDS}. *Acta Crystallographica Section D* **2010**, *66* (2), 125–132. https://doi.org/10.1107/S0907444909047337.

(119) Evans, P. R.; Murshudov, G. N. How Good Are My Data and What Is the Resolution? *Acta Crystallographica Section D: Biological Crystallography* **2013**, *69* (7), 1204–1214. https://doi.org/10.1107/S0907444913000061.

(120) Evans, P. Scaling and Assessment of Data Quality. In *Acta Crystallographica Section D: Biological Crystallography*; 2006; Vol. 62, pp 72–82. https://doi.org/10.1107/S0907444905036693.

(121) Sheldrick, G. M. Crystal Structure Refinement with SHELXL. *Acta Crystallographica Section C: Structural Chemistry* **2015**, *71*, 3–8. https://doi.org/10.1107/S2053229614024218.

(122) Farrugia, L. J. WinGX and ORTEP for Windows: An Update. *Journal of Applied Crystallography* **2012**, *45* (4), 849–854. https://doi.org/10.1107/S0021889812029111.

(123) Battye, T. G. G.; Kontogiannis, L.; Johnson, O.; Powell, H. R.; Leslie, A. G. W. IMOSFLM: A New Graphical Interface for Diffraction-Image Processing with MOSFLM. *Acta Crystallographica Section D: Biological Crystallography* **2011**, *67* (4), 271–281. https://doi.org/10.1107/S0907444910048675.

(124) Kabsch, W. XDS. *Acta Crystallographica Section D Biological Crystallography* **2010**, *66* (2), 125–132. https://doi.org/10.1107/S0907444909047337.

(125) Spek, A. L. {\it PLATON} SQUEEZE: A Tool for the Calculation of the Disordered Solvent Contribution to the Calculated Structure Factors. *Acta Crystallographica Section C* **2015**, *71* (1), 9–18. https://doi.org/10.1107/S2053229614024929.

(126) Agyei, D.; Tan, K.-X.; Pan, S.; Udenigwe, C. C.; Danquah, M. K. 9 - Peptides for Biopharmaceutical Applications; Koutsopoulos Biotechnology and Bioengineering, S. B. T.-P. A. in B., Ed.; Woodhead Publishing, 2018; pp 231–251. https://doi.org/https://doi.org/10.1016/B978-0-08-100736-5.00009-0.

(127) Fornaguera, C.; Solans, C. Methods for the In Vitro Characterization of Nanomedicines—Biological Component Interaction. *Journal of Personalized Medicine* **2017**, *7*, 2.

https://doi.org/10.3390/jpm7010002.

(128) Sheldrick, G. M. A Short History of {\it SHELX}. *Acta Crystallographica Section A* **2008**, *64* (1), 112–122. https://doi.org/10.1107/S0108767307043930.

ABREVIATIONS

AMP Antimicrobial peptides

AMR antimicrobial resistance

AP Aggregation Propensity

B1 Buffer 1

B2 Buffer 2

CD Circular Dichroism

DCM Dichloromethane

DIPEA N,N-Diisopropyl ethylamine

DMF Dimethylformamide

DMSO Dimethyl sulfoxide

DMSO-d6 Deutereted dimethyl sulfoxide

ESI-MS ElectroSpray Ionisation Mass Spectroscopy

F,f - **Phe** - Phenylalanine (Upper case L-series, Lowercase D-series)

Fmoc 9-Fluorenylmethoxycarbonyl

G,g Glycine (Upper case L-series, Lowercase D-series)

G' Elastic or storage modulus

G'' Viscous or loss modulus

HBTU (O-benzotriazol-1-yl)-1,1,3,3-tetramethyluronium hexafluorophoshate

HOAt 1-Hydroxy-7-azabenzotriazole

HPLC High Performance Liquid Chromatography

I,i - **Ile** - Isoleucine (Upper case L-series, Lowercase D-series)

L,l - **Leu**- Leucine (Upper case L-series, Lowercase D-series)

LC liquid chromatography

LC- MS Liquid Chromatography- Mass Spectrometry

LMWG Low Molecular Weight Gelators

LogP

LVR Linear Viscoelastic Regime

MGC Minimum Gelation Concentration

MIC Minimum inhibitory concentration

MS Mass spectroscopy

Nle Norleucine

NMR Nuclear Magnetic Resonance

NPN 1-N-phenylnaphthylamine

Nva Norvaline

PB Phosphate Buffered

PBS Phosphate Buffered Saline

Phe(4) Para iodine phenylalanine

Phe(F) Para fluorine phenylalanine

R&D research and development

RBC red blood cell

RP-HPLC Reversed Phase High Performance Liquid Chromatography

Rt Retention Time

RT Room Temperature

SFG sum frequency generation spectroscopy

$SOCl_2$ Thionyl chloride

SPPS Solid-phase peptide synthesis

t.g. transition from gel to crystals

TEM Transmission Electron Microscopy

TFA Trifluoroacetic acid

ThT Thioflavin T

TIPS Triisopropylsilane

Tm Melting temperature

TMS Tetramethylsilane

UV Ultraviolet irradiation

UV-Vis Ultraviolet-Visible irradiation

V,v – **Val** - Valine (Upper case L-series, Lowercase D-series)

XRD X-ray Diffraction

Additional works performed during PhD

Scientific Pubblications:

1. Iglesias, D.; Melle-Franco, M.; **Kurbasic, M.;** Melchionna, M.; Abrami, M.; Grassi, M.; Prato, M.; Marchesan, S. "Oxidized Nanocarbons-Tripeptide Supramolecular Hydrogels: Shape Matters!" ***ACS* Nano** 2018, 12, 5530.

2. Garcia, A.M.[1]; **Kurbasic, M.[1]**; Kralj, S.; Melchionna, M.; Marchesan, S. "A biocatalytic and thermoreversible hydrogel from a histidine-containing tripeptide" **Chem. Commun.** 2017, 53, 8110. – **Journal Cover**

3. **Kurbasic, M.;** Romano, C. D.; Garcia, A. M.; Kralj, S.; Marchesan, S. "Assembly of a Tripeptide and Anti-Inflammatory Drugs into Supramolecular Hydrogels for Sustained Release" **Gels** 2017, 3, 29. – **Feature Article**

4. Cringoli, M. C.; Kralj, S.; **Kurbasic, M.;** Urban, M.; Marchesan, S. "Luminescent supramolecular hydrogels from a tripeptide and nitrogen-doped carbon nanodots" **Beilstein J. Nanotechnol.** 2017, 8, 1553.

5. **Kurbasic, M.;** Semeraro, S.; Garcia, A.M.; Kralj, S.; Parisi, E.; Deganutti, C.; De Zorzi R.; Marchesan, S. "Microwave-assisted cyclization of unprotected dipeptides in water to 2,5-piperazinediones and self-assembly study of products and reagents" **Synthesis** 2019, 51(14), 2829.

6. **Kurbasic, M.;** Garcia, A. M.; Parisi, E.; Marchesan, S. "Self-Assembling, Ultrashort Peptides as Antimicrobial Agents" *Submitted to* **Curr. Top Med. Chem**., 2019 – Review

7. Garcia, A. M.; Lavendomme, R.; Kralj, S.; **Kurbasic, M.;** Bellotto, O.; Semeraro, S.; Bandiera, A.; De Zorzi, R.; Marchesan, S. "Self-assembly of an amino acid derivative into a hydrogel biomaterial", *In preparation,* 2019

8. **Kurbasic, M.;** Garcia, A. M.; Kralj, S.; Pelin, M.; Melchionna, M.; Pengo, P.; Vargiu, A.V.; Marchesan, S. "A water playground for self-assembly from fibrils to plates", *In preparation,* 2019

Conferences:

1. **Oral Presentation** - Conference on Interactions of Light and Biological Matter: Experiments meet Theory, Trieste (Italy) – 2018

2. **Oral Presentation** – VIII International Meeting on Antimicrobial Peptides, Edinburgh (United Kingdom) – 2018

3. **Poster Presentation** – XLIII edition of the "Attilio Corbella" International Summer School on Organic Synthesis, Gargnano (Italy) – 2018

4. **Poster Presentation** – XIV International Symposium on Macrocyclic and Supramolecular Chemistry (ISMSC2019), Lecce (Italy) – 2019

Internationally awarded scholarship:

1. **Scholarship from MPIP** - Max Planck Institute for Polymer Research - Mainz (Germany)
   Non-linear Spectroscopy Studies on Supramolecular Peptides

2. **Scholarship from MultiComp** - Training School on Spectroscopy Methods - Vienna (Austria)

3. **Scholarship from "Attilio Corbella"** - International School on Organic Synthesis - Gargnano (Italy)

Courses:

1. Advanced NMR for inorganic and organic chemistry: a practical approach" Prof. S.Antoniutti – UniVe – 2017
2. "Experimental design and optimization" Prof. C. Ebert – UniTs – 2017
3. "Biocatalysis and enzymatic technologies in the chemical and pharmaceutical industry" Prof. L. Gardossi – UniTS – 2018
4. "From enzyme models to artificial enzymes" Prof. F. Benedetti – UniTS – 2018
5. "Luminescent materials and optical characterizations" Dr. F. Enrichi – UniVe – 2019
6. "Nanostructured (Bio)materials" Prof. S. Marchesan – UniTS – 2019

Seminars:

1. "Design and Applications of Catalytic Reactions for Sustainable Synthesis and Energy" Prof. David Milstein
2. "Monolayer-protected metal clusters: Chirality and reactivity" Prof. Thomas Bürgi
3. "Ru(III) complexes for anticancer therapy: the importance of being nucleolipidic" Prof. Daniela Montesarchio
4. "Renewable chemistry from biogas: CH4 and CO2 as feedstock" Dr.Fabrizio Sibilla
5. "Peptide based nanostructures for biomedical applications" Dr. Antonella Accardo
6. "Design of Antibacterial Glyconjugate Vaccines" Prof.Luigi Lay
7. "How my PhD gave me a winning hand of cards for my career" Dr. Elisa Miniussi
8. "II Winter School - Mentoring for Chemists: bringing excellence to Grow Excellence"
9. "Nature inspires smart device for regenerative medicine and nanomedicine" Anna Tampieri, Simone Sprio, Monica Sandri, Monica Montesi and Silvia Panseri
10. "Multifunctional and stimuli- responsive Coordination Cages" Prof. Guido Clever
11. "Nano-architected materials" Prof. Lorenzo Valdevit
12. "Understanding and Tuning Catlytic Materilas Using Nanocrystal Precursors" Dr. Matteo Cargnello